MACQUARIE
University
SYDNEY·AUSTRALIA

Investigations of Novel Bacterial Drug Efflux Systems

Stephanie S. Nagy

Bachelor of Advanced Science (Chemistry)

Master of Research (MRes) in Chemistry and Biomolecular Sciences

Thesis presented in fulfilment with the requirements for the degree of

Doctor of Philosophy

July 2022

School of Natural Sciences

Macquarie University

Australia

Table of Contents

Author statements

Declaration:

I certify that the content of this thesis is my own work and contains no material that has been submitted for the award of any other degree or diploma to any other university or tertiary education institute. To the best of my knowledge, this thesis contains no material produced by any other person except where due reference has been made within the text. Ethics approval was not required for this work. The microbiological work presented throughout this thesis was conducted under notifiable low risk dealings approved by the International Biosafety Committee (Reference: 5201401141).

Signed:
Stephanie S. Nagy
22.07.2022

Statement of impact of COVID-19:

The research conducted in Chapter 6 was dependent on frequent travel to the University of Wollongong to perform single-cell epifluorescence microscopy and microfluidic fabrication as part of our collaboration on this project. Due to state-wide shutdowns for eight months, and sensitivity of this assay, travel to troubleshoot our microfluidic chip took longer than expected, which limited the scope of the project to just providing a proof-of-concept research chapter. Furthermore, local travel restrictions specific to my residential local government area meant my access to resources at Macquarie University became limited in my final year of research. In Chapters 3-5 we originally planned to validate our whole-cell phenotype findings with further protein purification and biophysical characterisation. However, the thesis research changed track to incorporate bioinformatic analyses to adapt to these restrictions.

Abstract

The antimicrobial resistance (AMR) crisis represents one of the greatest challenges to modern medicine this century and threatens a return to the pre-antimicrobial era. It is evident that novel therapeutic options are required. Multidrug efflux pumps are ancient integral membrane transporters that provide a direct avenue for the polyspecific export of noxious compounds out of the cell, including antimicrobial therapeutics, thus promoting cell survival under antimicrobial challenge. Advances in genome sequencing and genomic techniques have allowed researchers to sequence, screen, identify and characterise drug efflux systems of novel bacterial isolates at exceptional rates. Furthermore, advances in single cell technology have provided a unique opportunity to study subtleties in heterogeneous efflux function at the single-cell level. *Acinetobacter baumannii* is a Gram-negative coccobacillus that is classified as a global top priority for the development of novel antimicrobials. *A. baumannii* infections are opportunistic and primarily affect the most critically ill patients. The emergence of multidrug resistant *A. baumannii* isolates is a significant unsolved public health problem.

The work presented in this thesis explores a range of high-throughput genomic techniques to further understand antimicrobial resistance in this pathogen. Transposon directed insertion sequencing was used to investigate the core fitness genes that confer biocide tolerance in *A. baumannii*. Transcriptomics explored the global gene response to subinhibitory concentration exposure of tetracycline and ciprofloxacin on planktonic and biofilm cultures of *A. baumannii*.

The high-throughput genomic analyses identified various hypothetical membrane proteins of unknown function that were important for antimicrobial fitness that could potentially represent new drug efflux pumps. Investigations in this thesis focused on three novel membrane proteins that were important for fitness under subinhibitory silver nitrate exposure in *A. baumannii*. The ABC-2 transporter, YadGH, the ArAE transport protein, ABUW_0700 and the DUF817 family protein, ABUW_1191 were found to be highly conserved in regions related to cell envelope homeostasis, redox and virulence respectively. Heterologous expression in *Escherichia coli*

provided evidence for multidrug resistance phenotype and acriflavine efflux activity in comparison to the empty vector controls. Microscopy, flow cytometry and lipid composition analyses suggested that YadGH conferred various pleiotropic effects on the cell envelope. Further experimental work will be required to clarify whether these membrane proteins are multidrug efflux pumps or confer drug resistance via indirect effects on the cell envelope.

Advances in single-cell technology provide a unique opportunity to study heterogeneity of efflux activity at the individual cell level. In this thesis, we provide a proof-of-concept study where we designed a microfluidic chip that allows for the direct visualisation and quantitation of heterogeneous efflux rates of individual cells in an isogenic bacterial population. To validate this, we studied real-time R6G efflux heterogeneity in a wild-type population of *E. coli* cells and discover a broad distribution of different efflux rates in individual cells. Furthermore, our technique enabled visualisation of heterogeneous R6G efflux cycles at the single-molecule level.

Acknowledgements

Behind this PhD thesis is a whole team of academics, family, and friends who through varying degrees of my PhD journey have provided unwavering support, guidance, and encouragement, and without whom I would not have achieved this milestone. First and foremost, I would like to extend my deepest gratitude to my principal supervisor: Distinguished Professor Ian Paulsen, whose steadfast support, mentorship, and expertise has not only made this thesis possible but has also taught me to become a better scientist. I am tremendously grateful to Dr. Bhumika Shah and Dr. Sophie Goodchild for their mentorship and expertise, in addition to providing invaluable professional and personal advice throughout this journey. I would like to thank a whole team of friendly collaborators who have made this research journey exceptionally pleasant. I want to thank Dr. Bart Eijkelkamp and Maoge Zang from Flinders University, for their enthusiastic expertise and prompt collaboration on *A. baumannii* membranes. I want to especially thank Dr. Andrew Robinson, Dr. Joris Goudsmits and Distinguished Professor Antoine van Oijen at the University of Wollongong for opening their newly founded Molecular Horizons facility to me to pursue fluorescence-based single-cell microfluidics. I would also like to thank Professor Peter Henderson and the Henderson laboratory at the University of Leeds for opening your lab to me during my scholarship funded travel to Europe, and for sharing your expertise in membrane protein expression and purification. I want to thank all the past and current members of the Paulsen laboratory that I am fortunate to have met during this journey for creating a wonderful lab environment. I want to especially thank Dr. Liping Li for her friendly collaboration and trusting me with her findings on *A. baumannii* biocide tolerance that has provided the foundational basis of this thesis and Dr. Francesca Short, for her friendly expertise and for encouraging me to pursue bioinformatic analyses on *A. baumannii.* Finally, I want to thank my parents for their unwavering support and belief in me and for providing me with every opportunity possible to allow me to reach this milestone. I also need to especially thank my partner Brendan, whose unwavering support, kindness and understanding during this journey has made this thesis possible.

Author contributions

Chapter 2: Genomic fitness profiling of *Acinetobacter baumannii* reveals modes of action for common biocides and mechanism of biocide-antibiotic antagonism

(Under review at *Nature Microbiology*)

Li, Paulsen, Hassan and Cain designed this study. The transposon mutant library was provided by Stephen Baker's laboratory. TraDIS sequencing and data processing was performed by Amy Cain and Julian Parkhill's research group. Data analyses were performed by Li. Experimental work was performed by Li, Short, Pokhrel, Naidu and Nagy. Nagy analysed data and performed MICs to confirm biocide tolerance conferred by membrane proteins of unknown function. Manuscript was written by Li with contributions from Short, Paulsen, Cain, Nagy, Parkhill and Hassan.

Chapter 3: The ABC-2 transporter, YadGH from *Acinetobacter baumannii* has pleiotropic effects on membrane homeostasis and drug resistance

Nagy, Hassan and Paulsen designed the study. Nagy performed all experiments except where otherwise stated, as well as all data analyses, and drafted the manuscript. Li provided TraDIS data for analysis. Short constructed the pan-genome data and advised on genetic neighbourhood conservation analyses. Pokhrel performed TEM microscopy. Zang performed FAME GC-MS and flow cytometry. Eijkelkamp provided preliminary fluorescence microscopy data. Shah advised on protein structure predictions and downstream analyses. Paulsen, Eijkelkamp, Zang and Shah provided revisions and suggestions on the manuscript.

Chapter 4: Identification and characterisation of an Aromatic Acid Exporter (ArAE) family protein from *Acinetobacter baumannii*

Nagy, Hassan and Paulsen designed the study. Nagy performed all experiments, all data analyses, and drafted the manuscript. Li provided TraDIS data. Short constructed the pan-genome data and advised on genetic neighbourhood conservation analyses. Shah advised on protein structure

predictions and downstream analyses. Paulsen and Shah provided revisions and suggestions on the manuscript.

Chapter 5: Characterisation of the *Acinetobacter baumannii* DUF817 protein as a multidrug resistance protein

Nagy, Hassan and Paulsen conceptualised the study. Nagy designed and performed all experiments, performed all data analyses and drafted the manuscript. Li provided the TraDIS data. Short provided the pan-genome data and advised on genetic neighbourhood conservation analyses. Shah advised on protein structure predictions. Paulsen and Shah provided revisions and suggestions on the manuscript.

Chapter 6: A tool for the direct visualisation of rapid drug efflux out of individual bacterial cells

Nagy, Robinson, Goudsmits, Hassan, van Oijen and Paulsen designed the study. Nagy performed all experiments, data analyses and drafted the manuscript. Goudsmits designed the microfluidic chip and advised on microfluidics techniques. Robinson and Goudsmits assisted Nagy with fluorescence microscopy, microfluidics and troubleshooting. Goodchild assisted with troubleshooting and data analyses. Paulsen provided revisions and suggestions on the manuscript.

Chapter 7: Identification of a novel ciprofloxacin tolerance gene, *aciT*, which contributes to filamentation in *Acinetobacter baumannii*

(Published in *Antimicrobial Agents and Chemotherapy,* May 2021)

Naidu, Shah, and Paulsen designed this study. Experimental work was performed by Naidu, Kamath, Pokhrel, and Nagy. Naidu performed all experiments with the following acknowledgements. Pokhrel constructed the *aciT* complement strain. Kamath prepared samples for mass spectrometry and proteomics. Nagy advised and assisted with membrane protein expression analyses. All data analyses were performed by Naidu. The manuscript was written by Naidu with contributions from Shah, Hassan, Kamath, Molloy, Pokhrel, Nagy and Paulsen.

Chapter 8: Rapid microevolution of biofilm cells in response to antibiotics

(Published in *Nature Biofilms and Microbiomes,* November 2019)

Penesyan and Paulsen conceived the project and designed the experiments. Penesyan performed all experiments except for where otherwise stated and collected data. Nagy performed MICs for all biofilm isolates collected in the study. Penesyan performed all data analyses. Penesyan, Kjelleberg, Gillings, Nagy and Paulsen wrote the manuscript.

Abbreviations

ABC	ATP-binding cassette
AbgT	*p*-aminobenzoyl-glutamate transporter
ABPS	Adaptive Poisson-Boltzmann Solver
ADP	Adenosine diphosphate
AMR	Antimicrobial resistance
ANOVA	Analysis of variance
ArAE	Aromatic acid exporter
ATP	Adenosine triphosphate
BCA	Bicinchoninic acid
BLAST	Basic Local Alignment Search Tool
CCCP	Carbonyl cyanide *m*-chlorophenyl hydrazone
CDS	Coding sequence
C-terminal	Carboxy-terminal
DM	Dichroic mirror
DNA	Deoxyribonucleic acid
DUF	Domain of unknown function
EDTA	Ethylenediaminetetraacetate
EM	Electron microscopy
Em	Emission
EM-CCD	Electron multiplying charge coupled device
E-value	Expectation value
Ex	Excitation
FACS	Fluorescence-activated cell sorting
FAME	Fatty acid methyl ester
GC-MS	Gas chromatography-mass spectrometry

H_6	Hexa-histidine
HEPES	4-(2-hydroxyethyl)-1-piperazineethanesulfonic acid
HMM	Hidden Markov model
IPTG	Isopropyl ß-D-1-thiogalactopyranoside
LB	Luria-Bertani
LPSN	List of Prokaryotic Names with Standing Nomenclature
MATE	Multidrug and toxin extrusion family
MDR	Multidrug resistance
MFP	Membrane fusion protein
MFS	Major facilitator superfamily
MGE	Mobile genetic elements
MIC	Minimum inhibitory concentration
MMSeq2	Many-against-many sequence searching
mRNA	Messenger RNA
MS	Mass spectrometry
MSA	Multiple sequence alignment
MSD	Mass selective detector
MUSCLE	Multiple sequence comparison by log-expectation
MWM	Molecular weight marker
NA	Numerical aperture
NADPH	Reduced nicotinamide adenine dinucleotide phosphate
NanoDSF	Nanoscale differential scanning fluorimetry
NanoITC	Nano isothermal titration calorimetry
NAO	Nonyl-acridine orange
NaPi	Sodium phosphate buffer
NBD	Nucleotide binding domain
NCBI	National Center for Biotechnology Information

nres	Number of residues
N-terminal	Amino-terminal
OD	Optical density
OMP	Outer membrane protein
PACE	Proteobacterial antimicrobial compound efflux
PAGE	Polyacrylamide gel electrophoresis
PBS	Phosphate buffered saline
PDB	Protein Data Bank
PDMS	Polydimethylsiloxane
PE	Polyethylene
PM	Phenotype microarray
QAC	Quaternary ammonium compound
R6G	Rhodamine 6G
RMSD	Root-mean-square deviation
RNA	Ribonucleic acid
RNA-seq	RNA sequencing
RND	Resistance-nodulation-division
ROS	Reactive oxygen species
RPM	Rotations per minute
rRNA	Ribosomal RNA
SDS	Sodium dodecyl sulfate
SEM	Standard error of the mean
SMR	Small multidrug resistance
SOC	Super optimal broth with catabolite repression
SPR	Surface plasmon resonance
$t_{1/2}$	Half-life
TCDB	Transport classification database

TEM	Transmission electron microscopy
TMD	Transmembrane domain
TMH	Transmembrane helix
TMSOH	Trimethylsilanol
Tn	Transposon
TraDIS	Transposon directed insertion sequencing
TRIS	Tris(hydroxymethyl)aminomethane
UAR-EMS	Uranyl acetate replacement stain
WHO	World Health Organisation

Chapter 1: General Introduction

1.1 Antimicrobial resistance

Antimicrobial resistance (AMR) is defined as the ability of once susceptible microbes, including bacteria, to develop molecular mechanisms to confer resistance to once effective therapeutic antimicrobial compounds used in the treatment of infectious disease. In 1929, the first clinical antibiotic, penicillin, was discovered (1). In 1940, the first mechanism concerning penicillin resistance was attributed to the presence of an endogenous hydrolytic enzyme, known as penicillinase (2). Since this point, there has been an exponential rise in the emergence of multi-drug resistant (MDR) bacterial pathogens, non-susceptible to three or more antimicrobial classes, and pan-drug resistant (PDR) bacterial pathogens, non-susceptible to all antimicrobial categories isolated from clinical environments (3, 4). In 2019, 1.27 million deaths worldwide were attributed to AMR infections, where 73% of total deaths were attributed to infections caused by *Escherichia coli, Staphylococcus aureus, Klebsiella pneumoniae, Streptococcus pneumoniae, Pseudomonas aeruginosa* or *Acinetobacter baumannii* (3). MDR resistant isolates have been reported for all species listed above (5–10). Recently, the World Health Organisation published a list of priority bacterial pathogens for which there is an urgent and essential need for novel therapeutics, due to the limited prevention opportunities and therapeutic options available today to effectively treat infections caused by these pathogens (11). The top three priority pathogens listed includes carbapenem-resistant *A. baumannii* and *P. aeruginosa* and extended-spectrum β-lactamase producing *Enterobacteriaceae* spp. (11). Furthermore, pan-drug resistant (PDR) isolates of *A. baumannii* and *P. aeruginosa* have been reported (5, 6). Regrettably, these organisms act as opportunistic pathogens that afflict the most vulnerable patients with high rates of morbidity and mortality. Therefore, the emergence of PDR isolates of these species is of grave concern (5, 6).

A large number of therapeutic options used to treat bacterial infections today were discovered between 1950-1960, known as the golden era of antibiotic discovery (12). Research and discovery into novel therapeutic options has stalled since this era, despite the rise and prevalence of AMR. This is partly due to the fact that antimicrobial research and development are not a profitable venture for many major pharmaceutical companies; prescription lifetimes are expected to be short, strict pricing regulations exist and the rate of antimicrobial resistance development is extremely fast, hence, any novel therapeutics developed are likely to become irrelevant, and thus unprofitable, within a very short period of time (13). In addition, the abundance and misuse of remaining antimicrobials by humans and in livestock industry has rapidly accelerated the emergence of AMR worldwide (14). The current shortage in novel antimicrobial therapeutic options and rise of antibiotic misuse in clinical and community environments threatens the return of modern medicine back to the pre-antibiotic era (14). It is evident that novel therapeutics are essential to combat AMR. However, it is also imperative to investigate the specific mechanisms which drive and confer drug resistance to these pathogens to identify novel therapeutic targets for antibiotic research and development, and rational design of novel and effective antimicrobial therapies to combat AMR.

1.2 Mechanisms of antimicrobial resistance in bacteria

To defend against antimicrobial challenge, bacteria can achieve antimicrobial resistance through several distinct mechanisms. These mechanisms can either be intrinsic — through structural and functional differences that allow the bacteria to be inherently insensitive to certain antimicrobials — or adaptive — through mutational changes in the chromosome or acquired from the environment by horizontal gene transfer of mobile genetic elements harbouring resistance genes. Mechanisms in which drug resistance can be accomplished includes antimicrobial inactivation and modification, target modification, protection, and bypass, as well as reduced permeability of the cell envelope and increased drug efflux activity by transporters. These different mechanisms of antimicrobial resistance are briefly described below and surmised in Figure 1.

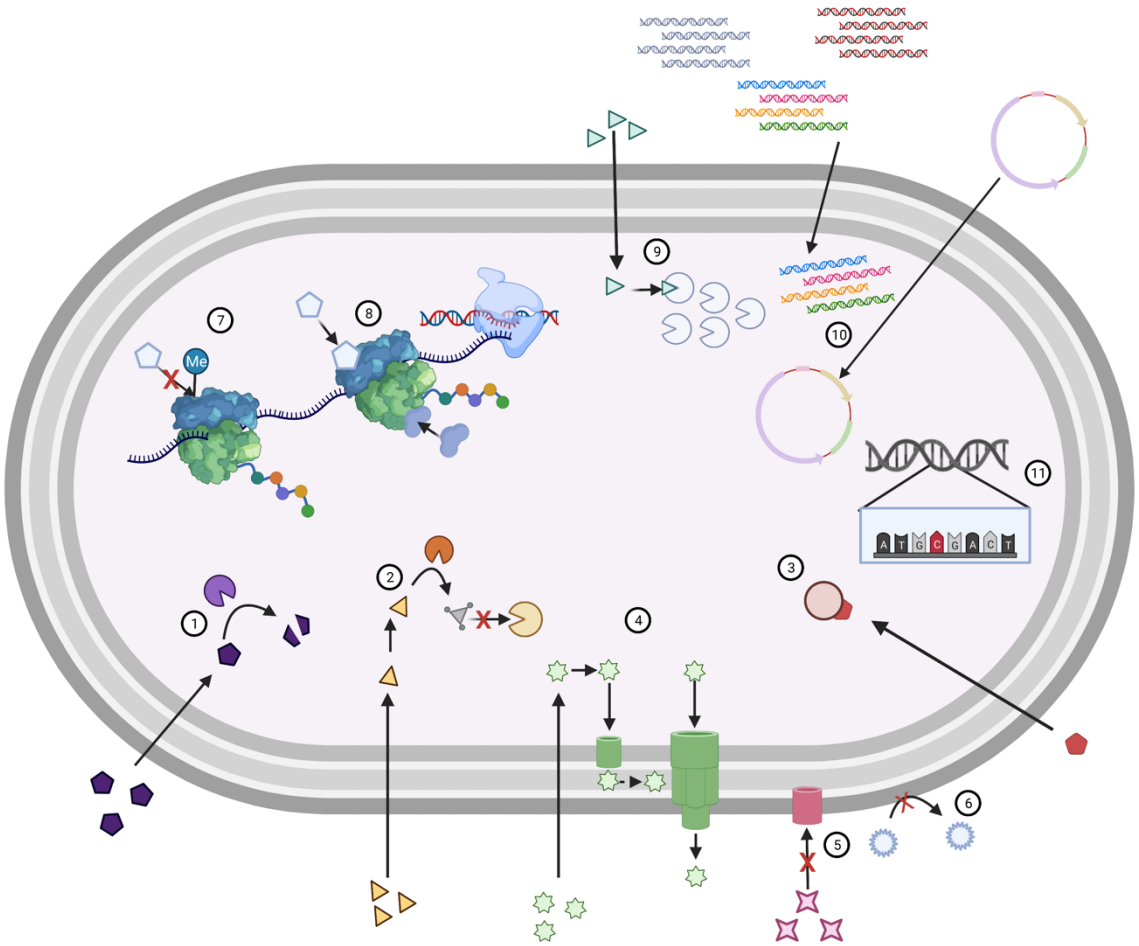

Figure 1: Schematic overview of antimicrobial resistance mechanisms in bacteria. Antimicrobials that penetrate the cell membrane to enter the cytoplasmic space can be inactivated in three distinct methods: expression or acquisition of enzymes that catalyse the degradation of an antimicrobial compound (1); expression or acquisition of enzymes modify the chemistry of the molecules and prevent target binding (2); and antimicrobial inactivation through drug-binding proteins to sequester the antibiotic and prevent access to the target (3). Accumulation of antimicrobial can be reduced by three methods: active drug efflux through direct transport of an antimicrobial out of the cell (4); lowered permeability through decreased expression and modification of non-specific outer-membrane proteins (5); and intrinsic and adaptive resistance due to presence and modification of outer-membrane lipids to reduce antimicrobial entry (6). Antimicrobial resistance can also be achieved through modification of protein target to prevent antibiotic binding (7); target protection to release and rescue protein targets from antimicrobial action when bound (8); and overproduction of target to minimise toxic effects of antimicrobials within the cell cytoplasm (9).

AMR can be intrinsic, adaptive through selective pressures or acquired from foreign DNA and resistance plasmids that carry AMR genes (10, 11). Figure created with BioRender.com.

1.2.1 Drug inactivation and modification

One of the first mechanisms of antibiotic resistance reported was the direct inactivation and degradation of an antibiotic compound to mediate resistance (2). In this mechanism, drug inactivation is mediated by degrading or modifying an antimicrobial by expressing endogenous enzymes to break covalent bonds (hydrolases, lyases, epoxidases and mono-oxidases), reduce antibiotics to ineffective forms (reductases), form inactive mutants to prevent pro-drug activation or transfer bulky functional groups to prevent target binding by means of steric hinderance (transferases) (15). Due to the diversity of drug inactivating enzymes reported, specific examples of antibiotic degradation and modification are provided in Table 1. Drug inactivation can also be achieved through antimicrobial sequestration where drug-binding proteins bind an antimicrobial with high-affinity to prevent the antimicrobial from binding to the target. Drug sequestration examples include the bleomycin binding genes *tmlA, blmA* and *zmbA* of *Streptoalloteichus hindustanus*, *Streptomyces verticillus* and *Streptomyces flavoviridis* (16).

Table 1: Examples of drug degradation and modification mechanisms

Antimicrobial	Degradation	Mechanism	Source
β-lactams	Hydrolysis via β-lactamases	Hydrolysis of the amide of the four-membered β-lactam ring	(17)
Macrolides	Hydrolysis by macrolide esterases	Hydrolysis of macrolactone ring	(18)
Fosfomycin	Hydrolysis by fosfomycin epoxidases or thiol transferases	Hydration of oxirane ring by epoxidase activity or thiol transfer and oxirane ring degradation by (FosA/B)	(19)
Tetracycline	Mono-oxidation by *tetX* monooxygenase enzymes	Incorporation of -OH and degradation of unstable intermediate 11A-hydroxyltetracycline	(20)
Rifamycins	Mono-oxidation by *rox* monooxygenase enzymes	Linearisation by incorporation of -OH in naphthyl group of rifamycin	(21)
Streptogramins	Ester bond cleavage via ring opening lyases	C-O bond cleavage and linearisation of streptogramin B	(22)
Antimicrobial	**Reduction**	**Mechanism**	**Source**
Nitrofurans	Loss-of-function nitro-reductase activity	Pro-drug remains inactivated and unable to exert antimicrobial activity	(23)
Nitroimidazoles	Loss-of-function nitro-reductase activity	Pro-drug remains inactivated and unable to exert antimicrobial activity	(24)
Chloramphenicol	Nitroreduction	Reduction of nitro-group to inactive form of amino-chloramphenicol	(25)
Antimicrobial	**Modification**	**Mechanism**	**Source**
Aminoglycoside	Acylation by aminoglycoside *N*-acetyltransferases	Acetylation of aminoglycoside amine ($-NH_2$) groups at position 1', 2',3' or 6' in the presence of acetyl coenzyme A	(26)
	Phosphorylation by aminoglycoside *O*-phosphotransferases	Phosphorylation of aminoglycoside at hydroxyl groups in position 2,3,4,6,7 and 9 by transfer of phosphate group	(26)
	Nucleotidylation by aminoglycoside *O*-nucleotidyltransferases	Adenylation of aminoglycoside hydroxyl moieties at position 2,3,4,6 and 9 by transfer of AMP in the presence of ATP donor molecule	(26)

Table 1 (*continued*)

Antimicrobial	Modification	Mechanism	Source
Macrolides	Phosphorylation	Phosphorylation at the macrolide hydroxyl moiety in the desosamine sugar	(27)
	Glycosylation	Transfer of UDP-glucose to glycosylate 6-deoxyhexose of the macrolactone ring	(28)
Lincosamides	Nucleotidylation by lincosamide o-nucleotidyltransferases	Nucleotidylation of lincosamide hydroxyl moiety at position 3 or 4, in the presence of nucleotide 5' triphosphate and magnesium co-factor	(29, 30)
Rifamycin	Glycosylation	Glycosylation at hydroxyl moiety at carbon 23 by *rgt* genes to form inactive glycosylated derivative	(31)
	Phosphorylation	Phosphorylation at hydroxyl group at carbon 21 to form inactive phosphorylated derivative by *rph* genes	(32)
	ADP-ribosylation by ADP-ribosyltransferase enzymes (*arr*)	Arr enzyme stabilises the hydroxyl group at C-23 to form an oxocarbenium intermediate state to allow for ribosylation to form an inactive ADP-ribosyl-rifampicin derivative	(33)
Chloramphenicol	Acetylation by chloramphenicol acetyltransferase (CAT)	Acetylation by chloramphenicol hydroxyl moiety at position 3 in the presence of acetyl coenzyme A by CAT enzymes	(34)
Streptogramins	Acetylation	Acetylation of hydroxyl moiety at C14 of streptogramin A antibiotics	(35)

1.2.2 Target modification, protection, and bypass

In addition to direct modification and inactivation of antimicrobial compounds, bacteria can also achieve resistance by changing the antimicrobial target to become insensitive to antimicrobial challenge. This can be achieved by three main mechanisms of resistance: i) target protection, ii) target modification and iii) target bypass.

Target protection

Target protection is a mechanism that explicitly involves the use of a protein to protect a target by complete displacement of the antibiotic, allosteric antibiotic displacement, or target rescue by allosteric binding and restoration of target function in the presence of bound antibiotic (36). Prototypical examples of target protection mediated resistance include the expression of quinolone resistance pentapeptide repeat proteins (PRPs) that recognise quinolone bound DNA-gyrase and topoisomerase IV to trigger the release of the quinolone antibiotic to rescue DNA transcription activity (37). Additionally, expression of the tetracycline resistance gene, *tetM,* rescues translation activity of the ribosome by direct displacement of the tetracycline antibiotic by the homologous elongation factor G (EF-G) and induced conformational change when bound to EF-G binding site of the ribosome (38). Further examples of target protection mediated resistance are provided in a recent review by Wilson *et al.*, 2020 (36).

Target modification

Bacteria can also become resistant to antimicrobial action by modification of an antimicrobial target under selective pressure driven by antimicrobial exposure. Spontaneous mutation can occur in an antimicrobial target to lower binding affinity and antimicrobial activity within bacteria, which can become the primary population under antimicrobial selection. Mutations in chromosomally encoded target genes that can alter the conformation and chemical properties of a binding site to lower binding affinity have been shown to be important mechanisms of resistance against DNA transcription inhibitors (quinolones), RNA polymerase inhibitors (rifamycin) and translation inhibitors (aminoglycosides, tetracycline, macrolides, lincosamides and oxazolidinones) (39–41). Mutations in gene regulators can also confer resistance to antimicrobials

by differential expression of a target, resulting in loss of susceptibility to an antimicrobial. This method of mutagenesis is best represented by resistance to cell-disrupting antimicrobials, where mutations in phospholipid biosynthesis genes can result in altered phospholipid composition and modification that can lead to overall changes in the net charge of the cell envelope (42). This mechanism is reported in polymyxin resistant Gram-negative pathogens, including *A. baumannii, P. aeruginosa* and *K. pneumoniae* (43–45).

Target modification can also occur through the expression of endogenous target modifying enzymes. This mechanism of resistance is primarily associated with the expression of ribosome modifying methyltransferases that alter the antimicrobial binding site to avert antimicrobial activity. The major methyltransferases recognised include: the erythromycin ribosome methyltransferase (*erm*) gene, which methylates the adenine 2058 of 23S rRNA, conferring resistance to antimicrobials including macrolides, lincosamides and streptogramins (46); and the chloramphenicol-florfenicol resistance (*cfr*) gene, which methylates adenine at position 2053, contributing resistance to phenicols, lincosamides, oxazolidinones, pleuromutilins and streptogramins (47).

Target replacement and bypass

Bacteria can substitute antimicrobial targets to avoid antimicrobial activity. For example, glycopeptide resistance is mediated through the acquisition of *van* gene clusters that remodel the peptidoglycan pentapeptide repeat sequence D-Ala-D-Ala to D-Ala-D-Lactate or D-Ala-D-Serine is effective at reducing glycopeptide-mediated peptidoglycan binding and inhibition of peptidoglycan cross-linking, and is an important mechanism of resistance in vancomycin-resistant *Enterococci* (48). Acquisition of antimicrobial insensitive variants of a target is often associated with target bypass, including: the acquisition of β-lactam insensitive penicillin binding protein, PBP2a, as associated with methicillin resistance in *S. aureus* (MRSA) (49); and the acquisition of insensitive variants of dihydrofolate reductase (DHFR) and dihydropteroic acid synthase (DHPS) within the folate biosynthesis pathway to promote trimethoprim and sulfonamide resistance (50). Bypass can also be achieved by overproduction of a target to limit toxicity and resume activity. In

an *E. coli* isolate resistant to trimethoprim, overproduction of DHFR by 100-fold allows for continued folate biosynthesis and high-level trimethoprim resistance (51).

1.2.3 Reduced permeability

Antimicrobials often have intracellular targets and require transport processes to enter the cell to exert their activity. Limiting the import of antimicrobial substrates directly from the extracellular environment is a first-line of defence for many bacterial species. Hydrophilic antimicrobials, including β-lactam, tetracyclines and fluoroquinolones, find opportunity to enter the bacterial cell through passive transport using non-specific water-filled channels (52). Antimicrobial resistance in porin channels can be mediated by porin loss and porin exchange. Porin loss is associated with carbapenem resistance in Gram-negative pathogens, for example the loss of OmpK35 has been identified in broad-spectrum carbapenem resistant *K. pneumoniae* isolates (53). Exposure to an antimicrobial can induce porin-exchange where large, non-specific porins are downregulated and 'exchanged' for the upregulation of smaller, more specific porin channels that reduce permeability to large, bulky antimicrobial compounds. Exposure to β-lactam antibiotics was found to induce porin-exchange between Omp35, a large, non-specific porin, for Omp36, resulting in imipenem resistance in a clinical isolate of *Enterobacter aerogenes* (54). Mutation of the porin genes themselves and/or regulators can also contribute to such resistance (42).

1.2.4 Increased efflux activity

Integral membrane transporters play an important role in the import and export of bioactive compounds required for survival. Transporters associated with the direct export of noxious compounds including antimicrobials and antibiotics are aptly named drug efflux pumps. Drug efflux systems can be substrate specific, including the tetracycline efflux transporters, *tet* of *E. coli* and macrolide resistance efflux pumps, *mef* of *Streptococcus pneumoniae* (55, 56). However, many drug efflux pumps exhibit a broad substrate specificity, often recognising a diverse range of unrelated antimicrobial classes, which contributes to multidrug resistance phenotypes when expressed in bacteria. The AcrAB-TolC drug efflux pump is an example of an efflux system that can recognise and transport a diverse range of antibiotics, including; phenicols, β-lactam,

quinolones, tetracyclines, rifampicin, novobiocin, fusidic acid, and antiseptics triclosan and acriflavine (57, 58). The AcrAB-TolC efflux pump is capable of pumping substrates from the outer leaflet of the inner membrane and periplasmic space of the *E. coli* cell envelope and has been linked to MDR phenotypes in bacterial strains overexpressing this transport system (59, 60).

1.3 Drug efflux systems of bacteria

Efflux pumps represent an important mechanism of drug resistance in bacterial pathogens and can lead to intrinsic or adaptive multidrug resistant phenotype through the overexpression of chromosomally encoded transporters or acquisition of multidrug efflux systems from mobile genetic elements. Currently, there are seven phylogenetically and mechanistically distinct families of transporters with defined drug efflux pump activity; the ATP-binding cassette (ABC) superfamily (61), the Resistance-Nodulation-Division (RND) superfamily (62), the Major Facilitator Superfamily (MFS) (63), the Small Multidrug Resistance (SMR) family of the Drug-Metabolite Transporter (DMT) superfamily (64, 65), the Multidrug and Toxin Extrusion (MATE) family of the Multidrug/Oligosaccharidyl-Lipid/Polysaccharide (MOP) Superfamily (66, 67), the *p*-Aminobenzoylglutamate transporter (AbgT) family and the Proteobacterial Antimicrobial Compound Extrusion (PACE) family (68, 69). A representative example from each of these transporter families is shown in Figure 2.

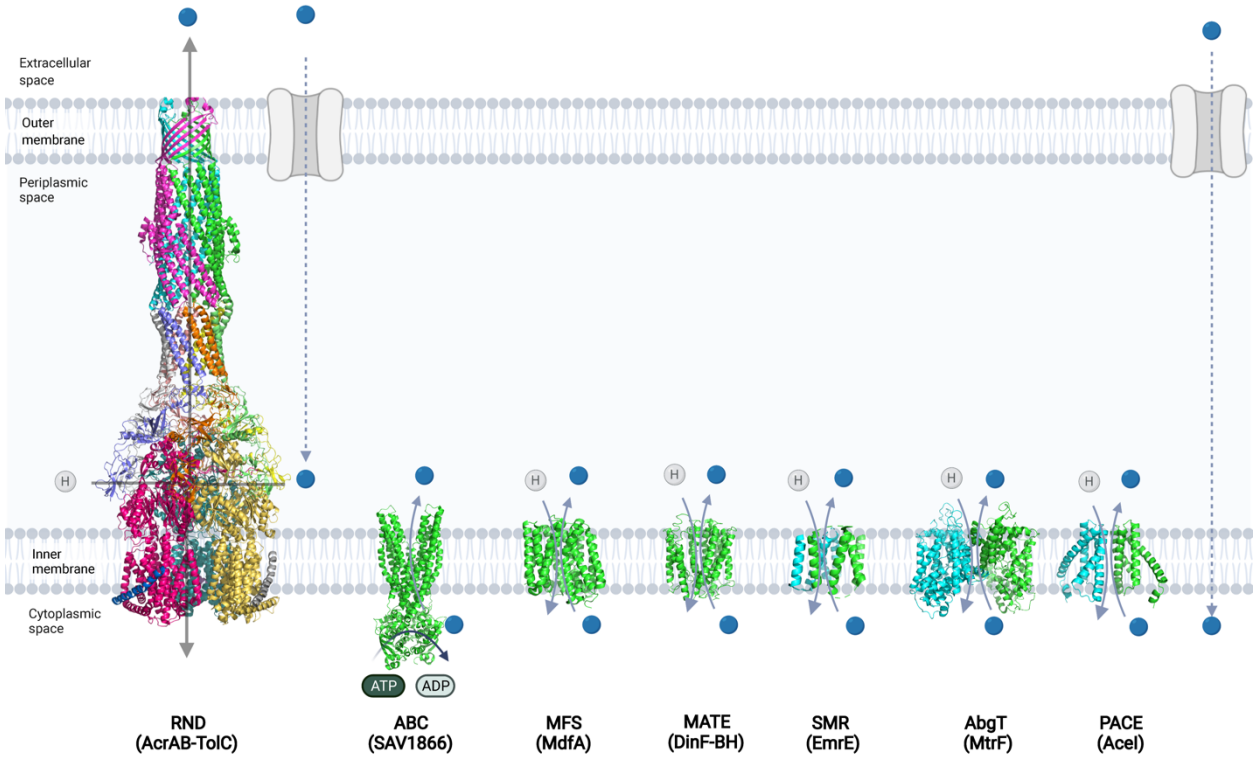

Figure 2: Representative structures of seven classes of efflux pumps in bacteria. The structural and mechanistic differences between all seven drug efflux families are shown, including; the tripartite RND transporter shown with MFP and OMP as represented by AcrAB-TolC (PDB:5O66) (70), ATP-binding cassette (ABC) transporter SAV1866 (PDB: 2ONJ) (71), the MFS transporter MdfA (PDB: 4ZP0) (72), the MATE transporter DinF-BH (4LZ6) (73), the SMR transporter EmrE (PDB: 2I68) (74), the AbgT transporter, MtrF (PDB: 4R1I) (75) and PACE transport protein, AceI (predicted structure provided by Dr. Bhumika Shah). MFS and ABC transporters can also associate with a MFP and OMP to form tripartite efflux pump structures (*not shown)*. Single-component transporters transport antimicrobials from the cytoplasmic space and release it to the periplasmic environment in Gram-negative organisms or extracellular environment in Gram-positive organisms. Tripartite efflux pumps, such as RND, MFS and ABC, can export antimicrobials from the periplasmic space or cytoplasmic space directly across the double membrane to the extracellular space of Gram-negatives (76, 77). Figure created with BioRender.com

1.3.1 The ATP-binding cassette family

The ABC transport superfamily represent one of the largest families of transport proteins across all domains of life (61). Bacterial ABC transporter can perform either substrate import or export of a diverse range of substrates including; ions, small metabolites, lipids, antimicrobials and macromolecular substrates, including proteins, siderophore and polysaccharides (61). ABC transporters are often 1000-2500 amino acids in length, comprising of two highly conserved nucleotide binding domains (NBD) and two α-helical transmembrane domains (TMDs) which contain 6 or 12 transmembrane helices that provide a translocation pathway and substrate selectivity (61, 78, 79). ABC transport proteins can be encoded by a single polypeptide, half-transporter (comprising one NBD and one TMH domain) or as two independent genes encoding the nucleotide binding domain and transmembrane permease separately. ABC import proteins also encode for an additional periplasmic binding protein to deliver substrate to the ABC transport complex; whereas exporters do not associate with a periplasmic binding protein (61). However, in Gram-negative bacteria, ABC exporters can also form tripartite ABC efflux systems in association with a membrane fusion protein (MFP) and outer membrane protein (OMP) to export substrates from the periplasm to the extracellular space (80, 81).

ABC efflux pumps are proposed to undergo an alternating access mechanism of transport, based on significant structural evidence of a range of ABC efflux pumps (79, 82–84). In this mechanism, substrate transport by ABC exporters is proposed to begin in the inward-facing conformation, allowing substrate loading into the transmembrane permease domain in the absence of ATP or with ADP bound (79). ATP-binding at the NBD interface triggers dimerization and strong conformational change from the inward-facing to outward-facing position of the transmembrane permease via an occluded state (79). Substrate is released to the periplasm or extracellular space due to loss of substrate affinity at the binding site (79). Subsequent ATP-hydrolysis and release of inorganic phosphate weakens dimerization of the NBD domain and the transporter transitions back to the inward-open conformational state for another cycle of transport (79). A prototypical example of multi-drug resistant ABC efflux pump includes the SAV1866 transporter from

S. aureus, reported to export a diverse range of chemotherapeutics and antimicrobial dyes including doxorubicin, vinblastine, verapamil, ethidium bromide and Hoechst 33342 (82, 85).

1.3.2 Resistance-nodulation-division superfamily

The Resistance-Nodulation-Division superfamily of transporters are a ubiquitous transporter family, found across all domains of life (62). RND efflux systems are typically 650–1000 amino acids in length and contain twelve integral membrane transmembrane helices connected by large periplasmic loop regions. In Gram-negative bacteria, the RND permease often associates with an additional MFP (also known as a periplasmic adaptor protein) and OMP to form a tripartite structure that spans across the inner membrane and outer membrane of the cell envelope. In Enterobacteria, an additional small protein <50 amino acids in length is conserved (86, 87). In *E. coli,* this protein is known as AcrZ and has been characterised to bind to AcrB to modulate substrate preference of the AcrAB-TolC efflux pump (86, 87). RND transporters are known for members hosting extensively diverse substrate profiles (see AcrAB-TolC in Section 1.2.4) (88). RND transport permease functions as a rotational trimer, in which each protomer rotates between access, binding and extrusion conformational states to achieve drug efflux through a peristaltic mechanism of substrate transport (89). In *E. coli* AcrB, a substrate can enter the RND transport permease through four separate entry channels via the periplasmic space or inner leaflet of the outer membrane, in the access state (90). The protomer responds to substrate binding in the occluded state which allows the substrate to travel to the appropriate binding site within the RND protomer (91, 92). The last protomer of the efflux system is in the extrusion state, where the substrate binding cavity is protonated, triggering substrate release to the extracellular space (91, 92).

1.3.3 The major facilitator superfamily

The MFS family is an ancient and diverse transport family, ubiquitously found across all domains of life (63). MFS transporters are typically 400–600 amino acids in length and contain 12 or 14 transmembrane helices connected by short hydrophilic loops forming a deep, hydrophobic

substrate cavity for substrate binding (93–95). MFS transporters can achieve transport via uniport, symport and antiport transport mechanisms to transport a diverse range of substrates, including ions, sugars, amino acids, nucleotides, peptides and a diverse range of antimicrobial compounds (63, 96, 97). The minimal functional unit of an MFS transporter is a single monomeric unit that drives transport across a single cell membrane interface. MFS transporters have been reported to form trimeric structures that span the double-membrane of Gram-negative bacteria for direct substrate transport from the cytoplasm across the double membrane into the extracellular space (76, 98). MFS exporters primarily use the proton-motive force to drive drug export via a rocker-switch model of alternating access mechanism of transport (99). In this mechanism, deprotonation of the substrate binding cavity in the inward-facing conformation triggers substrate loading and conformational change to the outward-facing state, via an occluded intermediate state for directional transport (99). MdfA is a prototypical example of a multidrug resistant MFS drug efflux pump. Expression of this MFS transporter is associated with resistance to a range of important antimicrobials including aminoglycosides, phenicols, fluoroquinolones, macrolides, rifampicin, tetracycline, puromycin and daunomycin and the antiseptic benzalkonium chloride, in addition to a variety of antimicrobial dyes (100).

1.3.4 The multidrug and toxin extrusion family.

The MATE transporters are a large and diverse family of drug efflux pumps of the greater multidrug/oligosaccharide-lipid/polysaccharide (MOP) superfamily that function exclusively as lipophilic and cation compound exporters (67). MATE transporters have been reported in bacteria, archaea, and eukaryotes. Typical MATE transporters are 400–700 amino acids in length comprising of twelve transmembrane helices connected by short hydrophilic loops (101). MATE transporters are monomeric and transport small cationic compounds using either proton- or sodium-motive force gradients operated by a predicted rocker-switch mechanism of transport as described for MFS transporters (Section 1.3.3), with the exception that loss of sodium ion binding to the substrate cavity can trigger conformational changes for sodium-coupled MATE transporters (73, 102, 103). MATE transporters also have more limited antimicrobial substrate ranges, selecting

for exclusively cationic antimicrobial compounds. The MATE transporters NorM of *Vibrio cholera* and NorM of *Neisseria gonorrhoea* contribute to resistance to aminoglycosides and fluoroquinolones, in addition to the cationic antimicrobial dye, ethidium bromide (102, 104).

1.3.5 Small multidrug resistance family

The small multidrug resistance family are a drug export subfamily within the greater drug/metabolite transport (DMT) superfamily (65). SMR transporters are small integral membrane transporters and are typically 110–140 amino acids in length comprised of four transmembrane helices (64). The SMR functional unit is proposed to be a dimer, where two protomers associate non-covalently in an antiparallel fashion to yield an eight transmembrane helical bundle for quaternary ammonium compound (QAC) export (105, 106). Transport is predicted to occur as a $2H^+$/drug antiport mechanism using a single-site alternating access mechanism of transport (105). In this mechanism, two protons bind to an SMR transporter to trigger a conformational change from outward-facing to inward-facing, where the bound substrate undergoes cation exchange via direct competition between substrate and cation at the binding site (105). This exchange of substrates triggers the conformational change back to the outward-facing state for substrate release (105). SMR transporters are restricted to prokaryotes (107). The major SMR transporter of *E. coli*, EmrE, is associated with conferred resistance to diverse range of cationic antimicrobial compounds including; acriflavine, ethidium bromide, tetraphenylphosphonium chloride, aminoglycosides, macrolides, tetracycline, methyl viologen, sulphonamides, crystal violet, benzalkonium chloride. cetyltrimethylammonium bromide and osmoprotectants, choline and betaine (108–113).

1.3.6 The *p*-Aminobenzoyl glutamate transport family

The AbgT family of transporters are a family of transporters present across bacteria and yeast species (68). In bacteria, members of the AbgT family have been reported to function in the import and export of folic acid intermediates. AbgT transporters are typically 475–525 amino acids in length, comprising a protomer that includes nine transmembrane helices (68). Recent crystal structures of two independent AbgT efflux pumps reveal a unique, concave bowl-like structure

formed by the dimerization of two protomers (75, 114). The concave basin formed by both protomers on the cytoplasmic side of the membrane is solvent accessible and reaches from the cytoplasmic space into the inner leaflet of the phospholipid bilayer. An entrance from the concave basin into a channel like structure is predicted to be the site of substrate binding and transport to the periplasmic space (75, 114). The AbgT family efflux pump is predicted to achieve transport across this channel by a proposed elevator-access mechanism (115, 116). Originally the AbgT family was named after the *E. coli* (AbgT) importer involved in *p*-aminobenzoyl glutamate uptake, an important intermediate for the *de novo* synthesis of folic acid (117). However, high-level characterisation of MtrF and YdaH revealed that these transporters are incapable of *p*-aminobenzoyl glutamate or *p*-aminobenzoic acid uptake and function in ion-motive force coupled *p*-aminobenzoic and sulfonamide efflux (68).

1.3.7 Proteobacterial antimicrobial compound efflux family

The PACE family of drug transport systems represents the first novel efflux family to be identified in the 15 years since discovery of the MATE family (118). PACE family members are restricted to the bacterial kingdom and are comprised of only approximately 150 amino acids arranged into four transmembrane α-helices (119). Like the SMR transport family, PACE family members are predicted to form a small homodimer to allow selective transport of QACs, primarily biocides and antimicrobial dyes (120). However, although the stoichiometry and predicted mechanism of PACE transport proteins is yet to be determined the physiological role of at least one PACE transport family member has been identified. AceI, a prototypical PACE transporter from *Acinetobacter baumannii* known for chlorhexidine efflux, was purified and reconstituted into proteoliposome and shown to export the polyamines cadaverine and putrescine (121, 122) and exclusively confer resistance to chlorhexidine (118). However, homologues of the PACE transporter across proteobacterial species are known to have broader substrate profiles, including VP1155, an AceI homologue from *Vibrio parahaemolyticus*, which shows conferred resistance to acriflavine, proflavine, chlorhexidine and benzalkonium chloride (120).

1.4 Physiological roles of drug efflux systems

The drug efflux families described above are phylogenetically, structurally, and mechanistically distinct from each other. The genes for multiple different drug efflux pumps are commonly encoded chromosomally in the core genome of most bacterial strains. However, many of these efflux systems share similar antimicrobial substrate profiles to each other (123). It is hypothesised that drug efflux systems may have arisen from the need for polyspecific substrate transport through convergent evolution multiple times throughout the history of the bacterial kingdom in order to survival a range of biologically unfavourable conditions (124). The evolution of these ancient transport systems may have incidentally provided a strong survival mechanism against substantial antimicrobial selection pressures in the mid-last century of modern medicine (107, 124, 125). These physiological roles of multidrug efflux pumps may differ between species, even within the same efflux family (124, 126). Some of these physiological phenotypes, such as biofilm formation and bile salt efflux are clearly linked to bacterial virulence (124). Examples of important physiological roles from known antimicrobial drug efflux pumps are discussed below.

1.4.1. Arabinose export

Arabinose is an important pentose sugar central to carbon metabolism in bacteria. Arabinose metabolite homeostasis can fluctuate vary considerably due to metabolic flux or changes in environmental conditions (127). Accumulation of excess arabinose or toxic metabolite intermediates can be detrimental to cell survival. Removal of excess arabinose from the bacterial cell is regulated by the sugar transport family, the SET subfamily of the MFS transport group (124, 127). However, few MFS drug efflux pumps, including MdfA, EmrD and MdtD have also been characterised with arabinose efflux phenotype (124, 127). It is implicated that arabinose efflux function of these transporters may act as metabolic relief valves in the presence of toxic levels of arabinose and/or arabinose metabolism intermediates and assist in osmoregulation and prevention of the sugar-phosphate stress response respectively (127).

1.4.2 L-cysteine export

Amino acids are a prime example of endogenous metabolites that require precise intracellular regulation for optimised cell function (128). The presence of extracellular amino acids within the bacterial cell environment has been linked to biofilm dispersal, bacterial cell growth and decline and adherence to mammalian cells during infection (129). The MFS transporter, Bcr, is an antimicrobial efflux pump known to confer resistance to acriflavine, tetracycline, kanamycin and fosfomycin (111). A recent study dedicated to the discovery of L-cysteine exporters found that Bcr is capable of efficient L-cysteine export out of bacterial cells (130). Additionally, known RND transport systems, AcrD and AcrEF and MFS tripartite EmrAB, may represent putative cysteine export proteins (130). Furthermore, TolC, an outer-membrane protein that associates with AcrD, AcrEF and EmrAB efflux systems in *E. coli* was found to play an important role in L-cysteine resistance and export out of *E. coli* (131, 132). Low concentrations of L-cysteine are cytotoxic to the bacterial cell (133). Therefore, these multidrug efflux systems may play an important role in L-cysteine homeostasis by preventing noxious accumulation of L-cysteine and preventing insufficient concentrations of such a biologically important amino acid from occurring (133).

1.4.3 Polyamine export

Polyamines are ancient metabolites defined by an aliphatic carbon chain with two or more amine groups. Polyamides play a critical role in cell function across all domains of life (134). In bacteria, polyamines perform central roles in a multitude of important physiological functions, including; cell metabolism, oxidative stress response, nucleic acid and protein metabolism, pH homeostasis, cell-cell communication and biofilm formation (121). High intracellular concentrations of polyamines, that can be encountered through dysregulation of endogenous polyamine metabolism or exposure to polyamine-rich conditions, are toxic to the bacterial cell. Several antimicrobial multidrug efflux pumps have been characterised as polyamine efflux systems that alleviate such polyamine toxicity. For example, the recently discovered PACE transporter AceI of *A. baumannii* was determined to directly export putrescine and cadaverine under short-chain diamine stress (122). The MFS transporter AmvA from *A. baumannii* was also found to be induced under

spermidine and spermine exposure to promote fitness against these polyamines, where lack of AmvA was linked to reduced tolerance to exogeneous spermine and spermidine that would naturally be present in the gut of a human host (135). The *E. coli* SMR transporter, MdtJI, and *Bacillus subtilis* MFS transporter, Blt, have also been characterised as multidrug resistance efflux systems that play a physiological role in the export of the polyamide spermidine (136, 137).

1.4.4 Guanidinium ion transport

Guanidine riboswitches are a group of regulatory regions in mRNA that bind guanidine to elicit post-transcriptional control of downstream genes (138). Guanidinium controlled RNA is proposed to be an ancient form of gene regulation in the primordial RNA world (124, 139). SMR family transporters have been found in gene clusters encoding for riboswitches in the *B. subtilis* genome (140). The guanidine moiety is found in many substrates of SMR drug efflux pumps including spermidine, arginine, guanine and biocides including ethidium and methyl viologen. Hence, it has been proposed that guanidine is the physiological substrate of the SMR efflux pumps, with happenstance export of these guanidine-like compounds (141). Recently, the MATE transporter, MepA, involved in tigecycline resistance was also found to be closely associated with a new class guanidine-controlled riboswitch (142, 143), suggesting MATE drug efflux transporters may also play a physiological role in a guanidinium ion transport (143).

1.4.5 Secondary metabolite export

Bacteria live in many environments where competition between bacterial species for limited resources is necessary for survival. Efflux pumps play an important role in the export of endogenously synthesised antimicrobials and efflux of cell permeating toxic metabolites from neighbouring microbes. Many antibiotics used to treat bacterial infections have been discovered from antibiotic producing environmental microbes, including *Streptomyces* spp., *Micromonospora* spp., *Bacillus* spp. and *Pseudomonas* spp. (144). It is possible that selection for polyspecific antimicrobial efflux pumps may have arisen from microbial competition events in the environment (124). The dissemination of efflux pumps from antibiotic producers to non-producers was shown in a recent study where two drug transporters from the MFS transport family, the MFS

chloramphenicol efflux pump (*cmx*) and the ABC lincosamide efflux pump (*lmrA*) from proteobacteria, were found to more similar to producer-strain homologs in the Actinobacteria phylum than any other phylum of bacteria (145).

1.4.6 Human antimicrobial peptide resistance

Antimicrobial peptides (AMPs) are an essential part of the human innate immunity. Over one-hundred structurally unique AMPs have been characterised across a diverse range of human tissue environments (146). Most AMPs can self-insert into the cell membrane to disrupt bacterial membranes and induce cell lysis due to their charged and amphiphilic nature (147). Efflux pumps can also recognise AMPs as native substrates for transport out of the cell. A recent example of AMP resistance includes the ABC tripartite efflux system, MacAB-TolC. MacAB-TolC is known for conferring macrolide resistance in Gram-negative pathogens (148–150), however, it has also been characterised to play a physiological role in exporting endogenous produced heat-stable enterotoxin II in enterotoxigenic *E. coli* during gut colonisation and invasion of the host (151). Recently, an outbreak of invasive non-typhoidal *Salmonella* was linked to the overexpression of MacAB-TolC in this strain due to mutation in regulation, leading to increased levels of resistance to human AMP, C18G, allowing for higher-levels of infection and invasion of the gut epithelium into bloodstream with high rates of mortality and morbidity (152).

1.4.7 Bile acid and salt resistance.

Bile acids and salts are steroid compounds that primarily function as surfactants to solubilize lipid soluble nutrients in a relatively hydrophilic gut environment (153). Due to their detergent-like amphipathic nature, bile salts also have demonstrable antimicrobial activity against bacteria, including cell membrane disruption, DNA damage, protein damage and metal chelation (154). LmrCD, is a major ABC multidrug efflux system of non-pathogenic probiotic bacterium, *Lactococcus lactis*. LmrCD is associated with ATP-dependent efflux of Hoechst 33342, daunomycin, rhodamine 6G and ethidium bromide (155, 156). Knockouts of LmrCD revealed the ABC transporter was an important resistance factor against bile salts is specifically important for

glycodeoxycholate resistance in the gastrointestinal tract, colonisation and survival in mammalian intestine (155).

1.4.8 Steroid hormone tolerance.

Steroid hormones such as progesterone play an important role in the mammalian endocrine and immune system and have been documented to both promote and inhibit growth in bacteria (157–162). The sexually transmitted pathogen *Neissseria gonorrhoea* colonises progesterone-rich mucosal surfaces of the female reproductive tract (163). The RND tripartite system, MtrCDE of *N. gonorrhoeae,* confers resistance to a diverse range of compounds including β-lactams, macrolides, ethidium bromide and cationic antimicrobial peptides (164, 165). *N. gonorrhoeae* strains lacking the MtrCDE efflux pump were found to be cleared from the genital tract of female mice more quickly than the wild-type control (163). This result suggests the importance of the MtrCDE efflux pump for colonisation and survival during gonorrhoeal infection, consistent with a role in progesterone export and tolerance, in addition to a multidrug resistance phenotype in this organism (163).

1.4.9 Plant colonisation, pathogenesis, and toxin resistance.

Plants depend on the secretion of diverse range of phytotoxins to defend against bacterial infection (166–168). Antimicrobial drug efflux pumps can confer tolerance to phytotoxins to assist with the colonisation of pathogenic bacteria and/or assist in export of toxins produced by competitive bacteria and other microbes during plant colonisation (169). The RND efflux system, AcrAB-TolC of plant pathogen *Erwinia amylovora* responsible for fire blight in apple blossoms, was found to play a critical role in plant colonisation and virulence by conferring resistance to phytoalexin compounds phloretin, quercetin, (+)-catechin and naringenin (170). The MATE transporter, NorM of *E. amylovora,* mediates resistance to antimicrobials norfloxacin and ethidium bromide, in addition to plant phytotoxin, berberine (171). NorM was determined to export antimicrobial toxins produced by co-colonising epiphytic bacteria, allowing for high density populations to be formed during plant colonisation and infection of rosaceous plants (171).

1.4.10 Lipid transport and antimicrobial fatty acid tolerance.

The bacterial cell envelope is rich in a diverse range of hydrophobic lipids, fatty acids, lipopolysaccharides (LPS), lipooligosaccharides (LOS) and extracellular polysaccharides (EPS). Membrane transporters have evolved to export many different lipid species for cell envelope biosynthesis and homeostasis. Several multidrug efflux pumps have also been reported to play significant, physiological roles in lipid transport (124). In *Mycobacteria spp*., a large set of dedicated RND transport systems, known as the MmpL transport family, is dedicated to the export of phospholipids and cell wall components unique to the organism, in addition to characterised roles in antimicrobial compound efflux and siderophore export (172). Outside of lipid export of cell membrane components, efflux of lipid species, such as antimicrobial fatty acids, can play an important role in skin colonisation and infection of certain pathogens. *S. aureus*, a commensal skin microbe known to cause difficult to treat skin infections, was found to overexpress the tetracycline-specific MFS transporter, Tet38, in staphylococcal subcutaneous abscesses (173). Free fatty acids are found in high concentrations common within staphylococcal subcutaneous abscesses (173). Tet38 efflux pump expression was found to be induced in the presence of human antimicrobial fatty acids, including palmitoleic, oleic, linoleic and undecanoic acids, and was found to directly transport palmitoleic acid and undecanoic acid out of membrane vesicles (173). Mouse skin colonisation models revealed that *S. aureus* strains lacking the Tet38 efflux pump had 5-fold lower colonisation rates than the wild-type *S. aureus* strain (173). Together, these results suggest that the tetracycline specific efflux MFS transporter plays a physiological role in fatty acid export and skin colonisation in *S. aureus* (173).

1.4.11 Quorum sensing

Bacteria populations often live as a collective population and require the use of quorum sensing to coordinate a range of important physiological functions such as cell survival, motility, adhesion and pathogenicity (174). Quorum sensing is dependent on the secretion of autoinducing signals throughout cell growth, allowing for co-ordinated responses at sufficient cell density and quorum signal concentrations within a population (175). In *P. aeruginosa*, the quorum sensing signal

molecule, *N*-(3-oxo)-dodecanoyl L-homoserine is an important autoinducer signal for co-ordinating virulence response and controlling biofilm development (175, 176). However, unlike many of the N-Acyl homoserine lactones (AHLs) molecules involved in bacterial quorum sensing, *N*-(3-oxo)-dodecanoyl L-homoserine is not membrane permeable. This, in turn, led to the discovery that the MexAB-OprM efflux system plays a key role in quorum sensing in *P. aeruginosa* (176).

1.4.12 Biofilm formation and nitrosative stress tolerance

Biofilms are a predominant form of lifestyle for many bacterial organisms present in moist environmental conditions such as chronic wound and indwelling device infections (177). The biofilm matrix is a highly hydrophobic, anoxic environment comprised of cells with decreased growth rate compared to planktonic cultures. Biofilm communities can confer up to 1000 × higher resistance to antimicrobial compounds compared to isogenic strains in planktonic culture (178, 179). Furthermore, biofilms have also been identified to express a higher level of antimicrobial efflux systems compared to planktonic cultures, suggesting an important, physiological role for efflux pumps in the biofilm lifecycle (179). Biofilm formation within a bacterial community is highly regulated by quorum sensing, mediated by the secretion of autoinducer (AI) signal compounds and highly regulated by the secretion of signal *N*-(3-oxo)-dodecanoyl L-homoserine lactone in *P. aeruginosa* biofilms (124). Secretion of *N*-(3-oxo)-dodecanoyl L-homoserine lactone in *P. aeruginosa* biofilms is largely mediated by the RND efflux pump MexAB-OprM (124). MexAB-OprM expression in biofilm communities has also been linked to biofilm-specific resistance to azithromycin is not observed to occur when expressed in planktonic cultures, thus conferring biofilm-specific antibiotic resistance in *P. aeruginosa* biofilms (180). Furthermore, biofilms are highly anoxic, and many biofilm-producing species often need to transition from aerobic to anaerobic respiration to adapt. Nitrosative stress can be induced by the formation of radical nitrogen species, including nitrosyl indole derivatives, via the anaerobic respiration pathway. The *E. coli* RND efflux pump, MdtEF, is found to be induced under anaerobic growth conditions and export reactive nitrosyl indole derivatives to support growth under anaerobic

growth conditions in biofilms (181–184). In *K. pneumoniae*, export of toxic nitrosyl indole derivatives during nitrosative stress is mediated by the SMR drug efflux system, KpnEF (185). In the case of *P. aeruginosa*, the RND efflux pump, MexEF-OprN is typically dormant under normal physiological conditions. However, in the presence of NO-generating compounds, *s*-nitrosoglutathione and diethylenetriamine, MexEF-OprN expression was inducible (186). The MexEF-OprN efflux pump has been proposed to have native, physiological role as a metabolic stress relieve pump (187).

1.4.13 Oxidative stress tolerance

Reactive oxygen species (ROS) such as superoxides, hydrogen peroxide and hydrogen radicals are a product of aerobic respiration, are generated upon exposure to radical forming antimicrobials or as innate defence against plant/mammalian host upon infection by the bacterium (188–190). Free radicals act upon bacteria by damaging nucleic acids (DNA/RNA), lipids (cell membranes) and proteins. The ROS stress response usually involves the expression of detoxification enzymes including peroxidases, catalases and superoxide mutases (188). Efflux pump expression have been shown to correlate with oxidative stress response. The *E. coli* MATE drug efflux transporter, NorM, is known for conferring resistance to a range of fluoroquinolones, aminoglycosides toxic organic cations (111, 191). Expression of NorM efflux pump was found to reduce mutagenesis and accumulation of ROS species upon H_2O_2-killing by direct export of ROS reactive species, conferring heightened protection against oxidative stress in *E. coli* (192).

1.4.14 Metal acquisition

Metal ions are also important co-factors for many enzymes required for normal bacterial function that cannot be synthesised by the cell (193). As a result, bioactive metals ions that are extremely valuable are tightly sequestered and regulated across the kingdom of life (193). Siderophores are important metal chelators that function to bind iron with high affinity, assisting in solubilising and transporting iron to the producing organism (194, 195). Genes encoding siderophores (small molecular ion chelators), siderophore export proteins and their synthesis intermediate are often organised in gene clusters (196–198). The RND efflux pump, MmpL5 of *Mycobacterium*

tuberculosis, confers resistance to azole antibiotics and antituberculosis antimicrobials, bedaquiline and clofazimine. MmpL5 was also shown to play an important function in transport of mycobacterial specific siderophores, mycobactin and carboxymycobactin (172, 199, 200).

1.4.15 pH and osmoregulation tolerance

Bacteria often inhabit niche environments that are not necessarily physiologically favourable to the organism, such as high pH conditions (alkaliphiles), low pH conditions (acidophiles) and high salt concentrations (halophiles) (201), and hence, have required adaptive evolution to survive in these conditions. Many bacteria also require adaptive responses to survive fluctuations in these conditions temporarily for survival. MdfA is an *E. coli* MFS drug efflux pump and is known for chloramphenicol resistance as well as a broad-substate specificity to a diverse range of antibiotics (100). In experiments investigating the impact of altered pH on drug transport activity, it was found that MdfA elevated survival in alkali pH conditions in the absence of antibiotic (202). Transport experiments in membrane vesicles revealed MdfA mediated the exchange of Na+/K+ ions for H+ to confer alkali tolerance in neutralophilic organism *E. coli* under pH stress (202). Alternatively, in acid-tolerance based experiments, TolC-dependent tripartite systems were found to be important for cell survival in extremely low pH environments, where the tripartite multidrug efflux pumps EmrAB-TolC (MFS) and MdtAB-TolC (RND) were important for tolerance to cell envelope stress and acid stress conditions (203). The SMR efflux pump of *E. coli,* EmrE, is known for antimicrobial quaternary cation compound efflux and biocide resistance (204). EmrE was also shown to confer a role in osmoregulation via the direct export of osmoprotective quaternary cation compounds, choline and betaine, and to regulate cell homeostasis and protect osmotic shock in the incidence of salt or pH stress in the environment (113).

1.4.16 Heavy metal tolerance

Bacteria can inhabit niche environments where the total concentration of heavy metal ions can be toxic to cell survival. Heavy metals act as important co-factors but cannot be synthesized or degraded within bacterial cells. Hence, metal efflux is a primary mechanism for the release of excess toxic metal accumulation from within the cell (193). Direct metal efflux often occurs via

metal-specific transport systems such as the heavy metal efflux (HME) transport family of the RND superfamily (205). However, a few antimicrobial multidrug efflux pumps have also been associated with heavy-metal tolerance in bacteria (205). For example, the RND transporter CusCFBA transport of *E. coli*, is important for the efflux of copper and silver ions, but also demonstrates the capacity to confer heightened resistance to chloramphenicol, fusaric acid, cefmetazole, oxalinic acid and lincomycin (206).

1.4.17 Solvent and hydrocarbon tolerance.

Polycyclic aromatic hydrocarbons are toxic pollutants that can occur naturally in the environment or can accumulate in the environment from industrial and anthropogenic pollution (207). Aromatic hydrocarbons are highly hydrophobic and planar in nature and exert toxicity by inserting into bacterial cell membranes to disrupt several processes including cell respiration processes, membrane protein functions and cell membrane integrity (207). Tolerance to toxic hydrocarbons and solvents have been associated with multidrug efflux pump expression. For example, the RND efflux systems MexAB-OprM, MexCD-OprJ and MexEF-OprN have been found to have physiological roles in polycyclic aromatic hydrocarbon and toluene export in solvent tolerant strains of *P. aeruginosa* and *Pseudomonas putida* (208–212).

1.5 Methods to study drug efflux systems

Drug efflux systems are found across all domains of life. The capability for drug efflux systems to perform polyspecific transport of bioactive molecules across a diverse range of chemical space makes drug efflux pumps a valuable target for membrane transport research. Generally, drug efflux pumps have primarily been investigated for their role in antimicrobial resistance (213). More recently, investigations have included the role of these transport proteins in bacterial virulence, fundamental cell biology and applications to harness bacterial efflux pumps for industrial processes (124, 214–216). Today, a range of computational, phenotypic, biophysical, and structural techniques have contributed to the improved identification and characterisation of drug efflux pumps of bacteria. A summary of these methods is provided in herein.

1.5.1 Bioinformatic tools to discover novel efflux candidates

Today, a range of bioinformatic tools have made identification of integral membrane transport proteins and putative efflux homologues more convenient. Due to the sequence similarity shared amongst the RND, ABC, MFS, PACE, SMR and AbgT families, it is possible to identify shared homologues amongst bacterial strains of interest. Such homologues can be readily identified using free to use webservers such as BlastP (217), PSI-BLAST (218) and HMMER (219, 220). Sequence homology of approximately 20% is sufficient for inferred similarity in structure and putative function. Expansive protein databases including UniProt (221), Pfam (222) and Interpro (223), and more specialised transporter databases such as TCDB (224), TransportDB (225) and mpstruc, provide a valuable knowledgebase of transport protein classification, structure and function. Phylogeny can also provide a powerful tool to identify the evolutionary history of a new protein target, and are potentially capable of identifying putative substrate specific classes within an efflux family, including the ABC, RND, MFS, MOP and DMT superfamilies (226–228).

In addition to seeking out homologues to guide putative function annotation, it is also important to analyse the host genome to investigate the genetic context of the protein of interest. Localisation of a gene of interest in an operon involved in a metabolic function may provide clues to the native role of the new efflux system. For example, the MFS family transporter Blt of *Bacillus subtillis* is co-transcribed with spermine/spermidine acetyltransferase and has a physiological role in the direct export of spermidine from the cell (137). The ABC transporter, BarAB of *A. baumannii* is immediately upstream of the acinetobactin biosynthesis cluster and functions in acinetobactin siderophore efflux (198). Recently, free-to-use software such as Clinker (229) and FlaGs (230) have been designed to visualise the level of gene conservation across local and distant homologue genetic clusters.

1.5.2 Conventional methods of efflux pump discovery

Usually, the discovery of new efflux candidates involved recognising and isolating drug resistance plasmids and transposons that conferred resistance when cloned into susceptible bacterial strains (55). Chromosomal drug efflux pumps were characterised by use of plasmid clone libraries, where

mass cloning of plasmid libraries into drug susceptible bacterial strains and culturing against specific antibiotic selection allowed the identification of plasmids that mediated host resistance to an antibiotic of interest, which included the discovery of a few novel drug efflux pump genes, including NorA and NorM of the MATE transporter family and MdfA of the MFS transport family (100, 231, 232). Following the advance of genome sequencing, it became possible to scrutinize the whole genome of a bacterial strain of interest to search for genes that may represent new drug efflux pumps due to sequence similarity. Once identified, it was common to clone the gene of interest, transform into a drug-susceptible host for heterologous characterisation or to delete the gene of interest from the strain of interest to investigate the role in drug resistance and susceptibility respectively (233–235). Today, due to the speediness and lowered cost of sequencing technologies, it is increasingly common to identify novel efflux pumps with genome-wide screening techniques, such as transcriptomics (see 1.5.3) and TraDIS (see 1.5.4).

1.5.3 Transcriptomic approach to efflux pump discovery

Transcriptomics provides an ideal experimental platform to study the regulatory response of efflux pumps via measuring the upregulation or downregulation of mRNA in response to antimicrobial challenge, which can help decipher efflux genes involved in an adaptive antimicrobial resistance response (236). Briefly, RNA is extracted from a control and sample that has been treated with antimicrobial of interest and is sent for RNA-sequencing (RNA-seq), RNA samples are usually depleted of ribosomal and transfer RNAs prior to RNA-seq and sequenced reads are mapped back to the reference genome to decipher regions undergoing active transcription in the control sample and treated sample (236). The level of coverage for each gene or genomic region can be used to decipher the level of regulatory response to a condition tested in the experiment. Analysis between the control and treated sample can also assist in identifying genes differentially expressed in response to treatment (236). This method is best exemplified by the case of the discovery of a novel efflux family the proteobacterial antimicrobial compound efflux (PACE) family (237). In this study, transcriptomics is used to screen for genes responding to shock exposure to chlorhexidine, a common antiseptic found in hospital handwashes (118). AceI, a small integral

membrane protein of unknown function, had greater than 10–fold higher transcription in response to chlorhexidine compared to a no treatment control of *A. baumannii* (118). This study led to the characterisation and discovery of chlorhexidine efflux transporter, AceI, which is the first described member of the PACE transport family (118).

1.5.4 TraDIS and TraDIS-Sort approach to efflux pump discovery

Transposon directed insertion sequencing (TraDIS) can also identify novel efflux genes or efflux pumps involved in antimicrobial resistance by analysing the fitness response of a sequenced bacterial genome to antimicrobial challenge. Briefly, TraDIS combines large-scale transposon mutagenesis with next generation sequencing, to determine fitness or essentiality of each gene within a bacterial genome in a singular experiment (238). TraDIS requires the construction of a saturated mutant library using transposon mutagenesis. The goal is to achieve a mutant library in which each cell carries a single transposon insertion in the genome. These cells are pooled, and each gene or genetic region should have multiple insertions at different sites within the library (238). Sequencing of a TraDIS mutant library before and after a selective treatment, such as antimicrobial exposure can be used to determine genes involved in promoting fitness in the condition tested, based on changed number of transposon insertions across the sequenced genome (238). For example, genetic regions that cannot tolerate transposon insertions can be evaluated as contributing to genetic fitness to that condition. Conversely, genetic regions that have increased transposon insertions compared to wild-type may be detrimental to cell survival in the condition tested (238). This technique was recently applied in a large-scale experiment where ten biocides were used as selective conditions against a TraDIS library of *Acinetobacter baumannii* (239). TraDIS sequencing identified numerous characterised antibiotic efflux pumps that were important for fitness under the biocide challenges, suggesting a protective role in antiseptic tolerance as well as antibiotic resistance (239).

An adapted technique of TraDIS, known as TraDIS-Sort was developed for precise identification of novel drug efflux pumps and regulators from a TraDIS mutant library. The technique combines traditional TraDIS experiment with fluorescence active cell sorting (FACs), which sorts cells

based on accumulation of a fluorescent dye (240). Many antimicrobial dyes such as ethidium bromide are fluorescent DNA intercalating agents and are also common substrates of drug efflux pumps (241). A TraDIS mutant library was treated with ethidium bromide and single cells are subjected to FACs sorted based on level of fluorescence accumulation (240). Single cells with high-level of ethidium bromide accumulation and low-level of ethidium bromide accumulation are collected to determine genes involved in drug efflux activity (238). Transposon insertions in drug efflux genes, are expected to have higher accumulation of ethidium bromide, as they have lowered activity in drug transport mediated export of ethidium out of the cell (238). Alternatively, cells with abnormally low levels of ethidium accumulation within the population, often have transposon mutations in drug efflux gene regulators, leading to increased efflux and lower fluorescence accumulation within the cell (238). This technique was successful in the identification and characterisation of two RND transporters (AdeABC and AdeIJK) and one MFS transporter (AmvA) as well as the transcriptional regulator (AmvR) implicated in ethidium bromide export in *A. baumannii* (238).

1.5.5 Characterisation of multidrug resistance phenotype in whole bacterial cells.

To determine the drug resistance phenotype, experiments can be performed to determine whether the overexpression of a putative drug efflux pump may confer heightened resistance to a range of antimicrobials of interest. For bacterial species, these experiments are often carried out as minimum inhibitory concentration assays, either on solid agar media supplemented with antimicrobials of interest across a range of concentrations or in broth conditions, such as microdilution method (242). The minimum inhibitory concentration assay approach has been automated in a high-throughput manner with the Biolog phenotype microarray system (243). In this method phenotype microarray plates (PM11-20) can screen the susceptibility of bacteria to 240 unique antimicrobial compounds in a single experiment, measured by respiration and oxidation of tetrazolium violet dye, allowing a diverse range of antimicrobial phenotypes to be analysed in a single experiment (243).

1.5.6 Characterisation of drug efflux phenotype in whole bacterial cells.

Preliminary characterisation of drug efflux activity of a gene can be achieved through the direct measurement of efflux or accumulation of a detectable antimicrobial substrate. Differences in efflux and accumulation rates can be attributed to a drug efflux phenotype.

Fluorometric whole cell transport assays are a convenient method to study drug export activity. Many antimicrobial fluorescent dyes are common substrates of drug efflux systems (241, 244). Furthermore, a few fluorescent antimicrobial dyes also reveal differential fluorescence intensity in and out of the cell. Dyes such as ethidium bromide and Hoechst 33342 fluoresce when bound to DNA and quench in aqueous solutions (241, 244). Conversely, DNA-intercalating dyes such as acriflavine or pyronin Y are quenched when bound to DNA and fluoresce brightly in aqueous conditions (120, 244). In these experiments, whole bacterial cells are loaded with a fluorophore of choice in the presence of proton-decoupling agent, such as carbonyl cyanide m-chlorophenyl hydrazone (CCCP), allowing for dye to accumulate passively within the bacterial cells. Active efflux can be observed by re-establishing the electrochemical gradient upon addition of a carbon source and measuring increase or decrease of florescence emission over time using standard fluorimetry (241).

Whole cell drug accumulation studies can offer an alternative method to measure drug efflux activity through fluorescence or radioactivity detection methods. These experiments are performed with prepared cells in solution with no substrate present and a baseline fluorescence or radioactivity is recorded. Substrate is then added to the cell population and samples are collected at dedicated time intervals to measure the rate of substrate accumulation over time until a steady state is reached. Results are compared in a relative manner, where an efflux proficient strain will have a lower level of substrate accumulation over time than an efflux deficient strain as it cannot efficiently export the substrate. In some cases, it may be difficult to detect differential efflux. Hence, the use of efflux deficient bacterial strains may allow drug efflux phenotypes from expressed genes to be observed with greater resolution. These novel technologies include the adaptation of single-cell microfluidics (245), flow cytometry (246–248) and mass spectrometry

(249) techniques to visualise substrate accumulation over time and determine drug efflux activity across a diverse range of substrates of interest.

1.5.7 Heterologous expression and purification methods

Drug transport proteins are integral membrane proteins. In wild-type organisms, the expression of a specific membrane protein of interest may represent only 1% of the total proteinaceous weight of the cell membrane (250). Hence, achieving the high membrane protein purification yields required for many biophysical and structural techniques is significantly challenging due to the limited expression, as well as the relative instability of membrane proteins out of their natural lipid bilayer environment. A common approach towards purification of a drug efflux pump is to clone membrane transport gene into an *E. coli* host and add an additional His-tag at the N-terminus or C-terminus to assist in the identification and purification of the gene from other membrane proteins present in the cell membrane extracts (251). Expression into *E. coli* BL21 host with pTTQ18 is usually used as a first-attempt vector/host combination for heterologous protein expression, however, a diverse range of other vector/host combinations have also been described (251). Large-scale culture, induction and cell disruption is followed by ultracentrifugation to isolate pure bacterial cell membranes from the cell lysate (251). Membranes are solubilised in appropriate buffer containing detergent to form micelles and stabilise the membrane protein outside of the cell membrane environment for further purification by immobilised metal affinity chromatography (251, 252). Once purified, excessive detergent is removed, and the protein is concentrated for further biophysical and structural characterisation. A comprehensive review on membrane protein purification techniques is provided in Smith *et al*., 2016 (253).

1.5.8 Biophysical studies to determine substrates of drug transport proteins

Once a protein is purified, it is important to test function and perform direct biophysical experiments to determine substrates of the efflux target. There are many different techniques to determine substrate binding affinity of a transporter and substrate of interest. A few methods amenable to membrane transporters are described in this section.

Tryptophan fluorescence quenching assay

Tryptophan fluorescence quenching is a simple fluorometric technique to determine substrate binding kinetics. The amino acid tryptophan is fluorescent and can undergo a significant shift in emission wavelength maxima upon a change in solvation environment due to a in conformation induced by substrate binding. Large conformational changes are common for highly dynamic and flexible membrane transport systems, and if tryptophan residues are available at appropriate locations on the transport protein studied, it is a worthwhile short experiment to determine the influence of ligand binding on a target protein of interest, in which the change in tryptophan fluorescence intensity at a given wavelength can be correlated to binding kinetics and binding affinity for substrate and transport protein interaction (254).

Circular dichroism

Circular dichroism (CD) is a simple spectroscopic technique that can provide information about secondary structure of a protein, either through near-UV spectrum wavelengths or far-UV wavelength ranges (255). Variation in the near-UV range of 250–350nm can reflect changes in the positioning of aromatic amino acid sidechains, indicating conformational change upon substrate binding. Measurements in the far-UV range (150–250 nm) can provide information about secondary structure of a transporter as α-helices and β-sheets have defined absorption spectrums (255). An advantage of this technique is that secondary structures are unravelled as temperature increases, causing protein denaturation (255). Binding to a substrate increases stabilisation of protein, and thus, measurement of denaturation rates of secondary structures between protein with and without substrate can be a useful technique to study putative ligands, as well as provide an avenue to study potential binding sites by comparing wildtype proteins against modified proteins with changed binding site residues (255).

Nano differential scanning fluorimetry (nano-DSF)

NanoDSF is a derivative of differential scanning fluorimetry (DSF) that monitors the change in local chemical environment of a protein, such as denaturation monitored through the analysis of intrinsic tryptophan and tyrosine fluorescence shifts (256). NanoDSF provides an opportunity for

efflux pump research as the method only requires low quantities of pure protein, does not require labelling with fluorescent dyes and is amenable to screening a diverse range of compounds across chemical space (256). Observed shifts in thermostability by nanoDSF can be coupled to chemical screens providing a high-throughput approach for rapid characterisation of putative ligands, co-factors or inhibitors of membrane proteins (256). NanoDSF technique has been applied to the characterisation of the physiological role of *A. baumannii* multidrug efflux pump, AmvA as a spermidine and spermine efflux pump (135). Furthermore, nanoDSF has also found applications in buffer, pH and detergent screens to assist optimisation of membrane protein purification methods (256–258).

1.5.9 Proteoliposome transport assays

The measurement of substrate transport in an isolated, synthetic liposome environment offers direct evidence for antimicrobial export mediated by drug efflux pump (251, 259). In these experiments, pure membrane proteins are reconstituted into synthetic liposome environments, mimicking a phospholipid membrane environment. Proteoliposomes are loaded with fluorophores or radiolabelled substrates and then measured using whole cell efflux and accumulation assays (see Section 1.5.6) where accumulation of substrate overtime can be evidence of efflux mediated transport out of the proteoliposome environment (260). Furthermore, this technique also provides an avenue to establish energy-coupling mechanisms of drug efflux transporters (260). Pyranine is a fluorescent dye that changes absorption according to pH environment and can report on direction of proton-coupled transport processes (122, 261). In the case of PACE transporter, AceI, pH change was coupled to export the polyamine cadaverine but not spermidine. The latter substrate was not determined to be a physiological substrate of the AceI transporter (122). Furthermore, proteoliposome transport assays have been recently coupled to single-molecule Förster resonance energy transfer (sm-FRET) experiments, to study real-time conformational dynamics of efflux pumps during directional substrate transport to study the precise mechanism of drug transport in these efflux systems (262). This approach was recently successful in the study of the real-time

conformational change of the rocker-switch mechanism of transport by MFS transporter MdfA (263).

1.5.10 Structure elucidation techniques

Elucidating the structure of a drug efflux pump is important to understand membrane transport function as well as to aid drug-discovery efforts to develop therapeutics to block their mechanism of action. Three main methods are available to solve the structure of membrane proteins; x-ray crystallography, nuclear magnetic resonance (NMR) and cryo-EM.

X-ray crystallography

X-ray crystallography is a common structural biology technique used x-ray to diffract crystalline atoms of a protein in which X-ray diffraction patterns can allow a 3D electron density map to be imaged and the position of atoms and their chemical bonds to be elucidated (264). Achieving high-resolution crystal structures of membrane transport systems is challenging process as high concentrations of pure protein are required. As they are often highly flexible and unstable outside of membrane lipid environment, membrane transporter protein are also typically very difficult to crystallise (265). Recent advances in membrane protein crystallisation and X-ray crystallography is provided in a review by Kermani, 2021 (266). Nonetheless, X-ray crystallography is still a powerful technique used to solve the structures of many membrane proteins including a variety of drug efflux pump across the ABC, RND, MFS, MATE, SMR and AbgT efflux families (72, 82, 104, 114, 204, 267).

Nuclear magnetic resonance (NMR) spectroscopy

Nuclear magnetic resonance (NMR) spectroscopy can elucidate the structure of membrane proteins by studying the nuclear spin oscillations that allow for the determination of how atoms are chemically linked, the spatial distance between atoms and ability to move in respect to each other (268). In this method, NMR does not require crystal structures and is accessible for small membrane protein structure elucidation. Solution NMR methods are limited to lipid micelles and nanodisc preparation methods, whilst solid-state methods can allow for structures to be solved in

lipid bilayer environment (268). However, NMR is limited due to anisotropic interactions, sample heterogeneity, spectral complexity and signal degeneration in locations of sequence repeats or in large membrane protein systems studied (268). The use and limitations of NMR spectroscopy to solve membrane protein structures is well reviewed by Yeh *et al.,* 2020 (268). NMR spectroscopy has recently been applied to solve structural elucidation of SMR transporter EmrE in a native lipid environment (269).

Cryo-EM technique for the elucidation of membrane protein structures.

Cryo-EM is a technique that has recently become a popular method for structure elucidation of membrane transport proteins. In this technique, electron diffraction and imaging of membrane protein structure can be solved in a near physiological, partially hydrated environment such as a liposome. Membrane protein specimens are rapidly frozen to bypass the need for crystals and loaded into an electron microscope at high-vacuum and low temperatures to minimise radiation damage (270). Structures can be solved by single-particle analysis where vitrified samples are distributed across a grid where thousands of copies of identical membrane proteins are frozen in random orientations and collated to create an averaged projection to solve protein structure. Alternatively, electron tomography can be used to convert 2D projections of heterogeneous particles into 3D tomogram by tilting the specimen stage and a 3D tomogram is calculated using a reconstruction algorithm. A review by Murata *et al.,* 2018 provides a comprehensive overview of cryo-EM applications to solve membrane protein structures (270). Cryo-EM has been useful for solving large tripartite efflux complexes including the tripartite RND transporter AcrAB-TolC and ABC transporter MacAB-TolC (86, 148).

1.6 *Acinetobacter baumannii*- a nosocomial pathogen of concern

In the early 20th century, the first type strain of *Acinetobacter* spp. was isolated from soil using calcium-acetate enriched minimal media and was aptly named, *Micrococcus calco-aceticus* (271). The nomenclature of the *Acinetobacter* genus was eventually defined by Brisou and Prévot in 1954 to distinguish non-motile species from motile species of *Achromobacter* spp. (272). Over 100 species within the genus *Acinetobacter* are acknowledged to date by the List of Prokaryotic names

with Standing in Nomenclature (LPSN) (273). Members of the *Acinetobacter* genus are defined as a Gram-negative coccobacillus, defined as a strictly aerobic, non-fermenting, pleomorphic, non-motile, catalase-positive, oxidase-negative, and high GC content (~39–47%) species of bacteria (5). *Acinetobacter* spp. are found in a variety of environments, including water, sewage, soil, plants, human and hospital environments (274).

Most members of *Acinetobacter* spp. are non-pathogenic, environmental species. However, a few members of *Acinetobacter* are opportunistic pathogens. The *Acinetobacter baumannii-Acinetobacter calcoacetius* (ACB) complex are a closely related group of species initially comprised of *Acinetobacter baumannii, Acinetobacter calcoaceticus, Acinetobacter nosocomialis and Acinetobacter pittii* (275). Subsequent additions to this complex include *Acinetobacter seifertii, Acinetobacter lactucae* (synonym *Acinetobacter dijkshooriniae*) and *Acinetobacter* genomic spp. 1–3 (275). Members of the ACB complex are frequently associated with hospital and community acquired infections (5). *A. baumannii* is the commonly isolated species associated with difficult to treat hospital acquired in clinical settings (5). *A. baumannii* is an opportunistic pathogen known to cause a range of hospital-acquired infections including ventilator-assisted pneumoniae, catheter-associated urinary tract infections, surgical-site infections, bloodstream infections, meningitis, soft-tissue infections, wound infections and skin infections (5, 276). Hospital-acquired risk factors include prolonged hospital stay, antibiotic use, major surgery and use of foreign medical equipment such as catheters, cannulas, tubing and ventilators (5, 276). Community acquired *A. baumannii* (CA-Ab) infections include pneumoniae, wound infections and bacteraemia/sepsis, and have been linked to wound infections from natural disasters and war zones, as well as at-risk populations in tropical and sub-tropical climates (277, 278). At risk populations include individuals with co-morbidities including diabetes mellitus, pulmonary disease, lung cancer, alcoholism, and chronic smoking (277).

Prior to the 1970s, *A. baumannii* infections were susceptible to a diverse range of antibiotic classes, including β-lactams, aminoglycosides, quinolones and tetracyclines (5, 279). Increased frequency of *A. baumannii* outbreaks and resistance have been reported as early as the 1980s (5). Multi-locus

sequence typing (MLST) has determined three international lineages of *A. baumannii*, known as international clones, I, II and III (280). International clones I and II are associated with MDR, PDR and carbapenem-resistant outbreaks which can be associated with the acquisition of multiple antimicrobial resistance mechanisms and resistance islands, integrons and transposons (280–283). The dissemination of carbapenem-resistant *A. baumannii* globally has caused concern as carbapenems, along with polymyxins and tigecycline, were used as a last resort antibiotics to treat MDR *A. baumannii* infections (282, 284–286). Furthermore, colistin and tigecycline resistant strains are also reported, indicating the start of a pan-drug resistant era for this opportunistic pathogen (284, 287–289). Recently, the WHO and Centers for Disease Control have recognised carbapenem-resistant *Acinetobacter* spp. as a critical threat to modern medicine, in which the development of novel therapeutic options for the treatment of carbapenem-resistant *Acinetobacter* infections is essential (11, 290). For this reason, understanding the mechanisms of resistance in this pathogen is an important step in developing effective therapeutics.

1.6.1 Virulence mechanisms in *A. baumannii*

The success of *A. baumannii* as an opportunistic pathogen can be largely attributed to the high level of genome plasticity, allowing *A. baumannii* to acquire mobile genetic elements, adapt and undergo mutagenesis and genome rearrangement to rapidly acclimatise to adverse conditions (291). Furthermore, the high abundance and diversity of virulence and antimicrobial resistance mechanisms contribute to the ability of *A. baumannii* to persist in harsh environmental conditions, invade host cells and persist against antimicrobial challenge during infection. A brief overview of *A. baumannii* virulence mechanisms is provided in the following paragraphs; for more detail please see the review by Morris *et al*., 2019 (292).

The main virulence mechanisms of *A. baumannii* includes cell adhesion, invasion of host epithelial cells, biofilm formation, cell motility and acquisition of micronutrients (291). In addition, the success of *A. baumannii* as a hospital pathogen is also due to its ability to persist in the hospital environment. *A. baumannii* can survive and persist in harsh, desiccation-like conditions, such as hospital abiotic surfaces for up to 100 days (293, 294). The ability to persist desiccation has been

linked to capsular polysaccharide, lipid A acetylation and biofilm formation allowing for water to be trapped within these dense polysaccharide rich environments to survive extremely dry conditions (291, 295, 296). In desiccation-stressed *A. baumannii,* genes involved in oxidative stress resistance and DNA protection and repair, including RecA were found to be significantly upregulated to protect from DNA damage and oxidative stress caused by desiccation conditions (297, 298). Disinfectants commonly used to sterilise abiotic surfaces and medical equipment in hospital environments as well as in handwashes and sanitisers to prevent hospital acquired infections. In a recent study, a range of *A. baumannii* antibiotic drug efflux transporters were found to be important to fitness upon exposure to disinfectants, suggesting hospital biocides may drive antimicrobial resistant phenotypes in *A. baumannii* (239). Furthermore, *A. baumannii* was found to upregulate the transcription of the disinfectant-specific antimicrobial efflux pump, AceI, in response to chlorhexidine exposure (118). Additionally, ethanol, a common surface disinfectant was also found to promote cell growth, pathogenicity, and virulence of *A. baumannii* (299, 300). Biofilm formation is an important mechanism to survive and persist on abiotic surfaces such as plastics, glass, metals, and porcelain, in addition to adherence to epithelial cells and persistence in wound infections (301, 302). The chaperone-usher pilus system, biofilm-associated protein, type I secretion system, capsular polysaccharides, poly-β-1,6-N-acetylglucosamine (PNAG) and autotransporter signal (Ata) are important features in the formation, adherence and maintenance of mature *Acinetobacter* biofilms (303–307).

Motility of *A. baumannii* is an important mechanism of infection. In contrast to the nomenclature as a 'non-motile' rod, *A. baumannii* is capable of motility through two defined mechanisms; twitching motility, and surface-associated motility which may assist infection of the host and persistence in nosocomial environments (308).

Colony-phase variation is a mechanism of virulence reported in *A. baumannii* isolate AB5075_UW, involving a switch between opaque-colony and translucent-colony variants in this pathogen (309). Opaque-colony variants have been reported to be greater surface-associated motility and virulence compared to translucent-colony variants within the same bacterial

population (309). *A. baumannii* also encodes many virulence mechanisms to assist with direct interactions with host and defence against host immune responses.

The cell membrane is the first layer of defence. Expression of glycans, glycoconjugates, lipooligosaccharides and peptidoglycan at the membrane play an important role in lowering antimicrobial permeability and trap water in desiccation survival, but also prevent complement-mediated killing, immune evasion and antibody recognition, as well as enhances biofilm production and maintenance (295, 305, 310–312). Lack of capsule has been linked to avirulent forms of *A. baumannii* that are easily targeted by complement-mediated killing mechanisms (313).

Transition metals such as zinc, manganese, and iron play an important role in innate host immunity against bacterial infection, and sequestration mechanisms are critical for *A. baumannii* survival in the host. *A. baumannii* has diverse set of mechanisms to acquire these transition metals *in vivo.* A common mechanism is the expression of siderophores, iron-chelating molecules, including acinetobactin, fimsbactins and baumannoferrins (314–316). Zinc is essential for the survival of *A. baumannii* against host-mediated nutritional immunity. *A. baumannii* can sequester zinc with extremely high affinity through the expression of the ZnuABC transporter (317). *A. baumannii* also express metallochaperone ZigA and a histidine utilization system to sequester and release zinc in a bioavailable form for utilisation within the cell as an important co-factor for many enzymes required for infection and resistance (318, 319). Manganese is an important co-factor for the breakdown of accumulated urea from bacterial metabolism (320). In metal-limited conditions during host infection, *A. baumannii* is shown to express manganese transport and urea metabolism to circumvent the toxic effect of manganese limitation (321).

A. baumannii also expresses several protein secretion mechanisms to survive within the environment and during host infection (322). Currently, there are five types of protein secretion systems in *A. baumannii*. Type I secretion system (T1SS) that are recognised as being important for cell adhesion to abiotic surfaces and biofilm formation (323). The type II secretion system (T2SS) is involved in the secretion of toxins and hydrolytic enzymes to assist nutrient acquisition

(324). The type IV secretion system (T4SS) mediate bacterial horizontal gene transfer and contribute to genomic plasticity of *A. baumannii* (325). Type V secretion system (T5SS) was the discovery of the adhesin autotransporter of *A. baumannii* (Ata) that plays an important role in secretion of extracellular matrix and membrane components (307, 322). The type VI secretion system (T6SS) involved in interbacterial competition and bacterial lysis, plays an important role in survival during polymicrobial infections (326). Further detail for each secretion system has been reviewed by Weber *et al*., 2017 (322).

1.6.2 AMR mechanisms of resistance in *A. baumannii*

Section 1.1 provided an overview of bacterial antimicrobial resistance mechanisms. The following section provides details of the known antimicrobial resistance determinants characterised in *A. baumannii*.

Drug inactivating enzyme mechanisms in *A. baumannii*

Clinical isolates of *A. baumannii* host a diverse range of drug inactivating enzymes to promote multi-drug resistance. Extended β-lactam and extended carbapenem resistance is a primary concern as it is usually antibiotic of choice for the treatment of multidrug resistant *A. baumannii* and carbapenem-resistant *A. baumannii* is a priority for urgent development of novel therapeutics (11, 290). β-lactam resistance is primarily mediated by the acquisition and expression β-lactamases (see Section 1.1.1) (327). *A. baumannii* has been reported to host all four β-lactamase groups to confer resistance. Class A β-lactamases are serine-dependent hydrolases that degrade penicillins and cephalosporins some carbapenem antibiotics (17). *A. baumannii* Class A β-lactamases span narrow-spectrum β-lactamase and extended-spectrum β-lactamases include TEM (328, 329), SHV (330), CTX-M (331, 332), SCO (333), PER (334–336), VEB (337), KPC (338, 339), GES (340–342) and CARB class of β-lactamases (343, 344). *A. baumannii* class B β-lactamases, known as metallo-β-lactamases, require zinc or heavy metal co-factor for hydrolysis (17). *A. baumannii* metallo-β-lactamases can hydrolyse all β-lactam antibiotic classes except for monobactams and span IMP (345–350), NDM (351–353), VIM (354–357) and SIM (358) metallo-β-lactamase classes (359). *A. baumannii* also host chromosomally encoded class C β-lactamases, also known

as AmpC cephalosporinases (327, 360, 361). This class of β-lactamases are serine-dependent, in which expression is correlated with the upstream insertion of Is*Aba*1 insertion sequence (17, 361). Constitutive overexpression of this class of enzymes are correlated with extended-spectrum cephalosporin resistance in this pathogen (327, 361, 362). *A. baumannii* class D β-lactamases, also known as oxacillinases is a major mechanism of carbapenem resistance in *A. baumannii*. Carbapenem-hydrolysing oxacillinases were first identified with OXA-23, the most prevalent oxacillinase in *A. baumannii* (363, 364). However, other class D β-lactamases subgroups including OXA-2 (365), OXA-10 (366), OXA-20 (367), OXA-24 (368), OXA-51 (369), OXA-58 (370), OXA-143 (371) and OXA-235 (372) have also been detected and sequenced from *A. baumannii* isolates worldwide (373). Insertion of IS*Aba*1 element upstream of OXA-23 and OXA-51 has been correlated with the overexpression of these oxacillinases and subsequent carbapenem resistance in *A. baumannii* (373, 374).

A. baumannii also host a diverse range of AMEs that confer aminoglycoside resistance, usually through the acquisition of mobile genetic elements (375). AMEs identified from *A. baumannii* isolates include: the AAC (3') group of aminoglycoside acetyltransferases (*aacC1, aacC2*) and the AAC (6') group of acetyltransferases (*aacA4*) (376); the ANT (2") (*aadB*) and ANT (3") (*aadA1*) nucleotidyltransferases (377, 378); and APH (3') and APH (3") classes of aminoglycoside phosphotransferases (378, 379).

Other antibiotic modifying classes reported in *A. baumannii* antimicrobial resistance include: the chloramphenicol acetyltransferases, including *catI* (380), *catB2* (343), *catB3* (381) catB8 (382, 383) to confer resistance to phenicol antibiotics; the ADP-ribosyltransferase (*arr*) to catalyse the ADP-ribosylation and inactivation of rifamycin antibiotics (381); and tetracycline monooxygenases from the TetX flavin-monooxygenase family including Tet(X3), Tet(X4), Tet(X5) and Tet(X6) that confer tigecycline, tetracycline, eravacycline and omadacycline resistance (289, 384, 385).

Target modification and protection mechanisms in *A. baumannii*

A. baumannii has several reported resistance mechanisms to confer resistance to a diverse range of antibiotics via target modification and protection (see Section 1.2.2). Tetracycline resistance has been identified to occur via target protection and rescue through the expression of TetM (38). Ribosome methylation mediated by the 16S rRNA methyltransferase, ArmA, is seen to promote aminoglycoside resistance (378, 386). Fluoroquinolone resistance in *A. baumannii* is primarily caused by selection for DNA gyrase (*gyrA*) and topoisomerase IV (*parC*) mutations and has been associated with nosocomial outbreaks of *A. baumannii* (387–389).

Antibiotic insensitive variants of targets have also been reported in *A. baumannii*. Examples include the acquisition and expression of insensitive variants of penicillin binding proteins in *A. baumannii* conferring imipenem resistance (390). Furthermore, insensitive variants of dihydrofolate reductase and dihydropteroate synthase, including *dfrA1, dfrA7, dfrA19, sul1 and sul2* conferring trimethoprim-sulphonamide resistance, have been reported in clinical isolates of MDR *A. baumannii* (391). In *A. baumannii,* polymyxin resistance is reported to occur from modification of outer membrane composition (392, 393). Specific resistance to the last resort antibiotic, colistin, has been linked to altered expression of the PmrAB two-component system leading to the phosphoethanolamine modification of lipid A and a changed net-charge in the outer-membrane of in response to polymyxin exposure (393).

Reduced antimicrobial permeability in *A. baumannii*

The cell envelope acts as a first layer of defence against antimicrobial activity towards many classes of antibiotics (see Section 1.2.3) (394). A primary mechanism of decreased permeability toward antimicrobial challenge is carried out by a range of outer membrane porins expressed in *A. baumannii* (52, 395). OmpA is the most prevalent outer membrane porin of *A. baumannii* and has been linked to membrane integrity (396, 397). Production of OmpA is associated with resistance to a diverse range of antimicrobials, including chloramphenicol, aztreonam and nalidixic acid and may contribute to antibiotic extrusion via association with drug efflux pumps (396). Furthermore, decreased expression of several porins have been attributed to carbapenem resistance phenotype

in *A. baumannii*, including outer membrane porins CarO, Omp22, Omp33-36, Omp37, Omp43, Omp44 and Omp47 (359, 398–402).

1.6.3 *A. baumannii* drug efflux pumps

Multidrug efflux pumps are a valuable mechanism of antibiotic resistance in *A. baumannii,* as the expression of one transporter can often mediate resistance diverse range of antibiotics and promote survival. Efflux pumps from the ABC, RND, MFS, MATE, SMR and PACE transport families have been identified and characterised to confer diverse range of antimicrobial resistance in *A. baumannii*.

A. baumannii RND efflux pumps

Currently, there are five RND efflux systems characterised in *A. baumannii* — AdeABC, AdeIJK, AdeFGH, ArpAB and AbeD (403–407). All RND members recognise diverse antibiotic substrate profiles. AdeABC was the first RND efflux system to be described in *A. baumannii* (403). AdeABC has been reported to confer resistance to a diverse range of antibiotics, including aminoglycosides, β-lactams, chloramphenicol, macrolides, tetracyclines, tigecycline, trimethoprim and pentamidine (403, 408). Expression of AdeABC is associated with biocide tolerance and multidrug resistance phenotype in *A. baumannii* (409, 410). The AdeFGH transporter confers resistance to chloramphenicol, clindamycin, fluoroquinolones, sulfamethoxazole, sodium dodecyl sulfate, trimethoprim, tetracycline and tigecycline and the dyes safranin O, acridine orange and ethidium bromide (405). AdeFGH expression has been linked to increased biofilm formation and has been shown to be increased in response to human serum albumin exposure and DNA damage, suggesting roles in pathogenicity and virulence (411–413). AdeFGH is regulated by AdeL, a LysR-type transcriptional regulator and mutations in AdeL regulator is linked to expression of AdeFGH and multidrug resistant phenotype in clinical isolates of *A. baumannii* (405, 414). AdeIJK is highly conserved across *A. baumannii*, in which constitutive expression of this transporter confers intrinsic multidrug resistance (404, 415). AdeIJK confers resistance to β-lactams, chloramphenicol, erythromycin, tetracyclines, lincosamides, fluoroquinolones, fusidic acid, novobiocin, rifampin and trimethoprim (395). AdeABC and

AdeIJK are proposed to act synergistically to promote tetracycline and tigecycline resistance (404). AdeIJK transport can be repressed by the TetR-type regulator, AdeN and mutations in this regulator has been associated with AdeIJK overexpression (415). AbeD is an orphan RND transporter in *A. baumannii*, as the corresponding MFP and OMP to form a tripartite structure for export has not been identified (407). AbeD expression confers resistance to tobramycin, gentamicin, ceftriaxone, rifampicin and benzalkonium chloride. AbeD expression is proposed to be regulated by the SoxSR two-component system, involved in regulation of oxidative stress response (407). ArpAB is an RND efflux pump characterised to play a role tobramycin and amikacin resistance in *A. baumannii* (406). The ArpAB efflux pump promotes opaque-to-translucent colony phase switching, suggesting important roles in antimicrobial export and virulence in *A. baumannii* (309, 406).

A. baumannii ABC drug efflux pumps

MacAB-TolC is a tripartite ABC efflux system in *A. baumannii* that plays a role in macrolide and tigecycline resistance (149). MacAB-TolC expression in *A. baumannii* is regulated by the BaeSR two-component system (416). MacAB-TolC expression is associated with cell envelope stress response and mature biofilm homeostasis (417).

A. baumannii MFS drug efflux pumps

CraA is a phenicol efflux pump that confers resistance to chloramphenicol, florfenicol and thiamphenicol, dequalinium chloride, benzalkonium chloride and chlorhexidine (418, 419). AmvA is an efflux pump known to export a diverse range of antimicrobials, dyes and disinfectants including erythromycin, acriflavine, benzalkonium chloride, ethidium bromide and methyl viologen (420). Recently, AmvA was shown to play a physiological role in spermidine and spermine export (135). AbaF is an MFS transporter involved in conferring specific resistance for fosfomycin (421). AbaQ is an efflux pump specific towards efflux of quinolone antimicrobials (422). In addition to chromosomally encoded efflux pumps, *A. baumannii* has acquired narrow spectrum efflux systems including a range of Tet-type efflux pumps (i.e., Tet(A) and Tet(B)) on mobile genetic elements that confer specific resistance to tetracycline and tigecycline (423, 424).

The MFS transporters, CmlA and FloR, that confer resistance to chloramphenicol and florfenicol, respectively, are encoded on the AbaR1 resistance island (424).

A. baumannii MATE drug efflux pumps

MATE transporters associated with antibiotic resistance profiles in *A. baumannii* include the AbeM, AbeM2 and AbeM4 MATE transporters. AbeM confers resistance to a diverse range of substrates including fluoroquinolones, aminoglycosides, chloramphenicol, trimethoprim, triclosan, daunorubicin, doxorubicin tetraphenylphosphonium chloride and dyes, rhodamine 6G, ethidium bromide, Hoechst 33342, DAPI and acriflavine (234). Expression of *A. baumannii* MATE transporters AbeM2 and AbeM4 confer resistance to ciprofloxacin (425). AbeM3, a MATE transporter has not been characterised to confer resistance to antimicrobials, however, deletion of this transporter led to reduced virulence and motility in *A. baumannii* suggesting an important role of this transporter in the virulence (426).

A. baumannii SMR efflux pumps

AbeS is the only chromosomally encoded SMR efflux pump characterised in *A. baumannii* (427). AbeS confers resistance to amikacin, erythromycin, novobiocin, fluoroquinolones, tetracycline, and trimethoprim as well as a range of antimicrobial dyes and detergents (427). The QacE efflux pump is encoded on mobile genetic elements conferring high-level resistance to quaternary ammonium compounds and biocides. Isolates harbouring *qacE* gene are frequently isolated in carbapenem and biocide resistant isolates of *A. baumannii* (428–431).

A. baumannii PACE efflux pumps

A novel family of drug efflux transporters, known as the PACE transporter family, was discovered in *A. baumannii.* PACE transporters are chromosomally encoded and conserved in *Acinetobacter baumannii.* AceI has been characterised to specifically efflux the bisbiguanide antiseptic chlorhexidine and polyamines cadaverine and putrescine (118, 122). AceI is regulated by AceR, a LysR-type regulator (432). *A. baumannii* also encodes a paralogue of AceI, A1S_1503, reported to confer resistance to antimicrobial dye acriflavine (120).

1.7 Scope of thesis

The main hypothesis of this thesis is that omics data can be used for the discovery of new classes of efflux pumps. The discovery of the PACE drug efflux family in *A. baumannii* revealed that, in addition to the five canonical drug efflux families described so far, there are potentially additional novel types of drug efflux pumps yet to be discovered in this pathogen. In a recent TraDIS study examining genes important for biocide fitness across ten distinct biocides in *A. baumannii* we identified three integral membrane proteins of unknown function to confer resistance to silver nitrate (Chapter 2). In this thesis, we investigate the possibility of an ABC transporter of unknown function (Chapter 3), an ArAE family protein of unknown function (Chapter 4) and a DUF817 protein of unknown function (Chapter 5) as potential new efflux systems of *A. baumannii*. Furthermore, through transcriptomics we report on a fourth membrane protein of unknown function which was discovered to be important for ciprofloxacin tolerance due to a role in cell filamentation in *A. baumannii* (Chapter 7).

In parallel to this work, a microfluidic device for the measurement of bacteria cell efflux was also developed. Previously, most studies on drug efflux pumps in bacteria have studied efflux systems at the population level, which may mask subtle differences in efflux function at the single-cell level. This thesis reports on the development of a novel microfluidic technique to examine bacterial drug efflux activity at the individual single cell level (Chapter 6).

Lastly, in addition to their role in antimicrobial resistance, there is data to suggest that efflux pumps play a role in biofilm formation and homeostasis. In this thesis we conducted a study to report on exposure of biofilm to subinhibitory concentrations of two different antibiotics to investigate genes important for biofilm formation and antimicrobial resistance, which highlighted the importance of a select few drug efflux pumps (Chapter 8).

1.8 References

1. A. Fleming, On the antibacterial action of cultures of a penicllium, with special reference to their use in the isolation of *B. influenzae*. *Br. J. Exp. Pathol.* **10**, 226–236 (1929).

2. E. Abraham, E. Chain, An enzyme from bacteria able to destroy penicillin. *Nature* **146**, 837 (1940).

3. C. J. L. Murray, *et al.*, Global burden of bacterial antimicrobial resistance in 2019: a systematic analysis. *Lancet* **399**, 629–655 (2022).

4. A.-P. Magiorakos, *et al.*, Multidrug-resistant, extensively drug-resistant and pandrug-resistant bacteria: an international expert proposal for interim standard definitions for acquired resistance. *Clin. Microbiol. Infect.* **18**, 268–281 (2012).

5. A. Y. Peleg, H. Seifert, D. L. Paterson, *Acinetobacter baumannii*: Emergence of a successful pathogen. *Clin. Microbiol. Rev.* **21**, 538–582 (2008).

6. K. Poole, *Pseudomonas aeruginosa*: resistance to the max. *Front. Microbiol.* **2** (2011).

7. M. Souli, I. Galani, H. Giamarellou, Emergence of extensively drug-resistant and pandrug-resistant Gram-negative bacilli in Europe. *Euro. Surveill.* **13**, 19045 (2008).

8. A. R. Golden, *et al.*, Characterization of MDR and XDR *Streptococcus pneumoniae* in Canada, 2007–13. *J. Antimicrob. Chemother.* **70**, 2199–2202 (2015).

9. H. W. Boucher, *et al.*, Bad bugs, no drugs: No ESKAPE! An update from the Infectious Diseases Society of America. *Clin. Infect. Dis.* **48**, 1–12 (2009).

10. B. Jubeh, Z. Breijyeh, R. Karaman, Resistance of Gram-positive bacteria to current antibacterial agents and overcoming approaches. *Molecules* **25**, 2888 (2020).

11. E. Tacconelli, *et al.*, Discovery, research, and development of new antibiotics: the WHO priority list of antibiotic-resistant bacteria and tuberculosis. *Lancet Infect. Dis.* **18**, 318–327 (2018).

12. J. Davies, Where have all the antibiotics gone? *Can. J. Infect. Dis. Med. Microbiol.* **17**, 287–290 (2006).

13. S. J. Projan, Why is big pharma getting out of antibacterial drug discovery. *Curr. Opin. Microbiol.* **6**, 427-430 (2003).

14. S. Baker, A return to the pre-antimicrobial era? *Science* **347**, 1064–1066 (2015).

15. G. D. Wright, Bacterial resistance to antibiotics: Enzymatic degradation and modification.

Adv. Drug Deliv. Rev. **57**, 1451–1470 (2005).

16. E. Peterson, P. Kaur, Antibiotic resistance mechanisms in bacteria: Relationships between resistance determinants of antibiotic producers, environmental bacteria, and clinical pathogens. *Front. Microbiol.* **9**, 2928 (2018).

17. R. A. Bonomo, β-lactamases: A focus on current challenges. *Cold Spring Harb. Perspect. Med.* **7**, a025239 (2017).

18. M. Morar, K. Pengelly, K. Koteva, G. D. Wright, Mechanism and diversity of the erythromycin esterase family of enzymes. *Biochemistry* **51**, 1740–1751 (2012).

19. K. L. Fillgrove, S. Pakhomova, M. E. Newcomer, R. N. Armstrong, Mechanistic diversity of fosfomycin resistance in pathogenic microorganisms. *J. Am. Chem. Soc.* **125**, 15730–15731 (2003).

20. W. Yang, *et al.*, TetX is a flavin-dependent monooxygenase conferring resistance to tetracycline antibiotics. *J. Biol. Chem.* **279**, 52346–52352 (2004).

21. K. Koteva, *et al.*, Rox, a rifamycin resistance enzyme with an unprecedented mechanism of action. *Cell Chem. Biol.* **25**, 403-412.e5 (2018).

22. M. Korczynska, T. A. Mukhtar, G. D. Wright, A. M. Berghuis, Structural basis for streptogramin B resistance in *Staphylococcus aureus* by virginiamycin B lyase. *Proc. Natl. Acad. Sci. U. S. A.* **104**, 10388–10393 (2007).

23. J. Osei Sekyere, Genomic insights into nitrofurantoin resistance mechanisms and epidemiology in clinical *Enterobacteriaceae*. *Future. Sci. OA* **4**, FSO293 (2018).

24. C. Thomas, C. D. Gwenin, The role of nitroreductases in resistance to nitroimidazoles. *Biology (Basel)* **10,** 388 (2021).

25. T. S. Crofts, *et al.*, Discovery and characterization of a nitroreductase capable of conferring bacterial resistance to chloramphenicol. *Cell Chem. Biol.* **26**, 559-570.e6 (2019).

26. M. S. Ramirez, M. E. Tolmasky, Aminoglycoside modifying enzymes. *Drug Resist. Updat.* **13**, 151–171 (2010).

27. P. F. Wiley, L. Baczynskyj, L. A. Dolak, J. I. Cialdella, V. P. Marshall, Enzymatic phosphorylation of macrolide antibiotics. *J. Antibiot. (Tokyo).* **40**, 195–201 (1987).

28. D. N. Bolam, *et al*., The crystal structure of two macrolide glycosyltransferases provides a blueprint for host cell antibiotic immunity. *Proc. Natl. Acad. Sci. U. S. A*. **104**, 5336–5341 (2007).

29. A. Brisson-Noël, P. Delrieu, D. Samain, P. Courvalin, Inactivation of lincosaminide antibiotics in *Staphylococcus*. Identification of lincosaminide *O*-nucleotidyltransferases and comparison of the corresponding resistance genes. *J. Biol. Chem.* **263**, 15880–15887 (1988).

30. B. Bozdogan, *et al.*, A new resistance gene, *linB*, conferring resistance to lincosamides by nucleotidylation in *Enterococcus faecium* HM1025. *Antimicrob. Agents Chemother.* **43**, 925–929 (1999).

31. P. Spanogiannopoulos, M. Thaker, K. Koteva, N. Waglechner, G. D. Wright, Characterization of a rifampin-inactivating glycosyltransferase from a screen of environmental actinomycetes. *Antimicrob. Agents Chemother.* **56**, 5061–5069 (2012).

32. P. Spanogiannopoulos, N. Waglechner, K. Koteva, G. D. Wright, A rifamycin inactivating phosphotransferase family shared by environmental and pathogenic bacteria. *Proc. Natl. Acad. Sci. U. S. A*. **111**, 7102–7107 (2014).

33. J. Baysarowich, *et al.*, Rifamycin antibiotic resistance by ADP-ribosylation: Structure and diversity of Arr. *Proc. Natl. Acad. Sci. U. S. A.* **105**, 4886–4891 (2008).

34. W. V. Shaw, Chloramphenicol acetyltransferase: Enzymology and molecular biology. *CRC Crit. Rev. Biochem.* **14**, 1–46 (1983).

35. J. Allignet, V. Loncle, C. Simenel, M. Delepierre, N. el Solh, Sequence of a staphylococcal gene, *vat*, encoding an acetyltransferase inactivating the A-type compounds of virginiamycin-like antibiotics. *Gene* **130**, 91–98 (1993).

36. D. N. Wilson, V. Hauryliuk, G. C. Atkinson, A. J. O'Neill, Target protection as a key antibiotic resistance mechanism. *Nat. Rev. Microbiol.* **18**, 637–648 (2020).

37. M. W. Vetting, *et al.*, Structure of QnrB1, a plasmid-mediated fluoroquinolone resistance factor. *J. Biol. Chem.* **286**, 25265–25273 (2011).

38. A. Dönhöfer, *et al.*, Structural basis for TetM-mediated tetracycline resistance. *Proc. Natl. Acad. Sci. U. S. A.* **109**, 16900–16905 (2012).

39. L. S. Redgrave, S. B. Sutton, M. A. Webber, L. J. V. Piddock, Fluoroquinolone resistance: Mechanisms, impact on bacteria, and role in evolutionary success. *Trends Microbiol.* **22**, 438–445 (2014).

40. B. P. Goldstein, Resistance to rifampicin: A review. *J. Antibiot.* **67**, 625–630 (2014).

41. D. N. Wilson, Ribosome-targeting antibiotics and mechanisms of bacterial resistance. *Nat. Rev. Microbiol.* **12**, 35–48 (2014).

42. J. M. A. Blair, M. A. Webber, A. J. Baylay, D. O. Ogbolu, L. J. V. Piddock, Molecular mechanisms of antibiotic resistance. *Nat. Rev. Microbiol.* **13**, 42–51 (2015).

43. M. D. Adams, *et al.*, Resistance to colistin in *Acinetobacter baumannii* associated with mutations in the PmrAB two-component system. *Antimicrob. Agents Chemother.* **53**, 3628–3634 (2009).

44. L. Fernández, *et al.*, Adaptive resistance to the "last hope" antibiotics polymyxin B and colistin in *Pseudomonas aeruginosa* is mediated by the novel two-component regulatory system ParR-ParS. *Antimicrob. Agents Chemother.* **54**, 3372–3382 (2010).

45. A. Cannatelli, *et al.*, *In vivo* emergence of colistin resistance in *Klebsiella pneumoniae* producing KPC-type carbapenemases mediated by insertional inactivation of the PhoQ/PhoP *mgrB* regulator. *Antimicrob. Agents Chemother.* **57**, 5521–5526 (2013).

46. M. C. Roberts, *et al.*, Nomenclature for macrolide and macrolide-lincosamide-streptogramin B resistance determinants. *Antimicrob. Agents Chemother.* **43**, 2823–2830 (1999).

47. K. S. Long, J. Poehlsgaard, C. Kehrenberg, S. Schwarz, B. Vester, The Cfr rRNA methyltransferase confers resistance to phenicols, lincosamides, oxazolidinones, pleuromutilins, and streptogramin A antibiotics. *Antimicrob. Agents Chemother.* **50**, 2500–2505 (2006).

48. Y. Cetinkaya, P. Falk, C. G. Mayhall, Vancomycin-resistant enterococci. *Clin. Microbiol. Rev.* **13**, 686–707 (2000).

49. J. Fishovitz, J. A. Hermoso, M. Chang, S. Mobashery, Penicillin-binding protein 2a of methicillin-resistant *Staphylococcus aureus*. *IUBMB Life*. **66**, 572–577 (2014).

50. O. Sköld, Sulfonamides and trimethoprim. *Expert Rev. Anti. Infect. Ther.* **8**, 1–6 (2010).

51. J. Flensburg, O. Sköld, Massive overproduction of dihydrofolate reductase in bacteria as a response to the use of trimethoprim. *Eur. J. Biochem.* **162**, 473–476 (1987).

52. L. Fernández, R. E. W. Hancock, Adaptive and mutational resistance: Role of porins and efflux pumps in drug resistance. *Clin. Microbiol. Rev.* **25**, 661–681 (2012).

53. A. Doménech-Sánchez, *et al.*, Role of *Klebsiella pneumoniae* OmpK35 porin in antimicrobial resistance. *Antimicrob. Agents Chemother.* **47**, 3332–3335 (2003).

54. J.-P. Lavigne, *et al.*, An adaptive response of *Enterobacter aerogenes* to imipenem: Regulation of porin balance in clinical isolates. *Int. J. Antimicrob. Agents* **41**, 130–136 (2013).

55. L. M. McMurry, R. E. J. Petrucci, S. B. Levy, Active efflux of tetracycline encoded by four genetically different tetracyline resistance determinants in *Escherichia coli*. *Proc. Natl. Acad. Sci. U. S. A.* **77**, 3974–3977 (1980).

56. A. Tait-Kamradt, *et al.*, *mefE* is necessary for the erythromycin-resistant M phenotype in *Streptococcus pneumoniae*. *Antimicrob. Agents Chemother.* **41**, 2251–2255 (1997).

57. C. A. Elkins, H. Nikaido, Substrate specificity of the RND-type multidrug efflux pumps AcrB and AcrD of *Escherichia coli* is determined predominantly by two large periplasmic loops. *J. Bacteriol.* **184**, 6490–6498 (2002).

58. J. Kobylka, *et al.*, AcrB: a mean, keen, drug efflux machine. *Ann. N. Y. Acad. Sci.* **1459**, 38–68 (2020).

59. X. Z. Li, P. Plésiat, H. Nikaido, The challenge of efflux-mediated antibiotic resistance in Gram-negative bacteria. *Clin. Microbiol. Rev.* **28**, 337–418 (2015).

60. H. Okusu, D. Ma, H. Nikaido, AcrAB efflux pump plays a major role in the antibiotic resistance phenotype of *Escherichia coli* multiple-antibiotic-resistance (Mar) mutants. *J. Bacteriol.* **178**, 306–308 (1996).

61. A. L. Davidson, J. Chen, ATP-binding cassette transporters in bacteria. *Annu. Rev. Biochem.* **73**, 241–268 (2004).

62. T. T. Tseng, *et al.*, The RND permease superfamily: An ancient, ubiquitous and diverse family that includes human disease and development proteins. *J. Mol. Microbiol. Biotechnol.* **1**, 107–125 (1999).

63. S. S. Pao, I. T. Paulsen, M. H. Saier, Jr., The major facilitator superfamily. *Microbiol. Mol. Biol. Rev.* **62**, 1–34 (1998).

64. D. C. Bay, K. L. Rommens, R. J. Turner, Small multidrug resistance proteins: A multidrug transporter family that continues to grow. *Biochim. Biophys. Acta.* **1778**, 1814–1838 (2008).

65. D. L. Jack, N. M. Yang, M. H. Saier, Jr., The drug/metabolite transporter superfamily. *Eur. J. Biochem.* **268**, 3620–3639 (2001).

66. T. Kuroda, T. Tsuchiya, Multidrug efflux transporters in the MATE family. *Biochim. Biophys. Acta.* **1794**, 763–768 (2009).

67. R. N. Hvorup, *et al.*, The multidrug/oligosaccharidyl-lipid/polysaccharide (MOP) exporter superfamily. *Eur. J. Biochem.* **270**, 799–813 (2003).

68. J. A. Delmar, E. W. Yu, The AbgT family: A novel class of antimetabolite transporters. *Protein Sci.* **25**, 322–337 (2016).

69. K. A. Hassan, *et al.*, Pacing across the membrane: The novel PACE family of efflux pumps is widespread in Gram-negative pathogens. *Res. Microbiol.* **169**, 450–454 (2018).

70. Z. Wang, *et al.*, An allosteric transport mechanism for the AcrAB-TolC multidrug efflux pump. *eLife* **6**, 1–19 (2017).

71. R. J. P. Dawson, K. P. Locher, Structure of the multidrug ABC transporter Sav1866 from *Staphylococcus aureus* in complex with AMP-PNP. *FEBS Lett.* **581**, 935–938 (2007).

72. J. Heng, *et al.*, Substrate-bound structure of the *E. coli* multidrug resistance transporter MdfA. *Cell Res.* **25**, 1060–1073 (2015).

73. M. Lu, M. Radchenko, J. Symersky, R. Nie, Y. Guo, Structural insights into H+-coupled multidrug extrusion by a MATE transporter. *Nat. Struct. Mol. Biol.* **20**, 1310–1317 (2013).

74. S. J. Fleishman, *et al.*, Quasi-symmetry in the Cryo-EM structure of EmrE provides the key to modeling its transmembrane domain. *J. Mol. Biol.* **364**, 54–67 (2006).

75. C. C. Su, *et al.*, Structure and function of *Neisseria gonorrhoeae* MtrF illuminates a class of antimetabolite efflux pumps. *Cell Rep.* **11**, 61–70 (2015).

76. N. Yousefian, *et al.*, Structural characterization of the EmrAB-TolC efflux complex from *E. coli*. *Biochim Biophys Acta Biomembr*. **1863**, 183488 (2021).

77. I. Alav, *et al.*, Structure, assembly, and function of tripartite efflux and type 1 secretion systems in Gram-negative bacteria. *Chem. Rev.* **121**, 5479–5596 (2021).

78. S. Srikant, R. Gaudet, A. W. Murray, Selecting for altered substrate specificity reveals the evolutionary flexibility of ATP-Binding Cassette transporters. *Curr. Biol.* **30**, 1689-1702.e6 (2020).

79. C. Thomas, R. Tampé, Structural and mechanistic principles of ABC transporters. *Annu. Rev. Biochem.* **89**, 605–636 (2020).

80. N. P. Greene, E. Kaplan, A. Crow, V. Koronakis, Antibiotic resistance mediated by the MacB ABC transporter family: A structural and functional perspective. *Front. Microbiol.* **9**, 950 (2018).

81. A. Crow, N. P. Greene, E. Kaplan, V. Koronakis, Structure and mechanotransmission mechanism of the MacB ABC transporter superfamily. *Proc. Natl. Acad. Sci. U. S. A.* **114**, 12572-12577 (2017).

82. R. J. P. Dawson, K. P. Locher, Structure of a bacterial multidrug ABC transporter. *Nature* **443**, 180–185 (2006).

83. A. Ward, C. L. Reyes, J. Yu, C. B. Roth, G. Chang, Flexibility in the ABC transporter MsbA: Alternating access with a twist. *Proc. Natl. Acad. Sci. U. S. A.* **104**, 19005–19010 (2007).

84. H. G. Choudhury, *et al.*, Structure of an antibacterial peptide ATP-binding cassette transporter in a novel outward occluded state. *Proc. Natl. Acad. Sci. U. S. A.* **111**, 9145–9150 (2014).

85. S. Velamakanni, Y. Yao, D. A. P. Gutmann, H. W. van Veen, Multidrug transport by the ABC transporter Sav1866 from *Staphylococcus aureus*. *Biochemistry* **47**, 9300–9308 (2008).

86. D. Du, *et al*., Structure of the AcrAB–TolC multidrug efflux pump. *Nature* **509**, 512–515 (2014).

87. E. C. Hobbs, X. Yin, B. J. Paul, J. L. Astarita, G. Storz, Conserved small protein associates with the multidrug efflux pump AcrB and differentially affects antibiotic resistance. *Proc. Natl. Acad. Sci. U.S.A*. **109**, 16696–16701 (2012).

88. V. K. Ramaswamy, A. V. Vargiu, G. Malloci, J. Dreier, P. Ruggerone, Molecular rationale behind the differential substrate specificity of bacterial RND multi-drug transporters. *Sci. Rep.* **7**, 8075 (2017).

89. M. A. Seeger, *et al.*, Structural asymmetry of AcrB trimer suggests a peristaltic pump mechanism. *Science* **313**, 1295–1298 (2006).

90. H.-K. Tam, *et al*., Allosteric drug transport mechanism of multidrug transporter AcrB. *Nat Commun.* **12**, 3889 (2021).

91. J. Anes, M. P. McCusker, S. Fanning, M. Martins, The ins and outs of RND efflux pumps in *Escherichia coli*. *Front. Microbiol.* **6**, 587 (2015).

92. A. Neuberger, D. Du, B. F. Luisi, Structure and mechanism of bacterial tripartite efflux pumps. *Res Microbiol.* **169**, 401–413 (2018).

93. J. Adler, E. Bibi, Membrane topology of the multidrug transporter MdfA: Complementary gene fusion studies reveal a nonessential C-terminal domain. *J. Bacteriol.* **184**, 3313–3320 (2002).

94. I. T. Paulsen, M. H. Brown, T. G. Littlejohn, B. A. Mitchell, R. A. Skurray, Multidrug resistance proteins QacA and QacB from *Staphylococcus aureus*: Membrane topology and identification of residues involved in substrate specificity. *Proc. Natl. Acad. Sci. U. S. A.* **93**, 3630 (1996).

95. N. J. Wood, T. Alizadeh, D. J. Richardson, S. J. Ferguson, J. W. B. Moir, Two domains of a dual-function NarK protein are required for nitrate uptake, the first step of denitrification in *Paracoccus pantotrophus*. *Mol. Microbiol.* **44**, 157–170 (2002).

96. M. H. Saier, Jr, *et al.*, The Transporter Classification Database (TCDB): Recent advances. *Nucleic Acids Res.* **44**, D372–D379 (2016).

97. M. H. Saier, Jr, A functional-phylogenetic classification system for transmembrane solute transporters. *Microbiol. Mol. Biol. Rev.* **64**, 354–411 (2000).

98. O. Lomovskaya, K. Lewis, *emr*, an *Escherichia coli* locus for multidrug resistance. *Proc. Natl. Acad. Sci. U. S. A.* **89**, 8938 (1992).

99. D. Drew, R. A. North, K. Nagarathinam, M. Tanabe, Structures and general transport mechanisms by the major facilitator superfamily (MFS). *Chem. Rev.* **121**, 5289–5335 (2021).

100. R. Edgar, E. Bibi, MdfA, an *Escherichia coli* multidrug resistance protein with an extraordinarily broad spectrum of drug recognition. *J. Bacteriol.* **179**, 2274–2280 (1997).

101. D. Du, H. W. van Veen, S. Murakami, K. M. Pos, B. F. Luisi, Structure, mechanism and cooperation of bacterial multidrug transporters. *Curr. Opin. Struct. Biol.* **33**, 76–91 (2015).

102. X. He, *et al.*, Structure of a cation-bound multidrug and toxic compound extrusion transporter. *Nature* **467**, 991–994 (2010).

103. Y. Tanaka, *et al.*, Structural basis for the drug extrusion mechanism by a MATE multidrug transporter. *Nature* **496**, 247–251 (2013).

104. M. Lu, *et al.*, Structures of a Na+-coupled, substrate-bound MATE multidrug transporter. *Proc. Natl. Acad. Sci. U. S. A.* **110**, 2099–2104 (2013).

105. I. Ubarretxena-Belandia, J. M. Baldwin, S. Schuldiner, C. G. Tate, Three-dimensional structure of the bacterial multidrug transporter EmrE shows it is an asymmetric homodimer. *EMBO J.* **22**, 6175–6181 (2003).

106. A. A. Kermani, *et al.*, The structural basis of promiscuity in small multidrug resistance transporters. *Nat. Commun.* **11**, 6064 (2020).

107. I. T. Paulsen, M. H. Brown, R. A. Skurray, Proton-dependent multidrug efflux systems. *Microbiol. Rev.* **60**, 575–608 (1996).

108. M. Morimyo, E. Hongo, H. Hama-Inaba, I. Machida, Cloning and characterization of the *mvrC* gene of *Escherichia coli* K-12 which confers resistance against methyl viologen toxicity. *Nucleic Acids Res.* **20**, 3159–3165 (1992).

109. A. S. Purewal, I. G. Jones, M. Midgley, Cloning of the ethidium efflux gene from *Escherichia coli*. *FEMS Microbiol. Lett.* **68**, 73–76 (1990).

110. H. Yerushalmi, M. Lebendiker, S. Schuldiner, EmrE, an *Escherichia coli* 12-kDa multidrug transporter, exchanges toxic cations and H+ and is soluble in organic solvents. *J. Biol. Chem.* **270**, 6856–6863 (1995).

111. K. Nishino, A. Yamaguchi, Analysis of a complete library of putative drug transporter genes in *Escherichia coli*. *J. Bacteriol.* **183**, 5803–5812 (2001).

112. I. Nasie, S. Steiner-Mordoch, S. Schuldiner, New substrates on the block: Clinically relevant resistances for EmrE and homologues. *J. Bacteriol.* **194**, 6766–6770 (2012).

113. D. C. Bay, R. J. Turner, Small multidrug resistance protein EmrE reduces host pH and osmotic tolerance to metabolic quaternary cation osmoprotectants. *J. Bacteriol.* **194**, 5941–5948 (2012).

114. J. R. Bolla, *et al.*, Crystal structure of the *Alcanivorax borkumensis* YdaH transporter reveals an unusual topology. *Nat. Commun.* **6**, 1–10 (2015).

115. M. Lu, Structure and mechanism of the divalent anion/Na+ symporter. *Int. J. Mol. Sci.* **20**, 440 (2019).

116. A. A. Garaeva, D. J. Slotboom, Elevator-type mechanisms of membrane transport. *Biochem. Soc. Trans.* **48**, 1227–1241 (2020).

117. E. L. Carter, *et al.*, *Escherichia coli abg* genes enable uptake and cleavage of the folate catabolite *p*-aminobenzoyl-glutamate. *J. Bacteriol.* **189**, 3329–3334 (2007).

118. K. A. Hassan, *et al.*, Transcriptomic and biochemical analyses identify a family of chlorhexidine efflux proteins. *Proc. Natl. Acad. Sci. U. S. A.* **110**, 20254–20259 (2013).

119. J. R. Bolla, A. C. Howes, F. Fiorentino, C. V. Robinson, Assembly and regulation of the chlorhexidine-specific efflux pump AceI. *Proc. Natl. Acad. Sci. U. S. A.* **117**, 17011–17018 (2020).

120. K. A. Hassan, Q. Liu, P. J. F. Henderson, I. T. Paulsen, Homologs of the *Acinetobacter baumannii* AceI transporter represent a new family of bacterial multidrug efflux systems. *mBio* **6**, e01982-14 (2015).

121. P. Shah, E. Swiatlo, A multifaceted role for polyamines in bacterial pathogens. *Mol. Microbiol.* **68**, 4–16 (2008).

122. K. A. Hassan, *et al.*, Short-chain diamines are the physiological substrates of PACE family efflux pumps. *Proc. Natl. Acad. Sci. U. S. A.* **116**, 18015–18020 (2019).

123. N. Tal, S. Schuldiner, A coordinated network of transporters with overlapping specificities provides a robust survival strategy. *Proc. Natl. Acad. Sci. U. S. A.* **106**, 9051–9056 (2009).

124. P. J. F. Henderson, *et al.*, Physiological functions of bacterial "multidrug" efflux pumps. *Chem. Rev.* **121**, 5417–5478 (2021).

125. A. A. Neyfakh, Mystery of multidrug transporters: The answer can be simple. *Mol. Microbiol.* **44**, 1123–1130 (2002).

126. G. Spengler, A. Kincses, M. Gajdács, L. Amaral, New roads leading to old destinations: Efflux pumps as targets to reverse multidrug resistance in bacteria. *Molecules* **22**, 468 (2017).

127. K. Koita, C. V. Rao, Identification and analysis of the putative pentose sugar efflux transporters in *Escherichia coli*. *PLoS One* **7**, e43700 (2012).

128. H. Tsuchiya, *et al.*, Structural basis for amino acid export by DMT superfamily transporter YddG. *Nature* **534**, 417–420 (2016).

129. A. Aliashkevich, L. Alvarez, F. Cava, New insights into the mechanisms and biological roles of D-amino acids in complex eco-systems. *Front. Microbiol.* **9,** 683 (2018).

130. S. Yamada, *et al.*, Effect of drug transporter genes on cysteine export and overproduction in *Escherichia coli*. *Appl. Environ. Microbiol.* **72**, 4735–4742 (2006).

131. H. I. Zgurskaya, G. Krishnamoorthy, A. Ntreh, S. Lu, Mechanism and function of the outer membrane channel TolC in multidrug resistance and physiology of enterobacteria. *Front. Microbiol.* **2,** 189 (2011).

132. N. Wiriyathanawudhiwong, I. Ohtsu, Z.-D. Li, H. Mori, H. Takagi, The outer membrane TolC is involved in cysteine tolerance and overproduction in *Escherichia coli*. *Appl. Microbiol. Biotechnol.* **81**, 903–913 (2009).

133. T. Daßler, T. Maier, C. Winterhalter, A. Böck, Identification of a major facilitator protein from *Escherichia coli* involved in efflux of metabolites of the cysteine pathway. *Mol. Microbiol.* **36**, 1101–1112 (2000).

134. A. J. Michael, Polyamines in eukaryotes, bacteria, and archaea. *J. Biol. Chem.* **291**, 14896–14903 (2016).

135. F. L. Short, *et al.*, The *Acinetobacter baumannii* disinfectant resistance protein, AmvA, is a spermidine and spermine efflux pump. *Commun. Biol.* **4**, 1114 (2021).

136. K. Higashi, *et al.*, Identification of a spermidine excretion protein complex (MdtJI) in *Escherichia coli*. *J. Bacteriol.* **190**, 872 (2008).

137. D. P. Woolridge, *et al.*, Efflux of the natural polyamine spermidine facilitated by the *Bacillus subtilis* multidrug transporter Blt. *J. Biol. Chem.* **272**, 8864-8866 (1997).

138. J. W. Nelson, R. M. Atilho, M. E. Sherlock, R. B. Stockbridge, R. R. Breaker, Metabolism of free guanidine in bacteria is regulated by a widespread riboswitch class. *Mol. Cell* **65**, 220-230 (2017).

139. R. R. Breaker, Riboswitches and the RNA world. *Cold Spring Harb. Perspect. Biol.* **4**, a003566 (2012).

140. J. E. Barrick, *et al.*, New RNA motifs suggest an expanded scope for riboswitches in bacterial genetic control. *Proc. Natl. Acad. Sci. U. S. A.* **101**, 6421-6426 (2004).

141. A. A. Kermani, C. B. Macdonald, R. Gundepudi, R. B. Stockbridge, Guanidinium export is the primal function of SMR family transporters. *Proc. Natl. Acad. Sci. U. S. A.* **115**, 3060–3065 (2018).

142. F. McAleese, *et al.*, A novel MATE family efflux pump contributes to the reduced susceptibility of laboratory-derived *Staphylococcus aureus* mutants to tigecycline. *Antimicrob. Agents Chemother.* **49**, 1865–1871 (2005).

143. H. Salvail, A. Balaji, D. Yu, A. Roth, R. R. Breaker, Biochemical validation of a fourth guanidine riboswitch class in bacteria. *Biochemistry* **59**, 4654-4662 (2020).

144. N. Chandra, S. Kumar, "Antibiotics Producing Soil Microorganisms." in *Antibiotics and Antibiotics Resistance Genes in Soil*, M. Z. Hashmi, V. Strezov, A. Varma, Eds. (Springer International Publishing, 2017), pp. 1–18.

145. X. Jiang, *et al.*, Dissemination of antibiotic resistance genes from antibiotic producers to pathogens. *Nat. Commun.* **8**, 1–7 (2017).

146. G. Wang, Human antimicrobial peptides and proteins. *Pharmaceuticals* **7**, 545-594 (2014).

147. A. H. Benfield, S. T. Henriques, Mode-of-action of antimicrobial peptides: Membrane disruption vs. intracellular mechanisms. *Front. Med. Technol.* **2**, 610997 (2020).

148. A. W. P. Fitzpatrick, *et al.*, Structure of the MacAB-TolC ABC-type tripartite multidrug efflux pump. *Nat. Microbiol.* **2**, 17070 (2017).

149. U. Okada, *et al.*, Crystal structure of tripartite-type ABC transporter MacB from *Acinetobacter baumannii*. *Nat. Commun.* **8**, 1336 (2017).

150. N. Kobayashi, K. Nishino, A. Yamaguchi, Novel macrolide-specific ABC-type efflux transporter in *Escherichia coli*. *J. Bacteriol.* **183**, 5639–5644 (2001).

151. H. Yamanaka, H. Kobayashi, E. Takahashi, K. Okamoto, MacAB is involved in the secretion of *Escherichia coli* heat-stable enterotoxin II. *J. Bacteriol.* **190**, 7693–7698 (2008).

152. J. D. Honeycutt, *et al.*, Genetic variation in the MacAB-TolC efflux pump influences pathogenesis of invasive *Salmonella* isolates from Africa. *PLoS Pathog.* **16**, 1–30 (2020).

153. J. Maldonado-Valderrama, P. Wilde, A. Macierzanka, A. Mackie, The role of bile salts in digestion. *Adv. Colloid Interface Sci.* **165**, 36–46 (2011).

154. V. Urdaneta, J. Casadesús, Interactions between bacteria and bile salts in the gastrointestinal and hepatobiliary tracts. *Front. Med.* **4**, 163 (2017).

155. A. H. Zaidi, *et al.*, The ABC-type multidrug resistance transporter LmrCD is responsible for an extrusion-based mechanism of bile acid resistance in *Lactococcus lactis*. *J. Bacteriol.* **190**, 7357–7366 (2008).

156. J. Lubelski, P. Mazurkiewicz, R. Van Merkerk, W. N. Konings, A. J. M. Driessen, *ydaG* and *ydbA* of *Lactococcus lactis* encode a heterodimeric ATP-binding cassette-type multidrug transporter. *J. Biol. Chem.* **279**, 34449–34455 (2004).

157. M. Hegde, T. K. Wood, A. Jayaraman, The neuroendocrine hormone norepinephrine increases *Pseudomonas aeruginosa* PA14 virulence through the *las* quorum-sensing pathway. *Appl. Microbiol. Biotechnol.* **84**, 763 (2009).

158. C. Vidaillac, *et al.*, Sex steroids induce membrane stress responses and virulence properties in *Pseudomonas aeruginosa*. *mBio* **11**, e01774-20 (2020).

159. M. Lyte, *et al.*, Stimulation of *Staphylococcus epidermidis* growth and biofilm formation by catecholamine inotropes. *Lancet* **361**, 130-135 (2003).

160. H. Neuman, J. W. Debelius, R. Knight, O. Koren, Microbial endocrinology: The interplay between the microbiota and the endocrine system. *FEMS Microbiol. Rev.* **39**, 509-521 (2015).

161. W. Yotis, R. Stanke, Bacteriostatic action of progesterone on staphylococci and other microorganisms. *J. Bacteriol.* **92**, 1285-1289 (1966).

162. S. A. Morse, T. J. Fitzgerald, Effect of progesterone on *Neisseria gonorrhoeae*. *Infect. Immun.* **10**, 1370-1377 (1974).

163. A. E. Jerse, *et al.*, A gonococcal efflux pump system enhances bacterial survival in a female mouse model of genital tract infection. *Infect. Immun.* **71**, 5576-5582 (2003).

164. D. Golparian, W. M. Shafer, M. Ohnishi, M. Unemo, Importance of multidrug efflux pumps in the antimicrobial resistance property of clinical multidrug-resistant isolates of *Neisseria gonorrhoeae*. *Antimicrob. Agents Chemother.* **58**, 3556–3559 (2014).

165. W. M. Shafer, X.-D. Qu, A. J. Waring, R. I. Lehrer, Modulation of *Neisseria gonorrhoeae* susceptibility to vertebrate antibacterial peptides due to a member of the resistance/nodulation/division efflux pump family. *Proc. Natl. Acad. Sci. U. S. A.* **95**, 1829-1833 (1998).

166. H. D. VanEtten, J. W. Mansfield, J. A. Bailey, E. E. Farmer, Two classes of plant antibiotics: Phytoalexins versus "phytoanticipins". *Plant Cell* **6**, 1191-1192 (1994).

167. B. Khameneh, M. Iranshahy, V. Soheili, B. S. F. Bazzaz, Review on plant antimicrobials: A mechanistic viewpoint. *Antimicrob. Resist. Infect. Control* **8**, 118 (2019).

168. R. González-Lamothe, *et al.*, Plant antimicrobial agents and their effects on plant and human pathogens. *Int. J. Mol. Sci.* **10**, 3400-3419 (2009).

169. N. A. Eckardt, Move it on out with MATEs. *Plant Cell* **13**, 1477–1480 (2001).

170. A. Burse, H. Weingart, M. S. Ullrich, The phytoalexin-inducible multidrug efflux pump AcrAB contributes to virulence in the fire blight pathogen, *Erwinia amylovora*. *Mol. Plant Microbe Interact.* **17**, 43-54 (2004).

171. A. Burse, H. Weingart, M. S. Ullrich, NorM, an *Erwinia amylovora* multidrug efflux pump involved in *in vitro* competition with other epiphytic bacteria. *Appl. Environ. Microbiol.* **70**, 693–703 (2004).

172. A. Viljoen, *et al.*, The diverse family of MmpL Transporters in mycobacteria: From regulation to antimicrobial developments. *Mol. Microbiol.* **104**, 889-904 (2017).

173. Q. C. Truong-Bolduc, R. A. Villet, Z. A. Estabrooks, D. C. Hooper, Native efflux pumps contribute resistance to antimicrobials of skin and the ability of *Staphylococcus aureus* to colonize skin. *J. Infect. Dis.* **209**, 1485–1493 (2014).

174. N. A. Whitehead, A. M. L. Barnard, H. Slater, N. J. L. Simpson, G. P. C. Salmond, Quorum-sensing in Gram-negative bacteria. *FEMS Microbiol. Rev.* **25**, 365–404 (2001).

175. J. P. Pearson, C. Van Delden, B. H. Iglewski, Active efflux and diffusion are involved in transport of *Pseudomonas aeruginosa* cell-to-cell signals. *J. Bacteriol.* **181**, 1203–1210 (1999).

176. S. Minagawa, *et al.*, RND type efflux pump system MexAB-OprM of *Pseudomonas aeruginosa* selects bacterial languages, 3-oxo-acyl-homoserine lactones, for cell-to-cell communication. *BMC Microbiol.* **12**, 70 (2012).

177. H. Wu, C. Moser, H.-Z. Wang, N. Høiby, Z.-J. Song, Strategies for combating bacterial biofilm infections. *Int. J. Oral Sci.* **7**, 1–7 (2015).

178. H. Ceri, *et al.*, The Calgary Biofilm Device: New technology for rapid determination of antibiotic susceptibilities of bacterial biofilms. *J. Clin. Microbiol.* **37**, 1771–1776 (1999).

179. D. Sharma, L. Misba, A. U. Khan, Antibiotics versus biofilm: An emerging battleground in microbial communities. *Antimicrob. Resist. Infect. Control* **8**, 76 (2019).

180. R. J. Gillis, *et al.*, Molecular basis of azithromycin-resistant *Pseudomonas aeruginosa* biofilms. *Antimicrob. Agents Chemother.* **49**, 3858–3867 (2005).

181. Y. Zhang, *et al.*, The multidrug efflux pump MdtEF Protects against nitrosative damage during the anaerobic respiration in *Escherichia coli*. *J. Biol. Chem.* **286**, 26576-26584 (2011).

182. M. A. Schembri, K. Kjaergaard, P. Klemm, Global gene expression in *Escherichia coli* biofilms. *Mol. Microbiol.* **48**, 253-267 (2003).

183. Z. Xu, A. Yan, Multidrug efflux systems in microaerobic and anaerobic bacteria. *Antibiotics* **4**, 379–396 (2015).

184. Z. Deng, Y. Shan, Q. Pan, X. Gao, A. Yan, Anaerobic Expression of the *gadE-mdtEF* multidrug efflux operon is primarily regulated by the two-component system ArcBA through antagonizing the H-NS mediated repression. *Front. Microbiol.* **4**, 194 (2013).

185. V. B. Srinivasan, G. Rajamohan, KpnEF, a new member of the *Klebsiella pneumoniae* cell envelope stress response regulon, is an SMR-type efflux pump involved in broad-spectrum antimicrobial resistance. *Antimicrob. Agents Chemother.* **57**, 4449–4462 (2013).

186. H. Fetar, *et al*., *mexEF-oprN* multidrug efflux operon of *Pseudomonas aeruginosa*: Regulation by the MexT activator in response to nitrosative stress and chloramphenicol. *Antimicrob. Agents Chemother.* **55**, 508–514 (2011).

187. A. Kumar, H. P. Schweizer, Evidence of MexT-independent overexpression of MexEF-OprN multidrug efflux pump of *Pseudomonas aeruginosa* in presence of metabolic stress. *PLOS ONE* **6**, e26520 (2011).

188. J. A. Imlay, The molecular mechanisms and physiological consequences of oxidative stress: Lessons from a model bacterium. *Nat. Rev. Microbiol.* **11**, 443–454 (2013).

189. Y. Yang, A. V Bazhin, J. Werner, S. Karakhanova, Reactive oxygen species in the immune system. *Int. Rev. Immunol.* **32**, 249-270 (2013).

190. C. Lamb, R. A. Dixon, The oxidative burst in plant disease resistance. *Annu. Rev. Plant Physiol. Plant Mol. Biol.* **48**, 251-275 (1997).

191. M. H. Brown, I. T. Paulsen, R. A. Skurray, The multidrug efflux protein NorM is a prototype of a new family of transporters. *Mol. Microbiol.* **31**, 394–395 (1999).

192. J. R. Guelfo, A. Rodríguez-Rojas, I. Matic, J. Blázquez, A MATE-family efflux pump rescues the *Escherichia coli* 8-oxoguanine-repair-deficient mutator phenotype and protects against H2O2 killing. *PLOS Genet.* **6**, e1000931 (2010).

193. P. Chandrangsu, C. Rensing, J. D. Helmann, Metal homeostasis and resistance in bacteria. *Nat. Rev. Microbiol.* **15**, 338–350 (2017).

194. S. C. Andrews, A. K. Robinson, F. Rodríguez-Quiñones, Bacterial iron homeostasis. *FEMS Microbiol. Rev.* **27**, 215–237 (2003).

195. R. C. Hider, X. Kong, Chemistry and biology of siderophores. *Nat. Prod. Rep.* **27**, 637–657 (2010).

196. J. L. Furrer, D. N. Sanders, I. G. Hook-Barnard, M. A. McIntosh, Export of the siderophore enterobactin in *Escherichia coli*: Involvement of a 43 kDa membrane exporter. *Mol. Microbiol.* **44**, 1225–1234 (2002).

197. C. K. Lim, A. Penesyan, K. A. Hassan, J. E. Loper, I. T. Paulsen, Disruption of transporters affiliated with enantio-pyochelin biosynthesis gene cluster of *Pseudomonas protegens* Pf-5 has pleiotropic effects. *PLoS One* **11**, e0159884 (2016).

198. J. R. Sheldon, E. P. Skaar, *Acinetobacter baumannii* can use multiple siderophores for iron acquisition, but only acinetobactin is required for virulence. *PLoS Pathog.* **6**, e1008995 (2020).

199. A. Milano, *et al.*, Azole resistance in *Mycobacterium tuberculosis* is mediated by the MmpS5–MmpL5 efflux system. *Tuberculosis* **89**, 84–90 (2009).

200. R. C. Hartkoorn, S. Uplekar, S. T. Cole, Cross-Resistance between clofazimine and bedaquiline through upregulation of MmpL5 in *Mycobacterium tuberculosis*. *Antimicrob. Agents Chemother.* **58**, 2979-2981 (2014).

201. J. A. Coker, Recent advances in understanding extremophiles. *F1000 Res.* **8**, F1000 Faculty Rev:1917 (2019).

202. O. Lewinson, E. Padan, E. Bibi, Alkalitolerance: A biological function for a multidrug transporter in pH homeostasis. *Proc. Natl. Acad. Sci. U. S. A.* **101**, 14073–14078 (2004).

203. K. N. W. Deininger, *et al.*, A requirement of TolC and MDR efflux pumps for acid adaptation and GadAB induction in *Escherichia coli*. *PLoS One* **6**, 1–7 (2011).

204. A. A. Kermani, *et al.*, Crystal structures of bacterial small multidrug resistance transporter EmrE in complex with structurally diverse substrates. *eLife* **11**, e76766 (2022).

205. D. H. Nies, Efflux-mediated heavy metal resistance in prokaryotes. *FEMS Microbiol. Rev.* **27**, 313–339 (2003).

206. O. Conroy, E. -H. Kim, M. M. McEvoy, C. Rensing, Differing ability to transport nonmetal substrates by two RND-type metal exporters. *FEMS Microbiol. Lett.* **308**, 115–122 (2010).

207. J. Sikkema, J. A. M. de Bont, B. Poolman, Mechanisms of membrane toxicity of hydrocarbons. *Microbiol. Rev.* **59**, 201–222 (1995).

208. X. Z. Li, L. Zhang, K. Poole, Role of the multidrug efflux systems of *Pseudomonas aeruginosa* in organic solvent tolerance. *J. Bacteriol.* **180**, 2987–2991 (1998).

209. X. Z. Li, K. Poole, Organic solvent-tolerant mutants of *Pseudomonas aeruginosa* display multiple antibiotic resistance. *Can. J. Microbiol.* **45**, 18 (1999).

210. F. J. Weber, L. P. Ooijkaas, R. M. Schemen, S. Hartmans, J. A. de Bont, Adaptation of *Pseudomonas putida* S12 to high concentrations of styrene and other organic solvents. *Appl. Environ. Microbiol.* **59**, 3502-3504 (1993).

211. A. Rojas, *et al.*, Three efflux pumps are required to provide efficient tolerance to toluene in *Pseudomonas putida* DOT-T1E. *J. Bacteriol.* **183**, 3967-3973 (2001).

212. J. L. Ramos, E. Duque, P. Godoy, A. Segura, Efflux pumps involved in toluene tolerance in *Pseudomonas putida* DOT-T1E. *J. Bacteriol.* **180**, 3323-3329 (1998).

213. L. J. V. Piddock, Clinically relevant chromosomally encoded multidrug resistance efflux pumps in bacteria. *Clin. Microbiol. Rev.* **19**, 382–402 (2006).

214. L. J. V. Piddock, Multidrug-resistance efflux pumps- not just for resistance. *Nat. Rev. Microbiol.* **4**, 629-636 (2006).

215. I. Alav, J. M. Sutton, K. M. Rahman, Role of bacterial efflux pumps in biofilm formation. *J. Antimicrob. Chemother.* **73**, 2003–2020 (2018).

216. D. B. Kell, N. Swainston, P. Pir, S. G. Oliver, Membrane transporter engineering in industrial biotechnology and whole cell biocatalysis. *Trends Biotechnol.* **33**, 237–246 (2015).

217. S. F. Altschul, W. Gish, W. Miller, E. W. Myers, D. J. Lipman, Basic local alignment search tool. *J. Mol. Biol.* **215**, 403–410 (1990).

218. S. F. Altschul, *et al.*, Gapped BLAST and PSI-BLAST: a new generation of protein database search programs. *Nucleic Acids Res.* **25**, 3389–3402 (1997).

219. S. R. Eddy, Profile hidden Markov models. *Bioinformatics* **14**, 755–763 (1998).

220. R. D. Finn, J. Clements, S. R. Eddy, HMMER web server: Interactive sequence similarity searching. *Nucleic Acids Res.* **39**, 29–37 (2011).

221. The Uniprot Consortium, UniProt: The universal protein knowledgebase in 2021. *Nucleic Acids Res.* **49**, D480–D489 (2021).

222. J. Mistry, *et al.*, Pfam: The protein families database in 2021. *Nucleic Acids Res.* **49**, D412–D419 (2021).

223. M. Blum, *et al*., The InterPro protein families and domains database: 20 years on. *Nucleic Acids Res.* **49**, D344–D354 (2021).

224. M. H. Saier Jr, *et al*., The Transporter Classification Database (TCDB): 2021 update. *Nucleic Acids Res.* **49**, D461–D467 (2021).

225. L. D. H. Elbourne, S. G. Tetu, K. A. Hassan, I. T. Paulsen, TransportDB 2.0: A database for exploring membrane transporters in sequenced genomes from all domains of life. *Nucleic Acids Res.* **45**, D320–D324 (2017).

226. M. H. Saier, Jr, I. T. Paulsen, Phylogeny of multidrug transporters. *Semin. Cell Dev. Biol.* **12**, 205–213 (2001).

227. M. H. Saier, Jr, Molecular phylogeny as a basis for the classification of transport proteins from bacteria, archaea and eukarya. *Adv. Microb. Physiol.* **40**, 81–136 (1998).

228. M. Zwama, A. Yamaguchi, K. Nishino, Phylogenetic and functional characterisation of the *Haemophilus influenzae* multidrug efflux pump AcrB. *Commun. Biol.* **2**, 340 (2019).

229. C. L. M. Gilchrist, Y.-H. Chooi, Clinker & Clustermap.Js: Automatic generation of gene cluster comparison figures. *Bioinformatics*. **37**, 2473-2475 (2021)

230. C. K. Saha, R. S. Pires, H. Brolin, M. Delannoy, G. C. Atkinson, FlaGs and webFlaGs: Discovering novel biology through the analysis of gene neighbourhood conservation. *Bioinformatics* **37**, 1312–1314 (2021).

231. K. Ubukata, N. Itoh-Yamashita, M. Konno, Cloning and expression of the *norA* gene for fluoroquinolone resistance in *Staphylococcus aureus*. *Antimicrob. Agents Chemother.* **33**, 1535–1539 (1989).

232. Y. Morita, *et al.*, NorM, a putative multidrug efflux protein, of *Vibrio parahaemolyticus* and its homolog in *Escherichia coli*. *Antimicrob. Agents Chemother.* **42**, 1778–1782 (1998).

233. Y. Yamada, K. Hideka, S. Shiota, T. Kuroda, T. Tsuchiya, Gene cloning and characterization of SdrM, a chromosomally-encoded multidrug efflux pump, from *Staphylococcus aureus*. *Biol. Pharm. Bull.* **29**, 554–556 (2006).

234. X.-Z. Su, J. Chen, T. Mizushima, T. Tsuchiya, AbeM, an H+-coupled *Acinetobacter baumannii* multidrug efflux pump belonging to the MATE family of transporters. *Antimicrob. Agents Chemother.* **49**, 4362–4364 (2005).

235. K. A. Hassan, *et al.*, Roles of DHA2 family transporters in drug resistance and iron homeostasis in *Acinetobacter* spp. *J. Mol. Microbiol. Biotechnol.* **20**, 116–124 (2011).

236. L. Li, S. G. Tetu, I. T. Paulsen, K. A. Hassan, “A Transcriptomic Approach to Identify Novel Drug Efflux Pumps in Bacteria” in *Bacterial Multidrug Exporters*, Methods in Molecular Biology., A. Yamaguchi, K. Nishino, Eds. (Springer New York, 2018), pp. 221–235.

237. K. A. Hassan, *et al.*, An ace up their sleeve: A transcriptomic approach exposes the AceI efflux protein of *Acinetobacter baumannii* and reveals the drug efflux potential hidden in many microbial pathogens. *Front. Microbiol.* **6**, 1–6 (2015).

238. A. K. Cain, *et al.*, A decade of advances in transposon-insertion sequencing. *Nat. Rev. Genet.* **21**, 526–540 (2020).

239. L. Li, *et al.*, Genomic fitness profiling of *Acinetobacter baumannii* reveals modes of action for common biocides and mechanisms of biocide-antibiotic antagonism. *Prepr. available Res. Sq.*, 1–16 (2021).

240. K. A. Hassan, *et al.*, Fluorescence-based flow sorting in parallel with transposon insertion site sequencing identifies multidrug efflux systems in *Acinetobacter baumannii. mBio* **7**, 3–8 (2016).

241. J. M. A. Blair, L. J. V. Piddock, How to measure export *via* bacterial multidrug resistance efflux pumps. *mBio* **7**, 1–6 (2016).

242. I. Wiegand, K. Hilpert, R. E. W. Hancock, Agar and broth dilution methods to determine the minimal inhibitory concentration (MIC) of antimicrobial substances. *Nat. Protoc.* **3**, 163–175 (2008).

243. B. R. Bochner, P. Gadzinski, E. Panomitros, Phenotype microarrays for high-throughput phenotypic testing and assay of gene function. *Genome Res.* **11**, 1246–1255 (2001).

244. B. A. Mitchell, I. T. Paulsen, M. H. Brown, R. A. Skurray, Bioenergetics of the staphylococcal multidrug export protein QacA. *J. Biol. Chem.* **274**, 3541–3548 (1999).

245. J. Cama, *et al.*, Single-cell microfluidics facilitates the rapid quantification of antibiotic accumulation in Gram-negative bacteria. *Lab Chip.* **20**, 2765–2775 (2020).

246. L. Paixão, *et al.*, Fluorometric determination of ethidium bromide efflux kinetics in *Escherichia coli*. *J. Biol. Eng.* **3**, 18 (2009).

247. M. A. Sánchez-Romero, J. Casadesús, Contribution of phenotypic heterogeneity to adaptive antibiotic resistance. *Proc. Natl. Acad. Sci.* **111**, 355–360 (2014).

248. E. E. Whittle, *et al.*, Flow cytometric analysis of efflux by dye accumulation. *Front. Microbiol*. **10** (2019).

249. A. R. Brown, *et al.*, A Mass spectrometry-based assay for improved quantitative measurements of efflux pump inhibition. *PLoS One* **10**, e0124814 (2015).

250. G. Szakonyi, *et al.*, A genomic strategy for cloning, expressing and purifying efflux proteins of the major facilitator superfamily. *J. Antimicrob. Chemother.* **59**, 1265–1270 (2007).

251. A. Ward, *et al.*, "The amplified expression, identification, purification, assay and properties of hexahistidine-tagged bacterial membrane transport proteins" in *Membrane Transport - A Practical Approach*, 1st Edition, S. A. Baldwin Ed. (Oxford University Press, 2000) pp. 141–166.

252. G. G. Privé, Detergents for the stabilization and crystallization of membrane proteins. *Methods* **41**, 388–397 (2007).

253. S. M. Smith, "Strategies for the Purification of Membrane Proteins" in *Protein Chromatography.* Methods in Molecular Biology, D. Walls, S. T. Loughran, Eds. (Springer New York, 2017), pp. 389–400.

254. A. Ward, *et al.*, *Membrane Transport: A Practical Approach* (2000).

255. A. J. Miles, B. A. Wallace, Circular dichroism spectroscopy of membrane proteins. *Chem. Soc. Rev.* **45**, 4859–4872 (2016).

256. K. Gao, R. Oerlemans, M. R. Groves, Theory and applications of differential scanning fluorimetry in early-stage drug discovery. *Biophys. Rev.* **12**, 85–104 (2020).

257. V. Kotov, *et al.*, High-throughput stability screening for detergent-solubilized membrane proteins. *Sci. Rep.* **9**, 10379 (2019).

258. C. Cecchetti, *et al.*, A novel high-throughput screen for identifying lipids that stabilise membrane proteins in detergent based solution. *PLoS One* **16**, e0254118 (2021).

259. R. Goers, *et al.*, Optimized reconstitution of membrane proteins into synthetic membranes. *Commun. Chem.* **1,** 35 (2018).

260. V. V Rybenkov, *et al.*, The whole is bigger than the sum of its parts: Drug transport in the context of two membranes with active efflux. *Chem. Rev.* **121**, 5597–5631 (2021).

261. K. Kano, J. H. Fendler, Pyranine as a sensitive pH probe for liposome interiors and surfaces. pH gradients across phospholipid vesicles. *Biochim. Biophys. Acta - Biomembr.* **509**, 289–299 (1978).

262. K. Bartels, T. Lasitza-Male, H. Hofmann, C. Löw, Single-molecule FRET of membrane transport proteins. *ChemBioChem* **22**, 2657–2671 (2021).

263. Y. Zhu, L. He, Y. Liu, Y. Zhao, X. C. Zhang, smFRET probing reveals substrate-dependent conformational dynamics of *E. coli* multidrug MdfA. *Biophys. J.* **116**, 2296–2303 (2019).

264. M. Nachiappan, *et al.*, "3D structural determination of macromolecules using X-ray crystallography methods" in *Molecular docking for computer-aided drug design*. S.M Coumar, Ed. (Academic Press, 2021), pp. 119–140.

265. E. P. Carpenter, K. Beis, A. D. Cameron, S. Iwata, Overcoming the challenges of membrane protein crystallography. *Curr. Opin. Struct. Biol.* **18**, 581–586 (2008).

266. A. A. Kermani, A guide to membrane protein X-ray crystallography. *FEBS J.* **288**, 5788–5804 (2021).

267. S. Murakami, R. Nakashima, E. Yamashita, T. Matsumoto, A. Yamaguchi, Crystal structures of a multidrug transporter reveal a functionally rotating mechanism. *Nature* **443**, 173–179 (2006).

268. V. Yeh, A. Goode, B. B. Bonev, Membrane protein structure determination and characterisation by solution and solid-state NMR. *Biology (Basel).* **9**, 396 (2020).

269. A. A. Shcherbakov, *et al.*, Structure and dynamics of the drug-bound bacterial transporter EmrE in lipid bilayers. *Nat. Commun.* **12**, 172 (2021).

270. K. Murata, M. Wolf, Cryo-electron microscopy for structural analysis of dynamic biological macromolecules. *Biochim. Biophys. Acta. Gen. Subj.* **1862**, 324–334 (2018).

271. M. W. Beijerinck, Pigments as products of oxidation by bacterial action. *K. Ned. Akad. van Wet. Proc. Ser. B Phys. Sci.* **13**, 1066–1077 (1910).

272. J. Brisou, A. R. Prévot, Studies on bacterial taxonomy. X. The revision of species under Acromobacter group. *Ann. Inst. Pasteur (Paris).* **86**, 722–728 (1954).

273. A. C. Parte, J. S. Carbasse, J. P. Meier-Kolthoff, L. C. Reimer, M. Göker, List of Prokaryotic names with Standing in Nomenclature (LPSN) moves to the DSMZ. *Int. J. Syst. Evol. Bacteriol.* **70**, 5607–5612 (2020).

274. A. Al Atrouni, M.-L. Joly-Guillou, M. Hamze, M. Kempf, Reservoirs of non-baumannii *Acinetobacter* species. *Front. Microbiol.* **7**, 49 (2016).

275. P. Villalón, *et al.*, Dynamics of a sporadic nosocomial *Acinetobacter calcoaceticus – Acinetobacter baumannii* complex population. *Front. Microbiol.* **10**, 593 (2019).

276. J.-L. García-Garmendia, *et al.*, Risk factors for *Acinetobacter baumannii* nosocomial bacteremia in critically ill patients: A cohort study. *Clin. Infect. Dis.* **33**, 939–946 (2001).

277. C. Dexter, G. L. Murray, I. T. Paulsen, A. Y. Peleg, Community-acquired *Acinetobacter baumannii*: Clinical characteristics, epidemiology and pathogenesis. *Expert Rev. Anti. Infect. Ther.* **13**, 567–573 (2015).

278. M. Eveillard, M. Kempf, O. Belmonte, H. Pailhoriès, M.-L. Joly-Guillou, Reservoirs of *Acinetobacter baumannii* outside the hospital and potential involvement in emerging human community-acquired infections. *Int. J. Infect. Dis.* **17**, e802–e805 (2013).

279. E. Bergogne-Bérézin, K. J. Towner, *Acinetobacter* spp. as nosocomial pathogens: Microbiological, clinical, and epidemiological features. *Clin. Microbiol. Rev.* **9**, 148–165 (1996).

280. L. Diancourt, V. Passet, A. Nemec, L. Dijkshoorn, S. Brisse, The population structure of *Acinetobacter baumannii*: Expanding multiresistant clones from an ancestral susceptible genetic pool. *PLoS One* **5**, e10034 (2010).

281. M. Hamidian, R. M. Hall, AbaR4 replaces AbaR3 in a carbapenem-resistant *Acinetobacter baumannii* isolate belonging to global clone 1 from an Australian hospital. *J. Antimicrob. Chemother.* **66**, 2484–2491 (2011).

282. M. Hamidian, S. J. Nigro, Emergence, molecular mechanisms and global spread of carbapenem-resistant *Acinetobacter baumannii*. *Microb. genomics* **5**, e000306 (2019).

283. P. Visca, H. Seifert, K. J. Towner, *Acinetobacter* infection- an emerging threat to human health. *IUBMB Life* **63**, 1048–1054 (2011).

284. L. D. de M. Carrasco, *et al.*, Polymyxin resistance among XDR ST1 carbapenem-resistant *Acinetobacter baumannii* clone expanding in a teaching hospital. *Front. Microbiol.* **12**, 622704 (2021).

285. M. J. Satlin, *et al.*, Clinical and Laboratory Standards Institute and European Committee on Antimicrobial Susceptibility Testing position statements on polymyxin b and colistin clinical breakpoints. *Clin. Infect. Dis.* **71**, e523–e529 (2020).

286. M. Hagihara, S. T. Housman, D. P. Nicolau, J. L. Kuti, *In vitro* pharmacodynamics of polymyxin B and tigecycline alone and in combination against carbapenem-resistant *Acinetobacter baumannii*. *Antimicrob. Agents Chemother.* **58**, 874–879 (2014).

287. J. Zhang, *et al.*, Genomic and phenotypic evolution of tigecycline-resistant *Acinetobacter baumannii* in critically ill patients. *Microbiol. Spectr.* **10**, e01593-21 (2022).

288. Y. Cai, D. Chai, R. Wang, B. Liang, N. Bai, Colistin resistance of *Acinetobacter baumannii:* clinical reports, mechanisms and antimicrobial strategies. *J. Antimicrob. Chemother.* **67**, 1607–1615 (2012).

289. T. He, *et al.*, Emergence of plasmid-mediated high-level tigecycline resistance genes in animals and humans. *Nat. Microbiol.* **4**, 1450–1456 (2019).

290. Centers for Disease Control and Prevention, "Antibiotic resistance threats in the United States 2019" (2019).

291. C. M. Harding, S. W. Hennon, M. F. Feldman, Uncovering the mechanisms of *Acinetobacter baumannii* virulence. *Nat. Rev. Microbiol.* **16**, 91–102 (2018).

292. F. C. Morris, C. Dexter, X. Kostoulias, M. I. Uddin, A. Y. Peleg, The mechanisms of disease caused by *Acinetobacter baumannii. Front. Microbiol.* **10**, 1601 (2019).

293. M. Giannouli, *et al.*, Virulence-related traits of epidemic *Acinetobacter baumannii* strains belonging to the international clonal lineages I-III and to the emerging genotypes ST25 and ST78. *BMC Infect. Dis.* **13**, 282 (2013).

294. L. C. S. Antunes, F. Imperi, A. Carattoli, P. Visca, Deciphering the multifactorial nature of *Acinetobacter baumannii* pathogenicity. *PLoS One* **6**, e22674 (2011).

295. J. M. Boll, *et al.*, Reinforcing lipid A acylation on the cell surface of *Acinetobacter baumannii* promotes cationic antimicrobial peptide resistance and desiccation survival. *mBio* **6**, e00478-15 (2015).

296. P. Espinal, S. Martí, J. Vila, Effect of biofilm formation on the survival of *Acinetobacter baumannii* on dry surfaces. *J. Hosp. Infect.* **80**, 56–60 (2012).

297. C. M. Gayoso, *et al.*, Molecular mechanisms involved in the response to desiccation stress and persistence in *Acinetobacter baumannii*. *J. Proteome Res.* **13**, 460–476 (2014).

298. J. Aranda, *et al.*, *Acinetobacter baumann*nii RecA protein in repair of DNA damage, antimicrobial resistance, general stress response, and virulence. *J. Bacteriol.* **193**, 3740–3747 (2011).

299. C. C. Nwugo, *et al.*, Effect of ethanol on differential protein production and expression of potential virulence functions in the opportunistic pathogen *Acinetobacter baumannii*. *PLoS One* **7**, e51936 (2012).

300. L. Camarena, V. Bruno, G. Euskirchen, S. Poggio, M. Snyder, Molecular mechanisms of ethanol-induced pathogenesis revealed by RNA-sequencing. *PLOS Pathog.* **6**, e1000834 (2010).

301. C. Greene, J. Wu, A. H. Rickard, C. Xi, Evaluation of the ability of *Acinetobacter baumannii* to form biofilms on six different biomedical relevant surfaces. *Lett. Appl. Microbiol.* **63**, 233–239 (2016).

302. M. G. Thompson, *et al.*, Validation of a novel murine wound model of *Acinetobacter baumannii* infection. *Antimicrob. Agents Chemother.* **58**, 1332–1342 (2014).

303. A. P. Tomaras, C. W. Dorsey, R. E. Edelmann, L. A. Actis, Attachment to and biofilm formation on abiotic surfaces by *Acinetobacter baumannii*: Involvement of a novel chaperone-usher pili assembly system. *Microbiology* **149**, 3473–3484 (2003).

304. T. W. Loehfelm, N. R. Luke, A. A. Campagnari, Identification and characterization of an *Acinetobacter baumannii* biofilm-associated protein. *J. Bacteriol.* **190**, 1036–1044 (2008).

305. J. A. Iwashkiw, *et al.*, Identification of a general *O*-linked protein glycosylation system in *Acinetobacter baumannii* and its role in virulence and biofilm formation. *PLoS Pathog.* **8**, e1002758 (2012).

306. A. H. K. Choi, L. Slamti, F. Y. Avci, G. B. Pier, T. Maira-Litrán, The *pgaABCD* locus of *Acinetobacter baumannii* encodes the production of poly-β-1-6-N-acetylglucosamine, which is critical for biofilm formation. *J. Bacteriol.* **191**, 5953–5963 (2009).

307. L. V Bentancor, A. Camacho-Peiro, C. Bozkurt-Guzel, G. B. Pier, T. Maira-Litrán, Identification of Ata, a multifunctional trimeric autotransporter of *Acinetobacter baumannii*. *J. Bacteriol.* **194**, 3950–3960 (2012).

308. B. A. Eijkelkamp, *et al.*, Adherence and motility characteristics of clinical *Acinetobacter baumannii* isolates. *FEMS Microbiol. Lett.* **323**, 44–51 (2011).

309. K. A. Tipton, D. Dimitrova, P. N. Rather, Phase-variable control of multiple phenotypes in *Acinetobacter baumannii* strain AB5075. *J. Bacteriol.* **197**, 2593–2599 (2015).

310. T. A. Russo, *et al.*, The K1 capsular polysaccharide of *Acinetobacter baumannii* strain 307-0294 is a major virulence factor. *Infect. Immun.* **78**, 3993–4000 (2010).

311. C. M. Harding, *et al.*, *Acinetobacter* strains carry two functional oligosaccharyltransferases, one devoted exclusively to type IV pilin, and the other one dedicated to *O*-glycosylation of multiple proteins. *Mol. Microbiol.* **96**, 1023–1041 (2015).

312. K. H. Piepenbrink, *et al.*, Structural diversity in the type IV pili of multidrug-resistant *Acinetobacter*. *J. Biol. Chem.* **291**, 22924–22935 (2016).

313. R. G. Lees-Miller, *et al.*, A common pathway for *O*-linked protein-glycosylation and synthesis of capsule in *Acinetobacter baumannii*. *Mol. Microbiol.* **89**, 816–830 (2013).

314. J. A. Gaddy, *et al.*, Role of acinetobactin-mediated iron acquisition functions in the interaction of *Acinetobacter baumannii* strain ATCC 19606T with human lung epithelial cells, *Galleria mellonella* caterpillars, and mice. *Infect. Immun.* **80**, 1015–1024 (2012).

315. A. Proschak, *et al.*, Structure and biosynthesis of fimsbactins A–F, siderophores from *Acinetobacter baumannii* and *Acinetobacter baylyi*. *Chembiochem* **14**, 633–638 (2013).

316. W. F. Penwell, *et al.*, Discovery and characterization of new hydroxamate siderophores, baumannoferrin A and B, produced by *Acinetobacter baumannii*. *Chembiochem* **16**, 1896–1904 (2015).

317. L. E. Hesse, Z. R. Lonergan, W. N. Beavers, E. P. Skaar, The *Acinetobacter baumannii* Znu system overcomes host-imposed nutrient zinc limitation. *Infect. Immun.* **87**, e00746-19 (2019).

318. B. L. Nairn, *et al.*, The response of *Acinetobacter baumannii* to zinc starvation. *Cell Host Microbe* **19**, 826–836 (2016).

319. S. F. Alquethamy, *et al.*, The role of zinc efflux during *Acinetobacter baumannii* infection. *ACS Infect. Dis.* **6,** 150-158 (2020).

320. L. J. Juttukonda, E. P. Skaar, Manganese homeostasis and utilization in pathogenic bacteria. *Mol. Microbiol.* **97**, 216–228 (2015).

321. L. J. Juttukonda, W. J. Chazin, E. P. Skaar, *Acinetobacter baumannii* coordinates urea metabolism with metal import to resist host-mediated metal limitation. *mBio* **7**, e01475-16 (2016).

322. B. S. Weber, R. L. Kinsella, C. M. Harding, M. F. Feldman, The secrets of *Acinetobacter* secretion. *Trends Microbiol.* **25**, 532–545 (2017).

323. C. M. Harding, *et al.*, Pathogenic *Acinetobacter* species have a functional type I secretion system and contact-dependent inhibition systems. *J. Biol. Chem.* **292**, 9075–9087 (2017).

324. T. L. Johnson, U. Waack, S. Smith, H. Mobley, M. Sandkvist, *Acinetobacter baumannii* is dependent on the type II secretion system and its substrate LipA for lipid utilization and *in vivo* fitness. *J. Bacteriol.* **198**, 711–719 (2015).

325. C.-C. Liu, H.-Y. Kuo, C. Y. Tang, K.-C. Chang, M.-L. Liou, Prevalence and mapping of a plasmid encoding a type IV secretion system in *Acinetobacter baumannii. Genomics* **104**, 215–223 (2014).

326. M. D. Carruthers, P. A. Nicholson, E. N. Tracy, R. S. Munson, Jr, *Acinetobacter baumannii* utilizes a type VI secretion system for bacterial competition. *PLoS One* **8**, e59388 (2013).

327. S. Corvec, *et al.*, AmpC cephalosporinase hyperproduction in *Acinetobacter baumannii* clinical strains. *J. Antimicrob. Chemother.* **52**, 629–635 (2003).

328. L. Krizova, L. Poirel, P. Nordmann, A. Nemec, TEM-1 β-lactamase as a source of resistance to sulbactam in clinical strains of *Acinetobacter baumannii*. *J. Antimicrob. Chemother.* **68**, 2786–2791 (2013).

329. A. Endimiani, *et al.*, Spread in an italian hospital of a clonal *Acinetobacter baumannii* strain producing the TEM-92 extended-spectrum β-lactamase. *Antimicrob. Agents Chemother.* **51**, 2211–2214 (2007).

330. T. Naas, F. Namdari, H. Réglier-Poupet, C. Poyart, P. Nordmann, Panresistant extended-spectrum β-lactamase SHV-5-producing *Acinetobacter baumannii* from New York City. *J. Antimicrob. Chemother.* **60**, 1174–1176 (2007).

331. N. Nagano, Y. Nagano, C. Cordevant, N. Shibata, Y. Arakawa, Nosocomial transmission of CTX-M-2 β-lactamase-producing *Acinetobacter baumannii* in a neurosurgery ward. *J. Clin. Microbiol.* **42**, 3978–3984 (2004).

332. A. Potron, L. S. Munoz-Price, P. Nordmann, T. Cleary, L. Poirel, Genetic features of CTX-M-15-producing *Acinetobacter baumannii* from Haiti. *Antimicrob. Agents Chemother.* **55**, 5946–5948 (2011).

333. L. Poirel, *et al.*, Identification of the novel narrow-spectrum β-lactamase SCO-1 in *Acinetobacter* spp. from Argentina. *Antimicrob. Agents Chemother.* **51**, 2179–2184 (2007).

334. S. H. Jeong, *et al.*, Investigation of a nosocomial outbreak of *Acinetobacter baumannii* producing PER-1 extended-spectrum β-lactamase in an intensive care unit. *J. Hosp. Infect.* **59**, 242–248 (2005).

335. F. Pasterán, *et al.*, Emergence of PER-2 and VEB-1a in *Acinetobacter baumannii* strains in the Americas. *Antimicrob. Agents Chemother.* **50**, 3222–3224 (2006).

336. R. A. Bonnin, *et al.*, PER-7, an extended-spectrum β-Lactamase with increased activity toward broad-spectrum cephalosporins in *Acinetobacter baumannii*. *Antimicrob. Agents Chemother.* **55**, 2424–2427 (2011).

337. T. Naas, *et al.*, VEB-1 Extended-spectrum β-lactamase-producing *Acinetobacter baumannii*, France. *Emerg. Infect. Dis.* **12**, 1214–1222 (2006).

338. T. Martinez, I. Martinez, G. J. Vazquez, E. E. Aquino, I. E. Robledo, Genetic environment of the KPC gene in *Acinetobacter baumannii* ST2 clone from Puerto Rico and genomic insights into its drug resistance. *J. Med. Microbiol.* **65**, 784–792 (2016).

339. I. E. Robledo, *et al.*, Detection of KPC in *Acinetobacter* spp. in Puerto Rico. *Antimicrob. Agents Chemother.* **54**, 1354–1357 (2010).

340. M. H. Al-Agamy, *et al.*, First detection of GES-5 carbapenemase-producing *Acinetobacter baumannii* isolate. *Microb. Drug Resist.* **23**, 556–562 (2017).

341. C. Moubareck, S. Brémont, M.-C. Conroy, P. Courvalin, T. Lambert, GES-11, a novel integron-associated GES variant in *Acinetobacter baumannii*. *Antimicrob. Agents Chemother.* **53**, 3579–3581 (2009).

342. P. Bogaerts, *et al.*, GES extended-spectrum β-lactamases in *Acinetobacter baumannii* isolates in Belgium. *Antimicrob. Agents Chemother.* **54**, 4872–4878 (2010).

343. M. S. Ramírez, S. Piñeiro, A. I. S. Group, D. Centrón, Novel insights about class 2 integrons from experimental and genomic epidemiology. *Antimicrob. Agents Chemother.* **54**, 699–706 (2010).

344. A. Potron, L. Poirel, J. Croizé, V. Chanteperdrix, P. Nordmann, Genetic and biochemical characterization of the first extended-spectrum CARB-type ß-Lactamase, RTG-4, from *Acinetobacter baumannii*. *Antimicrob. Agents Chemother.* **53**, 3010–3016 (2009).

345. M. L. Riccio, *et al.*, Characterization of the metallo-β-lactamase determinant of *Acinetobacter baumannii* AC-54/97 reveals the existence of *bla*(IMP) allelic variants carried by gene cassettes of different phylogeny. *Antimicrob. Agents Chemother.* **44**, 1229–1235 (2000).

346. Y. W. Chu, *et al.*, IMP-4, a novel metallo-β-lactamase from nosocomial *Acinetobacter* spp. collected in Hong Kong between 1994 and 1998. *Antimicrob. Agents Chemother.* **45**, 710–714 (2001).

347. T. H. Koh, L.-H. Sng, G. C. Y. Wang, L.-Y. Hsu, Y. Zhao, IMP-4 and OXA β-lactamases in *Acinetobacter baumannii* from Singapore. *J. Antimicrob. Chemother.* **59**, 627–632 (2007).

348. M. C. B. Tognim, A. C. Gales, A. P. Penteado, S. Silbert, H. S. Sader, Dissemination of IMP-1 metallo-β-lactamase-producing *Acinetobacter* species in a Brazilian teaching hospital. *Infect. Control Hosp. Epidemiol.* **27**, 742–747 (2006).

349. A. C. Gales, M. C. B. Tognim, A. O. Reis, R. N. Jones, H. S. Sader, Emergence of an IMP-like metallo-enzyme in an *Acinetobacter baumannii* clinical strain from a Brazilian teaching hospital. *Diagn. Microbiol. Infect. Dis.* **45**, 77–79 (2003).

350. M. Yamamoto, *et al.*, Interspecies dissemination of a novel class 1 integron carrying *bla*(IMP-19) among *Acinetobacter* species in Japan. *J. Antimicrob. Chemother.* **66**, 2480–2483 (2011).

351. Y. Chen, Z. Zhou, Y. Jiang, Y. Yu, Emergence of NDM-1-producing *Acinetobacter baumannii* in China. *J. Antimicrob. Chemother.* **66**, 1255–1259 (2011).

352. P. Espinal, *et al.*, Dissemination of an NDM-2-producing *Acinetobacter baumannii* clone in an Israeli rehabilitation center. *Antimicrob. Agents Chemother.* **55**, 5396–5398 (2011).

353. M. Kumar, Identification of a novel NDM variant, *blaNDM-3*, from a multidrug-resistant *Acinetobacter baumannii*. *Infect. Control Hosp. Epidemiol.* **37**, 747–748 (2016).

354. A. Tsakris, *et al.*, VIM-1 metallo-β-lactamase in *Acinetobacter baumannii*. *Emerg. Infect. Dis.* **12**, 981–983 (2006).

355. J. H. Yum, *et al.*, Molecular characterization of metallo-β-lactamase-producing *Acinetobacter baumannii* and *Acinetobacter* genomospecies 3 from Korea: Identification of two new integrons carrying the *bla*(VIM-2) gene cassettes. *J. Antimicrob. Chemother.* **49**, 837–840 (2002).

356. M.-F. Lee, C.-F. Peng, H.-J. Hsu, Y.-H. Chen, Molecular characterisation of the metallo-β-lactamase genes in imipenem-resistant Gram-negative bacteria from a university hospital in southern Taiwan. *Int. J. Antimicrob. Agents* **32**, 475–480 (2008).

357. A. Tsakris, *et al.*, Clusters of imipenem-resistant *Acinetobacter baumannii* clones producing different carbapenemases in an intensive care unit. *Clin. Microbiol. Infect.* **14**, 588–594 (2008).

358. K. Lee, *et al.*, Novel acquired metallo-β-lactamase gene, *bla*(SIM-1), in a class 1 integron from *Acinetobacter baumannii* clinical isolates from Korea. *Antimicrob. Agents Chemother.* **49**, 4485–4491 (2005).

359. C.-R. Lee, *et al.*, Biology of *Acinetobacter baumannii*: Pathogenesis, antibiotic resistance mechanisms, and prospective treatment options. *Front. Cell. Infect. Microbiol.* **7**, 55 (2017).

360. G. Bou, J. Martínez-Beltrán, Cloning, nucleotide sequencing, and analysis of the gene encoding an AmpC β-lactamase in *Acinetobacter baumannii*. *Antimicrob. Agents Chemother.* **44**, 428–432 (2000).

361. C. Héritier, L. Poirel, P. Nordmann, Cephalosporinase over-expression resulting from insertion of IS*Aba1* in *Acinetobacter baumannii*. *Clin. Microbiol. Infect. Off. Publ. Eur. Soc. Clin. Microbiol. Infect. Dis.* **12**, 123–130 (2006).

362. J.-M. Rodríguez-Martínez, L. Poirel, P. Nordmann, Genetic and functional variability of AmpC-type β-lactamases from *Acinetobacter baumannii*. *Antimicrob. Agents Chemother.* **54**, 4930–4933 (2010).

363. P. D. Mugnier, L. Poirel, T. Naas, P. Nordmann, Worldwide dissemination of the *bla*OXA-23 carbapenemase gene of *Acinetobacter baumannii*. *Emerg. Infect. Dis.* **16**, 35–40 (2010).

364. H. M. Donald, W. Scaife, S. G. Amyes, H. K. Young, Sequence analysis of ARI-1, a novel OXA β-lactamase, responsible for imipenem resistance in *Acinetobacter baumannii* 6B92. *Antimicrob. Agents Chemother.* **44**, 196–199 (2000).

365. J. Vila, M. Navia, J. Ruiz, C. Casals, Cloning and nucleotide sequence analysis of a gene encoding an OXA-derived β-lactamase in *Acinetobacter baumannii*. *Antimicrob. Agents Chemother.* **41**, 2757–2759 (1997).

366. M. Giannouli, *et al.*, Molecular epidemiology of carbapenem-resistant *Acinetobacter baumannii* strains in intensive care units of multiple Mediterranean hospitals. *J. Antimicrob. Chemother.* **63**, 828–830 (2009).

367. M. M. Navia, J. Ruiz, J. Vila, Characterization of an integron carrying a new class D β-lactamase (OXA-37) in *Acinetobacter baumannii*. *Microb. Drug Resist.* **8**, 261–265 (2002).

368. G. Bou, A. Oliver, J. Martínez-Beltrán, OXA-24, a novel class D β-lactamase with carbapenemase activity in an *Acinetobacter baumannii* clinical strain. *Antimicrob. Agents Chemother.* **44**, 1556–1561 (2000).

369. S. Brown, H. K. Young, S. G. B. Amyes, Characterisation of OXA-51, a novel class D carbapenemase found in genetically unrelated clinical strains of *Acinetobacter baumannii* from Argentina. *Clin. Microbiol. Infect.* **11**, 15–23 (2005).

370. L. Poirel, *et al.*, OXA-58, a novel class D β-lactamase involved in resistance to carbapenems in *Acinetobacter baumannii*. *Antimicrob. Agents Chemother.* **49**, 202–208 (2005).

371. P. G. Higgins, L. Poirel, M. Lehmann, P. Nordmann, H. Seifert, OXA-143, a novel carbapenem-hydrolyzing class D β-lactamase in *Acinetobacter baumannii*. *Antimicrob. Agents Chemother.* **53**, 5035–5038 (2009).

372. P. G. Higgins, *et al.*, OXA-235, a novel class D β-lactamase involved in resistance to carbapenems in *Acinetobacter baumannii*. *Antimicrob. Agents Chemother.* **57**, 2121–2126 (2013).

373. L. Poirel, P. Nordmann, Carbapenem resistance in *Acinetobacter baumannii*: Mechanisms and epidemiology, *Clin. Microbiol. Infect.* **12**, 826–836 (2006).

374. J. F. Turton, *et al.*, The role of IS*Aba1* in expression of OXA carbapenemase genes in *Acinetobacter baumannii*. *FEMS Microbiol. Lett.* **258**, 72–77 (2006).

375. R. J. Seward, T. Lambert, K. J. Towner, Molecular epidemiology of aminoglycoside resistance in *Acinetobacter* spp. *J. Med. Microbiol.* **47**, 455–462 (1998).

376. Y. Doi, *et al.*, Spread of novel aminoglycoside resistance gene *aac*(6')-*Iad* among *Acinetobacter* clinical isolates in Japan. *Antimicrob. Agents Chemother.* **48**, 2075–2080 (2004).

377. A. Nemec, L. Dolzani, S. Brisse, P. van den Broek, L. Dijkshoorn, Diversity of aminoglycoside-resistance genes and their association with class 1 integrons among strains of pan-European *Acinetobacter baumannii* clones. *J. Med. Microbiol.* **53**, 1233–1240 (2004).

378. Y. J. Cho, *et al.*, Genetic basis of resistance to aminoglycosides in *Acinetobacter* spp. and spread of *armA* in *Acinetobacter baumannii* sequence group 1 in Korean hospitals. *Diagn. Microbiol. Infect. Dis.* **64**, 185–190 (2009).

379. L. Gallego, K. J. Towner, Carriage of class 1 integrons and antibiotic resistance in clinical isolates of *Acinetobacter baumannii* from northern Spain. *J. Med. Microbiol.* **50**, 71–77 (2001).

380. B. G. Elisha, L. M. Steyn, Identification of an *Acinetobacter baumannii* gene region with sequence and organizational similarity to Tn*2670*. *Plasmid* **25**, 96–104 (1991).

381. E. T. S. Houang, Y.-W. Chu, W.-S. Lo, K.-Y. Chu, A. F. B. Cheng, Epidemiology of rifampin ADP-ribosyltransferase (*arr-2*) and metallo-β-lactamase (*bla*IMP-4) gene cassettes in class 1 integrons in *Acinetobacte*r strains isolated from blood cultures in 1997 to 2000. *Antimicrob. Agents Chemother.* **47**, 1382–1390 (2003).

382. X. Xu, *et al.*, Integron gene cassettes in *Acinetobacter* spp. strains from South China. *Int. J. Antimicrob. Agents* **32**, 441–445 (2008).

383. J. F. Turton, *et al.*, Detection and typing of integrons in epidemic strains of *Acinetobacter baumannii* found in the United Kingdom. *J. Clin. Microbiol.* **43**, 3074–3082 (2005).

384. L. Wang, *et al.*, Novel plasmid-mediated *tet*(X5) gene conferring resistance to tigecycline, eravacycline, and omadacycline in a clinical *Acinetobacter baumannii* isolate. *Antimicrob. Agents Chemother.* **64**, e01326-19 (2019).

385. C. Chen, *et al.*, Spread of *tet*(X5) and *tet*(X6) genes in multidrug-resistant *Acinetobacter baumannii* strains of animal origin. *Vet. Microbiol.* **253**, 108954 (2021).

386. Y. Yu, H. Zhou, Q. Yang, Y. Chen, L. Li, Widespread occurrence of aminoglycoside resistance due to ArmA methylase in imipenem-resistant *Acinetobacter baumannii* isolates in China. *J. Antimicrob. Chemother.* **60**, 454–455 (2007).

387. H. Wisplinghoff, *et al.*, Mutations in *gyrA* and *parC* associated with resistance to fluoroquinolones in epidemiologically defined clinical strains of *Acinetobacter baumannii*. *J. Antimicrob. Chemother.* **51**, 177–180 (2003).

388. J. Vila, J. Ruiz, P. Goñi, A. Marcos, T. Jimenez de Anta, Mutation in the *gyrA* gene of quinolone-resistant clinical isolates of *Acinetobacter baumannii*. *Antimicrob. Agents Chemother.* **39**, 1201–1203 (1995).

389. P. G. Higgins, H. Wisplinghoff, D. Stefanik, H. Seifert, Selection of topoisomerase mutations and overexpression of *adeB* mRNA transcripts during an outbreak of *Acinetobacter baumannii*. *J. Antimicrob. Chemother.* **54**, 821–823 (2004).

390. M. Gehrlein, H. Leying, W. Cullmann, S. Wendt, W. Opferkuch, Imipenem resistance in *Acinetobacter baumanii* is due to altered penicillin-binding proteins. *Chemotherapy* **37**, 405–412 (1991).

391. C. R. Taitt, *et al.*, Antimicrobial resistance determinants in *Acinetobacter baumannii* isolates taken from military treatment facilities. *Antimicrob. Agents Chemother.* **58**, 767–781 (2014).

392. J. H. Moffatt, *et al.*, Colistin resistance in *Acinetobacter baumannii* is mediated by complete loss of lipopolysaccharide production. *Antimicrob. Agents Chemother.* **54**, 4971–4977 (2010).

393. L. A. Arroyo, *et al.*, The *pmrCAB* operon mediates polymyxin resistance in *Acinetobacter baumannii* ATCC 17978 and clinical isolates through phosphoethanolamine modification of lipid A. *Antimicrob. Agents Chemother.* **55**, 3743–3751 (2011).

394. J. M. Pagès, C. E. James, M. Winterhalter, The porin and the permeating antibiotic: A selective diffusion barrier in Gram-negative bacteria. *Nat. Rev. Microbiol.* **6**, 893–903 (2008).

395. J. Vila, S. Martí, J. Sánchez-Céspedes, Porins, efflux pumps and multidrug resistance in *Acinetobacter baumannii*. *J. Antimicrob. Chemother.* **59**, 1210–1215 (2007).

396. Y. Smani, *et al.*, Role of OmpA in the multidrug resistance phenotype of *Acinetobacter baumannii*. *Antimicrob. Agents Chemother.* **58**, 1806–1808 (2014).

397. J. S. Park, *et al.*, Mechanism of anchoring of OmpA protein to the cell wall peptidoglycan of the Gram-negative bacterial outer membrane. *FASEB J.* **26**, 219–228 (2012).

398. G. Bou, G. Cerveró, M. A. Domínguez, C. Quereda, J. Martínez-Beltrán, Characterization of a nosocomial outbreak caused by a multiresistant *Acinetobacter baumannii* strain with a carbapenem-hydrolyzing enzyme: High-level carbapenem resistance in *A. baumannii* is not due solely to the presence of β-lactamases. *J. Clin. Microbiol.* **38**, 3299–3305 (2000).

399. M. del Mar Tomás, *et al.*, Cloning and functional analysis of the gene encoding the 33- to 36-kilodalton outer membrane protein associated with carbapenem resistance in *Acinetobacter baumannii*. *Antimicrob. Agents Chemother.* **49**, 5172–5175 (2005).

400. M. I. Hood, A. C. Jacobs, K. Sayood, P. M. Dunman, E. P. Skaar, *Acinetobacter baumannii* increases tolerance to antibiotics in response to monovalent cations. *Antimicrob. Agents Chemother.* **54**, 1029–1041 (2010).

401. M. Dupont, J.-M. Pagès, D. Lafitte, A. Siroy, C. Bollet, Identification of an OprD Homologue in *Acinetobacter baumannii*. *J. Proteome Res.* **4**, 2386–2390 (2005).

402. J. Quale, S. Bratu, D. Landman, R. Heddurshetti, Molecular epidemiology and mechanisms of carbapenem resistance in *Acinetobacter baumannii* endemic in New York City. *Clin. Infect. Dis.* **37**, 214–220 (2003).

403. S. Magnet, P. Courvalin, T. Lambert, Resistance-nodulation-cell division-type efflux pump involved in aminoglycoside resistance in *Acinetobacter baumannii* strain BM4454. *Antimicrob. Agents Chemother.* **45**, 3375–3380 (2001).

404. L. Damier-Piolle, S. Magnet, S. Brémont, T. Lambert, P. Courvalin, AdeIJK, a resistance-nodulation-cell division pump effluxing multiple antibiotics in *Acinetobacter baumannii*. *Antimicrob. Agents Chemother.* **52**, 557–562 (2008).

405. S. Coyne, N. Rosenfeld, T. Lambert, P. Courvalin, B. Périchon, Overexpression of resistance-nodulation-cell division pump AdeFGH confers multidrug resistance in *Acinetobacter baumannii*. *Antimicrob. Agents Chemother.* **54**, 4389–4393 (2010).

406. K. A. Tipton, M. Farokhyfar, P. N. Rather, Multiple roles for a novel RND-type efflux system in *Acinetobacter baumannii* AB5075. *MicrobiologyOpen* **6**, 1–10 (2017).

407. V. B. Srinivasan, M. Venkataramaiah, A. Mondal, G. Rajamohan, Functional characterization of AbeD, an RND-Type membrane transporter in antimicrobial resistance in *Acinetobacter baumannii*. *PLoS One* **10**, e0141314 (2015).

408. F. G. Adams, U. H. Stroeher, K. A. Hassan, S. Marri, M. H. Brown, Resistance to pentamidine is mediated by AdeAB, regulated by AdeRS, and influenced by growth conditions in *Acinetobacter baumannii* ATCC 17978. *PLoS One* **13**, e0197412 (2018).

409. G. Rajamohan, V. B. Srinivasan, W. A. Gebreyes, Novel role of *Acinetobacter baumannii* RND efflux transporters in mediating decreased susceptibility to biocides. *J. Antimicrob. Chemother.* **65**, 228–232 (2009).

410. S. Coyne, P. Courvalin, B. Périchon, Efflux-mediated antibiotic resistance in *Acinetobacter* spp. *Antimicrob. Agents Chemother.* **55**, 947–953 (2011).

411. X. He, *et al.*, Biofilm formation caused by clinical *Acinetobacter baumannii* isolates is associated with overexpression of the AdeFGH efflux pump. *Antimicrob. Agents Chemother.* **59**, 4817–4825 (2015).

412. B. Quinn, *et al.*, Human serum albumin alters specific genes that can play a role in survival and persistence in *Acinetobacter baumannii*. *Sci. Rep.* **8**, 14741 (2018).

413. M. A. Peterson, A. N. Grice, J. M. Hare, A corepressor participates in LexA-independent regulation of error-prone polymerases in *Acinetobacter*. *Microbiology* **166**, 212–226 (2020).

414. E.-J. Yoon, P. Courvalin, C. Grillot-Courvalin, RND-Type Efflux Pumps in multidrug-resistant clinical isolates of *Acinetobacter baumannii*: Major role for AdeABC overexpression and AdeRS mutations. *Antimicrob. Agents Chemother.* **57**, 2989–2995 (2013).

415. N. Rosenfeld, C. Bouchier, P. Courvalin, B. Périchon, Expression of the resistance-nodulation-cell division pump AdeIJK in *Acinetobacter baumannii* is regulated by AdeN, a TetR-type regulator. *Antimicrob. Agents Chemother.* **56**, 2504–2510 (2012).

416. M.-F. Lin, Y.-Y. Lin, C.-Y. Lan, The role of the two-component system BaeSR in disposing chemicals through regulating transporter systems in *Acinetobacter baumannii. PLoS One* **10**, e0132843 (2015).

417. B. Robin, *et al.*, MacAB-TolC contributes to the development of *Acinetobacter baumannii* biofilm at the solid–liquid interface. *Front. Microbiol.* **12** 785161 (2022).

418. I. Roca, *et al.*, CraA, a major facilitator superfamily efflux pump associated with chloramphenicol resistance in *Acinetobacter baumannii*. *Antimicrob. Agents Chemother.* **53**, 4013–4014 (2009).

419. W. E. Foong, H.-K. Tam, J. J. Crames, B. Averhoff, K. M. Pos, The chloramphenicol/H+ antiporter CraA of *Acinetobacter baumannii* AYE reveals a broad substrate specificity. *J. Antimicrob. Chemother.* **74**, 1192–1201 (2019).

420. G. Rajamohan, V. B. Srinivasan, W. A. Gebreyes, Molecular and functional characterization of a novel efflux pump, AmvA, mediating antimicrobial and disinfectant resistance in *Acinetobacter baumannii*. *J. Antimicrob. Chemother.* **65**, 1919–1925 (2010).

421. A. Sharma, R. Sharma, T. Bhattacharyya, T. Bhando, R. Pathania, Fosfomycin resistance in *Acinetobacter baumannii* is mediated by efflux through a major facilitator superfamily (MFS) transporter—AbaF. *J. Antimicrob. Chemother.* **72**, 68–74 (2017).

422. M. Pérez-Varela, J. Corral, J. Aranda, J. Barbé, Functional characterisation of AbaQ, a novel efflux pump mediating quinolone resistance in *Acinetobacter baumannii*. *Antimicrob. Agents Chemother.* **62**, e00906-18 (2018).

423. W. E. Foong, J. Wilhelm, H.-K. Tam, K. M. Pos, Tigecycline efflux in *Acinetobacter baumannii* is mediated by TetA in synergy with RND-type efflux transporters. *J. Antimicrob. Chemother.* **75**, 1135–1139 (2020).

424. P.-E. Fournier, *et al.*, Comparative genomics of multidrug resistance in *Acinetobacter baumannii*. *PLoS Genet.* **2**, 62–72 (2006).

425. B. A. Eijkelkamp, K. A. Hassan, I. T. Paulsen, M. H. Brown, Development of a high-throughput cloning strategy for characterization of *Acinetobacter baumannii* drug transporter proteins. *Microb. Physiol.* **20**, 211–219 (2011).

426. M. Pérez-Varela, J. Corral, J. Aranda, J. Barbé, Roles of efflux pumps from different superfamilies in the surface-associated motility and virulence of *Acinetobacter baumannii* ATCC 17978. *Antimicrob. Agents Chemother.* **63**, 1–11 (2019).

427. V. B. Srinivasan, G. Rajamohan, W. A. Gebreyes, Role of AbeS, a novel efflux pump of the SMR family of transporters, in resistance to antimicrobial agents in *Acinetobacter baumannii*. *Antimicrob. Agents Chemother.* **53**, 5312–5316 (2009).

428. I. T. Paulsen, *et al.*, The 3' conserved segment of integrons contains a gene associated with multidrug resistance to antiseptics and disinfectants. *Antimicrob. Agents Chemother.* **37**, 761–768 (1993).

429. M. R. Babaei, A. Sulong, R. A. Hamat, S. A. Nordin, V. K. Neela, Extremely high prevalence of antiseptic resistant Quaternary Ammonium Compound E gene among clinical isolates of multiple drug resistant *Acinetobacter baumannii* in Malaysia. *Ann. Clin. Microbiol. Antimicrob.* **14**, 11 (2015).

430. F. Lin, *et al.*, Molecular characterization of reduced susceptibility to biocides in clinical isolates of *Acinetobacter baumannii*. *Front. Microbiol.* **8,** 1836 (2017).

431. W. J. Liu, *et al.*, Frequency of antiseptic resistance genes and reduced susceptibility to biocides in carbapenem-resistant *Acinetobacter baumannii*. *J. Med. Microbiol.* **66**, 13–17 (2017).

432. Q. Liu, *et al.*, Regulation of the *aceI* multidrug efflux pump gene in *Acinetobacter baumannii*. *J. Antimicrob. Chemother.* **73**, 1492–1500 (2018).

Chapter 2: Genomic fitness profiling of *Acinetobacter baumannii* reveals modes of action for common biocides and mechanisms of biocide-antibiotic antagonism

Published as: Li, L., Short, F.L., Hassan, K.A. et al. Systematic analyses identify modes of action of ten clinically relevant biocides and antibiotic antagonism in *Acinetobacter baumannii*. *Nature Microbiology* (2023). https://doi.org/10.1038/s41564-023-01474-z

Genomic fitness profiling of *Acinetobacter baumannii* reveals modes of action for common biocides and mechanisms of biocide-antibiotic antagonism

Liping Li[1,7], Francesca L. Short[1,3], Karl A. Hassan[1,2,7], Varsha Naidu[1,2,7], Alaska Pokhrel[1,8], Stephanie S. Nagy[1], Farzana Tasum Prity[1,7], Bhumika Shah[1,7], Nusrat Afrin[1], Stephen Baker[4], Julian Parkhill[5,6], Amy K. Cain[1,7*], and Ian T. Paulsen[1,7*]

Authors' affiliations

1. Department of Molecular Sciences, Macquarie University, Sydney, NSW, Australia

2. School of Environmental and Life Sciences, University of Newcastle, Callaghan, NSW, Australia.

3. Current address: Department of Microbiology, Biomedicine Discovery Institute, Monash University, Clayton, Victoria

4. Cambridge Institute of Therapeutic Immunology & Infectious Disease (CITIID), University of Cambridge, Cambridge, United Kingdom

5. The Wellcome Trust Sanger Institute, Wellcome Trust Genome Campus, Hinxton, Cambridge CB10 1SA, United Kingdom

6. Current address: Department of Veterinary Medicine, University of Cambridge, Madingley Road, Cambridge, CB3 0ES

7. ARC Centre of Excellence in Synthetic Biology, Macquarie University, Sydney, NSW, Australia

8. Australian Institute for Microbiology and Infection (AIMI), University of Technology Sydney, NSW, Australia

*Corresponding authors: Prof. Ian T. Paulsen, ian.paulsen@mq.edu.au or A/Prof. Amy K. Cain amy.cain@mq.edu.au

Running Title: Biocide fitness determinants in *A. baumannii*

Key words: antimicrobial resistance, antibiotics, biocides, TraDIS, drug efflux pumps, membrane potential, biocide stewardship

Abstract

Biocides, such as antiseptics and disinfectants, are used ubiquitously for hygiene in households and for life-saving infection control in hospitals. An increasing concern is that the widespread use of biocides may contribute to the emergence and spread of multidrug-resistant bacteria. We performed transposon directed insertion site sequencing (TraDIS) to identify genes and key cellular pathways of the multidrug resistant nosocomial pathogen *Acinetobacter baumannii,* that affect host fitness during exposure to a panel of ten structurally-diverse and clinically-relevant biocides: silver nitrate, benzalkonium, cetyltrimethylammonium bromide (CTAB), chlorhexidine, triclosan, chloroxylenol, polyvidone iodine, bleach, glutaraldehyde and ethanol. Multiple genes encoding proteins localised either in the cell envelope or in the cytoplasm were shown to affect biocide susceptibility. These proteins are involved in multiple processes including fatty acid biogenesis, multidrug efflux, the tricarboxylic acid cycle, cell respiration and cell division, suggesting that these biocides may have intracellular targets in addition to their known effects on the cell envelope. Based on the importance of cell respiration genes for *A. baumannii* fitness on biocides, we proposed and confirmed that apart from triclosan and ethanol, the other 8 biocides at sub-inhibitory concentration can dissipate the membrane potential and lead to *A. baumannii* tolerance to antibiotics that have intracellular targets. Our results support the concern that residual biocides in clinical or community environments can promote the development of antibiotic resistance in pathogenic bacteria.

Introduction

Multiple drug resistance (MDR) in bacterial pathogens is an alarming public health issue[1]. Bacteria can resist drugs by expressing efflux pumps to export drugs out of the cell, altering outer membrane permeability to reduce drug accumulation, or expressing enzymes for drug inactivation by hydrolysis or modification[2]. Alternatively, bacteria can gain intrinsic resistance mutations which prevent target recognition or cause target bypass. The Gram-negative opportunistic human pathogen *A. baumannii* is a significant worldwide threat for immunocompromised patients who are hospitalized in Intensive Care Unit (ICU) wards. This is due to the emergence of *A. baumannii* clonal lineages with high level resistance to antibiotics and tolerance to desiccation[3,4]. The World Health Organisation (WHO) recently listed carbapenem resistant *A. baumannii* as a "top priority pathogen" for development of new therapies.

Biocides are widely used for disinfection and cleaning in both households and hospitals, but little is known about their impact on the emergence and spread of MDR infections. In contrast to antibiotics, the use of biocides is largely unregulated. The recommended in-use biocide concentrations are normally orders of magnitude higher than the bacterial minimum bactericidal concentration (MBC). Biocides are presumed to have multiple antibacterial targets or non-specific targets, reducing the likelihood of bacteria developing resistance to these compounds[5]. However, outbreaks of nosocomial MDR infections are not uncommon. There is evidence suggesting that biocide exposure at sublethal concentrations can select for antibiotic-resistant bacteria under laboratory conditions[6], and clinical antibiotic resistant isolates typically have reduced biocide susceptibilities[7]. One of the most commonly known biocide and antibiotic cross-

resistance mechanisms is the activity of MDR efflux pumps, such as AcrAB-TolC from *Escherichia coli*[8], AdeIJK and AdeABC from *Acinetobacter baumannii*[9], and NorA from *Staphylococcus aureus*[10].

Biocide modes of action are generally poorly characterized, except for cell lysis via interaction with the phospholipid membrane[5]. However, some biocides are known to have mode of action that start intracellularly. For example, silver ions can interact with the thiol group of exposed cysteine residues leading to enzyme inactivation and disruption of cellular iron homeostasis[11,12], and they also cause cell membrane proton leakage[13]. The known silver resistance determinants are primarily involved in reducing silver ion intracellular concentration, including membrane transporters for silver ion export[14], and proteins for neutralization or reduction of silver ions to the inactive metallic form[15]. Triclosan targets an intracellular essential enzyme enoyl reductase (FabI) in fatty acid synthesis[16]. The two key determinants for high-level triclosan resistance are MDR efflux pumps and either mutations in the *fabI* gene or the acquisition of alternative Fab proteins not recognizable by triclosan[17]. A recent study revealed that two cytoplasmic membrane import systems may mediate triclosan uptake[18]. Apart from the drug efflux pumps mentioned earlier, members from the proteobacterial antimicrobial compound efflux (PACE) family confer resistance to antibacterial surfactant compounds including chlorhexidine and benzalkonium[19]. These observations suggest the surfactant biocides are also likely to have intracellular targets, or these pumps can expel them from the membrane.

Knowledge of both biocide modes of action and tolerance mechanisms is important for improved biocide use for effective and sustainable infection control. Here we performed the first systematic genome-wide screen to identify genes that affect susceptibilities of an MDR *A. baumannii* strain

to ten clinically important biocides (Table S1), using transposon-directed insertion-site sequencing (TraDIS)[20,21].

Results

TraDIS experimental outcomes. TraDIS assays were performed on a global clone II multidrug resistant *A. baumannii* strain BAL062 transposon mutant library, containing >100,000 unique Tn*5* insertions (1 insertion every 38 bp)[22], to assess the global genetic response to biocide treatments. Ten structurally distinct biocides were chosen for this study; these are all either listed as "essential medicines" by the WHO or commonly used in clinical settings and/or as household products (Table S1). The *A. baumannii* TraDIS library was exposed to a sub-inhibitory concentration of each biocide (¼ × the minimum inhibitory concentration (MIC) of the wild-type strain) (Table S2), and genomic DNA was extracted for TraDIS sequencing and analysis as previously described[23]. Gene-wise mutant abundance data were compared to untreated control samples grown under identical conditions for the same length of time to identify mutations that affect fitness in the presence of biocides, while controlling for any general impacts on growth rate. Collectively, the biocide treatments revealed a range of genes harbouring a reduced mutant population (i.e. decreased insertion read counts; 3-120 genes), representing potential biocide tolerance determinants, or with an expanded mutant population (i.e. increased insertion read counts; 7-100 genes) whose inactivation is potentially beneficial under biocide-treatment (Table S1).

We examined genes previously associated with biocide resistance and found their functions reflected in the TraDIS results. For example, the MDR efflux pump-encoding operon *adeABC* and its activator genes (*adeRS*) showed significantly decreased insertion read counts (e.g. *adeB*

had a 115.4-fold decrease) after treatment with benzalkonium, a known substrate of AdeABC; whereas no change was seen after treatment with glutaraldehyde, which is not known to be a substrate of AdeABC (Figure 1A).

Genes previously associated with antibiotic resistance were identified, for example as *lpsB* – a glycosyltransferase and LOS-synthesis gene involved in polymyxin resistance in *A. baumannii*[24] but not previously implicated in biocide resistance – showed a 5.8-fold decrease in insertions following triclosan treatment (Figure 1A). We also revealed potential new roles in biocide resistance for previously characterised genes, e.g., the insertions in the pyrimidine synthesis gene *pyrC* showed a 35.9-fold increase in $AgNO_3$-treated cultures compared to the control (Figure 1A).

As proof-of-principle phenotypic validation of this TraDIS data, we measured the MICs or the growth curves of the thirteen isogenic single-gene knockout Tn*26* mutants from *A. baumannii* AB5075[25]. They include *trpA* (encoding tryptophan synthase subunit alpha), *gltA* (encoding citrate synthase), BAL062_00464 (ABUW_0466, encoding ribonuclease I), *adeJ* (encoding another key MDR efflux pump in *A. baumannii*), BAL062_00031 (ABUW_0035, encoding a putative drug efflux pump), *amvA* (MDR efflux pump gene), *lysA* (diaminopimelate decarboxylase encoding gene), *dsbA* (encoding thiol:disulfide interchange protein), *ruvB* (encoding Holliday junction DNA helicase) and the genes outlined above: *adeB*, *lpsB*, *pyrC* and *adeR*, for the ten biocides (Table S3). For *adeB*, *lpsB*, *pyrC* and *adeR* the biocide MIC fold change for the mutant relative to wild-type was essentially consistent with the TraDIS results (Figure 1B).

TraDIS data reflects subtle population dynamic changes, which is likely more sensitive than standard MIC assays. For the remaining nine genes, we additionally performed growth curve assays. The growth curve differences between the mutants and the parental strain are essentially consistent with the TraDIS data (Figure S1 and S2 and Table S3). For both the MIC and growth curve data, polyvidone iodine is the one compound that was not consistent with the TraDIS data, as we observed no changes in susceptibility to this compound in the mutants tested here. To ensure the phenotypes that we observed on these isogenic single-gene knockout transposon mutants were not derived from secondary mutations, we tested five representative genes for further growth curve assays using a second, independent transposon mutant of the same gene. We showed that the two transposon mutant pairs of each of these five genes share highly similar biocide tolerance phenotypes (Figure S2).

Outer membrane lipooligosaccharide. *A. baumannii* lacks a homolog of the O antigen ligase WaaL, which transfers O-antigen polysaccharide onto the outer-core of LPS, suggesting that *A. baumannii* LPS may comprise only lipid A and core oligosaccharide[26]. We observed that insertions in a lauroyl acyl-transferase encoding gene, *lpxL*, increased in frequency following treatment with the cationic surfactants chlorhexidine and cetyltrimethylammonium bromide (CTAB) (21- and 2.3-fold respectively), suggesting that this gene decreased fitness at sub-inhibitory concentrations of these two biocides (Figure 2A). The predominant glycolipid molecule in the outer leaflet of *A. baumannii* OM is hepta-acylated lipid A[27], whereas an *lpxL* mutant generates a hexa-acylated lipid A[28]. This change in fatty acid profile may impact the effectiveness of these biocides against *A. baumannii*.

Cell surface polysaccharides. In *A. baumannii*, there are two gene clusters known to be involved in capsule polysaccharide biosynthesis (K-locus) and LOS outer core oligosaccharide biosynthesis (OC-locus) respectively[29]. We identified 9 genes in the K-locus with significant changes in insertion counts after treatment with one or more biocides. For instance, insertions in the *gna* gene, encoding a UDP-glucose dehydrogenase, increased during treatment with chlorhexidine and bleach (207 and 3.2-fold, respectively), implicating capsule polysaccharide in biocide sensitivity.

Insertions in an initiating glycosyltransferase-encoding gene, *pglC*, had decreased read-coverage (9.9-fold) when treated with $AgNO_3$, while treatment with the other 9 compounds did not have an effect, suggesting this gene may mediate tolerance only for $AgNO_3$ (Figure 2A). *pglC* is located in the variable region of the K-locus, but its presence is conserved in this gene cluster across *A. baumannii* strains[29,30]. It is required for the construction of capsular glycan repeat-units and glycosylation of glycoproteins[30], and the deletion mutant affects capsule production not LOS[31]. In addition to *pglC*, insertions in 7 other genes in the K-locus also displayed decreased frequency following $AgNO_3$ treatment (Figure 2A), implying that the capsular polysaccharide may play a specific role in $AgNO_3$ tolerance, whereas alteration of LOS glycoforms impacts susceptibility to biocides more broadly.

Insertions in seven genes in the OC-locus had altered frequency following biocide treatment (Figure 2A). For instance, insertions in the glycosyltransferase gene *lpsC* decreased 5.8-fold following exposure to benzalkonium, suggesting a specific role for *lpsC* in benzalkonium tolerance. Further, insertions in another glycosyltransferase gene, *gtrOC3,* dropped dramatically (78.8-fold) upon chlorhexidine treatment, suggesting *gtrOC3* mediates chlorhexidine tolerance

(Figure 2A). Insertions in the glycosyltransferase gene *lpsB*, which is outside of the two polysaccharide biosynthesis loci and is involved in LOS core biosynthesis, also showed changes following exposure to 7 biocides (Figure 2A). Previously, it has been shown that disruption of these glycosyltransferases in *A. baumannii* produces truncated LOS[32,33]. Thus, genes predicted to encode glycosyltransferases, that catalyze the linking of sugars of the LOS outer oligosaccharide core, may be important in biocide tolerance.

Chaperone-usher pilus. Another potential cell surface biocide tolerance determinant identified in this study is a chaperone-usher (CU) pilus assembly gene cluster *csuA/BABCDE* (Figure 2A)[34], insertions in which decreased after treatment with eight biocides (Figure 2A). For example, insertions in all the *csu* genes decreased with most biocides: 2.2- to 3.2-fold decrease for $AgNO_3$, 2.8- to 3.8-fold decrease for benzalkonium, 7.2- to 8.4-fold decrease CTAB, and 5- to 7-fold decrease for triclosan (Figure 2A). Consistent with their known function as *csu* operon activators, insertions in the genes of the two-component system BfmRS were also shown to decrease following treatments with seven same biocides (Figure 2A). Interestingly, insertions in a transcriptional regulator (BAL062_01328) directly upstream of the *csu* operon also decreased in frequency following treatment with the same eight biocides and the fold change was similar to that of *csu* gene mutants (Figure 2A), indicating that BAL062_01328 encodes a potential local transcriptional activator of the *csu* operon. Together these results suggest that the mature pilus system is required for a biocide tolerance phenotype.

Membrane transport. Sixteen drug efflux systems have been characterized or identified in *A. baumannii*[19,35]. One of the most clinically significant drug transporters in *A. baumannii* is a tripartite efflux system AdeABC[36], comprised of a membrane fusion protein (MFP) AdeA, a

198 resistance-nodulation-division (RND) efflux pump AdeB, and an outer membrane factor (OMF)
199 AdeC, respectively. This system is constitutively overexpressed in various clinical *A. baumannii*
200 MDR strains, typically due to mutations in the two-component transcriptional activator genes
201 *adeRS* [37].

202 Tn*5* insertions in *adeB* significantly decreased in frequency 115.4-, 2.2-, 85.6-, 7.9- and 2.0-fold
203 in the mutant pools that were treated by benzalkonium, cetrimonium, chlorhexidine, triclosan
204 and chloroxylenol, respectively (Figure 2B), suggesting that *adeB* mediates resistance to these
205 compounds. Benzalkonium and chlorhexidine have previously been characterized as AdeB
206 substrates[9]. Surprisingly, changes in frequency of Tn*5* insertions in *adeA* and *adeC* were only
207 seen in the mutant pools treated by benzalkonium and chlorhexidine (Figure 2B), where
208 insertions in *adeA* had 3.3- and 78.8-fold decrease, and insertions in *adeC* had 2.4- and 11.2-
209 fold decrease, respectively (Figure 2B). This suggests AdeABC functions as a tripartite system
210 in pumping out these two compounds. These fold-changes were lower than the changes of *adeB*
211 caused by the same compounds, indicating that there might be alternative OMF and MFP
212 proteins that form a tripartite RND efflux system with AdeB.

213 Insertions in *adeR* decreased 7.6- and 26.7-fold, and those in *adeS* decreased 7.5- and 240-fold
214 when treated by benzalkonium and chlorhexidine respectively, whereas no change was
215 observed in the other three conditions that also selected against insertions in *adeB* (Figure 2B).
216 A chlorhexidine transcriptomics study showed that chlorhexidine at ½ MIC can induce the
217 expression of *adeABC* in *A. baumannii* ATCC17978[38]. Using q-RT-PCR, we further showed that
218 benzalkonium and chlorhexidine can induce higher levels of *adeB* transcription in *A. baumannii*
219 BAL062 (Figure 2C). The transposon mutant of *adeB* in *A. baumannii* AB5075 is more sensitive

220 to benzalkonium, chlorhexidine, triclosan, CTAB and chloroxylenol. However, the transposon
221 mutant of *adeR* only showed increased sensitivity to benzalkonium and chlorhexidine (Figure
222 S3). These observations align with our TraDIS data and suggest that benzalkonium and
223 chlorhexidine can induce the overexpression of AdeABC through AdeRS, whereas CTAB,
224 triclosan and chloroxylenol do not act as inducers.

225 The other important RND system that has been characterized in clinical *A. baumannii* MDR
226 strains is AdeIJK, which share some of the substrates of AdeABC[9]. The TraDIS data from this
227 study for *adeIJK* is similar to that for *adeABC* (Figure 2B)[9,39]. For instance, insertions in the OMF
228 encoding gene *adeK* decreased 1.7-, 17-, 79.9-, 27.3-, and 10.0-fold after treatment with $AgNO_3$,
229 benzalkonium, chlorhexidine, triclosan and chloroxylenol respectively (Figure 2B). These
230 phenotypes are confirmed by transposon mutants of *adeJ* and *adeB* in *A. baumannii* AB5075
231 through growth curves (Figure S3). The respective changes in frequency of insertions in the
232 RND pump encoding gene *adeJ* and MFP encoding gene *adeI* were lower than seen for *adeK*,
233 suggesting AdeK might not only form a tripartite drug efflux system with AdeI and AdeJ, but also
234 with AdeAB, consistent with previous reports[40,41]. Also consistent with previous findings that the
235 transcriptional regulator AdeN represses the transcription of *adeIJK*[42], the insertions in *adeN*
236 increased 1.5-, 99.7-, 1.7- and 1.3-fold after treatment with benzalkonium, chlorhexidine,
237 triclosan and chloroxylenol respectively (Figure 2B).

238 The frequency of Tn*5* insertions in another RND membrane transporter gene BAL062_00031
239 and MFP encoding gene BAL062_00030 reduced 7.31- and 7.41-fold respectively when
240 exposed to triclosan, suggesting these genes play a role in triclosan resistance (Figure 2B).
241 Triclosan resistance phenotype of BAL062_00031 was confirmed in the homolog transposon

mutant of *A. baumannii* AB5075 through growth curve assays (Figure S3). There is no OMF gene located adjacent to BAL062_00030 and BAL062_00031. This system may use AdeK as its OMF partner, because *adeK* is the only OMF gene in which insertions reduced in frequency (27-fold) in the mutant pool exposed to triclosan (Figure 2B).

Four other drug efflux pumps were also implicated in mediating biocide resistance. The MFS transporter AmvA is a multidrug exporter with substrates including benzalkonium, and chlorhexidine[43,44]. The frequency of insertions in *amvA* decreased 1.6- and 106.2-fold after exposure to benzalkonium and chlorhexidine respectively, and additionally showed a 19.4-fold decrease when treated by $AgNO_3$ (Figure 2B). Furthermore, the frequency of insertions in *amvR*, encoding a transcriptional repressor of *amvA*[22], increased 5.2- and 84.7-fold following exposure to $AgNO_3$ and chlorhexidine, respectively (Figure 2B). Through growth curves, we confirmed that the *amvA* transposon mutant has lower $AgNO_3$ resistance than the parental strain (Figure S3), suggesting AmvA may recognize silver ions as a substrate or may transport other compounds related to silver detoxification.

The frequency of insertions in *tetR*, immediately upstream of a tetracycline efflux pump gene *tetA*, increased 21.1-fold following exposure to chlorhexidine (Figure 2B). TetR is a known transcriptional repressor of *tetA*[45], and this result suggested that *tetA* overexpression reduces susceptibility to chlorhexidine. In contrast, chlorhexidine did not affect the frequency of insertions in *tetA*, which is likely because TetR does not recognize chlorhexidine as a ligand and is not responsive to it. These are consistent with our previous finding that *E. coli* expressing *A. baumannii* TetA had a significant increase in chlorhexidine resistance level[46].

263 **Cell Division.** Various genes that are involved in peptidoglycan (PG) synthesis, cell shape
264 determination and cell division were shown to have a decreased frequency of Tn*5* insertions
265 following treatment with silver nitrate and several other biocides (Figure S4). Insertions in the
266 bacterial rod shape determining genes *mreB*, *mreC*, *mreD*, *rodA* and *pbp2* decreased in
267 frequency (4.8-, 6.3-, 4.7-, 4.8- and 4.0-fold respectively) when treated by $AgNO_3$, suggesting
268 disruption of these genes resulted in greater sensitivity to $AgNO_3$. In line with the phenotype of
269 these mutants, Ag^+ solution has been shown to cause distortion in bacterial cell membranes and
270 morphology[47]. Hypochlorite and ethanol also showed similar effects on the frequency of these
271 mutants, though with lower fold changes (Figure S4), suggesting they may also affect cell
272 membranes and morphology.

273 The FtsZ-ring associated genes (*zipA*, *zapA* and *rlpA*) and six genes involved in peptidoglycan
274 synthesis and hydrolysis were also found to have a role in tolerance to multiple biocides (Figure
275 S4). Insertions in *zipA* decreased in frequency when treated with eight different biocides, for
276 instance a 6.9-fold decrease in the $AgNO_3$ pool, a 3.0-fold decrease in the chloroxylenol pool,
277 and a 2.5-fold decrease in the glutaraldehyde pool. The frequency of insertions in genes in the
278 *pal-tolQ* operon, which is required for OM invagination during cell division, was strongly reduced
279 (59.3 – 61.7-fold) upon chlorhexidine treatment.

280 The PMF was proposed to affect cell division because the cellular localization of MreB and FtsA
281 (FtsZ-ring associated) proteins has been shown to be PMF-dependent [48]. This may explain why
282 TraDIS revealed that mutations in both electron transfer and cell division genes affect *A.*
283 *baumannii* fitness in the presence of $AgNO_3$ and other biocides.

284 **Central Metabolism and Respiration**. Tn*5* insertional inactivation of several TCA cycle genes
285 had effects on *A. baumannii* susceptibility to silver nitrate. The frequency of insertions in the TCA
286 cycle genes *sucC* and *sucD* encoding succinyl-CoA synthetase β and α subunits both showed
287 a 12.3-fold increase upon silver nitrate treatment, suggesting that absence of succinyl-CoA
288 synthetase increased resistance to silver nitrate (Figure S4). Similarly, previous work
289 demonstrated that knockout strains of *E. coli* TCA cycle genes (*ΔsucB*, *Δmdh*) were less
290 sensitive to silver nitrate than the wild type[12]. In contrast, insertions in two other TCA cycle genes
291 *acnA_1* encoding aconitate hydratase 1 and *icd_2* encoding isocitrate dehydrogenase showed
292 11.7- and 12.5-fold decreases after silver nitrate treatment, respectively (Figure S4), suggesting
293 that these mutants had decreased fitness in silver nitrate. Silver nitrate may target SucC/SucD
294 in *A. baumannii*, requiring alteration of fluxes through the TCA cycle, such that there is a heavier
295 requirement for *icd_2* and *acnA*.

296 Another known antibacterial effect of $AgNO_3$ occurs via cytoplasmic membrane proton leakage
297 and attenuated or ceased cell respiration[13]. We measured the membrane potential change upon
298 exposure to $AgNO_3$ in *A. baumannii* BAL062 using 3,3'-Diethyloxacarbocyanine iodide
299 ($DiOC_2(3)$). $AgNO_3$ at a concentration as low as 1/32 MIC started to cause a dose-dependent
300 drop in the membrane potential of cells in exponential phase (Figure 3A). The dissipation of
301 membrane potential was reflected in decreased frequency of insertions in genes encoding
302 proteins involved in electron/proton shuttling during respiration. For example, Tn*5* insertions in
303 *cydB* and *cydA_1*, encoding cytochrome D ubiquinol oxidase decreased by 5.5- and 7.0-fold
304 respectively, and insertions in a ubiquinone biosynthesis gene BAL062_03562 decreased 4-fold
305 (Figure S4). We hypothesize that these genes might be involved in maintaining the PMF to resist

306 silver nitrate-induced cytoplasmic membrane proton leakage and the compromised electron
307 suppliers from the TCA cycle.

308 An electron transport-related operon encoding cytochrome O (*cyo*) ubiquinol oxidase subunits
309 had significantly reduced frequency of Tn*5* insertions upon chloroxylenol, benzalkonium or
310 ethanol treatment (Figure S4), suggesting that the electron transport chain is affected by these
311 compounds, but in a different way to silver nitrate.

312 **Biocide induced dissipation of membrane potential**. The finding that cell division and cell
313 respiration genes are required for fitness in the presence of multiple biocides indicated that, like
314 $AgNO_3$, these molecules may cause dissipation of membrane potential as part of their activity.
315 To explore this hypothesis, we first measured the membrane potential change of *A. baumannii*
316 BAL062 on exposure to $AgNO_3$ using 3,3'-Diethyloxacarbocyanine iodide ($DiOC_2(3)$). As
317 expected, given its known effect causing proton leakage, $AgNO_3$ caused a drop in membrane
318 potential of exponential phase cells (Figure 3A). This effect was apparent at as low as 1/32 MIC
319 and was dose dependent. We then measured the membrane potential of exponential-phase *A.*
320 *baumannii* BAL062 following exposure to the remaining biocides at ¼ MIC. Based on the
321 importance of cell division and cell respiration genes for fitness in the presence of all biocides
322 except triclosan (Figure S4), we predicted that nine of the biocides would impact membrane
323 potential. As shown in Figure 3B all compounds except for triclosan and ethanol caused a drop
324 in membrane potential. This suggests that dissipation of membrane potential might be a direct
325 or downstream antibacterial effect of multiple biocides.

326 Cell membrane transport activities are energy dependent. If the biocides in this study do induce
327 dissipation of membrane potential, they should also be able to compromise the solute efflux

efficacy of proton-coupled pumps that rely on membrane potential as an energy source. Acriflavine is a passively lipid membrane permeable fluorescent compound and a well-known substrate of multiple drug efflux transporters, including AmvA (Figure 4A), AdeB and AdeJ[49] in *A. baumannii*. Its intracellular accumulation likely correlates with membrane protein efflux activity. We showed that, at ¼ MIC, triclosan and ethanol, the two compounds that did not affect membrane potential, did not change acriflavine fluorescence in *A. baumannii* BAL062. The other 8 compounds and the positive control proton ionophore CCCP (carbonyl cyanide m-chlorophenyl hydrazone) increased acriflavine accumulation in the cells (Figure 4B). This suggests efflux activities in the cells may be compromised because of membrane de-polarization caused by these compounds or transporter substrate competition may lead to less acriflavine efflux. Benzalkonium, chlorhexidine, CTAB, chloroxylenol and triclosan are known substrates to AdeB and AdeJ (Figure 2B and FigureS2), suggesting these substrates could compete with acriflavine during the efflux activity of these two transporters. However, triclosan did not affect acriflavine fluorescence, indicating the elevated acriflavine cellular level was more likely caused by membrane depolarization and loss of efflux pump activity. Chlorhexidine and benzalkonium at ¼ MIC can increase *adeB* expression (Figure 2C), but rather than triggering the cells to export more acriflavine via AdeB and reducing fluorescence, these biocides increased acriflavine intracellular accumulation (Figure 4B). These data (Figure 4B and Figure 3B) suggest that the 8 biocides, as well as the positive control CCCP, can de-energise the cell membrane and compromise membrane transport activities.

It is possible that the 8 biocides could be permeabilizing the cell membrane rather than specifically impacting the membrane potential. To investigate this possibility, we examined intracellular fluorescence of SYTOX-Green, a fluorescent DNA dye impermeable to intact cell

351 membranes. Apart from glutaraldehyde, the other 9 biocides and the positive control CCCP had
352 little effect on SYTOX-Green fluorescence in the cells, suggesting these compounds at the
353 concentrations tested in this assay do not have an observable impact on cell membrane integrity
354 (Figure 4B). The observations from both acriflavine and SYTOX Green assays collectively
355 suggest that $AgNO_3$, benzalkonium, CTAB, chlorhexidine, chloroxylenol, sodium hypochlorite,
356 povidone iodine (at ¼ MIC) dissipate the membrane potential without causing systemic
357 membrane damage. In contrast, glutaraldehyde (at ¼ MIC) permeabilizes the cell membrane
358 which leads to membrane potential dissipation.

359 **Biocides' impact on antibiotic potency**. The uptake of the poly-cationic aminoglycosides
360 requires membrane potential (both the proton gradient (ΔH^+) and electrical potential ($\Delta\psi$) across
361 the cytoplasmic membrane) and drug-sensitive ribosomal binding sites for irreversible drug
362 uptake[50]. Our next hypothesis is that the biocides that cause membrane potential dissipation can
363 compromise aminoglycoside uptake and thus antagonise the killing effects of the antibiotic. As
364 resistant bacterial strains accumulate less aminoglycoside antibiotic than sensitive strains[51], we
365 used an aminoglycoside-sensitive strain *A. baumannii* ATCC17978 rather than the highly
366 resistant AB5075 or BAL062 strain to test our hypotheses. We showed that apart from triclosan,
367 the other biocides including benzalkonium, chlorhexidine, CTAB and povidone iodine at ¼ MIC
368 and CCCP increased *A. baumannii* ATCC17978 survival when treated with gentamicin (Figure
369 5A). AdeB does not confer resistance to gentamicin[41], the antagonism with these biocides is
370 unlikely due to drug efflux. Furthermore, *adeB* expression is inducible by benzalkonium and
371 chlorhexidine, but not by CTAB and povidone iodine. Ethanol at ¼ MIC did not dissipate
372 membrane potential (Figure 3B), while it did induce gentamicin antagonism (Figure 5A). The
373 mechanism for ethanol inducing gentamicin antagonism remains unclear at this point in time.

374 These observations raised a question whether the biocides can also compromise the
375 antibacterial effects of other antibiotics that have different intracellular targets, such as
376 fluoroquinolones and tetracyclines, or antibiotics that target cell envelopes, such as colistin and
377 β-lactams.

378 Uptake of tetracyclines into the cytoplasm is PMF dependent but likely involves passive diffusion
379 of the uncharged form[52]. Similarly, the zwitterionic form of the fluoroquinolones has been
380 proposed to passively cross the cytoplasmic membrane, but due to their different protonation
381 behaviour from tetracyclines, uptake of some fluoroquinolones has been shown to be negatively
382 correlated with PMF[52,53]. Benzalkonium and chlorhexidine significantly increased *A. baumannii*
383 survival rates when treated with amikacin (another aminoglycoside), ciprofloxacin
384 (fluoroquinolone) and tigecycline (glycylcycline) (Figure 5B). In contrast, triclosan had no effect
385 on the efficacy of these antibiotics.

386 The observed biocide antagonism with amikacin and tigecycline is consistent with our hypothesis
387 that low concentrations of biocides that dissipate the membrane potential will affect uptake and
388 efficacy of antibiotics that have intracellular targets and whose uptake is dependent on the PMF.
389 There are differing reports in the literature whether uptake of fluoroquinolones is dependent on
390 the PMF[53], our data is suggestive that uptake of ciprofloxacin is dependent on the PMF.

391 Dissipation of the membrane potential may not antagonise the antibacterial effects of imipenem
392 and colistin, because the primary targets of these antibiotics are located in the cell envelope. As
393 expected, triclosan, benzalkonium and chlorhexidine at ¼ MIC have no impact on imipenem
394 killing (Figure 5B). Synergism was observed between benzalkonium and colistin, but not for
395 triclosan (Figure 5B). Chlorhexidine also seemed to marginally enhance colistin killing. The

synergy between these compounds is likely because benzalkonium, chlorhexidine and colistin all target cell membranes. Collectively, our data suggest that the biocides that can dissipate membrane potential can promote *A. baumannii* tolerance to various classes of antibiotics which have intracellular targets.

Discussion

TraDIS enabled us to investigate the potential tolerance/resistance determinants and modes of action of 10 diverse biocides that are commonly used for disinfection in hospital and in personal hygiene products. Many of these biocides are known surfactants, causing cell membrane permeabilization, leakage of intracellular constituents, and cell lysis, which were mostly based on direct biochemistry examinations or observations on cellular phenotypic changes[5]. This study provides additional genetic evidence that these biocides have diverse impacts on the cell surface, including components such as the outer membrane lipooligosaccharide, capsule polysaccharide and chaperone-user pilus. For instance, transposon insertions in genes related to LOS and lipid A biosynthesis affected *A. baumannii* fitness in the presence of these ten compounds. In contrast to LOS, capsular polysaccharide affected only $AgNO_3$ susceptibility out of the ten biocides tested.

Bacterial cell envelope is an indispensable and instrumental cellular component that dictates energy generation, nutrient uptake, metabolic waste extrusion, extracellular signal transduction and so on. It is expected that biocide-induced cell membrane leakage will lead to downstream intracellular affects. We showed that insertions in genes from multiple cellular pathways had statistically significant changes in frequency as a result of the biocide treatments, including the TCA cycle, electron transport chain, amino acid biosynthesis, nucleoside biosynthesis and biotin biosynthesis (SI 2). Non-specific cell membrane disruption has long been proposed to be the

mode of action of charged surfactant biocides, such as chlorhexidine and benzalkonium[5,54]. Various bacterial drug efflux pumps, including AdeABC, AdeIJK, TetB, AmvA and ABUW_0035 in this study were shown to be tolerance/resistance determinants for multiple biocides. The RND pumps such as AdeABC and AdeIJK can extrude substrates from cytoplasm and cytoplasmic membrane out of cell and potentially protect cells from biocide-induced membrane damages.

While antibiotic stewardship has been a topic of increasing public health concern, the debate on whether biocide stewardship is necessary is continuing[55-58]. Despite some studies reporting increased biocide resistance level in bacterial pathogens in laboratory studies, biocides' in-use concentrations are normally much higher than their MBCs and are effective in real world disinfection practices. It should be emphasized that the biocides tested here are either WHO Essential Medicines or widely used hospital and household disinfectant products. There is an increasing number of papers reporting that some biocides, such as benzalkonium, triclosan, or heavy metals, at sublethal concentrations can facilitate AMR gene horizontal transfer and promote the emergence of AMR pathogens[59,60]. A recent study further demonstrated that benzalkonium at high dosage can induce persister formation in *E. coli*, which further promotes cell adaptation to various antibiotics [61].

This is the first study that has systematically looked at the effects of biocides at low concentrations. Most of the literature on biocide mechanisms of action dates back to the 1970s and 1980s and has examined the effects of biocides above MBC[5]. Our data suggests that residual levels of seven out of ten biocides at sub-MIC levels can dissipate the cellular membrane potential without compromising membrane permeability. The biocide-induced collapse of membrane potential can affect the potency of antibiotics with intracellular targets on

bacterial cells, likely through impacting antibiotic uptake. We further showed that the biocides that cause dissipation of the membrane potential significantly promote *A. baumannii* survival rate under treatment with various antibiotics that have intracellular targets, including aminoglycosides, ciprofloxacin and tigecycline. However, the biocides do not antagonise the killing effects of drugs targeting the cell envelope, such as colistin and imipenem.

Although drug efflux pumps generally confer low level resistance to antibiotics, compared to their parental strains, bacteria that lack key MDR efflux systems are much less likely to develop MDR[62,63]. Furthermore, intermittent antibiotic exposures have been shown to lead to more rapid evolution of tolerance and resistance[64-66] and antibiotic tolerance facilitates the evolution of resistance[67]. These studies and our data together suggest that factors affecting antibiotic intracellular accumulation or drug target accessibility are important in the development of drug tolerance and AMR. Previous studies have typically used direct measurement of bacterial susceptibilities to antibiotics and biocides to investigate co-selection of antibiotic resistance[68]. We propose that the principal concern with respect to biocide stewardship is not the emergence of biocide resistance or antibiotic cross-resistance, but rather the presence of residual biocides, especially chlorhexidine, benzalkonium and CTAB and others that are hard to remove from the environment, could induce antibiotic tolerance and AMR development.

Acknowledgements

This work was supported by NHMRC (National Health and Medical Research Council) project grants APP1127615, APP1060895 and APP1165135 to ITP and KAH. The sequencing was supported by the Wellcome Trust grant WT098051. The transposon mutant library was constructed by SB, supported by Wellcome Trust grant WT100087/Z/12/Z. ITP is supported by

462 ARC (Australian Research Council) Laureate Fellowship FL140100021. AKC is supported by
463 ARC DECRA (Discovery Early Career Research Award) Fellowship DE180100929. FLS is
464 supported by ARC DECRA Fellowship DE200101524. KAH is supported by ARC Future
465 Fellowship FT180100123.

466

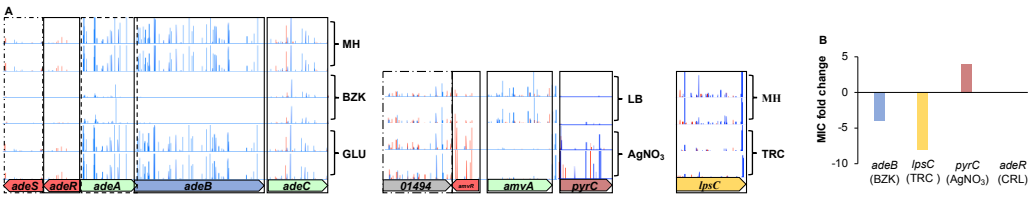

Figure 1. Biocide TraDIS data. (A) Representative genes and TraDIS insertion plots. Horizontal arrows represent gene length and direction, and gene names are within. Above each gene are lines representing reads mapped from each Tn*5* insertion site, the height of the line represents the number of reads. The black box height represents a maximum of 100 reads in all conditions, except *lpsB* with 10 reads. For each condition, two biological replicates of TraDIS results are presented (B) MIC fold change of four different mutants for relevant biocide compounds compared with the AB5075 wild-type strain. Biocides are listed in abbreviations (Table S1).

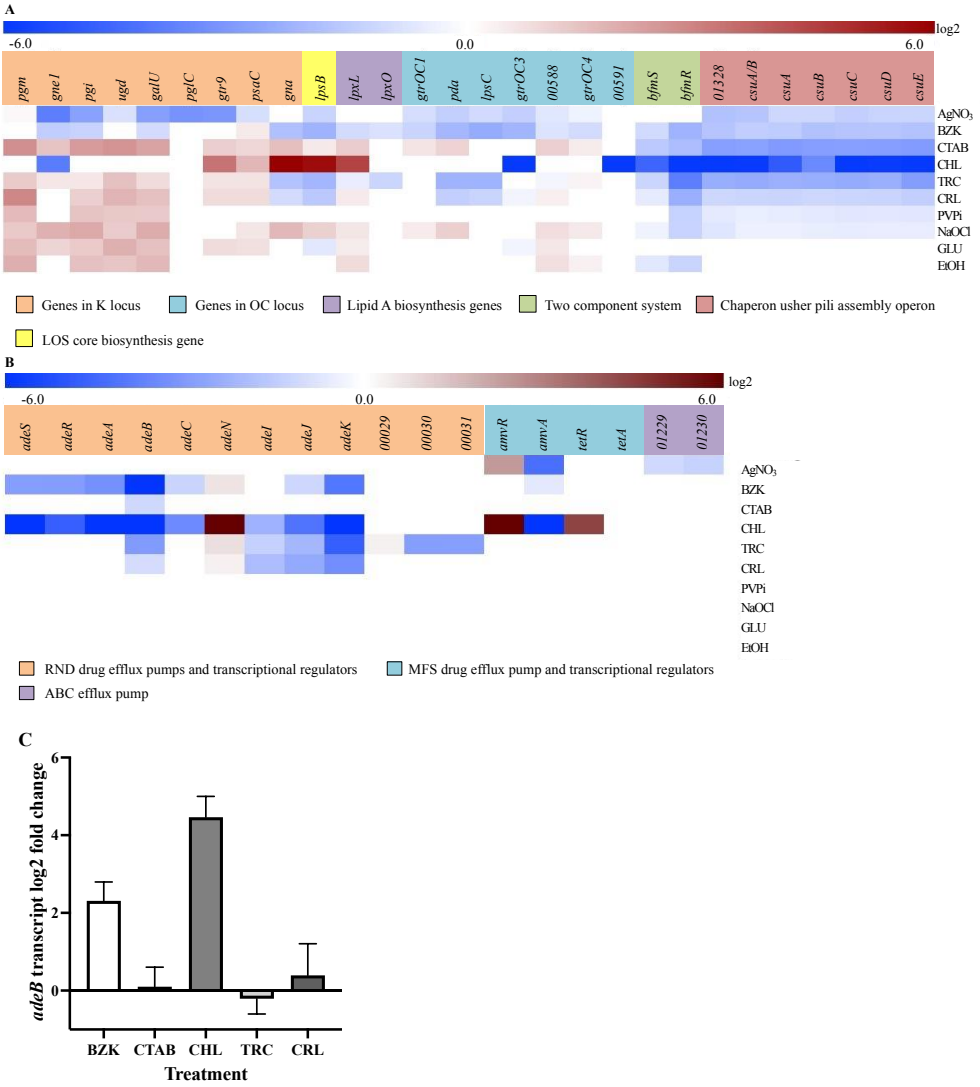

Figure 2 Genes with TraDIS insertion changes during biocide exposure. (A) Cell envelope-related genes. (B) Membrane transport-related genes. The colour-coded boxes represent the amount of Tn*5* insertion read coverage fold change, for each representative gene (above) and for each biocide (righthand side; abbreviations as in Table S1), where blue indicates a larger decrease in Tn*5* insertions and red shows an increase. Each gene's specific relationship to the cellular function is colour-coded, as stated below the heatmap. (C) Transcriptional response of *adeB* in *A. baumannii* BAL062 that was treated by the biocides at ¼ MIC, respectively.

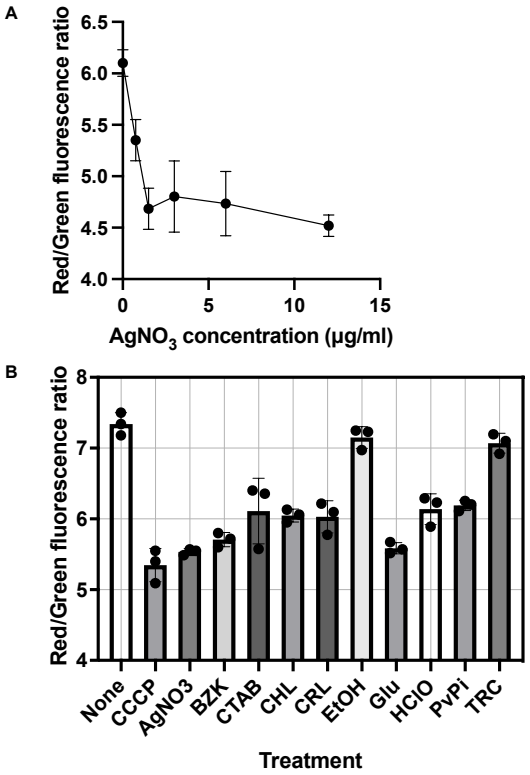

Figure 3. Effect of biocides on membrane potential. (A) Dose-dependent relationship between $AgNO_3$ and membrane potential in *A. baumannii* BAL062. Values on X-axis show $AgNO_3$ concentration (from 1/64 MIC to MIC). The membrane potential was measured with dye $DiOC_2(3)$ which emits green fluorescence in the cytosol, but shifts towards red fluorescence as the dye molecules self-associate at a higher cytoplasmic membrane potential. The ratio of red versus green fluorescence of $DiOC_2(3)$ shown here was calculated by the population mean of fluorescence intensities, which positively correlates with membrane potential. Three biological replicates were included. Each datapoint represents the mean of the ratio of Red/Green fluorescence intensity of three independent *A. baumannii BAL062* cultures that was treated by a biocide as specified. The error bars indicate the Red/Green ratio variation among the three biological replicates. (B) Relative membrane potential reduction in *A. baumannii* BAL062 after biocide exposure. Cells at OD_{600} 0.4-0.6 were treated by the 10 biocides at ¼ MIC, respectively. Three biological replicates were included.

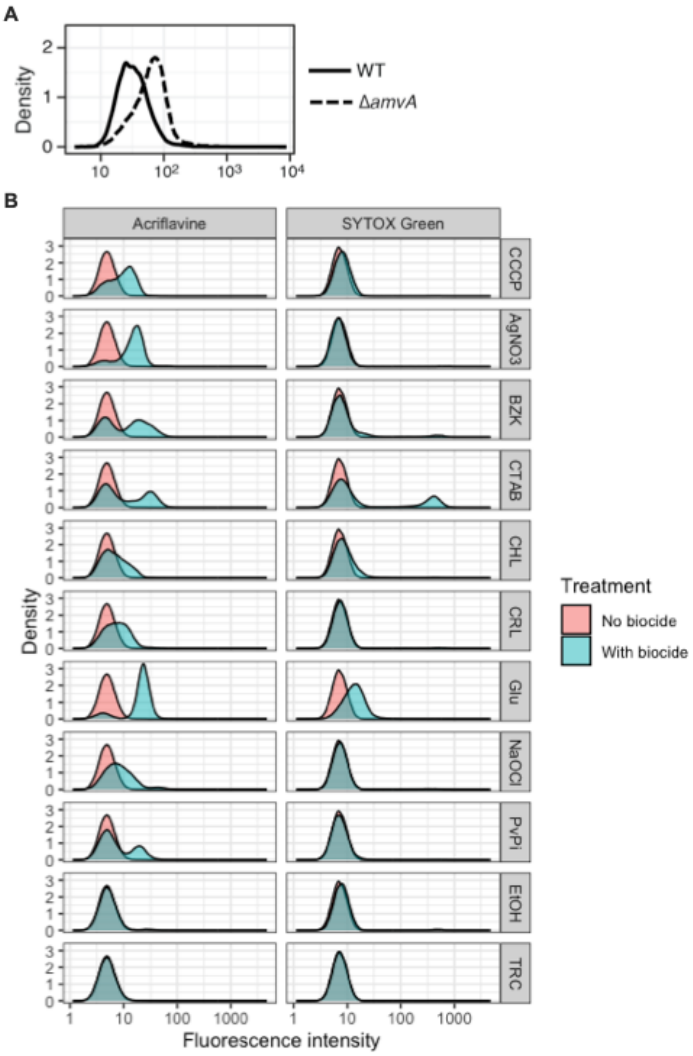

Figure 4. **Biocides' impact on acriflavine intracellular accumulation and cell membrane permeability.** (A) The transposon mutant of *amvA* derived from *A. baumannii* AB5075 accumulates more acriflavine then the parental strain does. (B) The difference of acriflavine and SYTOX Green accumulation between no treatment and biocide treated *A. baumannii* BAL062 were measured through flow cytometry (BD Influx™ Cell Sorter). The treatment concentration of the 10 biocides was at ¼ MIC, respectively. Each curve shows the fluorescence intensity for 50,000 cells. The cell populations show fluorescence profiles based on the concentration of acriflavine or SYTOX Green in the cell cytoplasm.

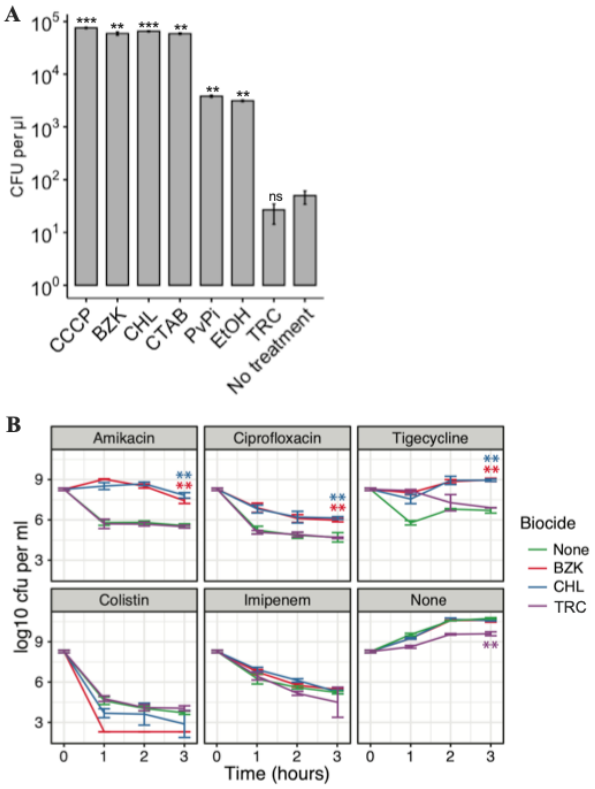

Figure 5. Biocides and antibiotics interactions in *A. baumannii*. (A) Biocides that dissipate membrane potential also reduce killing by gentamicin. Treatment of *A. baumannii* ATCC17978 with 4µg/ml Gentamicin (2x MIC) for 60 minutes killed 99.8% of cells. Addition of benzalkonium, ethanol, chlorhexidine, polyvidone iodine or CTAB at ¼ MIC did not influence bacterial growth, but dramatically reduced killing by gentamicin, with survival in the presence of biocide 100-1000 times higher than survival with gentamicin alone. Triclosan, which did not influence membrane potential at ¼ MIC, did not have this effect. Three biological replicates were included. Statistical significance was assessed by non-parametric t-test by comparing each biocide treatment to non-treatment survival CFU, respectively. (B) Biocide antagonism with a broader range of antibiotics of intracellular targets. Treatment of *A. baumannii* ATCC17978 with 2xMIC of amikacin, ciprofloxacin or 3xMIC of tigecycline for 1 hour killed more than 99% of cells. After 1 hour, there was no significant killing effects observed for either of the three conditions, which was possibly due to persisters or drug tolerance of the minority of the cell population. Addition of benzalkonium or chlorhexidine at ¼ MIC did not affect bacterial growth, but significantly inhibit killing of these three antibiotics, with survival in the presence of biocide 100-1000 times higher than survival with antibiotic alone. Triclosan did not have antagonistic effect with any of the antibiotics. Colistin at 2xMIC killed more than 99% of cells within 1 hour. Addition of ¼ MIC of triclosan did not influence bacterial growth and colistin killing, but benzalkonium and chlorhexidine increased the

killing rate for 10-100 times. None of the three biocides affected killing by 2xMIC of imipenem. Three biological replicates were included. Statistical significance overall was assessed by mixed-repeated measures ANOVA, followed by a one-way ANOVA with Dunnett's post-hoc test at t = 3 if the first test showed a significant effect.

530 **Materials and methods**

531 ***Bacterial strain and mutant library.*** The *A. baumannii* global clonal II MDR strain BAL062 was
532 used as the parental strain for mutant library construction as previously described [20,69], yielding
533 a saturated Tn*5* mutant library, containing >100k unique mutants, using electroporation. *A.*
534 *baumannii* AB5075-UW wild-type and Tn26 insertion mutants of *adeB* (ABUW_1975-150::T26),
535 *lpsB* (ABUW_3448-414::T26), *pyrC* (ABUW_2825-337::T26), *adeR* (ABUW_1973-195::T26)
536 and the remaining transposon mutants were obtained from the Manoil lab collection [25] (Table
537 S3).

538 ***Biocides and biocide-susceptibility test.*** The MICs of the parental strain *A. baumannii*
539 BAL062 against 10 biocides (Table S1) were tested through the 2-fold serial broth dilution
540 method. Due to different solubility of each compound, the media used were varied. Triclosan
541 and chloroxylenol were tested in DMSO complemented Mueller-Hinton II medium (MH) broth
542 (BD Biosciences), $AgNO_3$ in Luria Bertani broth without sodium chloride, and the rest of 7
543 compounds in MH broth. Three biological repeats were performed to confirm MIC values.

544 ***TraDIS assay.*** For each compound, two biological replicates of approximately 1×10^9 cells of *A.*
545 *baumannii* BAL062 mutant TraDIS library were inoculated into each 10 mL of growth media and
546 grown for 16hrs at 37ºC with shaking, yielding 18 sets of MH broth, 6 sets of DMSO-
547 complemented MH broth, and 4 sets of Luria Bertani broth without sodium chloride. Overnight
548 cultures were then diluted 1/100 in the same fresh media, which was then inoculated with
549 respective biocide compounds at ¼ × MIC, or without any addition for the six negative controls
550 (without biocide) and grown at 37ºC with shaking for 16 hrs. The genomic DNA from 2mL of this
551 overnight culture was extracted and purified using DNeasy Blood & Tissue Kit (Qiagen).

552 ***Sequencing and data analysis.*** 5 µg of gDNA was fragmented from 28 samples and TraDIS
553 sequencing libraries were constructed using methods previously described[20]. TraDIS
554 sequencing was performed on HiSeq2500 Illumina platform and generated 500k 50 bp single-
555 end reads per sample. The resulting FASTQ files were analysis using the TraDIS Toolkit using
556 parameters as previously described[22,69]. TraDIS sequencing data was deposited in the
557 European Nucleotide Database under project number PRJEB8707.

558 ***Membrane potential assay via flow cytometry*****.** Membrane potential was assessed using the
559 Bac*Light*^{TM} Bacterial Membrane Potential Kit (ThermoFisher Scientific). Multiple colonies of *A.*
560 *baumannii* BAL062 were inoculated into 5 ml growth media in 50-ml Falcon tube, including three
561 biological replicates, which were incubated at 37°C with shaking at 200rpm overnight or for 16
562 hours. 50 µl of the overnight culture was inoculate into 5 ml fresh media in 50-ml Falcon tube or
563 cell culture flask and incubated at 37°C with shaking at 200rpm, until the cells reached to early
564 (OD_{600} 0.4-0.6) exponential phase. AgNO3 media was in LB without sodium chloride, and the
565 media for all the other biocide membrane potential assays were prepared in MH broth. Cell
566 cultures that reached designated density were treated by biocide at ¼ MIC (Table S2) for 2-5
567 minutes at 37°C with shaking at 200rpm. 10 µl of the subculture then was inoculated in 1 ml filter
568 sterile phosphate buffered saline (PBS) that was supplemented with 8 µg/ml $DiOC_2(3)$, incubated
569 at room temperature up to 30 minutes, and followed by flow cytometry analysis in BD Influx^{TM}
570 Cell Sorter with an excitation wavelength of 488 nm. The peak emission wavelengths were at
571 530 nm (FITC or green) and 610 nm (Texas Red). The samples without $DiOC_2(3)$ treatment were
572 compared to the samples with the treatment to confirm that the fluorescent signals detected in
573 FITC and Texas Red channels were from $DiOC_2(3)$ and to gate the cell population of interest.
574 50,000 events of the gated population were counted for each sample. The red/green

575 fluorescence intensity ratio, that is proportional to membrane potential, was calculated based on
576 the total events of each sample.

577 ***Acriflavine cellular accumulation assay and membrane permeability assay via flow***
578 ***cytometry***. Overnight cultures of *A. baumannii BAL062* were prepared as described in
579 "Membrane potential assay via flow cytometry" and were sub-cultured at 1:100 in the respective
580 growth media and grown at 37 °C with shaking at 200rpm until OD_{600} reached 0.4-0.6. For
581 acriflavine cellular accumulation assay, biocides at ¼ MIC and acriflavine at 1/32 MIC (Table S2)
582 were then added to the cultures and incubate at 37°C with shaking at 200rpm for 2-5 minutes.
583 The cultures then were diluted 1/100 in fresh growth media supplemented with acriflavine at 1/32
584 MIC right before flow cytometry analysis in BD Influx™ Cell Sorter, with an excitation wavelength
585 of 488 nm and emission at 530 nm. For membrane permeability assay, biocides at ¼ MIC and
586 1 μM SYTOX™ Green were added to the subculture and incubate at 37°C with shaking at
587 200rpm for 2-5 minutes. The cultures were diluted 1/100 in the fresh growth media supplemented
588 with 1 μM SYTOX™ right before flow cytometry analysis in BD Influx™ Cell Sorter, with an
589 excitation wavelength of 488 nm and emission at 530 nm. Non-stained samples were also
590 analysed in BD Influx™ Cell Sorter to assist gating cell population of interest. 50,000 events of
591 the gated population were counted for each sample in both assays.

592 ***Antimicrobial killing assay.*** To examine the effect of biocides on gentamicin killing, overnight
593 cultures of ATCC17978 were subcultured at 1:100 in Mueller-Hinton II medium and grown at
594 37°C with vigorous shaking to an OD_{600} of 0.6-0.8. Biocides at ¼ MIC gentamicin at 2xMIC were
595 added to the cultures at room temperature. The cultures were returned to incubation at 37°C
596 200rpm, and were serially diluted and plated to enumerate viable bacteria after 60 minutes. The
597 effect of biocides on killing by amikacin (7.5 μg/ml), ciprofloxacin (1 μg/ml), tigecycline (7.5 μg/ml),

598 colistin (3.5 μg/ml) and imipenem (2.5 μg/ml) was measured similarly, except that cells were
599 grown to an OD_{600} of 0.4-0.6 and survival measured at 1-, 2- and 3-hour post-treatment.
600 Concentrations of biocides used were listed in Table S2.

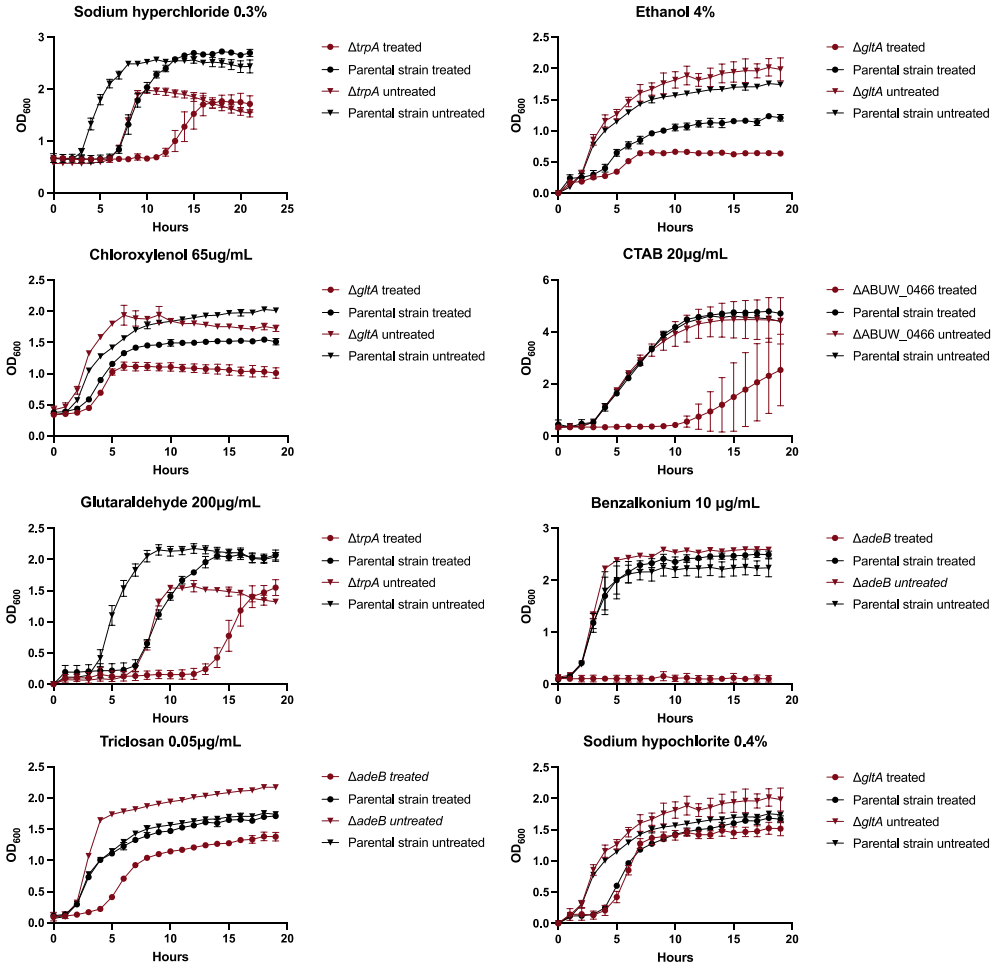

Figure S1. TraDIS data validation. The growth curves of an individual transposon mutant were compared to the parental strain *A. baumannii* AB5075, with or without biocide treatment. Three biological replicates were included. Despite not all the transposon mutants have the same growth fitness in the growth media as the parental strain, the biocides at the same concentration caused more significant growth inhibition in the mutants than in the parental strain. These observations are consistent with TraDIS results.

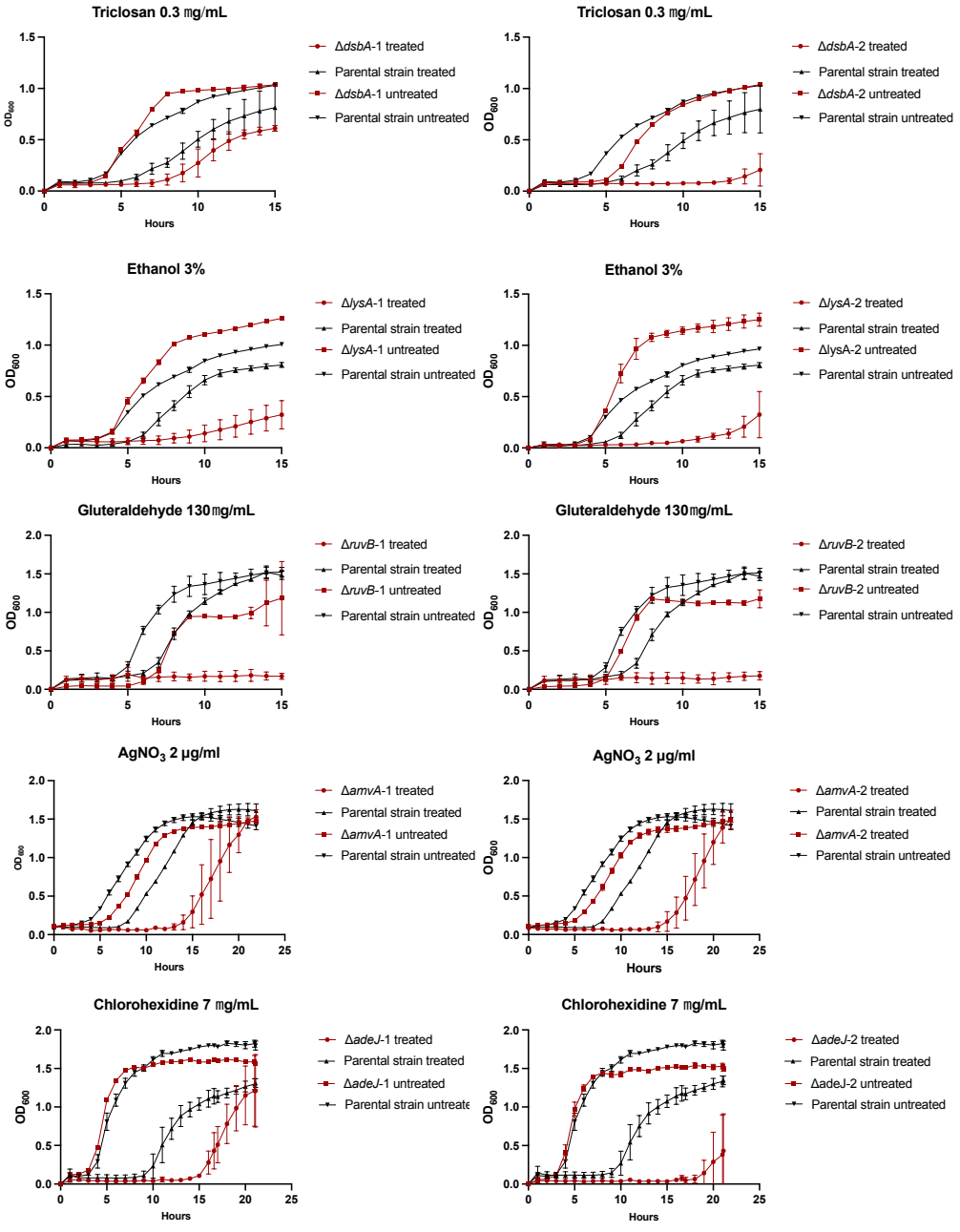
Triclosan 0.3 mg/mL
ΔdsbA-1 treated
Parental strain treated
ΔdsbA-1 untreated
Parental strain untreated
Triclosan 0.3 mg/mL
ΔdsbA-2 treated
Parental strain treated
ΔdsbA-2 untreated
Parental strain untreated
Ethanol 3%
ΔlysA-1 treated
Parental strain treated
ΔlysA-1 untreated
Parental strain untreated
Ethanol 3%
ΔlysA-2 treated
Parental strain treated
ΔlysA-2 untreated
Parental strain untreated
Gluteraldehyde 130mg/mL
ΔruvB-1 treated
Parental strain treated
ΔruvB-1 untreated
Parental strain untreated
Gluteraldehyde 130mg/mL
ΔruvB-2 treated
Parental strain treated
ΔruvB-2 untreated
Parental strain untreated
AgNO3 2 µg/ml
ΔamvA-1 treated
Parental strain treated
ΔamvA-1 untreated
Parental strain untreated
AgNO3 2 µg/ml
ΔamvA-2 treated
Parental strain treated
ΔamvA-2 treated
Parental strain untreated
Chlorohexidine 7 mg/mL
ΔadeJ-1 treated
Parental strain treated
ΔadeJ-1 untreated
Parental strain untreate
Chlorohexidine 7 mg/mL
ΔadeJ-2 treated
Parental strain treated
ΔadeJ-2 untreated
Parental strain untreated
OD600
Hours

608

Figure S2. Comparisons of biocide tolerance phenotype among the transposon mutants of the same gene. The transposon mutants of five genes, that showed changes in transposon insertion reads in the libraries treated by biocides, were chosen to be tested through growth curve assays. If the gene of interest do affect biocide sensitivity of the cell, the transposon mutants of different insertion sites should have similar phenotype. Alternatively, if the transposon mutants have distinct phenotypes, there maybe secondary mutations that can lead to phenotype variations. Two different and unique Tn*5* transposon mutants of each of the five genes were tested, and the pairs display similar biocide sensitivity changes, consistent with the respective TraDIS results. Three biological replicates were included for each mutant. The TraDIS results and transposon insertion sites of the mutants of choice are presented in Table S3.

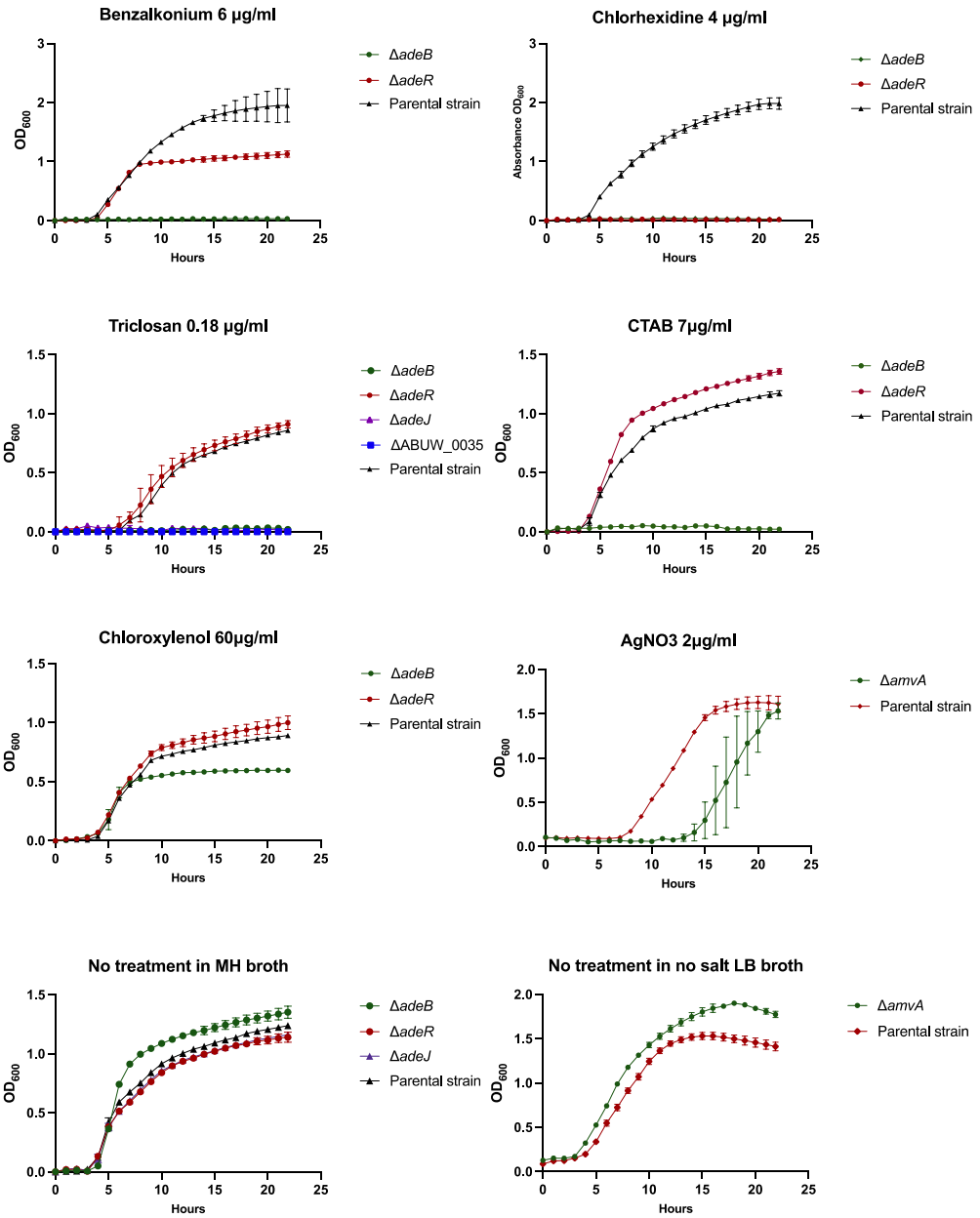
Benzalkonium 6 µg/ml
ΔadeB
ΔadeR
Parental strain
OD600
Hours
Chlorhexidine 4 µg/ml
Absorbance OD600
Triclosan 0.18 µg/ml
ΔadeJ
ΔABUW_0035
CTAB 7µg/ml
Chloroxylenol 60µg/ml
AgNO3 2µg/ml
ΔamvA
No treatment in MH broth
No treatment in no salt LB broth

619

620 **Figure S3. Validation of drug efflux pump's role in biocide resistance.** The growth curves of
621 an individual transposon mutant of an efflux gene or the transcriptional regulator of an efflux gene were
622 compared to the parental strain *A. baumannii* AB5075, with or without biocide treatment. Three
623 biological replicates were included. Despite not all the transposon mutants have the same growth
624 fitness in the growth media as the parental strain, the biocides at the same concentration caused more
625 significant growth inhibition in the mutants than in the parental strain. These observations are
626 consistent with TraDIS results.
627

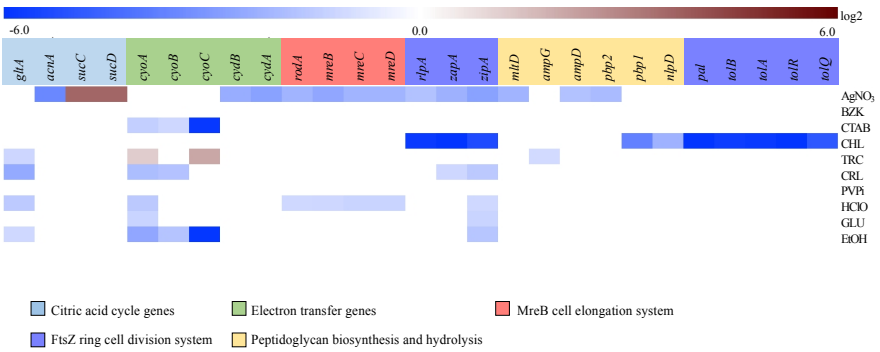

628
629 **Figure S4. TCA cycle, electron transfer and cell division**. As shown in the gradient bar at the
630 top, the boxes are colour coded by Tn*5* insertion read fold change, with darker blue indicating
631 higher decrease in Tn*5* insertion read coverage and darker red higher increase in Tn*5* insertion
632 read coverage for the gene in a library exposed to the biocide, in comparison with the respective
633 gene mutants in the control library. The genes are grouped by their predicted protein families,
634 with colour scheme underneath.

635

Table S1. Current knowledge of antibacterial actions and resistance mechanisms of the biocides tested in this study and a summary of the genes with statistically significant change of Tn5 insertion reads

Biocide (abbreviation)	Examples of clinical application	Proposed antibacterial action	Resistance mechanisms (resistance genes previously identified in *A. baumannii*)	Tn5 insertion read change [a]		TraDIS assay concentration at ¼ MIC [b]	References
				Genes > 2-fold increase	Genes > 2-fold decrease		
Silver nitrate ($AgNO_3$)	Silver impregnated nylon cloth as wound dressing, Ag coated catheters	Inactivation of proteins containing exposed thiol groups and Fe-S clusters, inhibition of DNA synthesis	Efflux, silver efflux system periplasmic chaperone, cation/copper transporter,	100	120		[15,47,70,71]
Benzalkonium (BZK)	Preoperative skin disinfection, hard-surface disinfection	Cell envelope disruption	Efflux (*abeS*, *adeABC*, *adeIJK*, *amvA*)	7	45		[43,72,73]
Cetyltrimethylammonium bromide (CTAB)	Preoperative skin disinfection, cosmetics additive	Cell envelope disruption	Efflux (*abeS*)	35	42		[72]
Chlorhexidine (CHL)	Pharmaceutical preservative, skin, hand and surgical disinfections	Phospholipid bilayer damage and unknown intracellular targets	Efflux (*aceI*, *abeS*, *adeABC*, *adeIJK*, *amvA*), unidentified chlorhexidine-degrading enzyme	68	34		[43,72-74]
Triclosan (TRC)	Antiseptic soap, hand rinses, dental hygiene	Inhibits the FabI enoyl-acyl carrier protein reductase and blocks fatty acid biosynthesis	Efflux (*abeM*, *adeABC*), mutations on enoyl-(acyl-carrier-protein) reductase FabI (*fabI*), expression of expression of alternative enoyl reductase FabK, FabL or FabV	24	57		[16,17,73,75,76]
Chloroxylenol (CRL)	Surgical hand scrubs and other hand-washing products	Probable cell membrane destabilization	Efflux (A1S_2795 and ABAYE_0913 MFS family, A1S_1535 ABC family)	13	44		[46]
Polyvidone iodine (PVPi)	First aid and treatments for skin infection and wounds	Probable binding to key proteins with exposed cysteine and methionine residues, nucleotides and fatty acids	None identified	9	3		
Sodium hypochlorite (NaOCl)	Hard-surface disinfection, disinfection of blood spillages	DNA damage and inhibition of DNA biosynthesis	Glutathione, antioxidant against NaOCl	14	34		[77]
Glutaraldehyde (GLU)	Endoscopes and surgical equipment disinfection	Probable cell envelope disruption, inhibition of DNA, RNA and protein synthesis	None identified	11	17		
Ethanol (EtOH)	Hand sanitising	Probable disruption of phospholipid bilayer and cell lysis	Cell membrane alteration	13	18		[78]

[a] Tn5 read coverage in the mutant pool treated with biocide compare to the control pool with no treatment. The fold-change was based on two biological replicates and with q-value lower than 0.01.

Table S2. The biocide MIC values and their concentrations used in this study.

Compound	MIC (μg/ml)[1]		TraDIS assay concentration (μg/ml)	Biocide concentration in membrane potential assay, acriflavine assays[2], and SYTOX™ Green assays[3] (μg/ml)	ATCC17978 time-kill curve assay (μg/ml)	Assay media
	BAL062	ATCC17978				
Triclosan (irgasan)	0.72	0.72	0.18	0.18	0.18	0.14% DMSO in MH
Chloroxylenol	240	240	60	60	N/A	0.14% DMSO in MH
Silver nitrate	24	8	6	6	N/A	LB without NaCl
Absolute ethanol	8%	12%	2%	2%	4%	MH
Sodium hypochlorite	0.24%	0.24%	0.06%	0.06%	N/A	MH
Glutaraldehyde	1800	1200	450	450	N/A	MH
Polyvidone iodine	4000	2000	1000	1000	600	MH
Chlorhexidine diacetate	20	16	5	5	2.5	MH
Benzalkonium chloride	16	16	4	4	4	MH
Cetyltrimethylammonium bromide	28	28	7	7	7	MH
CCCP (carbonyl cyanide m-chlorophenyl hydrazone)	N/A	N/A	N/A	5	5	MH
Gentamicin	10,000	2	N/A	N/A	4	MH
Amikacin	2000	3.5	N/A	N/A	7.5	MH
Tigecycline	2	2	N/A	N/A	7.5	MH
Ciprofloxacin	250	0.5	N/A	N/A	1	MH
Imipenem	80	1.25	N/A	N/A	2.5	MH
Colistin	5	1.5	N/A	N/A	3.5	MH

1. The antimicrobial MIC values are for *A. baumannii* BAL062 and ATCC17978, respectively.
2. Acriflavine at 3 μg/ml, equal to 1/32 MIC in *A. baumannii BAL062*, was used for its cellular accumulation assays in *A. baumannii* BAL062.
3. SYTOX™ Green at 1μM was used for cell membrane permeability assays in *A. baumannii* BAL062.

Table S3. Transposon mutants of *A. baumannii* AB5075 selected for growth curve assays in this study.

Locus tag	Gene name or function	Transposon insertion site/ gene length	Tn*5* insertion read change (log2)[1]								
			AgNO3	TRC	BZK	CTAB	CHL	CRL	NaOCl	Glu	EtOH
ABUW_0622	*trpA*	433/804	ns	ns	ns	-1.99	ns	-1.41	**-2.12**	**-1.45**	-1.89
ABUW_0867	*gltA*	563/1275	ns	-1.23	ns	-0.87	ns	**-2.56**	**-1.58**	ns	**-1.15**
ABUW_0466	Ribonuclease I	320/633	ns	-1.66	-1.54	**-1.97**	ns	-1.12	ns	-1.10	-0.77
ABUW_1975	*adeB*	150/3108	ns	**-2.99**	**-6.85**	**-1.15**	**-6.42**	**-1.02**	ns	ns	ns
ABUW_1973	*adeR*	195/744	ns	**ns**	**-2.92**	**ns**	**-4.74**	**ns**	ns	ns	ns
ABUW_0843	*adeJ*-1	1711/3177		**-2.14**	-1.12	ns	**-4.16**	**-2.55**	ns	ns	ns
	adeJ-2	956/3177									
ABUW_0035	RND efflux transporter	2427/3126	ns	**-2.87**	ns	ns	ns	ns	ns	ns	ns
ABUW_1679	*amvA*-1	495/1479	**-4.28**	ns	-0.64	ns	-6.73	ns	ns	ns	ns
	amvA-2	785/1497									
ABUW_3846	*dsbA*-1	184/618	-0.86	**-2.59**	-0.97	-1.09	ns	-0.98	ns	ns	ns
	dsbA-2	336/618									
ABUW_0953	*lysA*-1	390/1251	-0.79	0.58	ns	ns	ns	-0.87	-1.06	ns	**-2.83**
	lysA-2	721/1251									
ABUW_0999	*ruvB*-1	267/1005	ns	ns	ns	ns	ns	ns	-1.09	**-2.08**	ns
	ruvB-2	350/1005									
ABUW_2825	*pyrC*	337/1035	**5.17**	1.19	ns	0.58	ns	0.86	ns	ns	ns
ABUW_3448	*lpsB*	414/1101	-1.13	**-2.35**	1.00	ns	ns	-1.29	ns	ns	ns

1. The fold change values with bold font represent the biocide sensitivity of the respective mutants were selected for growth curve assays or MIC assays (Figure 1B, S1, S2 and S3).

References:

1 O'Neil, J. Tackling a crisis for the health and wealth of naions. (World Health Organization, 2014).

2 Blair, J. M. A., Webber, M. A., Baylay, A. J., Ogbolu, D. O. & Piddock, L. J. V. Molecular mechanisms of antibiotic resistance. *Nat. Rev. Microbiol.* **13**, 42-51 (2015).

3 Peleg, A. Y., Seifert, H. & Paterson, D. L. Acinetobacter baumannii: emergence of a successful pathogen. *Clini Microbial Rev.* **21**, 538-582 (2008).

4 Wong, D. *et al.* Clinical and Pathophysiological Overview of Acinetobacter Infections: a Century of Challenges. *Clin Microbiol Rev* **30**, 409-447, doi:10.1128/CMR.00058-16 (2017).

5 McDonnell, G. & Russell, A. D. Antiseptics and disinfectants: activity, action, and resistance. *Clini Microbial Rev.* **12**, 147-179 (1999).

6 Webber, M. A. *et al.* Parallel evolutionary pathways to antibiotic resistance selected by biocide exposure. *J. Antimicrob. Chemother.* **70**, 2241-2248 (2015).

7 Fernández-Cuenca, F. *et al.* Reduced susceptibility to biocides in Acinetobacter baumannii: association with resistance to antimicrobials, epidemiological behaviour, biological cost and effect on the expression of genes encoding porins and efflux. *J. Antimicrob. Chemother.* **70**, 3222-3229 (2015).

8 Alekshun, M. N. & Levy, S. B. The mar regulon: multiple resistance to antibiotics and other toxic chemicals. *Trends Microbiol.* **7**, 410-413 (1999).

9 Rajamohan, G., Srinivasan, V. B. & Gebreyes, W. A. Novel role of Acinetobacter baumannii RND efflux transporters in mediating decreased susceptibility to biocides. *J Antimicrob Chemother* **65**, 228-232 (2010).

10 Conceicão, T., Coelho, C., Lencastre, H. & Aires-de-Sousa, M. High prevalence of biocide resistance determinants in Staphylococcus aureus isolates from the three African countries. *Antimicrob. Agents Chemother.* **60**, 678-681 (2015).

11 Liau, S. Y., Read, D. C., Pugh, W. J., Furr, J. R. & Russell, A. D. Interaction of silver nitrate with readily identifiable groups: relationship to the antibacterial action of silver ions. *Lett. Appl. Microbiol* **25**, 279-283 (1997).

12 Morones-Ramirez, J. R., Winkler, J. A., Spina, C. S. & Collins, J. J. Silver enhances antibiotic activity against Gram-negative bacteria. *Sci Transl Med.* **5**, 190ra181 (2013).

13 Dibrov, P., Dzioba, J., Gosink, K. K. & Häse, C. C. Chemiosmotic mechanism of antimicrobial activity of Ag(+) in Vibrio cholerae. *Antimicrob Agents Chemother* **46**, 2668-2670 (2002).

14 Gupta, A., Matsui, K., Lo, J. F. & Silver, S. Molecular basis for resistance to silver cations in Salmonella. *Nat. Med.* **5**, 183-188 (1999).

15 Franke, S., Grass, G. & Nies, D. H. The product of the ybdE gene of the Escherichia chromosome is involved in detoxification of silver ions. *Microbiology* **147**, 965-972 (2001).

16 McMurry, L. M., Oethinger, M. & Levy, S. B. Triclosan targets lipid synthesis. *Nature* **394**, 531-532 (1998).

17 Chen, Y., Pi, B., Zhou, H., Yu, Y. & Li, L. Triclosan resistance in clinical isolates of Acinetobacter baumannii. *J. Med. Microbiol.* **58**, 1086-1091 (2009).

18 Yasir, M. *et al.* TraDIS-Xpress: a high-resolution whole-genome assay identifies novel mechanisms of triclosan action and resistance. *Genome Research* **30**, 239-249, doi:10.1101/gr.254391.119 (2020).
19 Hassan, K. A., Liu, Q., Henderson, P. J. F. & Paulsen, I. T. Homologs of the Acinetobacter baumannii AceI transporter represent a new family of bacterial multidrug efflux systems. *mBio* **6**, e01982-01914 (2015).
20 Langridge, G. C. *et al.* Simultaneous assay of every Salmonella Typhi gene using one million transposon mutants. *Genome Res.* **19**, 2308-2316 (2009).
21 Cain, A. K. *et al.* A decade of advances in transposon-insertion sequencing. *Nat Rev Genet* **21**, 526-540, doi:10.1038/s41576-020-0244-x (2020).
22 Hassan, K. A. *et al.* Fluorescence-Based Flow Sorting in Parallel with Transposon Insertion Site Sequencing Identifies Multidrug Efflux Systems in Acinetobacter baumannii. *mBio* **7**, e01200-01216 (2016).
23 Barquist, L. *et al.* The TraDIS toolkit: sequencing and analysis for dense transposon mutant libraries. *Bioinformatics* **32**, 1109-1111, doi:10.1093/bioinformatics/btw022 (2016).
24 Hood, M. I., Becker, K. W., Roux, C. M., Dunman, P. M. & Skaar, E. P. genetic determinants of intrinsic colistin tolerance in Acinetobacter baumannii. *Infect Immun* **81**, 542-551, doi:10.1128/IAI.00704-12 (2013).
25 Gallagher, L. A. *et al.* Resources for Genetic and Genomic Analysis of Emerging Pathogen Acinetobacter baumannii. *J Bacteriol* **197**, 2027-2035, doi:10.1128/JB.00131-15 (2015).
26 Kenyon, J. J., Nigro, S. J. & Hall, R. M. Variation in the OC locus Acinetobacter baumannii genomes predicts extensive structural diversity in the lipoologosaccharide. *PLoS ONE* **9**, e107833 (2014).
27 Arroyo, L. A. *et al.* The pmrCAB operon mediates polymyxin resistance in Acinetobacter baumannii ATCC 17978 and clinical isolates through phosphoethanolamine modification of lipid A. *Antimicrob Agents Chemother* **55**, 3743-3751 (2011).
28 Boll, J. M. *et al.* Reinforcing Lipid A Acylation on the Cell Surface of Acinetobacter baumannii Promotes Cationic Antimicrobial Peptide Resistance and Desiccation Survival. *mBio* **6**, e00478-00415 (2015).
29 Kenyon, J. J. & Hall, R. M. Variation in the complex carbohydrate biosynthesis loci of Acinetobacter baumannii genomes. *PLoS ONE* **8**, e62160 (2013).
30 Lees-Miller, R. G. *et al.* A common pathway for O-linked protein-glycosylation and synthesis of capsule in Acinetobacter baumannii. *Mol. Microbiol.* **89**, 816-830 (2013).
31 Geisinger, E. & Isberg, R. R. Antibiotic modulation of capsular exopolysaccharide and virulence in Acinetobacter baumannii. *PLoS. Pathogens* **11**, e1004691 (2015).
32 Luke, N. R. *et al.* Identification and characterization of a glycosyltransferase involved in Acinetobacter baumannii lipopolysaccharide core biosynthesis. *Infect. Immun.* **78**, 2017-2023 (2010).
33 Kenyon, J. J., Holt, K. E., Pickard, D., Dougan, G. & Hall, R. M. Insertions in the OCL1 locus of Acinetobacter baumannii lead to shortened lipooligosaccharides. *Res Microbiol* **165**, 472-475 (2014).

34 Pakharukova, N. *et al.* Structural insight into archaic and alternative chaperone-usher pathways reveals a novel mechanism of pilus biogenesis. *PLoS Pathog* **11**, e1005269 (2015).
35 Coyne, S., Courvalin, P. & Périchon, B. Efflux-mediated antibiotc resistance in Acinetobacter spp. *Antimicrob. Agents Chemother.* **55**, 947-953 (2011).
36 Chapman-Smith, A. & Cronan, J. E. The enzymatic biotinylation of proteins: a post-translational modification of exceptional specificity. *Trends Biochem. Sci.* **24**, 359-363 (1999).
37 Yoon, E. J., Courvalin, P. & Grillot-Courvalin, C. RND-type efflux pumps in multidrug-resistant clinical isolates of Acinetobacter baumannii: major role for AdeABC overexpression and AdeRS mutations. *Antimicrob Agents Chemother* **57**, 2989-2995 (2013).
38 Hassan, K. A. *et al.* Transcriptomic and biochemical analyses identify a family of chlorhexidine efflux proteins. *Proc Natl Acad Sci U S A* **110**, 20254-20259 (2013).
39 Yoon, E. J. *et al.* Contribution of resistance-nodulation-cell division efflux systems to antibiotic resistance and biofilm formation in Acinetobacter baumannii. *mBio* **6**, e00309-00315 (2015).
40 Leus, I. V. *et al.* Substrate Specificities and Efflux Efficiencies of RND Efflux Pumps of Acinetobacter baumannii. *J Bacteriol* **200**, doi:10.1128/JB.00049-18 (2018).
41 Sugawara, E. & Nikaido, H. Properties of AdeABC and AdeIJK efflux systems of Acinetobacter baumannii compared with those of the AcrAB-TolC system of Escherichia coli. *Antimicrob Agents Chemother* **58**, 7250-7257, doi:10.1128/AAC.03728-14 (2014).
42 Rosenfeld, N., Bouchier, C., Courvalin, P. & Périchon, B. Expression of the resistance-nodulation-cell division pump AdeIJK in Acinetobacter baumannii is regulated by AdeN, a TetR-type regulator. *Antimicrob Agents Chemother* **56**, 2504-2510 (2012).
43 Rajamohan, G., Srinivasan, V. B. & Gebreyes, W. A. Molecular and functional characterization of a novel efflux pump, AmvA, mediating antimicrobial and disinfectant resistance in Acinetobacter baumannii. *J. Antimicrob. Chemother.* **65**, 1919-1925 (2010).
44 Hassan, K. A. *et al.* Roles of DHA2 family transporters in drug resistance and iron homeostasis in Acinetobacter spp. *J Mol Microbiol Biotechnol* **20**, 116-124 (2011).
45 Orth, P., Schnappinger, D., Hillen, W., Saenger, W. & Hinrichs, W. Structural basis of gene regulation by the tetracycline inducible Tet repressor-operator system. *Nat Struct Biol* **7**, 215-219 (2000).
46 Li, L., Hassan, K. A., Brown, M. H. & Paulsen, I. T. Rapid multiplexed phenotypic screening identifies drug resistance functions for three novel efflux pumps in Acinetobacter baumannii. *J. Antimicrob. Chemother.* **71**, 1223-1232 (2016).
47 Jung, W. K. *et al.* Antibacterial activity and mechanism of action of the silver ion in Staphylococcus aureus and Escherichia coli. *Appl Environ Microbiol* **74**, 2171-2178 (2008).

48 Strahl, H. & Hamoen, L. W. Membrane potential is important for bacterial cell division. *Proc Natl Acad Sci U S A* **107**, 12281-12286, doi:10.1073/pnas.1005485107 (2010).
49 Rajamohan, G., Srinivasan, V. B. & Gebreyes, W. A. Novel role of Acinetobacter baumannii RND efflux transporters in mediating decreased susceptibility to biocides. *J Antimicrob Chemoth* **65**, 228-232, doi:10.1093/jac/dkp427 (2010).
50 Taber, H. W., Mueller, J. P., Miller, P. F. & Arrow, A. S. Bacterial uptake of aminoglycoside antibiotics. *Microbiol Rev* **51**, 439-457 (1987).
51 Holtje, J. V. Induction of streptomycin uptake in resistant strains of Escherichia coli. *Antimicrob Agents Chemother* **15**, 177-181, doi:10.1128/aac.15.2.177 (1979).
52 Nikaido, H. & Thanassi, D. G. Penetration of lipophilic agents with multiple protonation sites into bacterial cells: tetracyclines and fluoroquinolones as examples. *Antimicrob Agents Chemother* **37**, 1393-1399, doi:10.1128/aac.37.7.1393 (1993).
53 Piddock, L. J. Mechanism of quinolone uptake into bacterial cells. *J Antimicrob Chemother* **27**, 399-403, doi:10.1093/jac/27.4.399 (1991).
54 Morente, E. O. *et al.* Biocide tolerance in bacteria. *Int J Food Microbiol* **162**, 13-25, doi:10.1016/j.ijfoodmicro.2012.12.028 (2013).
55 LaBreck, P. T. *et al.* Systematic Analysis of Efflux Pump-Mediated Antiseptic Resistance in Staphylococcus aureus Suggests a Need for Greater Antiseptic Stewardship. *mSphere* **5**, doi:10.1128/mSphere.00959-19 (2020).
56 Wand, M. E., Bock, L. J., Bonney, L. C. & Sutton, J. M. Mechanisms of Increased Resistance to Chlorhexidine and Cross-Resistance to Colistin following Exposure of Klebsiella pneumoniae Clinical Isolates to Chlorhexidine. *Antimicrob Agents Chemother* **61**, doi:10.1128/AAC.01162-16 (2017).
57 Oggioni, M. R. *et al.* Significant Differences Characterise the Correlation Coefficients between Biocide and Antibiotic Susceptibility Profiles in Staphylococcus aureus. *Curr Pharm Des* **21**, 2054-2057, doi:10.2174/1381612821666150310103238 (2015).
58 Wales, A. D. & Davies, R. H. Co-Selection of Resistance to Antibiotics, Biocides and Heavy Metals, and Its Relevance to Foodborne Pathogens. *Antibiotics (Basel)* **4**, 567-604, doi:10.3390/antibiotics4040567 (2015).
59 Zhao, Y. *et al.* Evidence for co-selection of antibiotic resistance genes and mobile genetic elements in metal polluted urban soils. *Sci Total Environ* **656**, 512-520, doi:10.1016/j.scitotenv.2018.11.372 (2019).
60 Samreen, Ahmad, I., Malak, H. A. & Abulreesh, H. H. Environmental antimicrobial resistance and its drivers: a potential threat to public health. *J Glob Antimicrob Re* **27**, 101-111, doi:10.1016/j.jgar.2021.08.001 (2021).
61 Nordholt, N., Kanaris, O., Schmidt, S. B. I. & Schreiber, F. Persistence against benzalkonium chloride promotes rapid evolution of tolerance during periodic disinfection. *Nat Commun* **12**, 6792, doi:10.1038/s41467-021-27019-8 (2021).
62 Papkou, A., Hedge, J., Kapel, N., Young, B. & MacLean, R. C. Efflux pump activity potentiates the evolution of antibiotic resistance across S. aureus isolates. *Nat Commun* **11**, 3970, doi:10.1038/s41467-020-17735-y (2020).

63 El Meouche, I. & Dunlop, M. J. Heterogeneity in efflux pump expression predisposes antibiotic-resistant cells to mutation. *Science* **362**, 686-690, doi:10.1126/science.aar7981 (2018).
64 Fridman, O., Goldberg, A., Ronin, I., Shoresh, N. & Balaban, N. Q. Optimization of lag time underlies antibiotic tolerance in evolved bacterial populations. *Nature* **513**, 418-421, doi:10.1038/nature13469 (2014).
65 Van den Bergh, B. *et al.* Frequency of antibiotic application drives rapid evolutionary adaptation of Escherichia coli persistence. *Nat Microbiol* **1**, 16020, doi:10.1038/nmicrobiol.2016.20 (2016).
66 Baym, M. *et al.* Spatiotemporal microbial evolution on antibiotic landscapes. *Science* **353**, 1147-1151, doi:10.1126/science.aag0822 (2016).
67 Levin-Reisman, I. *et al.* Antibiotic tolerance facilitates the evolution of resistance. *Science* **355**, 826-830, doi:10.1126/science.aaj2191 (2017).
68 Kampf, G. Antibiotic ResistanceCan Be Enhanced in Gram-Positive Species by Some Biocidal Agents Used for Disinfection. *Antibiotics (Basel)* **8**, doi:10.3390/antibiotics8010013 (2019).
69 Boinett, C. J. *et al.* Clinical and laboratory-induced colistin-resistance mechanisms in Acinetobacter baumannii. *Microb Genom* **5**, doi:10.1099/mgen.0.000246 (2019).
70 Odermatt, A., Krapf, R. & Solioz, M. Induction of the putative copper ATPase, CopA and CopB, of Enterococcus hirae by Ag+ and Cu2+ extrusion by CopB. *Biochem. Biophys. Res. Commun.* **202**, 44-48 (1994).
71 Maillard, J. Y. & Hartemann, P. Silver as an antimicrobial: facts and gaps in knowledge. *Crit Rev Microbiol* **39**, 473-483 (2013).
72 Srinivasan, V. B., Rajamohan, G. & Gebreyes, W. A. Role of AbeS, a novel efflux pump of the SMR family of transporters, in resistance to antimicrobial agents in Acinetobacter baumannii. *Antimicrob. Agents Chemother.* **53**, 5312-5316 (2009).
73 Rajamohan G, Srinivasan VB & Gebreyes, W. A. Novel role of Acinetobacter baumannii RND efflux transporters in mediating decreased susceptibility to biocides. *J. Antimicrob. Chemother.* **65**, 228-232 (2010).
74 Ogase, H., Nagal, I., Kameda, K., Kume, S. & Ono, S. Identification and quantitative analysis of degradation products of chlorhexidine with chlorhexidine-resistant bacteria with three-dimensional high performance liquid chromatography. *J. Appl. Bacteriol* **73**, 71-78 (1992).
75 Su, X. Z., Chen, J., Mizushima, T., Kuroda, T. & Tsuchiya, T. AbeM, an H+-coupled Acinetobacter baumannii multidrug efflux pump belonging to the MATE family of transporters. *Antimicrob. Agents Chemother.* **49**, 4362-4364 (2005).
76 Zhu, L., Lin, J., Ma, J., Cronan, J. E. & Wang, H. Triclosan resistance of Pseudomonas aeruginosa PAO1 is due to FabV, a triclosan-resistant enoyl-acyl carrier protein reductase. *Antimicrob. Agents Chemother.* **54**, 689-698 (2010).
77 Chesney, J. A., Eaton, J. W. & Mahoney, J. R. Bacterial glutathione: a sacrificial defense against chlorine compounds. *J. Bacteriol* **178**, 2131-2135 (1996).
78 Fried, V. A. & Novick, A. Organic solvents as probes for the structure and function of the bacterial membrane: effects of ethanol on the wild type and an

229 ethanol-resistant mutant of Escherichia coli K-12. *J. Bacteriol* **114**, 239-248
230 (1973).
231
232

Supplementary data files from the biocide TraDIS experiment are available in Appendix A.

Chapter 3: The ABC-2 transporter, YadGH from *Acinetobacter baumannii* has pleiotropic effects on membrane homeostasis and drug resistance

Authors

Stephanie S. Nagy[1,2], Maoge Zang[3], Alaska Pokhrel[1], Francesca L. Short[4], Liping Li[1,2], Bart A. Eijkelkamp[3], Bhumika S. Shah[1,2], Peter J.F. Henderson[5], Karl A. Hassan[2,6] and Ian T. Paulsen.[1,2]

Author Affiliations

[1]School of Natural Sciences, Faculty of Science and Engineering, Macquarie University, Sydney, NSW, Australia

[2]ARC Centre of Excellence in Synthetic Biology, Macquarie University, Sydney, NSW, Australia

[3]Molecular Science and Technology, College of Science and Engineering, Flinders University, Adelaide, SA, Australia

[4]Department of Microbiology, Monash University, Melbourne, VIC, Australia

[5]School of Biomedical Sciences and Astbury Centre for Structural Biology, University of Leeds, Leeds, West Yorkshire, United Kingdom

[6]School of Environmental and Life Sciences, University of Newcastle, Newcastle, NSW, Australia

Corresponding author: Distinguished Professor Ian T. Paulsen, ian.paulsen@mq.edu.au

Abstract

Multidrug efflux systems are a main mechanism of multidrug resistance in *Acinetobacter baumannii*, a member of the 'ESKAPE' group, known to cause multidrug resistant infections in hospital settings. In a recent TraDIS study, we identified the ABC-2 type transporter genes *yadG* and *yadH* to confer increased fitness against the anti-infective agent silver nitrate. In this study, we heterologously expressed *yadGH* in *Escherichia coli* to examine whether YadGH protein complex confers a multidrug-resistance and efflux phenotype. Antimicrobial resistance studies reveal YadGH expression increased survival against a range of antimicrobials including sulfanilamides, tetracyclines, fluoroquinolones and quaternary ammonium compounds. We performed whole-cell fluorometric transport assays which demonstrated increased acriflavine efflux activity in *E. coli* expressing YadGH. Further analyses into the impact of *yadH* inactivation in *A. baumannii* revealed additional phenotypes including compromised capsule and changes in the cellular membrane fatty acid composition. This suggests that, in addition to conferring a multidrug resistance phenotype, YadGH may also play a physiological role in cell envelope homeostasis in *A. baumannii.*

Introduction

Acinetobacter baumannii is a Gram-negative coccobacillus, known to cause difficult-to-treat, hospital-acquired infections in susceptible patients (1). As an opportunistic pathogen, *A. baumannii* infections are associated with high morbidity and mortality rates in healthcare settings (1–3). A major contributor to multidrug resistance in *A. baumannii* is associated with the intrinsic and adaptive expression of multidrug efflux pumps. In *A. baumannii*, six efflux pump families have been found to play a role in drug resistance of this organism — the Resistance-Nodulation-Division (RND) superfamily, the Major Facilitator Superfamily (MFS), the Multidrug and Toxin Extrusion (MATE) family, the proteobacterial antimicrobial compound efflux (PACE) family, the Small Multidrug Resistance (SMR) family and the ATP-binding cassette superfamily (ABC) (4).

ABC transport proteins are one of the largest families of integral membrane proteins found across all domains of life (5). In bacteria, ABC transporters use ATP-hydrolysis to drive the transport of a diverse range of biologically active molecules in and out of the cell spanning from large macromolecular structures to small molecules and ions (6). This diversity allows ABC transporters to play a role in many key functions in bacterial cell survival, fitness, and pathogenicity (6). According to the TransportDB, approximately 30% of *A. baumannii* encoded transporters belong to the ABC transport family (7).

Recently, we performed a TraDIS study on *A. baumannii* to identify genes important for resistance against common biocides used in hospital environments (Chapter 2). This study led to the identification of ABC transporter genes of unknown function, *yadG* and *yadH,* that are important for bacterial fitness in the presence of topical antiseptic silver nitrate (Chapter 2). The YadGH ABC transporter is a member of the ABC-type 2 transport family, typically known to export complex carbohydrates (8). This family includes members responsible for the efflux of lipopolysaccharides (RfbAB/Wzm-Wzt), lipochitin oligosaccharides (NodIJ), teichoic acids (TagGH), capsular polysaccharides (KpsMT) and drug efflux (DrrAB) (9-13). Phylogenetically, the YadH transport permease clusters closely with the NodJ transport system and one other

transporter permease of unknown function YhhJ (8). However, there is no clear functional role determined for YadGH or any of its related homologs. In *Escherichia coli*, a *yadH* mutant was found to cause a hyperpermeable outer membrane phenotype (14). The *E. coli yadG* and *yadH* genes are located in close to the Mla-complex genes which maintain outer membrane lipid asymmetry through selective phospholipid transport to the outer membrane (14). In *Burkholderia cepacia*, *yadG* and *yadH* genes were found adjacent to the Mla-complex operon (15). Recent TraDIS research on *Burkholderia cenocepacia* revealed *yadG* and *yadH* genes were required for gold tolerance in this organism (16). In *A. baumannii* the *yadG* and *yadH* genes are not found adjacent to the Mla-complex genes. In this study, we performed a range of bioinformatic and phenotypic characterization assays of YadGH from *A. baumannii* AB5075_UW to attempt to clarify the role of this transporter in this pathogen.

Materials and methods

Bioinformatic analyses

All FASTA format sequences were downloaded from the National Centre for Biotechnology Information (NCBI). The coding region of *yadG* and *yadH* was retrieved from *Acinetobacter baumannii* AB5075_UW genome (CP008706.1). Homologous sequences of *yadH* were collected using the HMMER webserver (v. 2.41.2) against reference proteomes (17, 18). Full-length sequences with *E*-values $\leq 10^{-20}$ were deemed homologous. Multiple sequence alignments (MSAs) of *yadH* homologues were performed using MUSCLE (19). A phylogenetic tree of YadH homologues was constructed using the neighbor-joining method with n=1000 bootstrap replicates with default parameters using MEGAX software and visualised in iTOL (20-24). Pan-genome data of *A. baumannii* AB5075_UW from our previous published work was used to determine conservation of *yadG* and *yadH* across the *A. baumannii* species (25). *A. baumannii* genomes included in the analysis cover all complete genomes deposited to the NCBI assembly database as of March 26, 2020. The data was further examined to determine conservation of genetic neighbourhood of *yadG* and *yadH* genes and was visualised using Clinker (26). Gene conservation

analysis of *yadG* and *yadH* genes across more distantly related bacteria was performed using the WebFLaGs server with default parameters (27).

In silico prediction of the structure of YadGH

All *in silico* predictions of the ABC transport complex was performed using AlphaFold2 (28). AlphaFold2 models were generated using ColabFold notebook with default parameters (29). Individual models of YadG and YadH were generated using MMseq2 generated sequence MSAs (29, 30). The multimeric structure of YadGH was predicted using mixed paired and unpaired MSA alignments generated by MMseq2 using the ColabFold_Advanced notebook (29, 30). Amino acid conservation was mapped to YadG and YadH structures using the Consurf webserver (31, 32). Structural homologues of YadGH complex were identified using the DALI server (last accessed 26th of February 2022) (33). All PDB files were visualised with Pymol (34). Ramachandran plots of YadG and YadH models were generated with PROCHECK (35).

Bacterial strains, plasmids, and culture conditions

Bacterial strains used in this study include *A. baumannii* AB5075_UW and Tn*26* insertion mutant derivative in *yadH* (ABUW_1247::Tn*26*). *A. baumannii* AB5075_UW and transposon mutant strains were purchased from the Manoil three-allele collection (Manoil laboratory, University of Washington) (36). *A. baumannii* cultures were grown in LB-Lennox media (5 g/L NaCl, 10 g/L tryptone, 5 g/L yeast extract) at 37°C, 200 rpm unless otherwise specified.

Expression of YadGH^{AB5075} in an *E. coli* host was achieved as follows. As the coding sequence of *yadG* and *yadH* from *A. baumannii* AB5075_UW overlap at the stop and start codon of *yadG* and *yadH* respectively, the native coding region was chemically synthesised and cloned in-frame of the endogenous *tac* promotor and hexa-histidine tag of pTTQ18-RSGH6 expression vector by Genscript (Piscataway, USA). The coding region was cloned between *EcoR*I and *Pst*I restriction sites of the pTTQ18 expression vector to incorporate a hexa-histidine tag ($RSGH_6$) at the C-terminal end of the YadH to achieve the pTTQ18-$YadGH_{RSGH6}$ expression construct (37-39).

Chemically competent *E. coli* BL21 (DE3) (Bioline, USA) were transformed with pTTQ18-RSGH6 (empty vector) and pTTQ18-YadGH$_{RSGH6}$ according to the heat-shock method (40). Briefly, 50 µL of chemically competent *E. coli* were thawed on ice and incubated with 5 ng of plasmid DNA for 30 minutes, followed by heat-shock at 42°C for 40 seconds. *E. coli* samples were immediately transferred to ice to incubate for 2 minutes prior to recovery in S.O.C media (Thermo Fischer) for 1 hour at 37°C, 200 rpm. Recovered cell culture was plated on LB-agar supplemented with 100 µg/mL ampicillin for selection and incubated overnight at 37°C. Following transformation, all *E. coli* cultures harbouring pTTQ18-RSGH$_6$ (empty vector) or pTTQ18-YadGH$_{RSGH6}$ were prepared in LB-media supplemented with 100 µg/mL ampicillin and grown at 37°C, 200 rpm unless otherwise specified.

Small scale culture and expression in *E. coli*

Overnight cultures of *E. coli* were grown in 50 mL of Luria-Bertani (LB) broth (10 g/L NaCl, 10 g/L tryptone, 5 g/L yeast extract) supplemented with 100 µg/mL carbenicillin and 20 mM glycerol at 37°C, shaking at 200 rpm. Overnight cultures were diluted 1:100 in fresh LB media supplemented with 100 µg/mL carbenicillin and 20 mM glycerol and grown at 37°C, shaking at 200 rpm to an optical density (OD) of OD_{600nm} = 0.8. Expression of YadGH was induced with isopropyl ß-D-1-thiogalactopyranoside (0.2 mM final concentration) for 3 hours. Cell cultures were harvested by centrifugation (12,000 × g) for 15 minutes at 4°C.

E. coli mixed membranes were extracted according to the water-lysis spheroplast method as published, with minor modification (39). Briefly, cell pellets were resuspended in 10 mL 0.2 M Tris-HCl, pH 8.0 and stirred on rollers for 20 minutes at room temperature. At time zero, 4.85 mL of sucrose buffer (0.2 M Tris-HCl, pH 8.0, 1 M sucrose, 1 mM EDTA) was added. At 1.5 minutes, 65 µL of freshly prepared 10 mg/mL lysozyme solution was added. At 2 minutes, 9.6 mL MilliQ water was added and the mixture was stirred on rollers for a further 20 minutes. The spheroplasts were sedimented at 25,000 × g for 20 minutes, then resuspended in 15 mL MilliQ water and incubated at room temperature for 30 minutes. Mixed membranes were sedimented at 25,000 × g for 20 minutes, washed thrice with NaPi buffer (0.1 M disodium hydrogen phosphate, 0.1 M

sodium dihydrogen phosphate, pH 7.2). Membrane pellets were resuspended in 500 µL NaPi buffer, pH 7.2 containing 1 mM β-mercaptoethanol, snap-frozen with liquid nitrogen and stored at –80°C prior to further SDS-PAGE and western blot analyses.

Total protein content was quantified using Pierce™ BCA Protein Assay Kit (Thermo Scientific) (41). SDS-PAGE of mixed membrane samples followed the method published by Henderson and MacPherson (42). YadH expression in mixed membranes was detected by Western blotting using an anti-$RGSH_6$–horseradish peroxidase conjugate (Bio-Rad) according to manufacturer instructions.

Biolog phenotype microarrays of *E. coli* transformed with YadGH^{AB5075}

Biolog phenotype microarrays (PMs) using bacterial chemical sensitivity panels PM11-20 were used to determine whether expression of YadGH^{AB5075} in *E. coli* BL21 (DE3) cells could confer antimicrobial resistance (43-45). Briefly, *E. coli* BL21 (DE3) harbouring pTTQ18-$RSGH_6$ (empty vector) or pTTQ18-$YadGH_{RSGH6}$ were streaked onto LB agar plates supplemented with 100 µg/mL ampicillin and grown overnight at 37°C. Individual colonies were streaked onto a fresh LB-ampicillin agar plate and grown overnight at 37°C. Colonies were collected and suspended in Biolog GN IF-0a solution to 85% transmittance, measured by Biolog turbidimeter. Cell suspensions were diluted 1:200 in Biolog IF-10b solution and supplemented with 1:100 dilution of Biolog redox dye mix A. PM plates were inoculated with IPTG (0.05 mM final concentration) and 100 µL of bacterial cell culture in each well across chemical sensitivity panels PM11-PM20. PM plates were sealed with Breathe-Easy® plastic film (Diversified Biotech) to allow for gas exchange. Plates were incubated at 37°C, with shaking at 200 rpm for 72 hours and imaged using a Biolog OmniLog instrument to measure for colorimetric change.

Minimum inhibitory concentration assays of *E. coli* transformed with YadGH^{AB5075}

Minimum inhibitory concentration (MICs) was performed according to the microbroth serial dilution method as described (46). MICs of *E. coli* BL21 (DE3) harbouring pTTQ18-$RSGH_6$ (empty vector) or pTTQ18-$YadGH_{RSGH6}$ were performed in LB media. Overnight bacterial

cultures were diluted in fresh bacteriological media (1:100) supplemented with ampicillin for plasmid selection and grown to mid-exponential phase (OD_{600nm} = 0.6). Cells were further diluted in media (1:100) and inoculated into 96-well plates containing LB media supplemented with 0.05 mM and two-fold serial dilution of the antimicrobial. Plates were sealed with Breathe-Easy® film (Diversified Biotech) and incubated at 37°C, at 200 rpm for 24 hours before growth was measured using absorbance (OD_{600nm}) with the PheraSTAR FSX (BMG LabTech).

Fluorometric transport assays

Overnight cell cultures of *E. coli* BL21 (DE3) harbouring pTTQ18-$RSGH_6$ (empty vector) or pTTQ18-$YadGH_{RSGH6}$ were grown in LB media supplemented with 100 µg/mL ampicillin at 37°C, 200 rpm shaking. Protein expression was induced at OD_{600nm} = 0.8 with 0.05 mM IPTG for 1 hour. Cells were washed thrice with HEPES buffer (20 mM HEPES-KOH pH 7.0, 145 mM NaCl, 5 mM KCl) and resuspended to a final OD_{600nm} = 3 in 1 mL of HEPES buffer. Cells were treated with 10 µM CCCP and 5 µM acriflavine. Fluorescence transport assay was carried out as described (47) with modification for analyses of acriflavine transport using Biotek HT synergy multiplate (Biotek). Excitation and emission wavelengths were set to 450 nm and 510 nm respectively to detect differential acriflavine fluorescence. Assays began with an initial read to adjust for autofluorescence, followed by the injection of 5 µL of 65 µM sodium formate to initiate active transport of acriflavine out of the *E. coli* cells.

Lipid extraction and FAME GC-MS

Lipid extraction and FAME GC-MS were achieved as previous (48, 49). *A. baumannii* AB5075_UW and transposon mutant *A. baumannii* AB5075_UW *yadH*::Tn*26* cultures were grown overnight in LB-Lennox media (5 g/L NaCl, 10 g/L tryptone, 5 g/L yeast extract) at 37°C, 200 rpm shaking. Overnight cultures were inoculated into 20 mL of fresh LB-Lennox media at an initial optical density of OD_{600nm} = 0.05 and grown to a mid-log phase (OD_{600nm} = 0.7). Cell cultures were pelleted at 7,000 × g for 10 minutes and washed in phosphate buffered saline (PBS). Pellets were resuspended in 50 µL of 1.5% sodium chloride buffer. Cell suspension was treated with a 2:1 (v/v) chloroform:methanol and shaken for two minutes before further incubation at

room temperature for 10 minutes. A volume of 200 µL of 1.5% sodium chloride solution was added and mixed further for 1 minute before phase separation by centrifugation of cell suspension at 6,000 × g for 5 minutes. The lower phase was collected for fatty acid analyses and stored at −20°C prior to GC-MS. For FAME analyses, lipid extractions were concentrated and prepared in a 1:1 solution of chloroform:TMSOH. GC-MS analyses were performed on an Agilent 7890 GC system with an Agilent DB-FastFAME column (30 m) and MS was performed on a coupled Agilent 5975C MSD system (Agilent Technologies). FAME species were identified and compared to C4-24 Fatty Acid Methyl Ester standard (Sigma-Aldrich). Data was analysed using Agilent MassHunter Qualitative Navigator Software (Agilent Technologies).

Flow cytometry

A. baumannii AB5075_UW and transposon mutant *A. baumannii* AB5075_UW *yadH*::Tn26 cultures were inoculated into LB-Lennox media with appropriate selection and grown at 37°C, 200 rpm shaking. Overnight cultures were diluted to an OD_{600nm}= 0.05 in 20 mL of LB-Lennox media and grown to mid-log phase (OD_{600nm} = 0.7). Cultures were harvested by centrifugation at 13,300 × g for 5 minutes and resuspended to a final volume of 1 mL in PBS. A 100 µL aliquot of the cell suspensions were treated with 100 µL of PBS containing FM 4-64 (Biotium) or SYTOX Green (Invitrogen) at a final concentration of 5 µM. Cell cultures were incubated in the dark at room temperature for 15 minutes and further diluted with 800 µL PBS prior to analysis using an Attune NxT flow cytometer with an excitation set at 488 nm (Thermo Fisher Scientific). Heterologous cell populations were determined manually by gating cells on the forward and side scatter plot and was kept consistent across four biological replicates.

Fluorescence microscopy

A. baumannii AB5075_UW parental strain and the transposon derivative *yadH*::Tn*26* were cultured in LB-Lennox media overnight. Bacterial cell cultures were diluted to an OD_{600nm} = 0.05 in LB-Lennox media and incubated for 2 hours to mid-exponential phase. Bacterial cell cultures were treated with 10 µM nonyl-acridine orange (NAO) or 10 µM FM 4-64 (Biotium) and incubated

for 15 minutes in the dark at room temperature. Treated cultures were washed thrice in PBS solution and resuspended into a final volume of 200 µL PBS. Fluorescence microscopy of cell cultures was performed on an Olympus BX53 fluorescent microscope. FM4-64 stained cells were imaged (Ex/Em: 510/750 nm) with fluorescence filter cube U-FBN (Ex. 470-495 nm/Em. 510 nm/DM at 509 nm) (Olympus). NAO-stained cells were imaged (Ex/Em at 495/522 nm) with a U-FGFP filter cube (Ex. at 460-480 nm/Em. at 495-540 nm/DM at 490 nm) (Olympus). Images were acquired using cellSens software (Olympus Life Sciences).

Transmission electron microscopy

A. baumannii AB5075_UW parental strain and transposon derivative *yadH*::Tn*26* were grown in LB-Lennox media overnight at 37°C, 200 rpm shaking. Cell pellets were collected by centrifugation (800 × g for 15 minutes) and fixed in 3% glutaraldehyde in 0.1 M PBS for 1 hour at room temperature. Cell suspensions were gently washed thrice with PBS solution. Cell pellets were resuspended and embedded in 2% agarose. Each agarose block was stained with 1% osmium tetroxide for 1 hour at room temperature and washed with PBS, followed by treatment with uranyl acetate replacement stain (UAR-EMS) in aqueous solution (1:3) for 1 hour, before being washed gently with PBS solution. Agarose blocks were subject to ethanol dehydration series (30%, 50%. 70%, 90%, 95% and 100%) for 10 minutes each. Samples were embedded in epoxy resin in increasing concentration series (1:3 resin:ethanol for 1 hour, 2:3 resin:ethanol for 1 hour and 100% resin solution overnight). Resin samples were polymerised at 70°C for 12 hours and thin sections were prepared at 50-70 nm using a Leica EM UC7 Ultramicrotome. Samples were mounted into copper mesh grids and post-stained with UAR-EMS for 1 hour and lead citrate for an hour. Copper grids were washed thrice in 60°C MilliQ water between post-stain treatments. All TEM sections were imaged on a Phillips CM10 transmission electron microscope set to 100 kV.

Results and discussion

YadGH is part of the core genome of *A. baumannii*

Pan-genome analysis of all complete *A. baumannii* genomes was explored to investigate the distribution and genomic context of *yadGH* within the *A. baumannii* species. *yadGH* was found to be conserved across all *A. baumannii* genomes (at the time of analysis, n =172) at the time of analysis with high-level synteny, signifying that it is conserved as a part of the core genome within the *A. baumannii* species (Figure 1). Analysis of the top three local pathways across *A. baumannii*, representing 85% of all genomes analysed reveal *yadGH* is located in a region with a high number of cell envelope maintenance genes; namely *rlpA*, an endolytic peptidoglycosylase (ABUW_1242), *mltB*, membrane-bound lytic murein transglycosylase B (ABUW_1243) and *mrdB*, peptidoglycan glycosyltransferase (ABUW_1244) (Figure 1) (50, 51). In Chapter 2, *rlpA* and *mrdB* were alos shown to confer significant fitness to silver nitrate challenge under the same experimental conditions as *yadG* and *yadH*. Given the majority of *A. baumannii* genome sequences available in the pan-genome database are primarily isolated from nosocomial environments rather than environmental origins, this analysis may offer a more accurate depiction of *yadGH* conservation in clinical isolates rather than the species as a whole. For these reasons, further gene conservation across more distant evolutionary homologs, and phylogenetic analyses were pursued. Further analysis of *yadGH* genetic regions across local *A. baumannii* species and more distant evolutionary homologs reveal *yadGH* is located almost always adjacent to *queF* which encodes an NADPH-dependent 7-cyano-7-deazaguanine reductase involved in quenosine biosynthesis (Figure 2) (52, 53). Quenosine is an important molecule for tRNA modification that is essential for protein translational efficiency and accuracy (54). However, there is no clear functional link between YadGH and QueF.

YadH is highly conserved amongst *Acinetobacter* spp. and proteobacterial lineages.

The ABC transport permease are typically less conserved than the nucleotide-binding domains of an ABC transporter that have highly conserved ATP-hydrolysis function (55). For this reason, we

chose to construct a YadH phylogenetic tree to investigate the phylogeny of ABC transport protein and its homologs. HMM sequence searching using the HMMER webserver (v. 2.41.2) revealed homologous sequences across all kingdoms of life, as would be expected for an ABC transport member with high-level conservation within the bacterial kingdom (*n*= 6836 bacteria, *n*= 358 archaea, *n=6* eukaryotes). A phylogenetic tree of highly homologous YadH representatives is presented in Figure 3. Across *n* = 1000 sequences, the phylogenetic tree shows clear delineation of YadH homologs across two main clusters: Cluster 1 (comprising families I-V) and cluster 2 (comprising families VI-XIII). Most phyla represented across the phylogenetic tree belong to proteobacterial lineages, suggesting significant conservation of YadH function within this phylum (Figure 3). Cluster 1 is predominately comprised of sequences of Gammaproteobacteria class from Pasteurellales and Enterobacterales, in addition to selected firmicute representatives from Lactobacillales order. Cluster 2 is represented by Gammaproteobacteria, prominently from Xanthamonadales, Vibrionales, Oceanospirillales and Pseudomonadales order. All *Acinetobacter* spp. orthologs of YadH are in cluster 2 from family XIII and are closely related to orthologs from *Pseudomonas* spp. and Oceanospirillales order in the Gammaproteobacteria. Overall, the phylogenetic tree suggests homologs of $YadH^{AB5075}$ are highly conserved within the proteobacteria phylum and found in select other bacterial phyla.

Predicted structure of $YadGH^{AB5075}$ reveals a type V fold ABC transport protein

In the absence of high-resolution protein structure data for YadGH, AlphaFold2 was used to model the structure of the ABC transport complex. The tertiary and quaternary structure of the $YadGH^{AB5075}$ ABC transporter revealed high-level similarity to Type V fold ABC transporters (Figure 4) (5, 56). YadGH was modelled with high confidence as a homodimer, comprising two copies of the YadG (NBD) and YadH (TMH) protomers (Figure 4 and 5). AlphaFold2 mapped confidence to the YadGH complex reveal high level of confidence prediction for TMH and NBD regions (>90%), with lower regions of confidence for the cytoplasmic accessory domain and periplasmic loops (60-70%) and a singular α-helix that emerges perpendicular to the NBD domain (<10%) (Figure 5). Ramachandran plot analyses show 95.7% of residues lied in favoured and 4.3%

in allowed regions; no residues were found in disallowed regions (Figure 5). The predicted structure of the YadH transport permease is 257 amino acids in length comprising of six α-transmembrane helices; two re-entrant α-helices, one short coupling helix and an N-terminal connecting helix that kinks at a ~90° angle at the interface between the TMH domain and NBD domain (Figure 4). The NBD domain of ABC transporters is highly conserved in nature and our structure reveals that the YadG domain adopts the characteristic fold of NBD transporters of the ABC family (Figure 4 and 6). YadG is 311 amino acids long and is comprised of 14 β-sheets and 10 α-helices in total (Figure 4 and 6). Conserved motifs were identified, including: the Walker A and LSGGX motif involved in ATP binding; the H-motif for γ-phosphate binding; and the Q-loop and Walker B motif for magnesium ion and TMH-NBD coordination (Figure 6). In addition to the NBD domain, YadG reveals an additional cytoplasmic domain comprised of the last 92 amino acids of YadG that forms three α-helices and four antiparallel β-sheets (Figure 4 and 6). Consurf analyses reveal the internal region of the TMD and NBD to be highly conserved as expected for an ABC transporter (Figure 4). ABPS (Adaptive Poisson-Boltzmann Solver) electrostatics was used to determine distribution of charge across the transport protein. ABPS electrostatics confirms hydrophobic TMD region, polar NBD as expected for ABC transporters and negatively charged cytoplasmic domain (Figure 4). The cytoplasmic domain is less conserved compared to the rest of the structure but has been observed feature of some members of the Type V fold ABC transport family (Figure 4) (57, 58). DALI analyses were performed to search for homologous ABC transporter folds within known PDB repository, which revealed YadG and YadH have common features to ABC lipid transporters, alluding to a putative role in lipid transport for YadGH^{AB5075} (Table S2 and S3).

YadGH confers increased tolerance to multiple drugs and efflux activity.

To determine whether YadGH may demonstrate a multidrug resistance phenotype, we studied the capacity of YadGH^{AB5075} to confer resistance to over 240 unique antimicrobial compounds using Biolog phenotype microarray bacterial sensitivity panels PM11-20. A complete list of antimicrobials tested in this assay is available (Appendix B). To test this, the coding regions of

YadGH^{AB5075} were chemically synthesised and cloned into the pTTQ18-RSGH$_6$ expression vector and transformed into *E. coli* BL21 (DE3) cells. Expression of the YadGH construct was confirmed by the presence of YadH at ~20 kDa on SDS-PAGE and western blot (Appendix C). A band at ~30 kDa is also observed in the SDS-PAGE, consistent with YadG. On the western blot, there is a faint band at ~37 kDa that might represent a YadH dimer or alternatively a His-rich protein contaminant.

E. coli cells harbouring pTTQ18-YadGH displayed significantly increased respiration in the presence of a diverse set of antimicrobials compared to *E. coli* cells harbouring empty pTTQ18-RSGH$_6$ plasmid (Figure 7). Specifically, YadGH conferred stronger respiration, and presumably stronger growth in the presence of sulfonamides, fluoroquinolones, ceftriaxone, heterocyclic nitrogen antibiotics such as nitroimidazoles and nitrofurans, in addition to the detergent-like quaternary ammonium compound (QAC) disinfectants domiphen bromide and dequalinium chloride (Figure 7). In addition to these compounds, YadGH also conferred strong respiration in the presence of the phenylsulfamide fungicides tolyfluanid and dichlofluanid, suggesting a pleiotropic drug tolerance profile for YadGH (Figure 7).

To validate the findings of Biolog phenotype microarrays we followed this experiment with MICs to confirm strong hits for QACs — domiphen bromide and dequalinium chloride — and tinidazole. *E. coli* harbouring pTTQ18-YadGH$_{RSGH6}$ revealed log 2-fold increased MIC to domiphen bromide, dequalinium chloride and tinidazole compared to *E. coli* pTTQ18-RSGH$_6$ (empty vector control), suggesting an increased tolerance profile across multiple drugs in cells expressing YadGH^{AB5075} compared to cells without YadGH^{AB5075} (Table 1). Following this result, we screened for fluorescent antimicrobial substrates amenable for whole-cell transport assays. *E. coli* harbouring pTTQ18-YadGH$_{RSGH6}$ revealed log 2-fold increased MIC to acriflavine compared to *E. coli* pTTQ18-RSGH$_6$ (empty vector control) suggesting acriflavine is also a recognised antimicrobial by YadGH (Table 1). Further whole cell acriflavine transport assays were carried out to compare differential acriflavine efflux rates between *E. coli* expressing YadGH^{AB5075} and empty vector control. Cells expressing YadGH showed greater acriflavine efflux compared to *E. coli* control,

indicative of a putative drug efflux phenotype conferred by the overexpression of YadGH^{AB5075} in *E. coli* BL21 (DE3) cells (Figure 8).

YadH inactivation impacts cell membrane integrity of *A. baumannii*

Our bioinformatic data suggested a potential role of YadGH in cell envelope homeostasis and the TraDIS, Biolog, MIC and transport assay suggest a potential pleiotropic role in drug resistance. However, this phenotype has been observed when YadGH is highly expressed from a multicopy plasmid in *E. coli* and may not always be comparable in phenotype to the intrinsic expression of YadGH in host. Due to these observations, we set out to investigate the impact of *yadH* inactivation on the cell envelope of *A. baumannii* using a *yadH* knockout strain (*yadH*::Tn*26*) and its isogenic parent. Fatty acid methyl ester GC-MS analysis of the *A. baumannii* cell membrane between AB5075 wild type and *yadH* mutant revealed significant changes in the abundance of major unsaturated fatty acids of *A. baumannii*, with significant depletion of palmitoleic acid and a corresponding increase in oleic acid abundance (Figure 9).

To investigate whether these changes in lipid composition affected cell membrane permeability, we followed these experiments with flow cytometry using SYTOX green and FM 4-64 to investigate cell permeability and membrane morphology respectively (59, 60). SYTOX Green fluoresces bright green only when bound to DNA and can only enter deceased cells or living cells with compromised cell membrane integrity, offering an ideal probe to detect membrane permeability changes in live bacterial cells (59). FM 4-64 is a lipophilic dye that intercalates within the lipid bilayer and stains anionic phospholipids such as phosphatidylglycerol and cardiolipin, commonly found in bacterial cell membranes, providing valuable insights into overall changes in cell membrane morphology in live bacterial cells, including *Acinetobacter baumannii* (60). Flow cytometry showed a more significant accumulation of SYTOX green and FM 4-64 in *yadH* transposon mutants compared to wild type AB5075_UW, suggesting a change in cell membrane permeability in the AB5075_UW *yadH* mutant (Figure 10). Furthermore, flow cytometry data revealed a significant shift towards a predominately large cell population compared to wildtype AB5075_UW, suggesting change in cell shape morphology (Figure 10). Fluorescence microscopy

of nonyl acridine orange and FM 4-64 dye-loaded cells revealed greater cell size and cell aggregation in *yadH* mutant compared to wild type, providing further evidence for larger cell morphology in *A. baumannii* (Figure 11). To gather more direct evidence that *yadH* inactivation may compromise the cell membrane, we investigated the cell envelope structure of *A. baumannii* AB5075_UW (*yadH*::Tn*26*) using TEM microscopy. TEM microscopy showed the *yadH* mutant had a compromised capsule structure, providing further evidence that *yadH* inactivation shifted the cell envelope homeostasis in *A. baumannii* (Figure 12). All phenotypic assays in *A. baumannii* were performed across two independent transposon mutants of *yadH*, hence, phenotypes related to change in membrane composition and integrity more likely to be an effect of direct loss of the pump, rather than a product caused by indirect, downstream effect at the site of transposon insertion.

Conclusions

This study represents the first functional characterisation of YadGH, an ABC transporter of unknown function from *A. baumannii* AB5075_UW, a highly drug resistant and virulent isolate of *A. baumannii*. YadGH is an ABC-2 type transporter of unknown function, previously identified to confer fitness towards silver nitrate. In this study, the observed our bioinformatic, phylogenetic and structural analyses are suggestive of a putative physiological role for YadGH in cell membrane homeostasis, possibly through lipid transport. Further studies of a YadH mutant revealed a series of pleiotropic phenotypes related to a role within the cell envelope. This included altered lipid composition, lost capsule and altered drug resistance and efflux. This study suggests YadGH may play a role in cell envelope homeostasis however, it has not ascertained what the direct substrates of YadGH might be. The true substrate may be involved in cell envelope biogenesis and changes in resistance can be either directly through drug efflux or indirect via changes in the cell membrane or capsule structure. Previous studies have indicated that YadGH orthologs in Gram-negative pathogens indicate YadGH may associate with the Mla-complex to maintain outer-membrane asymmetry (14-16). Furthermore, *E. coli yadH* inactivation also induced a hyperpermeable phenotype of the *E. coli* cell membrane (14) similar to our findings that *yadH* inactivation in

A. baumannii led to greater cell membrane permeability and loss of capsule. Although YadGH was not found near the Mla-complex, our data does support the potential role of YadGH in cell envelope homeostasis.

Collectively, this work suggests YadGH may represent a new ABC-type efflux system in *A. baumannii*. Further work will focus on defining the specific substrate profile of YadGH and characterisation of YadGH transport activity in proteoliposomes in order to determine the direct roles this transporter plays in cell envelope homeostasis and drug resistance in this pathogen.

References

1. A. Y. Peleg, H. Seifert, D. L. Paterson, *Acinetobacter baumannii*: Emergence of a successful pathogen. *Clin. Microbiol. Rev.* **21**, 538–582 (2008).

2. C. J. L. Murray, *et al.*, Global burden of bacterial antimicrobial resistance in 2019: a systematic analysis. *Lancet* **399**, 629–655 (2022).

3. L. D. de M. Carrasco, *et al.*, Polymyxin resistance among XDR ST1 carbapenem-resistant *Acinetobacter baumannii* clone expanding in a teaching hospital. *Front. Microbiol.* **12,** 622704 (2021).

4. V. Kornelsen, A. Kumar, Update on multidrug resistance efflux pumps in *Acinetobacter* spp. *Antimicrob. Agents Chemother.* **65**, e00514-21 (2021).

5. C. Thomas, R. Tampé, Structural and mechanistic principles of ABC Transporters. *Annu. Rev. Biochem.* **89**, 605–636 (2020).

6. A. L. Davidson, E. Dassa, C. Orelle, J. Chen, Structure, function, and evolution of bacterial ATP-binding cassette systems. *Microbiol. Mol. Biol. Rev.* **72**, 317–364 (2008).

7. L. D. H. Elbourne, S. G. Tetu, K. A. Hassan, I. T. Paulsen, TransportDB 2.0: A database for exploring membrane transporters in sequenced genomes from all domains of life. *Nucleic Acids Res.* **45**, D320–D324 (2017).

8. I. T. Paulsen, A. M. Beness, M. H. Saier, Computer-based analyses of the protein constituents of transport systems catalysing export of complex carbohydrates in bacteria. *Microbiology* **143**, 2685–2699 (1997).

9. D. Bronner, B. R. Clarke, C. Whitfield, Identification of an ATP-binding cassette transport system required for translocation of lipopolysaccharide O-antigen side-chains across the cytoplasmic membrane of *Klebsiella pneumoniae* serotype O1. *Mol. Microbiol.* **14**, 505-519 (1994).

10. H. P. Spaink, A. H. Wijfjes, B. J. Lugtenberg, *Rhizobium* NodI and NodJ proteins play a role in the efficiency of secretion of lipochitin oligosaccharides. *J. Bacteriol.* **177**, 6276–6281 (1995).

11. V. Lazarevic, D. Karamata, The *tagGH* operon of *Bacillus subtilis* 168 encodes a two-component ABC transporter involved in the metabolism of two wall teichoic acids. *Mol. Microbiol.* **16**, 345–355 (1995).

12. A. N. Smith, G. J. Boulnois, I. S. Roberts, Molecular analysis of the *Escherichia coli* K5 kps locus: identification and characterization of an inner-membrane capsular polysaccharide transport system. *Mol. Microbiol.* **4**, 1863–1869 (1990).

13. W. Li, M. Sharma, P. Kaur, The DrrAB efflux system of *Streptomyces peucetius* is a multidrug transporter of broad substrate specificity. *J. Biol. Chem.* **289**, 12633–12646 (2014).

14. M. Babu, *et al.*, Global landscape of cell envelope protein complexes in *Escherichia coli*. *Nat. Biotechnol.* **36**, 103–112 (2018).

15. S. P. Bernier, S. Son, M. G. Surette, The Mla pathway plays an essential role in the intrinsic resistance of *Burkholderia cepacia* complex species to antimicrobials and host innate components. *J. Bacteriol.* **200**, e00156-18 (2018).

16. S. Gualdi, K. Agnoli, A. Vitale, S. Higgins, L. Eberl, Identification of genes required for gold and silver tolerance in *Burkholderia cenocepacia* H111 by transposon sequencing. *Environ. Microbiol.* **00,** 737-751 (2021).

17. S. R. Eddy, Profile hidden Markov models. *Bioinformatics* **14**, 755–763 (1998).

18. S. C. Potter, *et al.*, HMMER web server: 2018 update. *Nucleic Acids Res.* **46**, W200–W204 (2018).

19. R. C. Edgar, MUSCLE: Multiple sequence alignment with high accuracy and high throughput. *Nucleic Acids Res.* **32**, 1792–1797 (2004).

20. N. Saitou, M. Nei, The neighbor-joining method: a new method for reconstructing phylogenetic trees. *Mol. Biol. Evol.* **4**, 406–425 (1987).

21. J. Felsenstein, Confidence limits on phylogenies: an approach using the bootstrap. *Evolution (N. Y).* **39**, 783–791 (1985).

22. E. Zuckerkandle, L. Pauling, Evolutionary Divergence and Convergence in Proteins. *Evol. Genes Proteins*, 97–166 (1965).

23. S. Kumar, G. Stecher, M. Li, C. Knyaz, K. Tamura, MEGA X: Molecular evolutionary genetics analysis across computing platforms. *Mol. Biol. Evol.* **35**, 1547–1549 (2018).

24. I. Letunic, P. Bork, Interactive tree of life (iTOL) v5: an online tool for phylogenetic tree display and annotation. *Nucleic Acids Res.* **49**, W293-296 (2021).

25. F. L. Short, *et al.*, The *Acinetobacter baumannii* disinfectant resistance protein, AmvA, is a spermidine and spermine efflux pump. *Commun. Biol.* **4** (2021).

26. C. L. M. Gilchrist, Y.-H. Chooi, clinker & clustermap.js: Automatic generation of gene cluster comparison figures. *Bioinformatics* **37**, 2473–2475 (2021).

27. C. K. Saha, R. S. Pires, H. Brolin, M. Delannoy, G. C. Atkinson, FlaGs and webFlaGs: Discovering novel biology through the analysis of gene neighbourhood conservation. *Bioinformatics* **37**, 1312–1314 (2021).

28. J. Jumper, *et al.*, Highly accurate protein structure prediction with AlphaFold. *Nature*, 1–12 (2021).

29. M. Mirdita, *et al.*, ColabFold: making protein folding accessible to all. *Nat. Methods* **19**, 679–682 (2022).

30. M. Steinegger, J. Söding, MMseqs2 enables sensitive protein sequence searching for the analysis of massive data sets. *Nat. Biotechnol.* **35**, 1026–1028 (2017).

31. M. Landau, *et al.*, ConSurf 2005: The projection of evolutionary conservation scores of residues on protein structures. *Nucleic Acids Res.* **33**, W299-302 (2005).

32. H. Ashkenazy, *et al.*, ConSurf 2016: An improved methodology to estimate and visualize evolutionary conservation in macromolecules. *Nucleic Acids Res.* **44**, W344–W350 (2016).

33. L. Holm, DALI and the persistence of protein shape. *Protein Sci.* **29**, 128–140 (2020).

34. W. Delano, The PyMOL Molecular Graphics System. *CCP4 Newsl. Protein Crystallogr.* **40**, 82–92 (2002).

35. R. A. Laskowski, M. W. MacArthur, D. S. Moss, J. M. Thornton, PROCHECK: A program to check the stereochemical quality of protein structures. *J. Appl. Crystallogr.* **26**, 283–291 (1993).

36. L. A. Gallagher, *et al.*, Resources for genetic and genomic analysis of emerging pathogen *Acinetobacter baumannii*. *J. Bacteriol.* **197**, 2027–2035 (2015).

37. M. J. R. Stark, Multicopy expression vectors carrying the *lac* repressor gene for regulated high-level expression genes in *Escherichia coli*. *Gene* **51**, 255–267 (1987).

38. M. V. Dilworth, *et al.*, Microbial expression systems for membrane proteins. *Methods* **147**, 3–39 (2018).

39. A. Ward, *et al.*, "The amplified expression, identification, purification, assay and properties of hexahistidine-tagged bacterial membrane transport proteins" in *Membrane Transport - A Practical Approach*, S. A. Baldwin, Ed. (2000), pp. 141–166.

40. A. Froger, J. E. Hall, Transformation of plasmid DNA into *E. coli* using the heat shock method. *J. Vis. Exp.*, 253 (2007).

41. P. K. Smith, *et al.*, Measurement of protein using bicinchoninic acid. *Anal. Biochem.* **150**, 76–85 (1985).

42. P. J. F. Henderson, A. J. S. Macpherson, "Assay, genetics, proteins, and reconstitution of proton-linked galactose, arabinose, and xylose transport systems of *Escherichia coli*" in *Methods in Enzymology*, (1986), pp. 387–429.

43. B. R. Bochner, P. Gadzinski, E. Panomitros, Phenotype microarrays for high-throughput phenotypic testing and assay of gene function. *Genome Res.* **11**, 1246–1255 (2001).

44. A. M. Mackie, K. A. Hassan, I. T. Paulsen, S. G. Tetu, "Biolog Phenotype Microarrays for Phenotypic Characterisation of Microbial Cells" in *Methods in Molecular Biology*, (2014), pp. 123–130.

45. L. Li, K. A. Hassan, M. H. Brown, I. T. Paulsen, Rapid multiplexed phenotypic screening identifies drug resistance functions for three novel efflux pumps in *Acinetobacter baumannii*. *J. Antimicrob. Chemother.* **71**, 1223–1232 (2016).

46. I. Wiegand, K. Hilpert, R. E. W. W. Hancock, Agar and broth dilution methods to determine the minimal inhibitory concentration (MIC) of antimicrobial substances. *Nat. Protoc.* **3**, 163–175 (2008).

47. B. A. Mitchell, I. T. Paulsen, M. H. Brown, R. A. Skurray, Bioenergetics of the staphylococcal multidrug export protein QacA. *J. Biol. Chem.* **274**, 3541–3548 (1999).

48. S. F. Alquethamy, *et al.*, The molecular basis of *Acinetobacter baumannii* cadmium toxicity and resistance. *Appl. Environ. Microbiol.* **87,** e0171821 (2021).

49. M. Zang, *et al.*, The membrane composition defines the spatial organization and function of a major *Acinetobacter baumannii* drug efflux system. *MBio* **12**, e01070-21 (2021).

50. M. A. Jorgenson, Y. Chen, A. Yahashiri, D. L. Popham, D. S. Weiss, The bacterial septal ring protein RlpA is a lytic transglycosylase that contributes to rod shape and daughter cell separation in *Pseudomonas aeruginosa*. *Mol. Microbiol.* **93**, 113–128 (2014).

51. S. Crépin, *et al.*, The lytic transglycosylase MltB connects membrane homeostasis and *in vivo* fitness of *Acinetobacter baumannii*. *Mol. Microbiol.* **109**, 745–762 (2018).

52. S. G. Van Lanen, *et al.*, From cyclohydrolase to oxidoreductase: Discovery of nitrile reductase activity in a common fold. *Proc. Natl. Acad. Sci. U. S. A.* **102**, 4264–4269 (2005).

53. A. Mohammad, *et al.*, Protection of the queuosine biosynthesis enzyme QueF from irreversible oxidation by a conserved intramolecular disulfide. *Biomolecules* **7**, 30 (2017).

54. Y. Yifeng, *et al.*, Discovery of novel bacterial queuine salvage enzymes and pathways in human pathogens. *Proc. Natl. Acad. Sci.* **116**, 19126–19135 (2019).

55. A. L. Davidson, J. Chen, ATP-binding cassette transporters in bacteria. *Annu. Rev. Biochem.* **73**, 241–268 (2004).

56. C. Thomas, *et al.*, Structural and functional diversity calls for a new classification of ABC transporters. *FEBS Lett.* **594**, 3767–3775 (2020).

57. C. A. Caffalette, J. Zimmer, Cryo-EM structure of the full-length WzmWzt ABC transporter required for lipid-linked O antigen transport. *Proc. Natl. Acad. Sci. U. S. A.* **118**, e2016144118 (2021).

58. S. G. Aller, J. P. Segrest, The regulatory domains of the lipid exporter ABCA1 form domain swapped latches. *PLoS One* **17**, e0262746 (2022).

59. P. Lebaron, P. Catala, N. Parthuisot, Effectiveness of SYTOX Green stain for bacterial viability assessment. *Appl. Environ. Microbiol.* **64**, 2697–2700 (1998).

60. I. Fishov, C. L. Woldringh, Visualization of membrane domains in *Escherichia coli*. *Mol. Microbiol.* **32**, 1166–1172 (1999).

61. V. Mariani, M. Biasini, A. Barbato, T. Schwede, lDDT: A local superposition-free score for comparing protein structures and models using distance difference tests. *Bioinformatics* **29**, 2722–2728 (2013).

62. X. Robert, P. Gouet, Deciphering key features in protein structures with the new ENDscript server. *Nucleic Acids Res.* **42**, W320–W324 (2014).

63. J. F. Scortecci, *et al.*, Cryo-EM structures of the ABCA4 importer reveal mechanisms underlying substrate binding and Stargardt disease. *Nat. Commun.* **12**, 5902 (2021).

64. A. Harris, *et al.*, Structure and efflux mechanism of the yeast pleiotropic drug resistance transporter Pdr5. *Nat. Commun.* **12**, 5254 (2021).

65. Y. Sun, *et al.*, Molecular basis of cholesterol efflux via ABCG subfamily transporters. *Proc. Natl. Acad. Sci. U. S. A.* **118**, e2110483118 (2021).

66. Q. Yu, *et al.*, Structures of ABCG2 under turnover conditions reveal a key step in the drug transport mechanism. *Nat. Commun.* **12**, 4376 (2021).

67. H. Qian, *et al.*, Structure of the human lipid exporter ABCA1. *Cell* **169**, 1228-1239 (2017).

68. N. Zeytuni, *et al.*, Structural insight into the *Staphylococcus aureus* ATP-driven exporter of virulent peptide toxins. *Sci. Adv.* **6**, eabb8219 (2020).

69. C. Li, *et al.*, Cryo-electron microscopy structure and transport mechanism of a wall teichoic acid ABC transporter. *MBio* **11**, e02749-19 (2022).

70. C. Zhou, *et al.*, Structural insight into phospholipid transport by the MlaFEBD complex from *P. aeruginosa*. *J. Mol. Biol.* **433**, 166986 (2021).

71. T. Xie, Z. Zhang, Q. Fang, B. Du, X. Gong, Structural basis of substrate recognition and translocation by human ABCA4. *Nat. Commun.* **12**, 3853 (2021).

72. E. Johnson, P. T. Nguyen, T. O. Yeates, D. C. Rees, Inward facing conformations of the MetNI methionine ABC transporter: Implications for the mechanism of transinhibition. *Protein Sci.* **21**, 84–96 (2012).

73. S. Newstead, *et al.*, Insights into how nucleotide-binding domains power ABC transport. *Structure* **17**, 1213–1222 (2009).

74. U. Okada, *et al.*, Crystal structure of tripartite-type ABC transporter MacB from *Acinetobacter baumannii*. *Nat. Commun.* **8**, 1336 (2017).

75. H. R. Sikkema, *et al.*, Gating by ionic strength and safety check by cyclic-di-AMP in the ABC transporter OpuA. *Sci. Adv.* **6**, eabd7697 (2020).

76. F. Liu, *et al.*, Structural basis of trehalose recycling by the ABC transporter LpqY-SugABC. *Sci. Adv.* **6**, eabb9833 (2020).

77. H. G. Choudhury, *et al.*, Structure of an antibacterial peptide ATP-binding cassette transporter in a novel outward occluded state. *Proc. Natl. Acad. Sci.* **111**, 9145–9150 (2014).

Figures and tables

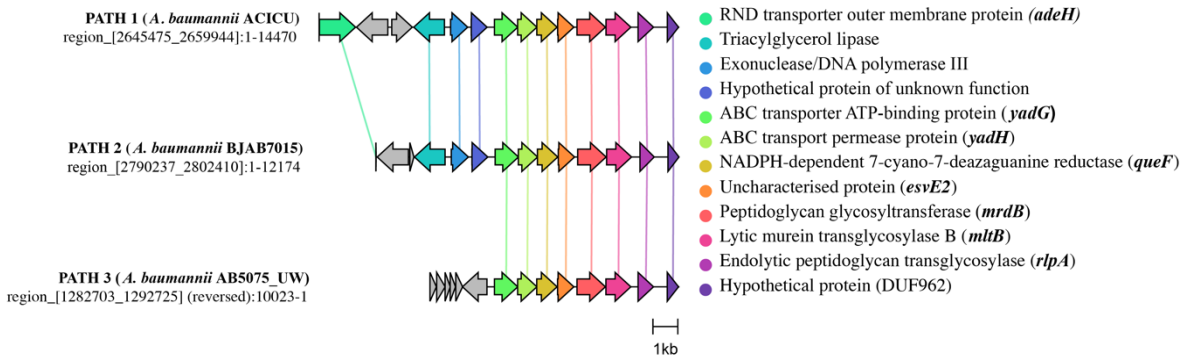

Figure 1: The genomic context of *yadGH* across *A. baumannii* genomes (*n* = 172). YadGH is conserved across all genomes with high-level of synteny. The top three alternate pathways are numbered 1-3 respectively. Path 1 (number of genomes = 93/172) is represented by *A. baumannii* ACICU. Path 2 (number of genomes = 45/172) is represented by *A. baumannii* BJAB7015 and Path 3 (number of genomes = 9/172) is represented by *A. baumannii* AB5075_UW. *Coloured* genes are conserved genes with 100% identity across genomes. *Grey* genes represent unique genes across pathways. Gene conservation was visualised with Clinker software (26) and further modified in Illustrator.

Figure 2: Conserved genetic neighborhood analysis of distant homologues**.** Genes that are present in two or more regions are colored and numbered (Table S1). Non conserved genes are blank. *yadH* and *yadG* are colored as *black* and *pink* adjacent arrows. *Purple* and *green* outlined genes are pseudogenes and RNA genes respectively. Branch values are provided in bootstrap support values. Figure generated by WebFLaGs web server (27).

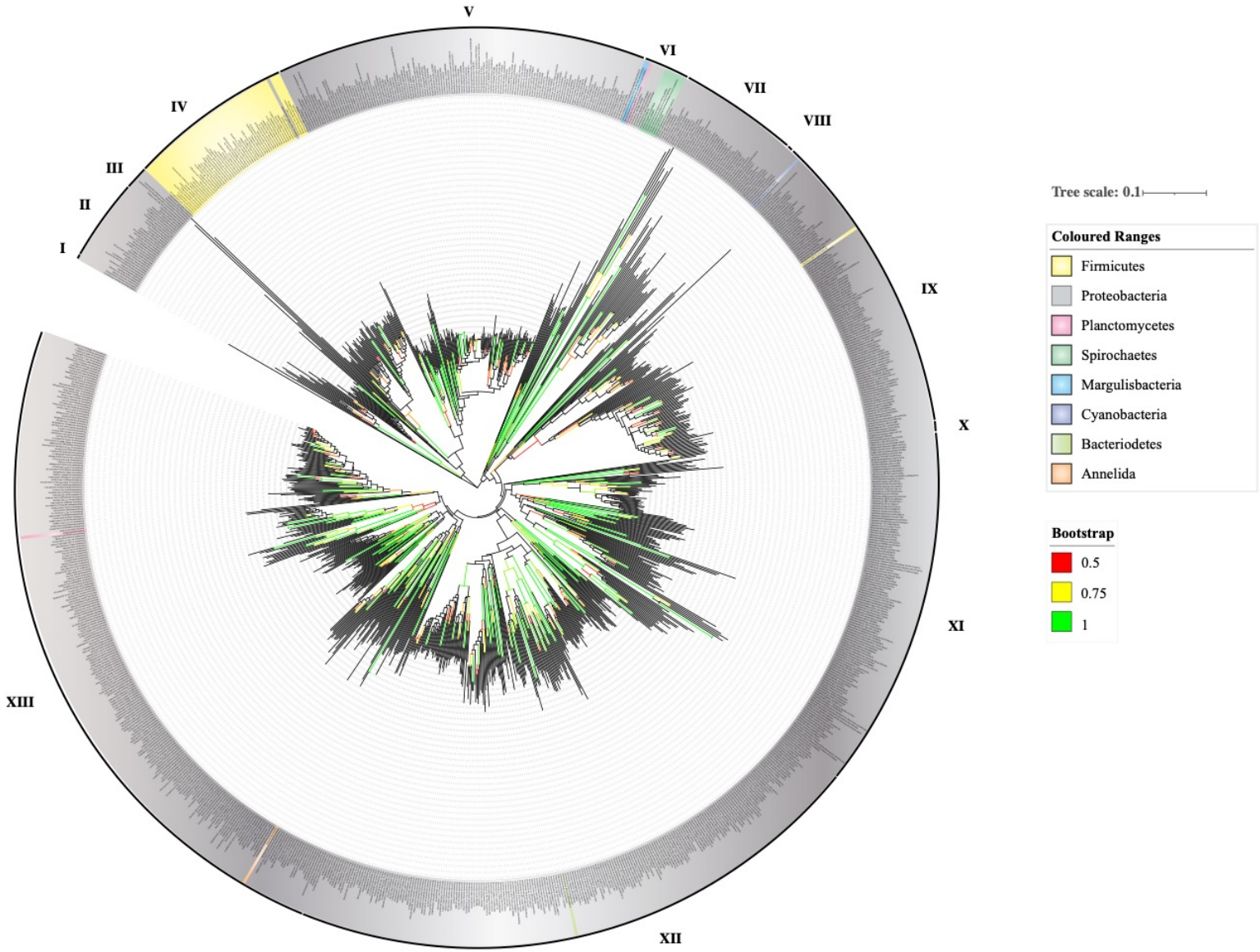
V
VI
VII
VIII
IX
X
XI
XII
XIII
IV
III
II
I
Tree scale: 0.1
Coloured Ranges
Firmicutes
Proteobacteria
Planctomycetes
Spirochaetes
Margulisbacteria
Cyanobacteria
Bacteriodetes
Annelida
Bootstrap
0.5
0.75
1

Figure 3: Phylogenetic tree of YadH^{AB5075} homologs (n = 1000) constructed by the neighbor-joining method (20). The phylogenetic tree was constructed in MEGAX (23), visualised in iTOL (24), and annotated in Illustrator. The phylogenetic tree was drawn scale where branch lengths were measured as number of substitutions per site. The tree is colorised according to taxonomic phylum. Bootstrap values of at least n=1000 iterations ≤0.5 are coloured from *red* to *green* (0.5-1.0), respectively (21). Distinct phylogenetic families are numbered from I to XIII.

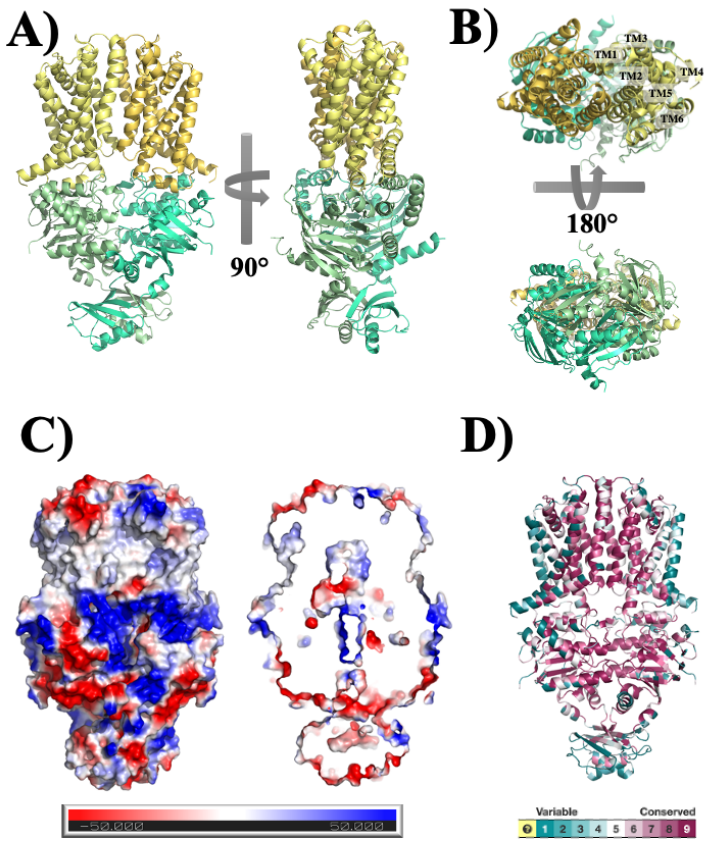

Figure 4: AlphaFold2 prediction of the YadGH. A) Cartoon ribbon representation of YadH transmembrane permease dimer (*pale yellow* and *yellow orange*) and YadG dimer (*pale green* and *green-cyan*) in two different side-view orientations visualised in Pymol. B) Top-down view of the tightly packed TMD domain of YadH with TMH annotation, followed by bottom-up view of the additional cytoplasmic domain, showing both YadG protomers intercalate to form an eight-member antiparallel β-sheet. C) APBS electrostatics view of the distribution of charge on the surface and within YadGH. D) ConSurf analysis of YadGH, where amino acids are coloured by conservation from variable (*cyan*) to conserved (*magenta*). All figures were visualised in PyMol software (34)

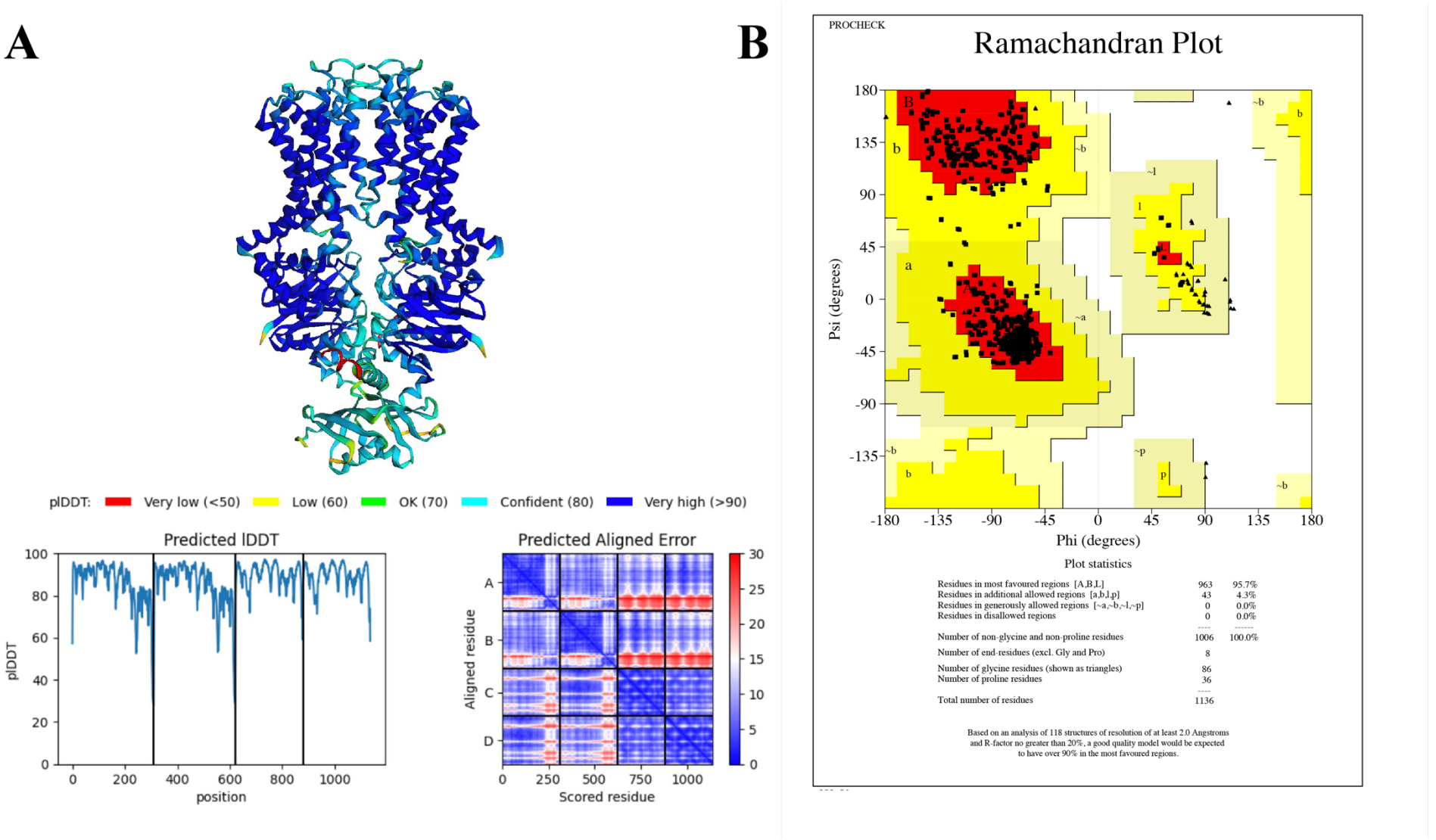

Figure 5: Assessment of YadGH model quality. **A)** lDDT confidence analysis of YadGH model by AlphaFold2 (28, 61). **B)** YadGH Ramachandran plot generated by PROCHECK for the assessment of model quality (35).

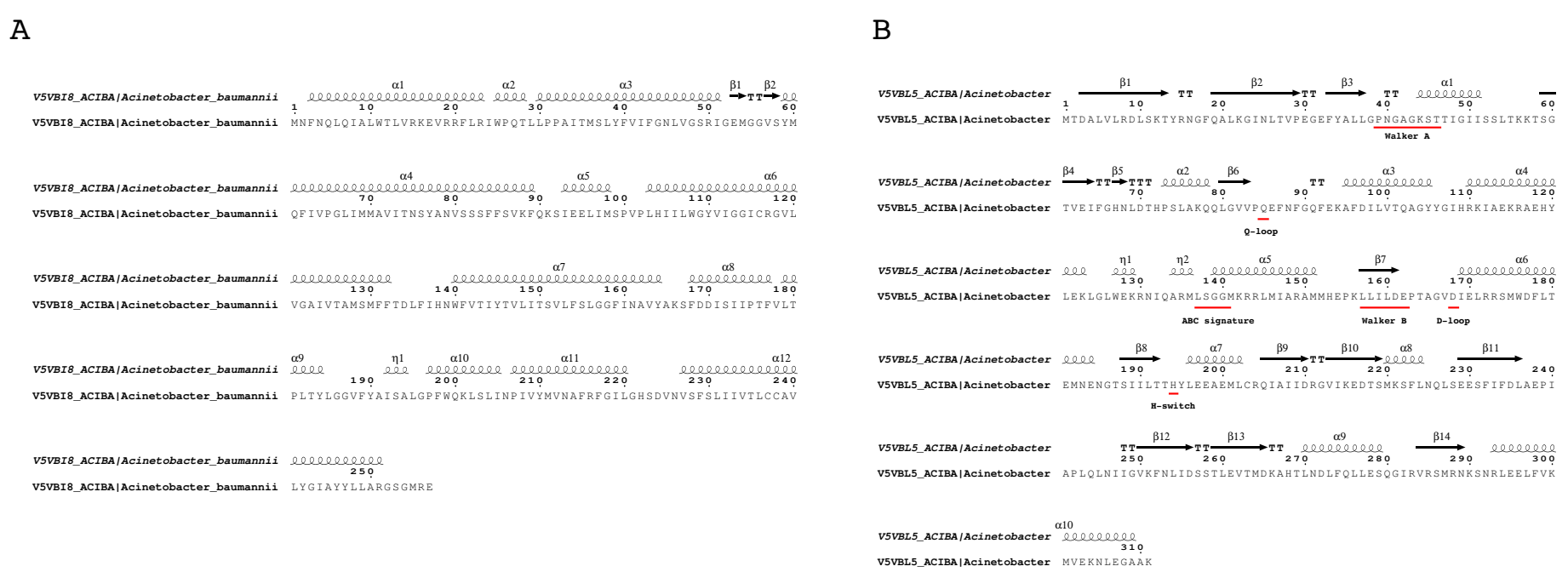

Figure 6: Sequence alignment with predicted secondary structure features from AlphaFold structures of with highlighted secondary structures and with NBD sequence motifs. A) YadH, reveals presence of 12 a-helices, one 310-helix and 1 beta turn. B) YadG reveals 14 β-strands, 10 α-helices, and two 310-turn helices (η). Figure prepared with ESPript webserver (62). NBD Motifs of YadG were annotated in PowerPoint.

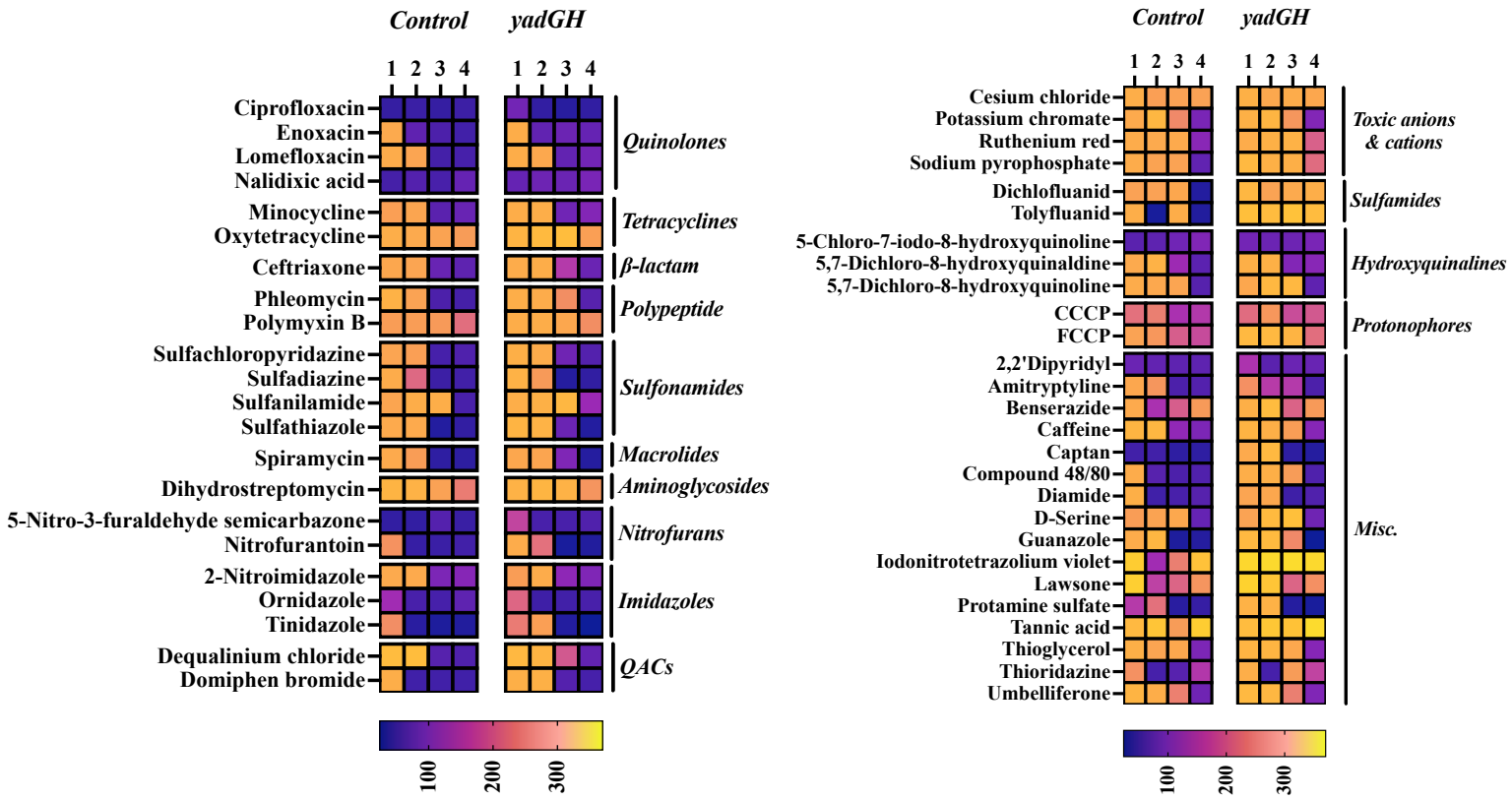

Figure 7: Resistance profile of YadGH from *A. baumannii*. Antimicrobial resistance phenotypes determined from the expression of ABC transporter YadGH^{AB5075} in *E. coli* BL21. Results are displayed as a heatmap using a colored scale from no respiration (*dark blue*) to maximum respiration (*yellow*). Biolog phenotypes are represented in two heatmap panels. A) antimicrobials and B) toxic bioactive compounds. Phenotypes are organized according to antimicrobial class. Columns represent log 2-fold increase in antimicrobial concentration across four wells of the Biolog PM

Table 1: Drug resistance of *E. coli* BL21 (DE3) pTTQ18 (control) or pTTQ18 (*yadGH*)

Drug	MIC (µg/mL) for cells transformed with		Drug category
	pTTQ18	pTTQ18 (*yadGH*)	
Dequalinium chloride	**8**	**16**	QAC
Domiphen bromide	**0.39**	**0.78**	QAC
Tinidazole	**125**	**250**	Nitroimidazole
Ethidium Bromide	37.5	37.5	Dye
Acriflavine	**9.38**	**18.75**	Dye
Hoechst 33342	**2.34**	**3.4**	Dye

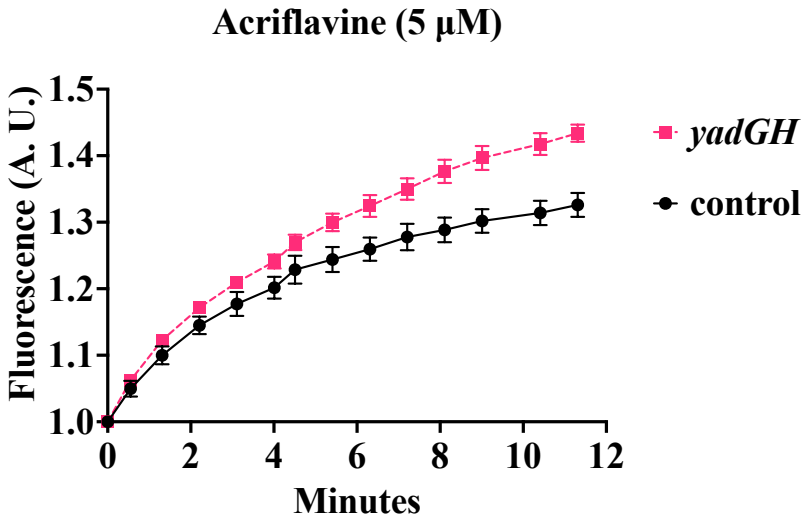

Figure 8: Acriflavine transport assay. Direct efflux of acriflavine associated with YadGH overexpression in *E. coli* cells. Acriflavine loaded cells after one hour of incubation in the presence of CCCP were measured to determine difference in efflux rate of acriflavine between IPTG induced *E. coli* BL21 (DE3) expressing YadGH (*pink*) verses an pTTQ18 empty vector control (*black*). Values are a means of three biological replicates and error bars are represented by the SEM. Statistical significance was determined using an unpaired t-test. Acriflavine efflux was found to be statistically significant between YadGH and control groups (p-value <0.05).

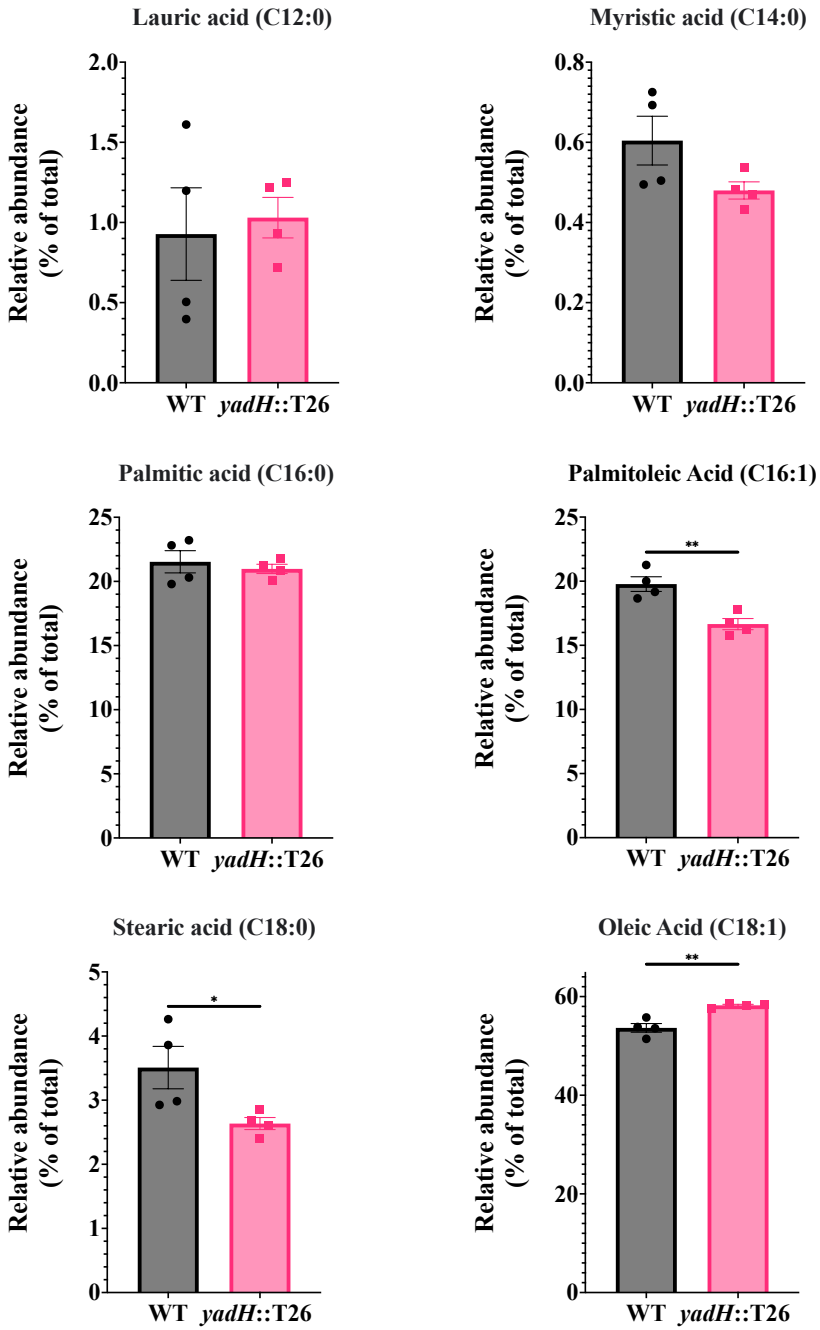

Figure 9: Fatty acid composition of the major fatty acid methyl ester (FAME) species of *A. baumannii* determined by GC-MS. **A)** *A. baumannii* fatty acid composition for *A. baumannii* AB5075_UW (*black*) and *yadH*::T26 mutant (*pink*) as determined by GC-MS. The data represents the mean of four biological replicates. Statistical analyses were performed by one-way ANOVA (*p <0.05, ** p<0.01).

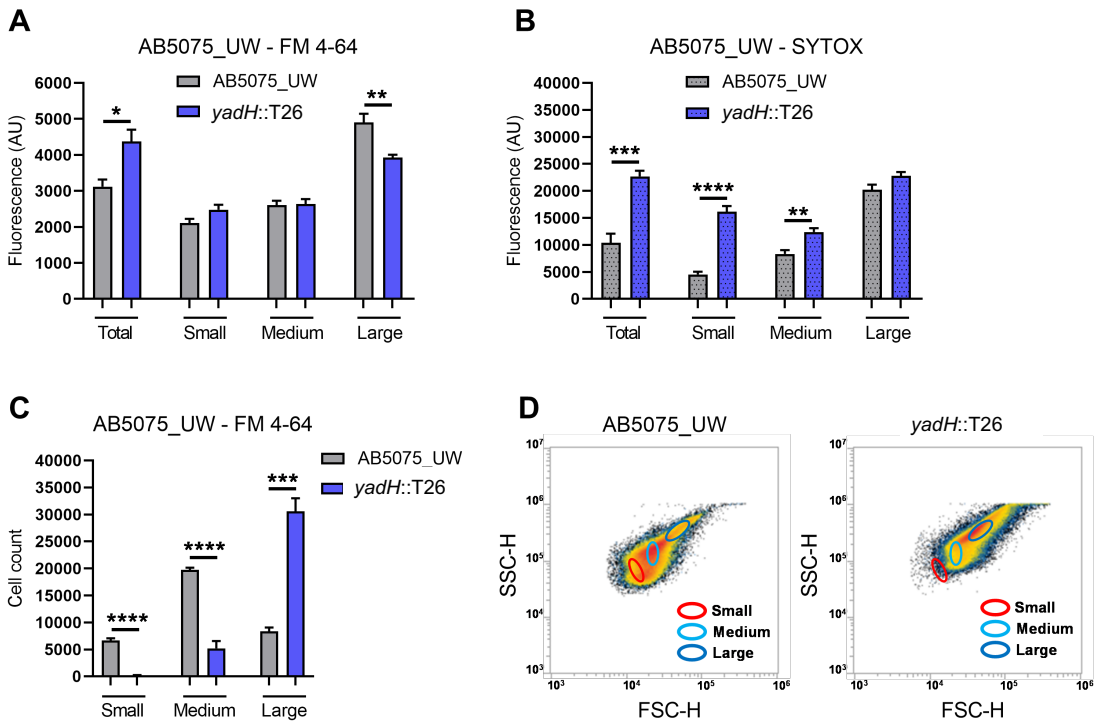

Figure 10: Flow cytometry analysis of *A. baumannii* AB5075_UW (*grey*) and *yadH*::Tn*26* populations (*blue*). A) Flow cytometry of FM 4-64 dye accumulation against *A. baumannii* AB5075_UW and *yadH*::Tn*26* populations, showing heightened accumulation of FM 4-64 in *yadH*::Tn*26* mutant compared to wild type. B) Flow cytometry analysis of SYTOX green accumulation against *A. baumannii* AB5075_UW and *yadH*::Tn*26* populations demonstrating a heightened accumulation of SYTOX green in *yadH*::Tn*26* strains compared to wild type. C) Total cell count appears significantly higher in the large population category in *yadH*::Tn*26* strains compared to wild type *A. baumannii* AB5075_UW. D) Forward vs side scatter plot of *A. baumannii* AB5075_UW population and *yadH*::Tn26 population showed cell size distribution across three distinct cell size categories (small, medium, and large). Statistical analyses were performed by one-way ANOVA (*p <0.05, ** p<0.01, *** p<0.001 and ****p<0.0001).

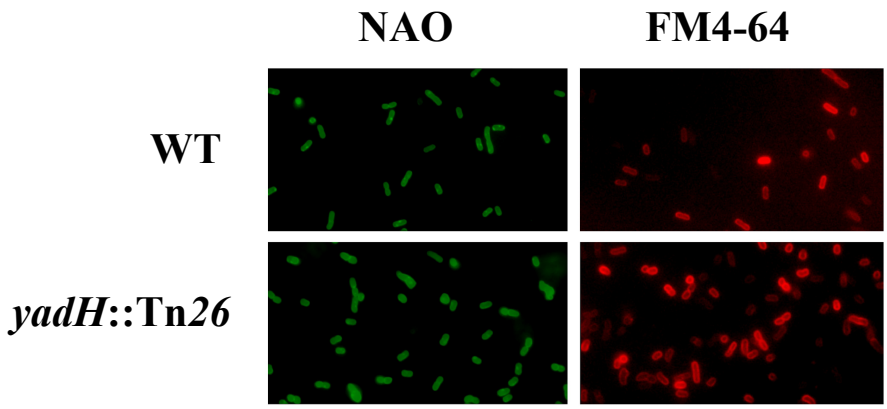

Figure 11: Nonyl-acridine orange (NAO) and FM 4-64 fluorescence microscopy across *A. baumannii* AB5075_UW cells and *yadH*::Tn*26*. The *yadH* mutant revealed increased cell density, cell size and dye accumulation of both NAO and FM 4-64 dyes compared to wild type. Fluorescence microscopy was performed on an Olympus BX53 fluorescent microscope. FM 4-64 stained cells were imaged (Ex/Em: 510/750 nm) and NAO-stained cells were imaged (Ex/Em: 495/522 nm). Images were acquired using cellSens software (Olympus Life Sciences).

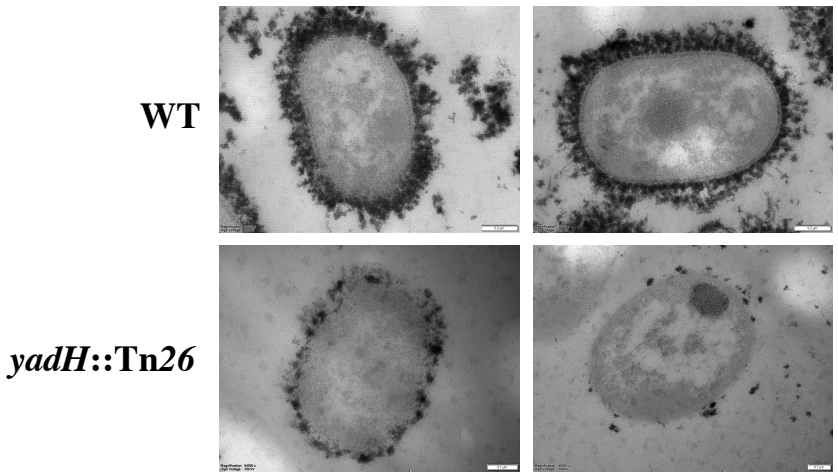

Figure 12: Transmission electron microscopy comparison of *A. baumannii* AB5075_UW wild type and *yadH*::Tn*26* mutant highlights the differences between in capsule formation. Top row: TEM images of wild-type *A. baumannii* AB5075_UW cells at 200 nm scale, stained with uranyl-acetate replacement stain to visualize the intact capsule- a dark, thick outer surface layer surrounding the cell. Bottom row: TEM images of the *yadH*::T26 mutant at a scale of 100 nm, displaying minimal capsule presence with thin and incomplete areas (depicted as black spots) around the cell. TEM images were captured using a Phillips CM10 transmission electron microscope at 100 kV.

Supporting information

Table S1: Legend of conserved genes across RefSeq homologs of *yadH*

Number	Accession	Gene
1	WP_072324479.1	ABC transporter ATP-binding protein
2	WP_205778954.1	NADPH-dependent 7-cyano-7-deazaguanine reductase QueF
3	WP_044399693.1	hypothetical protein
4	WP_009577357.1	EAL domain-containing protein
5	WP_014870944.1	nitroreductase
6	WP_045481168.1	acyl-CoA dehydrogenase
7	WP_003090883.1	sensor histidine kinase
8	WP_017134193.1	glutathione S-transferase
9	WP_001177236.1	septal ring lytic transglycosylase RlpA family
10	WP_004679678.1	hypothetical protein
11	WP_067660221.1	lytic murein transglycosylase B
12	WP_016657068.1	rod shape-determining protein RodA
13	WP_116579969.1	LysR family transcriptional regulator
14	WP_052675622.1	DNA internalization-related competence protein ComEC/Rec2
15	WP_102700915.1	transglutaminase family protein
16	WP_036506982.1	YiiD C-terminal domain-containing protein
17	WP_074780074.1	DUF4404 family protein
18	WP_005011198.1	DUF962 domain-containing protein
19	WP_013661162.1	3-oxoacyl-ACP reductase FabG
20	WP_049586866.1	tetraacyldisaccharide 4'-kinase
21	WP_029532388.1	biopolymer transporter ExbD
22	WP_010448848.1	MotA/TolQ/ExbB proton channel family protein
23	WP_067660200.1	DUF3820 family protein
24	WP_047276270.1	DUF2062 domain-containing protein
25	WP_068508956.1	HD-GYP domain-containing protein
26	WP_161466653.1	Trm112 family protein
27	WP_076462865.1	Fe(3+) ABC transporter substrate-binding protein
28	WP_136869966.1	VacJ family lipoprotein
29	WP_037039172.1	STAS domain-containing protein
30	WP_067338526.1	c-type cytochrome
31	WP_037039178.1	PilZ domain-containing protein
32	WP_016493378.1	methyl-accepting chemotaxis protein
33	WP_068476557.1	iron ABC transporter permease
34	WP_008938122.1	PilZ domain-containing protein
35	WP_068476543.1	flagellar basal body rod protein FlgB
36	WP_016493373.1	efflux RND transporter permease subunit
37	WP_222899608.1	efflux RND transporter periplasmic adaptor subunit
38	WP_227497952.1	hypothetical protein
39	WP_015046195.1	hypothetical protein
40	WP_040482103.1	peptide-methionine (R)-S-oxide reductase MsrB
41	WP_036159890.1	beta-ketoacyl-ACP synthase II
42	WP_067017871.1	acyl carrier protein
43	WP_013661161.1	ACP S-malonyltransferase
44	WP_047013348.1	dUTP diphosphatase

45	WP_064617175.1	proline--tRNA ligase
46	WP_070058841.1	DUF962 domain-containing protein
47	WP_068476541.1	flagellar basal body rod protein FlgC
48	WP_008042824.1	TIGR01777 family oxidoreductase
49	WP_070115477.1	pyrroloquinoline quinone-dependent dehydrogenase
50	WP_197027510.1	peptidyl-prolyl cis-trans isomerase
51	WP_011104753.1	hypothetical protein
52	WP_014993945.1	histidine phosphatase family protein
53	WP_011467650.1	hypothetical protein
54	WP_014993949.1	AbgT family transporter
55	WP_009019074.1	4-phosphoerythronate dehydrogenase
56	WP_004777211.1	hypothetical protein
57	WP_058021589.1	Fe-S biogenesis protein NfuA
58	WP_071263207.1	organic solvent ABC transporter permease
59	WP_083421080.1	DUF1499 domain-containing protein
60	WP_115346508.1	DUF4230 domain-containing protein
61	WP_008042821.1	hypothetical protein
62	WP_187147120.1	tryptophan synthase subunit beta
63	WP_076554830.1	phosphoribosylanthranilate isomerase
64	WP_230198464.1	elongation factor P hydroxylase
65	WP_000782592.1	alpha/beta fold hydrolase
66	WP_011912811.1	hypothetical protein
67	WP_023271755.1	serine hydroxymethyltransferase
68	WP_023659409.1	ISL3 family transposase
69	WP_035458621.1	MAPEG family protein
70	WP_036547862.1	DUF6134 family protein
71	WP_017245727.1	aspartate aminotransferase family protein
72	WP_038414390.1	fimbrial protein
73	WP_043253354.1	sodium/proline symporter PutP
74	WP_043253360.1	hypothetical protein
75	WP_005770647.1	type VI secretion system tip protein VgrG
76	WP_011104750.1	DUF4123 domain-containing protein
77	WP_045481146.1	hypothetical protein
78	WP_004903785.1	translation elongation factor Ts
79	WP_004903798.1	dihydroxy-acid dehydratase
80	WP_004903801.1	acyltransferase family protein
81	WP_008250006.1	hypothetical protein
82	WP_037039194.1	succinylglutamate desuccinylase
83	WP_052830263.1	4-alpha-glucanotransferase
84	WP_053102368.1	C40 family peptidase
85	WP_067384296.1	heavy metal translocating P-type ATPase
86	WP_067552817.1	hypothetical protein
87	WP_014870934.1	AMP-binding protein
88	WP_068997465.1	formaldehyde dehydrogenase, glutathione-independent
89	WP_025167491.1	LysE family translocator
90	WP_069516899.1	benzoate/H(+) symporter BenE family transporter
91	WP_069516901.1	NADP-dependent oxidoreductase
92	WP_070068784.1	phosphate ABC transporter permease PstA
93	WP_070068786.1	substrate-binding domain-containing protein

94	WP_070115473.1	hypothetical protein
95	WP_070115474.1	hypothetical protein
96	WP_071263201.1	flagellar hook assembly protein FlgD
97	WP_027590272.1	hypothetical protein
98	WP_072324475.1	2-dehydropantoate 2-reductase
99	WP_023271746.1	DUF3465 domain-containing protein
100	WP_064604400.1	lactoylglutathione lyase
101	WP_076554837.1	carbonic anhydrase
102	WP_064617873.1	hypothetical protein
103	WP_062334157.1	beta-N-acetylhexosaminidase
104	WP_083704680.1	mechanosensitive ion channel
105	WP_008739302.1	bile acid:sodium symporter family protein
106	WP_049341445.1	crotonase/enoyl-CoA hydratase family protein
107	WP_175487759.1	DUF308 domain-containing protein
108	WP_205778952.1	hypothetical protein
109	WP_051632752.1	helix-turn-helix domain-containing protein

Table S2 Structural homologues of YadH

PDB	Protein	Substrate	Organism	rmsd	z-score	%ID	align	nres	ref
6M96	WzmWzt	O-specific polysaccharides	*Aquifex aeolicus*	3.0	19.6	17	228	256	(57)
7M1P	ABCA4	N-retinylidene-phosphatidylethanolamine	*Homo sapiens*	3.4	19.2	9	236	1938	(63)
7P04	PDR5	Multiple drugs, sterols, peptides	*Saccharomyces cerevisiae*	3.6	19.1	10	238	1353	(64)
7R8D	ABCG1	Cholesterol	*Homo sapiens*	3.7	18.8	12	238	545	(65)
7OJ8	ABCG2	Multiple drugs	*Homo sapiens*	4.0	18.0	11	238	575	(66)
7R8A	ABCG5/ G8	Cholesterol	*Homo sapiens*	3.8	18.3	11	238	529	(65)
5XJY	ABCA1	Cholesterol, Phospholipids	*Homo sapiens*	3.4	18.0	12	236	1901	(67)
6XJH	PmtD	Phenol-soluble modulins	*Staphylococcus aureus*	3.6	16.7	12	220	251	(68)
6JBH	TarH	Teichoic acids	*Alicyclobacillus herbarius*	3.4	16.1	14	228	267	(69)
7CH7	MlaE	Phospholipids	*Pseudomonas aeruginosa*	3.3	10.4	9	181	284	(70)

Table S3 Structural homologues of YadG

PDB	Protein	Substrate	Organism	rmsd	z-score	%ID	align	nres	ref
7E7I	ABCA4	N-retinylidene-phosphatidylethanolamine	*Homo sapiens*	2.5	28.9	27	298	2011	(71)
3TUZ	MetN	Methionine	*Escherichia coli*	3.9	28.6	26	261	345	(72)
3FVQ	FbpC	Fe(3+) ions	*Neisseria gonorrhoea*	3.0	28.1	27	234	349	(73)
5GKO	MacB	Macrolides	*Acinetobacter baumannii*	2.2	26.9	30	234	650	(74)
7AHE	OpuA	Glycine betaine	*Lactococcus lactis*	2.5	26.6	23	244	382	(75)
6XJI	PmtC	Phenol-soluble modulins	*Staphylococcus aureus*	3.6	25.3	22	241	290	(68)
7ROQ	ABCA1	Cholesterol/Phospholipids	*Homo sapiens*	3.2	25.3	29	293	1831	(58)
7CAD	SugC	Trehalose	*Mycobacterium smegmatis*	3.2	25.3	22	246	384	(76)
7K2T	Wzm/ Wzt	O-linked polysaccharides	*Aquifex aeolicus*	2.0	24.9	27	220	374	(57)
4PL0	McjD	Antibacterial peptide (microcin J25)	*Escherichia coli*	2.3	24.1	21	221	576	(77)

Chapter 4: Identification and characterisation of an Aromatic Acid Exporter (ArAE) family protein from *Acinetobacter baumannii*

Authors

Stephanie S. Nagy[1,2], Francesca L. Short[3], Liping Li[1,2], Bhumika S. Shah[1,2], Peter J. F. Henderson[4], Karl A. Hassan[5] and Ian T. Paulsen.[1,2*]

Author affiliations

[1]School of Natural Sciences, Faculty of Science and Engineering, Macquarie University, Sydney, NSW, Australia

[2]ARC Centre of Excellence in Synthetic Biology, Macquarie University, Sydney, NSW, Australia

[3]Department of Microbiology, Monash University, Melbourne, VIC, Australia

[4]School of Biomedical Sciences and Astbury Centre for Structural Biology, University of Leeds, Leeds, West Yorkshire, United Kingdom

[5]School of Environmental and Life Sciences, University of Newcastle, Newcastle, NSW, Australia.

Corresponding author: Distinguished Professor Ian T. Paulsen, ian.paulsen@mq.edu.au

Abstract

Acinetobacter baumannii is an opportunistic, nosocomial pathogen commonly associated with hospital-acquired infections in immunocompromised and severely ill patients. The rise of multidrug and pandrug resistant isolates worldwide has prompted the classification of *A. baumannii* as a top priority pathogen for the urgent development of novel therapeutics. It is equally as imperative to understand the mechanism of resistance to combat this pathogen. Recently, we investigated the fitness of a library of *A. baumannii* transposon mutants to silver nitrate and found that ABUW_0700 conferred increased fitness towards silver nitrate. This gene belongs to the Aromatic Acid Exporter (ArAE) family, previously not characterised in *A. baumannii.* ABUW_0700 is conserved in the core genome across *A. baumannii* species. *In silico* prediction of the ABUW_0700 structure revealed a novel protein structure not previously seen in prokaryotic membrane transporters. Heterologous expression of the ABUW_0700 protein in *E. coli* confirmed that it conferred silver nitrate resistance, in addition to a range of antimicrobials including tetracyclines, fluoroquinolones, cefmetazole and sulfonamides and toxic ions. Whole cell transport assays suggested that ABUW_0700 conferred acriflavine efflux. Altogether, this study suggests that ABUW_0700 may represent a new class of multidrug efflux pumps, and potential target for therapeutic development.

Introduction

Acinetobacter baumannii is a nosocomial pathogen of which the rapid rise of multidrug and pan-drug resistant isolates worldwide has led to calls for the urgent development of novel therapeutics to combat resistance. It is equally important to identify putative resistance factors that contribute to the multidrug resistant phenotype of this organism. The aromatic acid export (ArAE) family of transporters, also known as the putative efflux transport (PET) family, are present across bacteria and eukaryotic kingdoms, and have been identified in plants, yeast, fungi, protozoa, and bacterial lineages (1). Members of this family are approximately 655-755 amino acids in length and have evolved as a result of an internal gene duplication event (1, 2). In plants, members of the ArAE are characterised as aluminium activated malate transporters and are recognised as necessary for resistance to aluminium toxicity in soil (3). However, in bacteria some members of the ArAE family are found adjacent to membrane fusion proteins and have been suggested to encode for tripartite efflux systems in Gram-negative bacteria (1, 4). However, only one member of the ArAE family has been experimentally characterized in bacteria (5). The AaeB efflux pump (synonym YhcP) of *Escherichia coli*, associates with the MFP protein, AaeA (synonym YhcQ) to transport *p*-hydroxybenzoic acid (pHBA) out of the cell in a proton-dependent manner, to relieve *E. coli* of unbalanced metabolism and acid stress (4). During our recent TraDIS study to investigate genes important for biocide tolerance in this pathogen, we noted that the ArAE gene, ABUW_0700 was involved in conferring increased fitness to silver nitrate (Chapter 2). Accordingly, further work to understand the role of this protein in conferring resistance to antimicrobials as a putative efflux pump was investigated in this study.

Materials and methods

Bioinformatic analyses

All FASTA format sequences were downloaded from the National Centre for Biotechnology Information (NCBI). The coding region of ABUW_0700 was retrieved from the *Acinetobacter baumannii* AB5075_UW genome (CP008706.1). Homologous sequences of ABUW_0700 were collected using the HMMER webserver (v. 2.41.2) against reference proteomes (6, 7). Full-length sequences with *E*-values $\leq 10^{-20}$ were deemed homologous. Multiple sequence alignments (MSAs) of ABUW_0700 homologues was performed using MUSCLE (8). A phylogenetic tree of ABUW_0700 homologs was constructed using the neighbor-joining method with $n = 1000$ bootstrap replicates and default parameters using MEGAX software and visualised with iTOL (9-13). The pan-genome of *A. baumannii* AB5075_UW was analysed from data from our previous publication (14) to investigate the conservation of ABUW_0700 and its genetic neighbourhood and was visualised using Clinker (15). *A. baumannii* genomes included in the analysis cover all complete genomes deposited to the NCBI assembly database as of March 26, 2020. Gene conservation analysis of ABUW_0700 homologs across more distantly related bacteria was performed using the WebFLaGs server with default parameters (16).

In silico prediction of the structure of ABUW_0700

In silico prediction of the structure of ABUW_0700 was performed using AlphaFold2 (17). AlphaFold2 models were run using a ColabFold notebook with default parameters and MMseq2 generated sequence MSAs (18, 19). A Ramachandran plot of the AlphaFold2 predicted structure of ABUW_0700 was generated with PROCHECK (20). Amino acid conservation was mapped to the ABUW_0700 structure with ConSurf (21, 22). Predictions of the pore region were visualised with MOLEonline (ver. 1.5.2.1) (23). Structural homologs of ABUW_0700 were reviewed with DALI (accessed on 13th April 2022) (24). All PDB files and figures were visualised and generated with Pymol (25).

Bacterial strains and plasmids

The coding region of ABUW_0700 from the AB5075_UW genome (CP008706.1) was chemically synthesised and cloned between the *EcoR*I and *Sal*I sites within the MCS for in-frame transcription with the endogenous *tac* promotor and C-terminal hexa-histidine tag ($RSGH_6$) of pTTQ18-$RSGH_6$ plasmid (26–28). Gene synthesis and cloning into the expression vector to yield pTTQ18-ABUW_0700_{RSGH6} was purchased from Genscript (Piscataway, USA). For heterologous expression of ABUW_0700 in *E. coli*, chemically competent *E. coli* BL21 (DE3) were purchased from Bioline, USA. *E. coli* BW25113 Δ*emrE*, Δ*mdfA* and Δ*acrB::kan* cells was used for acriflavine transport assays against an efflux sensitive background (29).

Preparation of chemically competent *E. coli* cells

Chemically competent cells of the *E. coli* triple efflux mutant were prepared according to the calcium wash method. Briefly, *E. coli* cells were grown to the mid-exponential phase (OD_{600nm} = 0.4) and immediately incubated on ice for 30 minutes. Cells were harvested at 3000 × g for 15 minutes at 4°C and resuspended with ice-cold 100 mM $MgCl_2$ solution. Cell suspensions were pelleted at 2000 × g for 15 minutes at 4°C. Cell pellets were resuspended in ice-cold 100 mM $CaCl_2$ solution and chilled on ice for 20 minutes. Cell suspensions were pelleted at 2000 × g for 15 minutes at 4°C and resuspended in ice cold 85 mM $CaCl_2$ with 15% glycerol. Cell suspensions were pelleted at 1000 × g for 15 minutes and resuspended to a final OD_{600nm} = 200 in 2 mL of ice cold 85 mM $CaCl_2$ with 15% glycerol. Samples were snap-frozen in liquid nitrogen and stored at −80°C for transformation.

Transformation of chemically competent *E. coli* cells.

E. coli BL21 (DE3) or BW25113 (Δ*emrE*, Δ*mdfA* and Δ*acrB::kan)* cells were transformed with pTTQ18-$RSGH_6$ or pTTQ18-ABUW_0700_{RSGH6} were transformed using the heat shock method (30) with the following modifications. Briefly, 50 µL of chemically competent *E. coli* were thawed on ice and incubated with 5 ng of plasmid DNA for 30 minutes, followed by a heat-shock at 42°C for 40 seconds. *E. coli* samples were immediately transferred to ice to incubate for 2 minutes before recovery in S.O.C media (Thermo Fischer) for 1 hour at 37°C, 200 rpm. Recovered cell

cultures were plated on LB-agar supplemented with 100 μg/mL ampicillin for selection and incubated overnight at 37°C. Following transformation, all *E. coli* cultures harbouring pTTQ18-RSGH$_6$ (empty vector) or pTTQ18-ABUW_0700$_{RSGH6}$ were prepared in LB-media supplemented with 100 μg/mL ampicillin and grown at 37°C, 200 rpm unless otherwise specified.

Small scale culture and expression of ABUW_0700 in *Escherichia coli*

Overnight cultures of *E. coli* BL21 (DE3) harbouring pTTQ18-RSGH$_6$ and pTTQ18-ABUW_0700$_{RSGH6}$ were grown in 50 mL of Luria-Bertani (LB) broth (10 g/L NaCl, 10 g/L tryptone, 5 g/L yeast extract) supplemented with 100 μg/mL carbenicillin and 20 mM glycerol at 37°C, shaking at 200 rpm. Overnight cultures were diluted 1:100 in fresh LB media supplemented with 100 μg/mL carbenicillin and 20 mM glycerol and grown at 37°C, shaking at 200 rpm to a final OD_{600nm} = 0.8. Expression of ABUW_0700 was induced with IPTG (0.2 mM final concentration) for 3 hours. Cell cultures were harvested by centrifugation (12,000 × g) for 15 minutes at 4°C. *E. coli* mixed membranes were extracted according to the water-lysis spheroplast method as published (28). Briefly, cell pellets were resuspended in 10 mL 0.2 M Tris-HCl, pH 8.0 and stirred on rollers for 20 minutes at room temperature. At time zero, 4.85 mL of sucrose buffer (0.2 M Tris-HCl, pH 8.0, 1 M sucrose, 1 mM EDTA) was added. At 1.5 minutes, 65 μL of freshly prepared 10 mg/mL lysozyme solution was added. At 2 minutes, 9.6 mL MilliQ water was added and the sample was gently mixed on rollers for 20 minutes. The spheroplasts were sedimented at 25,000 × g for 20 minutes, then resuspended in 15 mL MilliQ water and incubated at room temperature for 30 minutes. Mixed membranes were sedimented at 25,000 × g for 20 minutes, washed thrice with NaPi buffer (0.1 M disodium hydrogen phosphate, 0.1 M sodium dihydrogen phosphate, pH 7.2). Membrane pellets were resuspended in 500 μL of NaPi buffer, pH 7.2 containing 1 mM β-mercaptoethanol and were snap-frozen with liquid nitrogen and stored at −80°C prior to further SDS-PAGE and western blot analyses. Total protein content was quantified using the Pierce™ BCA Protein Assay Kit (Thermo Scientific) (31). SDS-PAGE of mixed membrane samples followed the method published by Henderson and MacPherson (32). Heterologous expression of ABUW_0700 in mixed membranes of *E. coli* was

detected by western blotting using an anti-$RGSH_6$–horseradish peroxidase conjugate (Bio-Rad) according to manufacturer instructions.

Antimicrobial sensitivity screening

Biolog phenotype microarrays (PMs) were used to explore the antimicrobial profile of ABUW_0700 against 240 unique antimicrobials using the bacterial chemical sensitivity panel (PM11-20) (33). A complete list antimicrobials tested is available (Appendix B). Biolog phenotype microarrays were performed as described (34). Briefly, *E. coli* cells were streaked onto LB agar plates supplemented with 100 μg/mL ampicillin and grown overnight at 37°C. Individual colonies were streaked onto a fresh LB-ampicillin agar plate and grown overnight at 37°C. Colonies were collected and suspended in Biolog GN IF-0a solution to 85% transmittance, measured by a Biolog turbidimeter. Cell suspensions were diluted 1:200 in Biolog IF-10b solution and supplemented with 1:100 dilution of Biolog redox dye mix A. PM plates were inoculated with IPTG (0.05 mM final concentration) and inoculated with 100 μL of bacterial cell culture in each well across PM11-PM20. PM plates were sealed with Breathe-Easy® plastic film to allow for gas exchange (Diversified Biotech). Plates were incubated and imaged using a Biolog OmniLog instrument to measure for colorimetric change at 37°C, with shaking for 72 hours.

Minimum inhibitory concentration assays

Minimum inhibitory concentration (MICs) assays were performed according to the microbroth serial dilution method as previously described (35), with the following modifications. LB media was used throughout all MICs, except for silver nitrate where LB media excluding sodium chloride was used throughout this assay to avoid the precipitation of silver salt. Briefly, fresh transformants of *E. coli* BL21 (DE3) harbouring pTTQ18-$RSGH_6$ or pTTQ18-ABUW_0700_{RSGH6} were grown in fresh media overnight supplemented with 100 μg/mL ampicillin. Overnight bacterial cultures were diluted 1:100 in fresh media supplemented with ampicillin (100 μg/mL) for positive selection and grown to mid-exponential phase (OD_{600nm} = 0.6). Cells were further diluted 1:100 in fresh media and inoculated into 96-well plate containing media supplemented with 0.05 mM and two-fold serial dilution of dye or silver nitrate. Plates were sealed with Breathe-Easy® film

(Diversified Biotech) and incubated at 37°C at 200 rpm for 24 hours before absorbance, measured at OD_{600nm} was determined using the PheraSTAR FSX (BMG LabTech).

Fluorometric transport assays

Overnight cell cultures of *E. coli* were grown in LB media containing 100 μg/mL ampicillin at 37°C, 200 rpm shaking. Protein expression was induced at OD_{600nm} = 0.8 with 0.05 mM IPTG for 1 hour. Cells were washed thrice with HEPES buffer (20 mM HEPES-KOH pH 7.0, 145 mM NaCl, 5 mM KCl) and resuspended to a final OD_{600nm} = 3 in 1 mL of HEPES buffer. Cells were treated with 10 μM CCCP and 5 μM acriflavine and incubated at 37°C in the dark for 1 hour. Cells were washed thrice with HEPES buffer to remove excess dye and protonophore. Cell pellets were resuspended immediately before transport assay initiation. All transport assays were performed using a Biotek HT synergy multiplate reader with excitation and emission wavelengths set to 450 nm and 510 nm respectively. Assays began with an initial read to adjust for autofluorescence, followed by the injection of 0.5% v/v glucose (final concentration) in HEPES buffer (final concentration) to initiate transport-mediated efflux of acriflavine out of the *E. coli* cells.

Results and discussion

ABUW_0700 is part of the core genome of *A. baumannii*

The pan-genome analysis confirmed the presence of the ArAE gene ABUW_0700 and its paralog ABUW_0338 across all complete genomes of *A. baumannii* (*n* = 172 genomes) revealing that both of these ArAE genes are part of the core genome of *A. baumannii*. Local genetic neighbourhood analysis revealed that ABUW_0700 is always adjacent to genes encoding an MFS transporter of unknown function (ABUW_0701) and a membrane protein of unknown function (ABUW_0699). ABUW_0700 always appears in the same genetic region (*n* = 172 genomes) (Figure 1). Typically, ArAE family genes are located adjacent to MFP and OMF family genes (1, 4). However, no known MFP gene was located within the local genetic region of ABUW_0700. Similarly, the paralogous ArAE gene, ABUW_0338 is also found adjacent to an MFS transporter gene, and no MFP gene is

located nearby. Analysis of more distant homologs of ABUW_0700 from more distant species revealed that the genetic region in which the ArAE gene is conserved is unique to *Acinetobacter* spp. (Figure 2). In contrast, in all other *Enterobacterales* the ortholog of ABUW_0700 is conserved in a region of high-synteny adjacent to genes encoding an inner membrane protein YccF (DUF307 family) and a transcriptional regulator TfoX linked to natural competence in *Enterobacteriaceae* (36).

Phylogenetic tree reveals conservation of ArAE homologs across diverse environments

The ArAE transport family is a large family that spans bacteria, archaea, and plant kingdom (1). To investigate the phylogeny of ABUW_0700 and orthologs, we performed HMM seq search to identify distant evolutionary homologs against reference proteomes. The HMM seq searching using HMMER (v. 2.41.2) with default parameters revealed the presence of homologous sequences across all three kingdoms of life (bacteria $n = 3241$, eukaryotes $n = 13$, archaea $n = 11$).

A phylogenetic tree of the ABUW_0700 homologs is presented in Figure 3. Across $n = 1000$ sequences, the phylogenetic tree shows clear groups of ABUW_0700 orthologs across three main clusters, cluster 1 (Family I), cluster 2 (Family II-V) and cluster 3 (Family VI-XI). Most bacterial members of this family are encoded within the Proteobacteria and Bacteroidetes phyla. ABUW_0700, its orthologs and paralogs across the *Acinetobacter* spp. are located within cluster 2 along with homologs from *Enterobacterales* and *Xanthomonadales* of Gammaproteobacteria with a few representatives from *Marinilabiliales* order in the Bacteroidetes phylum. Cluster I consists of paralogs from the *Enterobacterales* order in the Gammaproteobacteria but includes no members in the *Acinetobacter* genus. Members of cluster 3 are predominantly from the Bacteroidetes lineage, mostly from *Flavobacteriales* and *Sphingomonadales* order with some representatives from the *Burkholderiales* order in the Betaproteobacteria.

***In silico* predicted structure of ABUW_0700 reveals a novel fold in prokaryotes**

Currently, there is no solved structure of a prokaryotic member of the ArAE family of transporter proteins. To further investigate the putative function of ABUW_0700, we decided to examine the

predicted tertiary structure of ABUW_0700 using AlphaFold2. The predicted tertiary structure of ABUW_0700 reveals a large monomeric structure comprised exclusively of α-helical and 310-helical secondary structures, with a topology that alternates between the transmembrane and cytoplasmic domains as predicted by Harley and Saier (1) (Figure 4 and 5). The predicted structure of ABUW_0700 comprises one large transmembrane domain containing 10 α-transmembrane helices and two asymmetrical helical cytoplasmic domains (CD) (Figure 5). AlphaFold2 mapped confidence using lDDT parameters reports a very high level of confidence for the transmembrane region and cytoplasmic domains (>90%) of ABUW_0700 with lower confidence around the loop regions (80%) connecting the helices between TMH domain and CD domains (≤50-60%) (Figure 6). A Ramachandran plot confirms 95.3% of residues are located in favourable, 4.5% residues in allowed and 0.3% are in generously allowed regions. No residues were plotted in disallowed regions according to the Ramachandran plot (Figure 6). The ABUW_0700 model reveals a large, central transmembrane pore formed within the transmembrane region that reaches into the CHD domains (Figure 5). ABPS (Adaptive Poisson-Boltzmann Solver) electrostatics show a predominantly hydrophobic transmembrane permease, with largely polar cytoplasmic domains (Figure 5). Cross-section analysis reveals that the central cavity in the transmembrane region is positively charged (Figure 5). MOLEonline analyses identified this feature as a large pore 64.6 Å in length and 8 Å in width, with 4 ionizable residues that are located within the pore region (Figure 5, Figure S1, Table S2). DALI analyses could not match the predicted structure of ABUW_0700 to any known PDB structure with significant confidence. Recently, the cryo-EM structure of ALMT, an anion channel from *Glycine max*, a member of the ArAE family was solved (37). The cryo-EM structure reveals a similar structural fold to the tertiary structure predicted for ABUW_0700 by AlphaFold2 with a RMSD of 10.76 (Figure 5). The overlap in protein fold between the ALMT anion channel and the predicted structure of ABUW_0700, together with the positively charged pore of ABUW_0700, suggests the possibility that the natural substrate of ABUW_0700 is anionic.

ABUW_0700 confers increased tolerance to a diverse range of antimicrobials in *E. coli*

ABUW_0700 was heterologously expressed in *E. coli* BL21 (DE3) as a hexa-histidine C-terminal fusion. Western blot analysis confirmed the expression of the fusion protein ~70 kDa (Appendix C). As this gene was identified initially as conferring increased fitness to silver nitrate, we investigated its capacity when heterologously expressed in *E. coli* to confer resistance to a range of 240 other antimicrobials using Biolog phenotype microarrays. *E. coli* cells expressing ABUW_0700 displayed increased respiration on tetracycline, enoxacin, ciprofloxacin, tobramycin, cefmetazole, tobramycin, phleomycin, tinidazole, 2-nitroimdiazole and a range of sulfanilamides (Figure 7). In addition to these antimicrobials, ABUW_0700 also conferred increased respiration in the presence of bioactive compounds including dichlofluanid, tolyfluanid, guanidine, guanazole, L-aspartic-β-hydroxamate, protamine sulfate, caffeine, 6-mercaptopurine, menadione, compound 48/80 and umbelliferone (Figure 7). MIC analyses confirmed that heterologous expression of ABUW_0700 conferred log 2-fold increased MIC to sulfadiazine and to silver nitrate (Table 1). We also tested whether ABUW_0700 conferred resistance to acriflavine to identify suitable antimicrobial fluorophore for whole cell transport assays, and found that ABUW_0700 conferred a log 2-fold increased MIC to acriflavine.

Fluorometric transport assay demonstrates efflux mediated by ABUW_0700 expression

As *E. coli* encodes a variety of efflux pumps for fluorescent antimicrobials such as acriflavine and ethidium bromide, we undertook whole cell fluorometric transport assays using *E. coli* BW25113 (Δ*emrE*, Δ*mdfA* and Δ*acrB::kan*). This strain has the three primary drug efflux systems knocked out, providing a more sensitive background for transport assays. Efflux activity was measured as an increase in acriflavine fluorescence intensity overtime as acriflavine is quenched when bound to DNA within the bacterial cell and fluoresces brightly in an aqueous solution. Expression of ABUW_0700 revealed an increase in total acriflavine fluorescence exported over time compared to cells harbouring an empty vector as a control (pTTQ18-RSGH$_6$) (Figure 8). These results suggest that the antimicrobial resistance profile conferred by ABUW_0700 may be via an efflux mechanism.

Conclusions

This study provides a preliminary investigation of the ABUW_0700 putative ArAE transporter. Biolog phenotype microarrays, MIC analysis and fluorescent transport assays support that ABUW_0700 confers increased tolerance to multiple drugs via an efflux mechanism. This is consistent with its initial identification as a potential silver nitrate resistance determinant (Chapter 2). The structural similarity between the predicted fold of ABUW_0700 and the cryo-EM structure of ALMT, together with the positively charged pore of ABUW_0700 provides a possible alternative role in the transport of anionic metabolites. Purification of the ABUW_0700 protein with screening potential ligands by nano-DSF or nano-ITC, as well as reconstitution of the transporter in proteoliposomes, should clarify the biochemical and physiological function of this transporter. Its conservation in the core genome of *A. baumannii* suggests it plays an essential functional role in this opportunistic pathogen.

References

1. K. T. Harley, M. H. Saier, A novel ubiquitous family of putative efflux transporters. *J. Mol. Microbiol. Biotechnol.* **2**, 195–198 (2000).

2. M. H. Saier, Tracing pathways of transport protein evolution. *Mol. Microbiol.* **48**, 1145–1156 (2003).

3. T. Sharma, I. Dreyer, L. Kochian, M. A. Piñeros, The ALMT family of organic acid transporters in plants and their involvement in detoxification and nutrient security. *Front. Plant Sci.* **7**, 1488 (2016).

4. I. T. Paulsen, J. H. Park, P. S. Choi, M. H. Saier, A family of Gram-negative bacterial outer membrane factors that function in the export of proteins, carbohydrates, drugs and heavy metals from Gram-negative bacteria. *FEMS Microbiol. Lett.* **156**, 1–8 (1997).

5. T. K. Van Dyk, L. J. Templeton, K. A. Cantera, P. L. Sharpe, F. S. Sariaslani, Characterization of the *Escherichia coli* AaeAB efflux pump: A metabolic relief valve? *J. Bacteriol.* **186**, 7196–7204 (2004).

6. S. R. Eddy, Profile hidden Markov models. *Bioinformatics* **14**, 755–763 (1998).

7. S. C. Potter, *et al.*, HMMER web server: 2018 update. *Nucleic Acids Res.* **46**, W200–W204 (2018).

8. R. C. Edgar, MUSCLE: Multiple sequence alignment with high accuracy and high throughput. *Nucleic Acids Res.* **32**, 1792–1797 (2004).

9. N. Saitou, M. Nei, The neighbor-joining method: A new method for reconstructing phylogenetic trees. *Mol. Biol. Evol.* **4**, 406–425 (1987).

10. J. Felsenstein, Confidence limits on phylogenies: an approach using the bootstrap. *Evolution (N. Y).* **39**, 783–791 (1985).

11. E. Zuckerkandle, L. Pauling, Evolutionary divergence and convergence in proteins. *Evol. Genes Proteins*, 97–166 (1965).

12. S. Kumar, G. Stecher, M. Li, C. Knyaz, K. Tamura, MEGA X: Molecular evolutionary genetics analysis across computing platforms. *Mol. Biol. Evol.* **35**, 1547–1549 (2018).

13. I. Letunic, P. Bork, Interactive tree of life (iTOL) v5: An online tool for phylogenetic tree display and annotation. *Nucleic Acids Res.* **49**, W293-296 (2021).

14. F. L. Short, *et al.*, The *Acinetobacter baumannii* disinfectant resistance protein, AmvA, is a spermidine and spermine efflux pump. *Commun. Biol.* **4,** 1114 (2021).

15. C. L. M. Gilchrist, Y.-H. Chooi, Clinker & clustermap.js: Automatic generation of gene cluster comparison figures. *Bioinformatics* **37**, 2473–2475 (2021).

16. C. K. Saha, R. S. Pires, H. Brolin, M. Delannoy, G. C. Atkinson, FlaGs and webFlaGs: Discovering novel biology through the analysis of gene neighbourhood conservation. *Bioinformatics* **37**, 1312–1314 (2021).

17. J. Jumper, *et al.*, Highly accurate protein structure prediction with AlphaFold. *Nature*, 583–589 (2021).

18. M. Mirdita, *et al.*, ColabFold: making protein folding accessible to all. *Nat. Methods* **19**, 679–682 (2022).

19. M. Steinegger, J. Söding, MMseqs2 enables sensitive protein sequence searching for the analysis of massive data sets. *Nat. Biotechnol.* **35**, 1026–1028 (2017).

20. R. A. Laskowski, M. W. MacArthur, D. S. Moss, J. M. Thornton, PROCHECK: a program to check the stereochemical quality of protein structures. *J. Appl. Crystallogr.* **26**, 283–291 (1993).

21. M. Landau, *et al.*, ConSurf 2005: The projection of evolutionary conservation scores of residues on protein structures. *Nucleic Acids Res.* **33**, W299-302 (2005).

22. H. Ashkenazy, *et al.*, ConSurf 2016: an improved methodology to estimate and visualize evolutionary conservation in macromolecules. *Nucleic Acids Res.* **44**, W344–W350 (2016).

23. L. Pravda, *et al.*, MOLEonline: A web-based tool for analyzing channels, tunnels and pores (2018 update). *Nucleic Acids Res.* **46**, W368–W373 (2018).

24. L. Holm, DALI and the persistence of protein shape. *Protein Sci.* **29**, 128–140 (2020).

25. W. Delano, The PyMOL molecular graphics system. *CCP4 Newsl. Protein Crystallogr.* **40**, 82–92 (2002).

26. M. J. R. Stark, Multicopy expression vectors carrying the *lac* repressor gene for regulated high-level expression genes in *Escherichia coli*. *Gene* **51**, 255–267 (1987).

27. M. V. Dilworth, *et al.*, Microbial expression systems for membrane proteins. *Methods* **147**, 3–39 (2018).

28. A. Ward, *et al.*, "The amplified expression, identification, purification, assay and properties of hexahistidine-tagged bacterial membrane transport proteins" in *Membrane Transport - A Practical Approach*, S. A. Baldwin, Ed. (2000), pp. 141–166.

29. N. Tal, S. Schuldiner, A coordinated network of transporters with overlapping specificities provides a robust survival strategy. *Proc. Natl. Acad. Sci. U. S. A.* **106**, 9051–9056 (2009).

30. A. Froger, J. E. Hall, Transformation of plasmid DNA into *E. coli* using the heat shock method. *J. Vis. Exp.*, 253 (2007).

31. P. K. Smith, *et al.*, Measurement of protein using bicinchoninic acid. *Anal. Biochem.* **150**, 76–85 (1985).

32. P. J. F. Henderson, A. J. S. Macpherson, "Assay, genetics, proteins, and reconstitution of proton-linked galactose, arabinose, and xylose transport systems of *Escherichia coli*" in *Methods in Enzymology*, (1986), pp. 387–429.

33. B. R. Bochner, Global phenotypic characterization of bacteria. *FEMS Microbiol. Rev.* **33**, 191–205 (2009).

34. A. M. Mackie, K. A. Hassan, I. T. Paulsen, S. G. Tetu, "Biolog phenotype microarrays for phenotypic characterisation of microbial cells" in *Methods in Molecular Biology*, (2014), pp. 123–130.

35. I. Wiegand, K. Hilpert, R. E. W. W. Hancock, Agar and broth dilution methods to determine the minimal inhibitory concentration (MIC) of antimicrobial substances. *Nat. Protoc.* **3**, 163–175 (2008).

36. S. Sinha, R. J. Redfield, Natural DNA uptake by *Escherichia coli*. *PLoS One* **7**, e35620–e35620 (2012).

37. L. Qin, *et al.*, Cryo-EM structure and electrophysiological characterization of ALMT from *Glycine max* reveal a previously uncharacterized class of anion channels. *Sci. Adv.* **8**, 1–16 (2022).

38. X. Robert, P. Gouet, Deciphering key features in protein structures with the new ENDscript server. *Nucleic Acids Res.* **42**, W320–W324 (2014).

39. V. Mariani, M. Biasini, A. Barbato, T. Schwede, lDDT: A local superposition-free score for comparing protein structures and models using distance difference tests. *Bioinformatics* **29**, 2722–2728 (2013).

Figures and tables

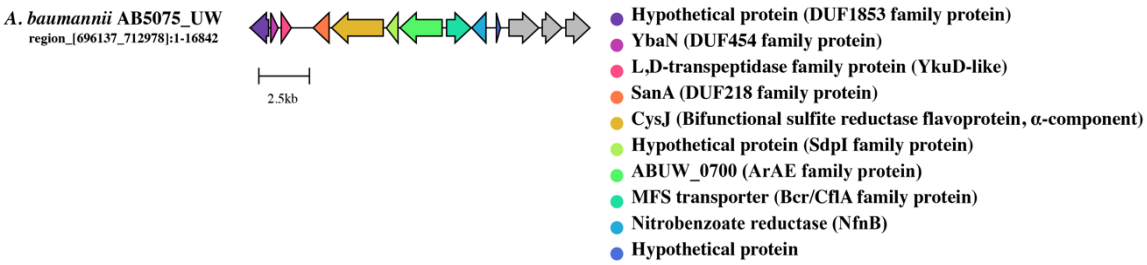

Figure 1: Visualization of the genomic context of ABUW_0700 across all complete *A. baumannii* genomes (*n* = 172). ABUW_0700 is conserved across all genomes with high-level of synteny. The conserved pathway is represented by *A. baumannii* AB5075_UW. *Coloured* genes are conserved genes with 100% identity across genomes analysed. *Grey* genes represent unique genes across genomes. Gene conservation and pathway mapping was visualised by Clinker (15) and annotated in Illustrator.

Figure 2: Conserved genetic neighbourhood analysis across distant RefSeq homologs of ABUW_0700 from family V of the phylogenetic tree. Genes that are present in two or more genetic regions are coloured and numbered (Table S1). Non-conserved genes are blank. ABUW_0700 and homologs are coloured as a *black* arrow. *Purple* outlined arrows are pseudogenes and *green* outlined arrows are RNA genes. Branch values are provided in bootstrap support values. The figure was generated by the WebFlaGs server with default parameters (16).

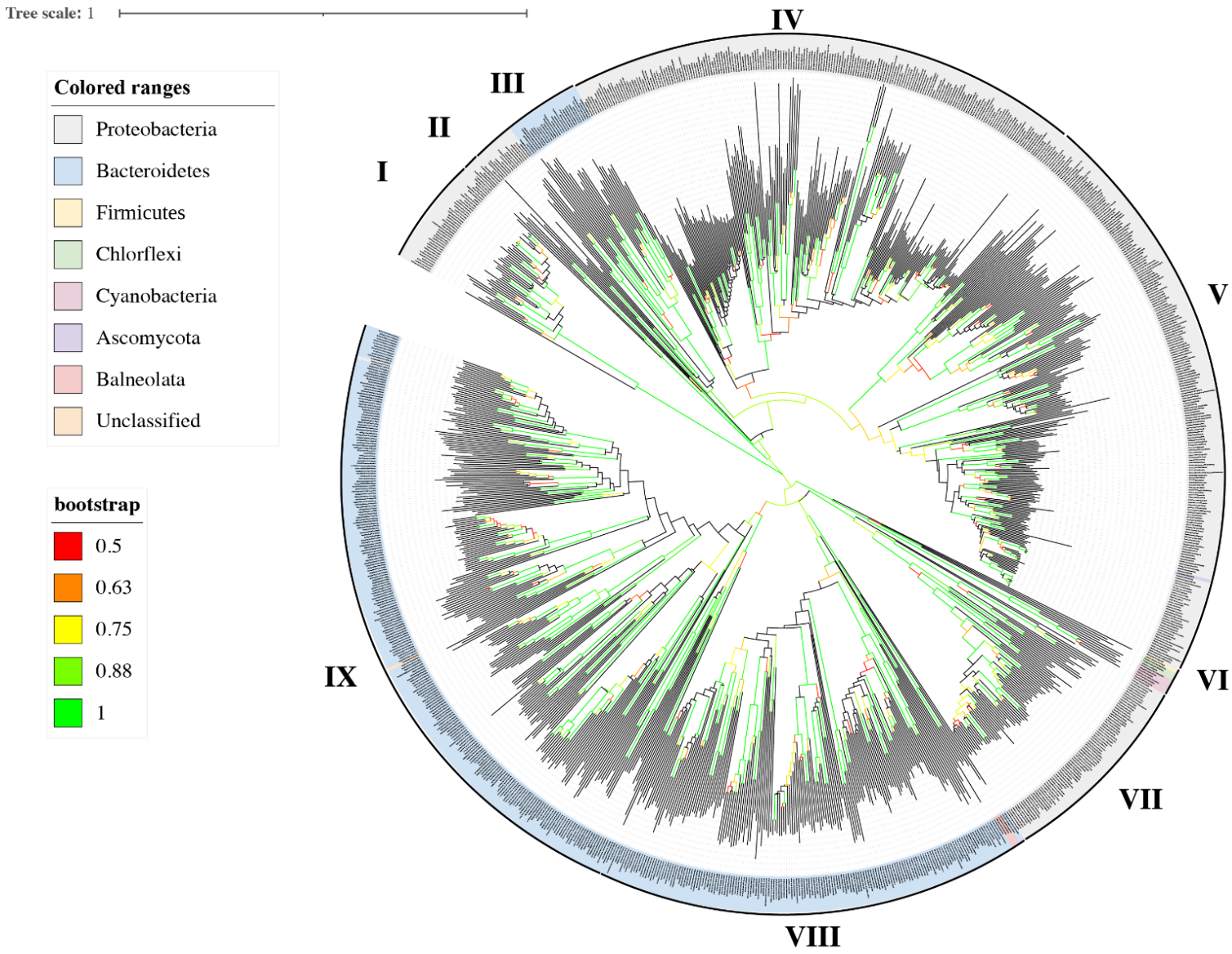
Tree scale: 1
Colored ranges
Proteobacteria
Bacteroidetes
Firmicutes
Chlorflexi
Cyanobacteria
Ascomycota
Balneolata
Unclassified
bootstrap
0.5
0.63
0.75
0.88
1
I
II
III
IV
V
VI
VII
VIII
IX

Figure 3: Phylogenetic tree of ABUW_0700 homologs ($n = 1000$) constructed by the neighbor-joining method in MEGAX and visualised in iTOL (9–13). The phylogenetic tree was drawn to a scale where branch lengths represent the number of substitutions per site. The tree is coloured according to taxonomic phylum. Bootstrap values of at least $n = 1000$ iterations ≤ 0.5 are represented as coloured branches from *red* to *green* (0.5-1.0), respectively.

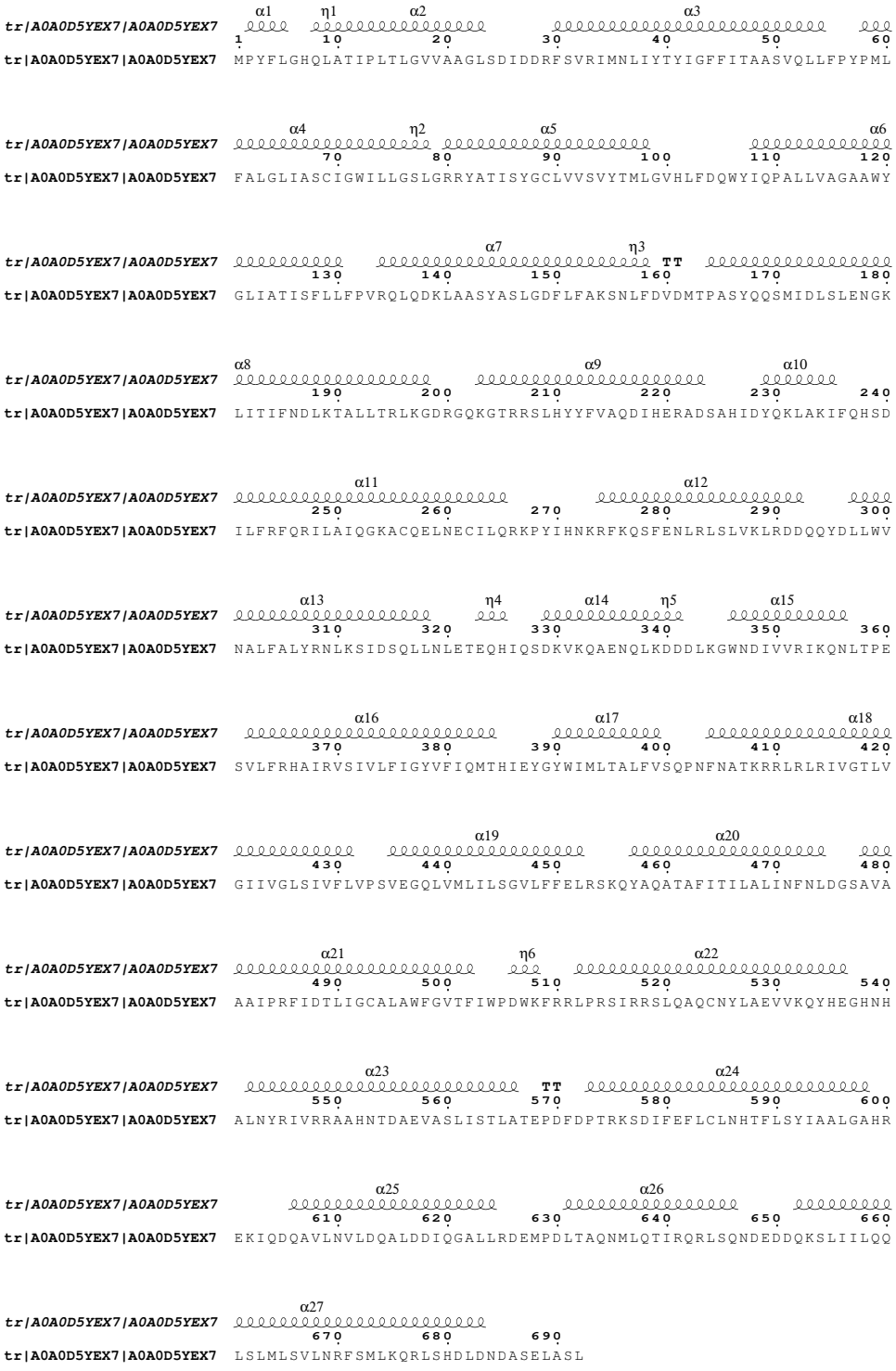

Figure 4: ABUW_0700 sequence with predicted secondary structure features aligned from AlphaFold2, revealed the presence of 27 α-helices and six 3_{10}-helices. The figure was prepared with the ESPript webserver (38).

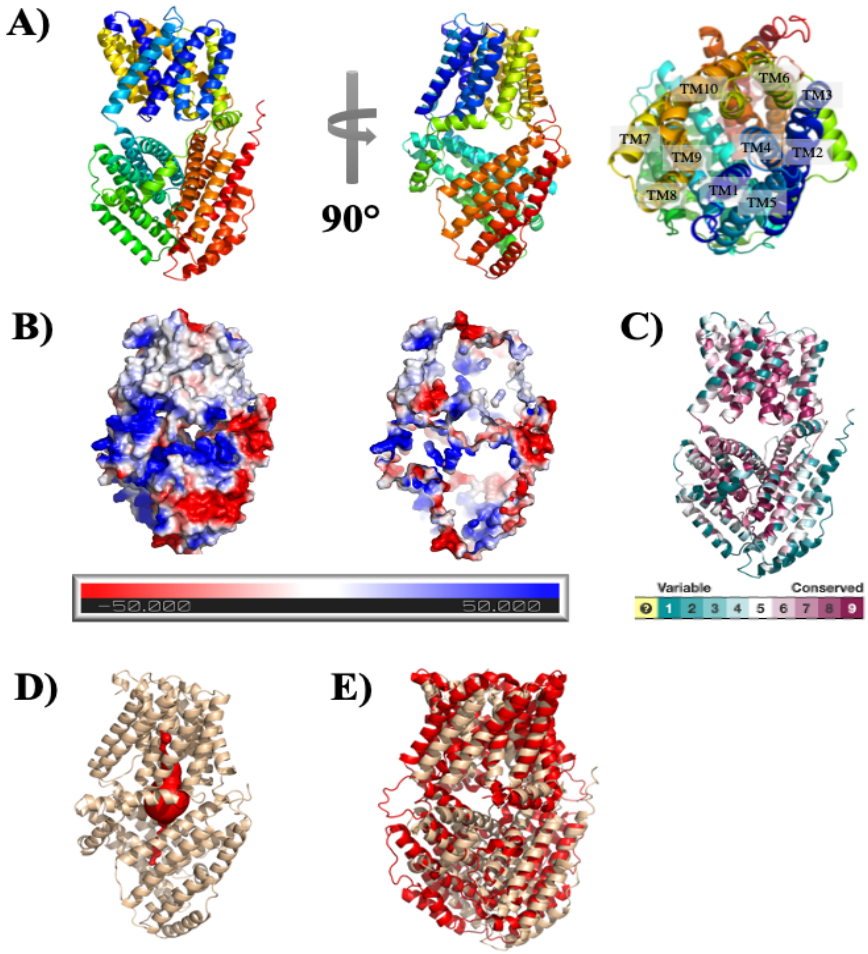

Figure 5: AlphaFold2 prediction of ABUW_0700. A) Overall rainbow ribbon representation of ABUW_0700 monomer showing the front profile, side profile, and top-down profile views revealing novel protein fold comprised only helices that include three distinct domains, a transmembrane domain region with a large central cavity and two large helical cytoplasmic domains that sit ajar from a transmembrane region located in the cytoplasm. B) APBS electrostatics view revealing the distribution of electrostatic charge across and within ABUW_0700. C) ConSurf analysis of ABUW_0700 structure, revealing amino acid conservation from variable (*cyan*) to conserved (*magenta*) (21, 22). D) MOLEonline estimate of central pore 64.6Å in length, spanning the transmembrane and cytoplasmic regions of ABUW_0700 (Figure S2, Table S2) (23). E) Overlay of AlphaFold2 predicted structure of ABUW_0700 (*wheat*) and cryo-EM structure of ALMT of *Glycine max* (*red*) with an RMSD value of 10.76 revealing novel protein fold is shared between ArAE family members (PDB: 7W6K) (37). All figures visualised in Pymol (25)

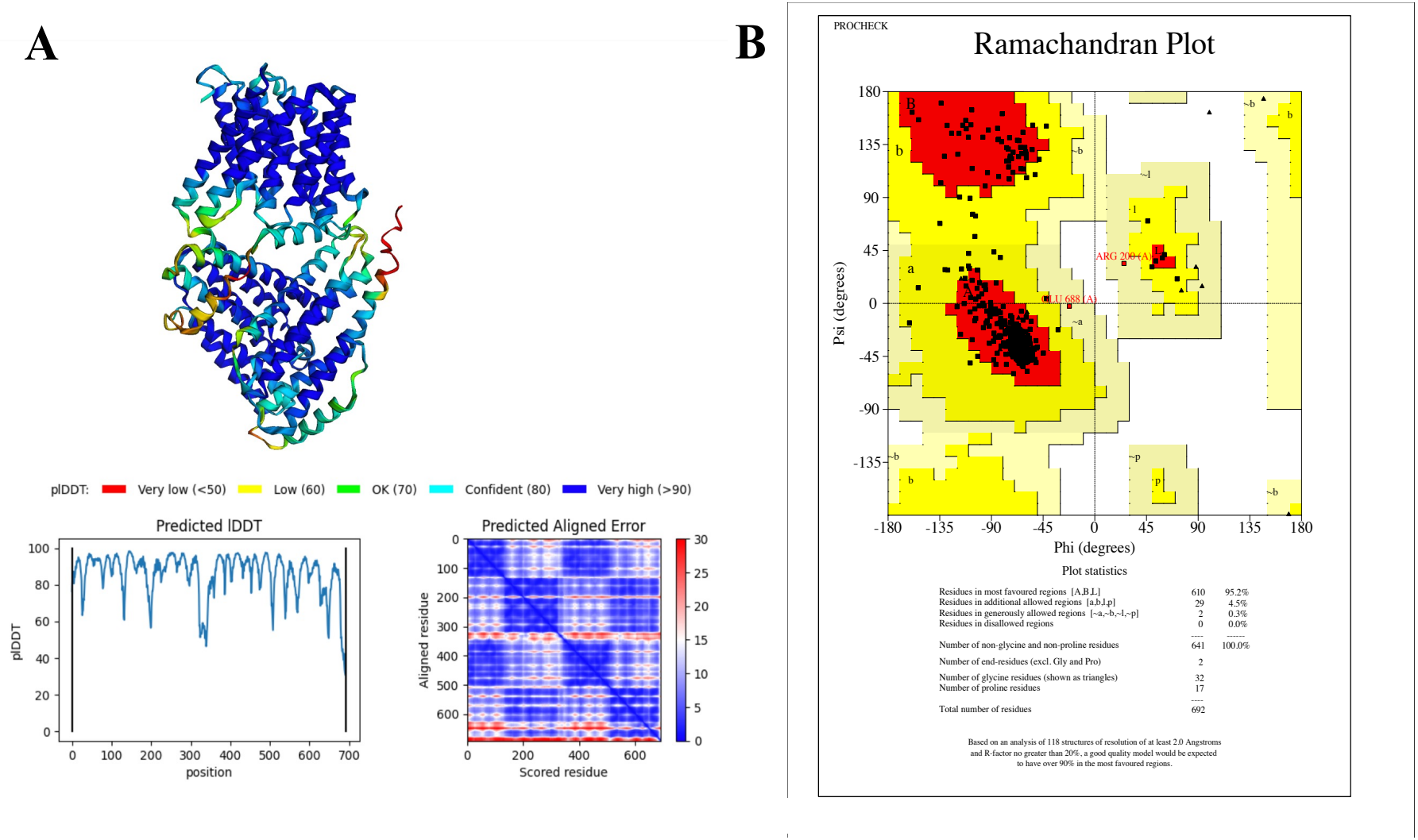

Figure 6: Assessment of ABUW_0700 AlphaFold2 model quality. A) lDDT confidence analysis provided by AlphaFold2 (17, 39). B) Ramachandran plot summary generated by PROCHECK (20).

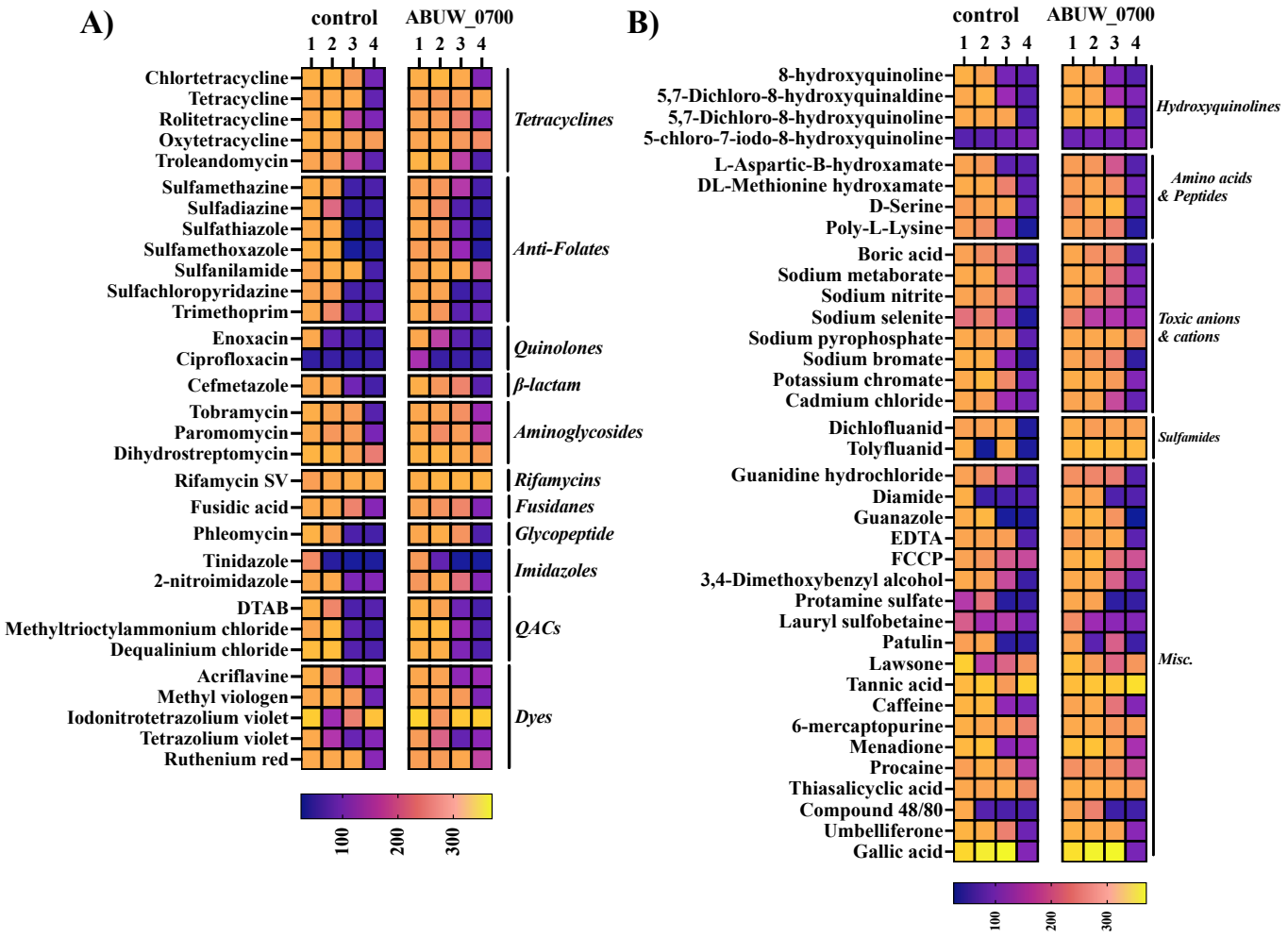
A)
control
ABUW_0700
1 2 3 4
1 2 3 4
Chlortetracycline
Tetracycline
Rolitetracycline
Oxytetracycline
Troleandomycin
Tetracyclines
Sulfamethazine
Sulfadiazine
Sulfathiazole
Sulfamethoxazole
Sulfanilamide
Sulfachloropyridazine
Trimethoprim
Anti-Folates
Enoxacin
Ciprofloxacin
Quinolones
Cefmetazole
β-lactam
Tobramycin
Paromomycin
Dihydrostreptomycin
Aminoglycosides
Rifamycin SV
Rifamycins
Fusidic acid
Fusidanes
Phleomycin
Glycopeptide
Tinidazole
2-nitroimidazole
Imidazoles
DTAB
Methyltrioctylammonium chloride
Dequalinium chloride
QACs
Acriflavine
Methyl viologen
Iodonitrotetrazolium violet
Tetrazolium violet
Ruthenium red
Dyes
100
200
300
B)
control
ABUW_0700
1 2 3 4
1 2 3 4
8-hydroxyquinoline
5,7-Dichloro-8-hydroxyquinaldine
5,7-Dichloro-8-hydroxyquinoline
5-chloro-7-iodo-8-hydroxyquinoline
Hydroxyquinolines
L-Aspartic-B-hydroxamate
DL-Methionine hydroxamate
D-Serine
Poly-L-Lysine
Amino acids & Peptides
Boric acid
Sodium metaborate
Sodium nitrite
Sodium selenite
Sodium pyrophosphate
Sodium bromate
Potassium chromate
Cadmium chloride
Toxic anions & cations
Dichlofluanid
Tolyfluanid
Sulfamides
Guanidine hydrochloride
Diamide
Guanazole
EDTA
FCCP
3,4-Dimethoxybenzyl alcohol
Protamine sulfate
Lauryl sulfobetaine
Patulin
Lawsone
Tannic acid
Caffeine
6-mercaptopurine
Menadione
Procaine
Thiasalicyclic acid
Compound 48/80
Umbelliferone
Gallic acid
Misc.
100
200
300

Figure 7: Biolog phenotype microarray profile of ABUW_0700. Antimicrobial resistance phenotypes were determined from the expression of ABUW_0700 in *E. coli* BL21 (DE3). Results are displayed as a heatmap using a coloured scale from no growth (*dark blue*) to maximum growth (*yellow*). Biolog phenotypes are represented across two heatmap panels. A) common antimicrobial therapeutics and B) toxic bioactive compounds. Phenotypes are organised according to chemical class. Columns represent a log 2-fold increase in antimicrobial concentration across four wells of the Biolog PM plate.

Table 1: MICs of *E. coli* BL21 (DE3) pTTQ18 (control) or pTTQ18 (ABUW_0700)

Drug	MIC (μg/mL) for cells transformed with		Drug category
	pTTQ18	pTTQ18 (ABUW_0700)	
Sulfadiazine	500	1000	Sulfonamides
Silver nitrate	3	6	Biocide
Acriflavine	9.38	18.75	Dye

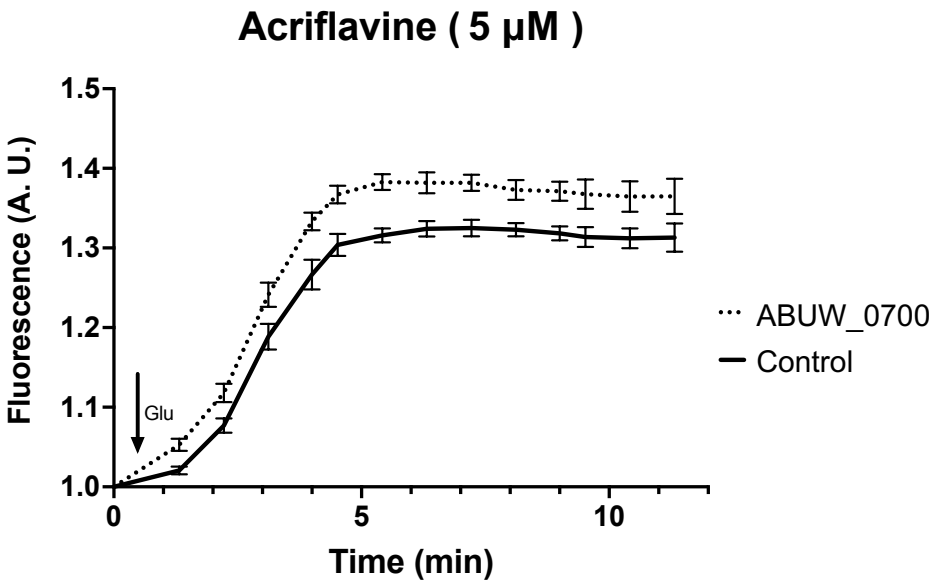

Figure 8: Acriflavine transport assay. Direct efflux of acriflavine associated ABUW_0700 expression in a triple efflux gene knockout mutant *E. coli* BW25113 (Δ*emrE*, Δ*acrB* and Δ*mdfA*::kan) (*dotted line*) compared to an empty vector control (*solid line*). Values are the means of three independent experiments and error bars are represented by the standard error of the mean. Statistical significance was determined using an unpaired t-test. Acriflavine efflux was found to be statistically significant between ABUW_0700 and control groups (p-value <0.05).

Supporting information

Table S1: FlaGs output of conserved flanking genes of ABUW_0700 homologs

Number	RefSeq Accession	Gene
1	NP_415483.2	methylglyoxal synthase
2	WP_005047455.1	DNA helicase IV
3	WP_011146055.1	TfoX/Sxy family DNA transformation protein
4	WP_002898408.1	porin OmpA
5	WP_024913558.1	cell division inhibitor SulA
6	WP_024132586.1	CoA-binding protein
7	WP_038269315.1	macrodomain Ter protein MatP
8	WP_006118670.1	YccF domain-containing protein
9	WP_048638491.1	Lon protease family protein
10	WP_004718942.1	heat shock protein HspQ
11	WP_048638490.1	Bifunctional3-hydroxydecanoyl-ACP dehydratase/ trans-2-decenoyl-ACP isomerase
12	WP_005654151.1	DUF2057 domain-containing protein
13	WP_011146063.1	acylphosphatase
14	WP_012987337.1	sulfurtransferase TusE
15	WP_004923900.1	MFS transporter
16	WP_006717573.1	metal ABC transporter permease
17	WP_023490460.1	23S rRNA (cytosine(1962)-C(5))-methyltransferase RlmI
18	WP_005179510.1	YcxB family protein
19	WP_003692100.1	PilT/PilU family type 4a pilus ATPase
20	WP_001047593.1	nitroreductase
21	WP_004678244.1	sulfite reductase flavoprotein subunit alpha
22	WP_025330027.1	DUF3304 domain-containing protein
23	WP_005008078.1	YdcF family protein
24	WP_016657636.1	ABC transporter ATP-binding protein
25	WP_000811534.1	patatin-like phospholipase family protein
26	WP_004678249.1	DUF2750 domain-containing protein
27	WP_004678228.1	alanine/glycine:cation symporter family protein
28	WP_016659325.1	sodium/glutamate symporter
29	WP_016657628.1	AI-2E family transporter
30	WP_004923912.1	ParA family protein
31	WP_004923917.1	hypothetical protein
32	WP_115723668.1	sugar transporter
33	WP_003690201.1	YggS family pyridoxal phosphate-dependent enzyme
34	WP_002243932.1	hypothetical protein
35	WP_003692093.1	GIY-YIG nuclease family protein
36	WP_002215267.1	RNA polymerase-binding protein DksA
37	WP_005694403.1	electron transport complex subunit RsxA
38	WP_005650033.1	electron transport complex subunit RsxB
39	WP_005753769.1	50S ribosomal protein L3 N(5)-glutamine methyltransferase
40	WP_005721623.1	endonuclease SmrB
41	WP_009485781.1	hypothetical protein
42	WP_010906619.1	porin

43	WP_011848606.1	patatin-like phospholipase family protein
44	WP_016657624.1	hypothetical protein
45	WP_016657626.1	hypothetical protein
46	WP_016659326.1	DcaP family trimeric outer membrane transporter
47	WP_021016829.1	NupC/NupG family nucleoside CNT transporter
48	WP_009875205.1	threonine synthase
49	WP_033111985.1	aldo/keto reductase
50	WP_002641665.1	rRNA pseudouridine synthase
51	WP_002641673.1	3-methyl-2-oxobutanoate hydroxymethyltransferase
52	WP_033111986.1	MdtA/MuxA family multidrug efflux RND transporter periplasmic adaptor subunit
53	WP_039104787.1	deoxyribonuclease IV
54	WP_005598741.1	DNA starvation/stationary phase protection protein
55	WP_045970052.1	hypothetical protein
56	WP_047761669.1	FKBP-type peptidyl-prolyl cis-trans isomerase
57	WP_067655516.1	hypothetical protein
58	WP_067655535.1	superoxide dismutase family protein
59	WP_067655513.1	phosphoglycerate dehydrogenase
60	WP_067662671.1	FAD-binding oxidoreductase
61	WP_164924999.1	IS3-like element IS600 family transposase
62	WP_225905354.1	pyrroline-5-carboxylate reductase

Transmembrane pore of ABUW_0700

Physico-chemical Properties

Length:	64.6	Bottleneck:	0.5
Hydropathy:	-0.31	Charge:	-2
Polarity:	12.44	Mutability:	90
LogP:	0.44	LogD:	0.14
LogS:	0.09	Ionizable:	4

3D view

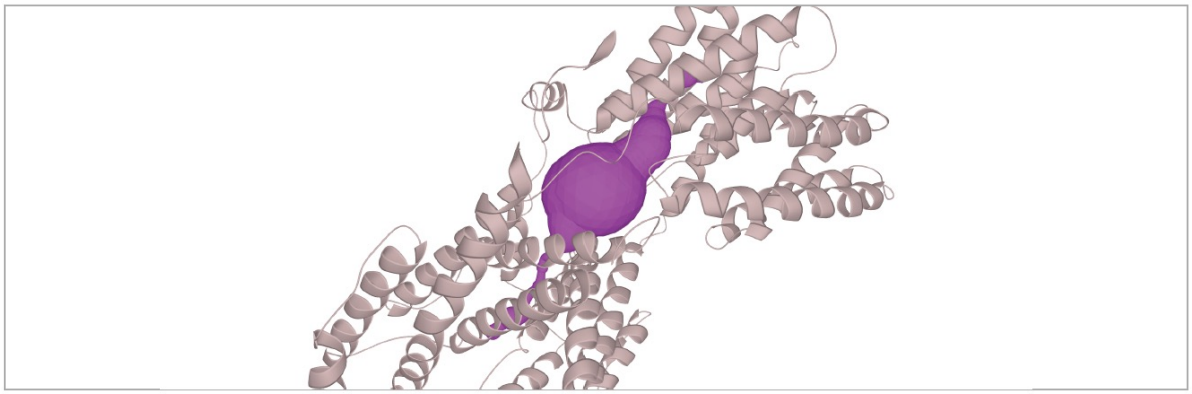

2D view

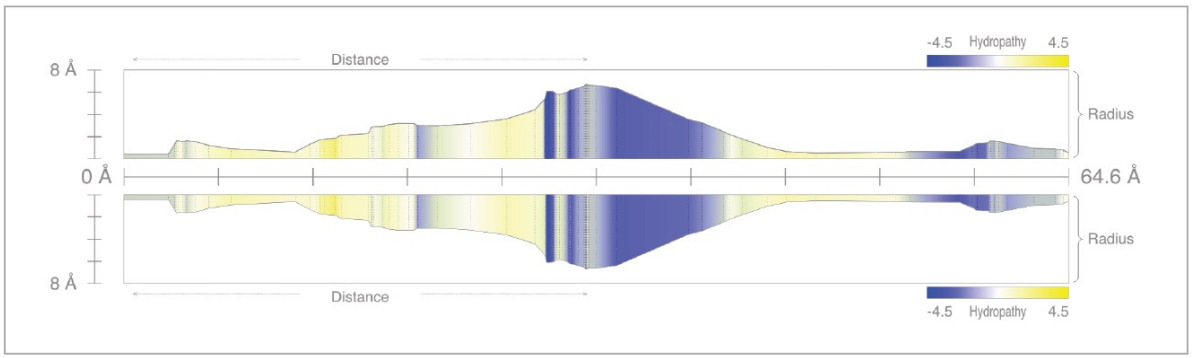

Figure S1: Predicted ABUW_0700 transmembrane pore region visualised in 3D, showing transmembrane cavity spanning cytoplasmic domain into the central cavity of the transmembrane domain of ABUW_0700. The 2D view reveals diameter and length of pore region in Angstroms. Mapped colours represent hydropathic (*yellow*) and hydrophilic (*blue*) respectively. The figure generated from MOLEonline (23).

Table S2: Residues lining ABUW_0700 putative pore

ABUW_0700 pore-lining residues		
THR47	SER93	HIS366
TRP72	ILE182	PRO402
ILE73	THR183	ASN403
GLY76	ASN186	HIS552
ARG80	HIS219	ASN553
ALA83	GLU220	ALA556
SER86	ASP223	GLU557
TYR87	SER224	SER560
CYS89	VAL362	ALA594
LEU90	LEU363	

Chapter 5: Characterisation of the *Acinetobacter baumannii* DUF817 protein as a multidrug resistance protein

Authors

Stephanie S. Nagy[1,2], Francesca L. Short[3], Liping Li[1,2], Bhumika S. Shah[1,2], Peter J. F. Henderson[4], Karl A. Hassan[5] and Ian T. Paulsen.[1,2*]

Author affiliations

[1]School of Natural Sciences, Faculty of Science and Engineering, Macquarie University, Sydney, NSW, Australia

[2]ARC Centre of Excellence in Synthetic Biology, Macquarie University, Sydney, NSW, Australia

[3]Department of Microbiology, Monash University, Melbourne, VIC, Australia

[4]School of Biomedical Sciences and Astbury Centre for Structural Biology, University of Leeds, Leeds, West Yorkshire, United Kingdom

[5]School of Environmental and Life Sciences, University of Newcastle, Newcastle, NSW, Australia.

Corresponding author: Distinguished Professor Ian T. Paulsen, ian.paulsen@mq.edu.au.

Abstract

The DUF817 family of proteins are unique to the bacterial kingdom, however their function within bacteria is unknown. In our recent work, the DUF817 protein ABUW_1191 from *Acinetobacter baumannii*, was found to promote fitness of this pathogen under silver nitrate challenge. Silver is membrane-active and is known to disrupt bacterial cell membranes and induce the prokaryotic oxidative stress response. Gram-negative resistance mechanisms against silver include expression of active efflux systems and down regulation of outer membrane proteins. This work sets out to investigate ABUW_1191 from a highly drug resistant, clinical isolate of *Acinetobacter baumannii*, AB5075_UW. Bioinformatic analysis revealed that the ABUW_1191 gene is conserved as part of the soft-core genome of *A. baumannii.* AlphaFold2 prediction of the structure of ABUW_1191 revealed an integral membrane protein comprised of eight transmembrane helices and five antiparallel β-sheets arranged in a novel protein fold. Heterologous expression of ABUW_1191 in *Escherichia coli* confers resistance to silver nitrate and a diverse range of therapeutics including clinically important β-lactams. Whole-cell fluorometric transport assays revealed increased acriflavine efflux activity in *E. coli* expressing ABUW_1191. Together, this data suggests provides a foundational characterisation of a previously uncharacterised class of integral membrane proteins characterized to exhibit antimicrobial resistance and efflux activity within bacteria.

Introduction

Domain of unknown function proteins, DUFs, are defined by the Pfam database as proteins of unknown function with no annotation or any level of experimental characterisation (1). As of 2021, 4435 Pfam families belonged to domain of unknown function or uncharacterized protein families, representing 23% of the Pfam database (1). The DUF817 protein family (PF05675) is a small family of DUF proteins (n = 916) unique to the bacterial kingdom that comprise of ~260 amino acids.

Silver is an ancient anti-infective agent that has pleiotropic mechanisms of antimicrobial activity against bacteria, which includes irreversible binding to thiol-groups of enzymes, disruption of iron homeostasis and cell membrane disruption and proton leakage, in addition to promotion of the prokaryotic oxidative stress response (2–4). In Gram-negative pathogens, silver resistance is commonly mediated by the upregulation of metal ion efflux pumps and down-regulation of non-specific outer-membrane porins (5, 6). *Acinetobacter baumannii* is a highly drug resistant and virulent opportunistic human pathogen that is a common cause of hospital-acquired infections in critically ill patients (7). In a recent TraDIS study to investigate the effects of biocide exposure we discovered that DUF817 family gene ABUW_1191 confers fitness against silver nitrate in *A. baumannii* (Chapter 2).

Although there is no direct evidence for the function of ABUW_1191 there is some clues to its function from high-throughput genomic studies. In *A. baumannii* AB5075_UW, a TraDIS study showed that ABUW_1191 was important for survival of the pathogen in heat-inactivated human serum, suggesting a possible role in virulence and bloodstream infections (8). A separate TraDIS study on *A. baumannii* AB0057 found that the ABUW_1191 ortholog AB57_2745 was identified as one of the top 25 fitness factors required for spleen infection in a mouse model of bacteraemia (9). Herein, we set out to perform the first experimental characterisation of a DUF817 family protein from *A. baumannii* AB5075_UW (ABUW_1191), following our TraDIS work (Chapter 2). In this study we use a combination of bioinformatics and resistance assays to experimentally

determine whether the DUF817 family may represent a novel family of multidrug resistant efflux pumps in bacteria.

Materials and methods

Bioinformatic analyses

All FASTA format sequences were downloaded from the National Centre for Biotechnology Information (NCBI). The coding region of ABUW_1191 was retrieved from the *A. baumannii* AB5075_UW genome (CP008706.1). Homologous sequences of ABUW_1191 were collected using the HMMER webserver (v. 2.41.2) against reference proteomes (10, 11). Full-length sequences with *E*-values $\leq 10^{-20}$ were deemed homologous. A multiple sequence alignment (MSA) of DUF817 homologues was performed using MUSCLE (12). The phylogenetic tree of DUF817 homologs was constructed using the neighbor-joining method with $n = 1000$ bootstrap replicates with default parameters using MEGAX software and was visualised with iTOL (13–17). The pan-genome of *A. baumannii* AB5075_UW was analysed from data from our previous publication (18) to investigate the conservation of ABUW_0700 and its genetic neighbourhood and was visualised using Clinker (19). *A. baumannii* genomes included in the pan-genome analysis comprise all complete genomes deposited to the NCBI assembly database as of March 26, 2020. Gene conservation analysis of ABUW_1191 homologs across more distantly related bacteria using the WebFLaGs server with default parameters (20).

In silico prediction of the structure of DUF817 protein, ABUW_1191

In silico predictions of the ABUW_1191 was performed using AlphaFold2 (21). AlphaFold2 models were run using ColabFold notebook with default parameters and MMseq2 generated sequence MSAs (22, 23). Ramachandran plots of the AlphaFold2 predicted structure were generated with PROCHECK (24). Amino acid conservation was mapped to the ABUW_1191 structure with ConSurf (25, 26). Predictions of the channel regions were visualised with MOLEonline (v. 1.5.2.1) (27). Structural homologs of ABUW_1191 were reviewed with DALI

(accessed on the 26th February, 2022) (28). All PDB files and figures were visualised and generated with Pymol (29).

Bacterial strains and plasmids

The coding region of ABUW_1191 from the AB5075_UW genome (CP008706.1) was chemically synthesised and cloned between the *EcoR*I and *Pst*I sites within the MCS for in-frame transcription with the endogenous *tac* promotor and C-terminal hexa-histidine tag ($RSGH_6$) of pTTQ18-$RSGH_6$ plasmid (30–32). Gene synthesis and cloning into the expression vector to yield pTTQ18-ABUW_1191_{RSGH6} was purchased from Genscript (Piscataway, USA). For heterologous expression of ABUW_1191 in *E. coli*, chemically competent *E. coli* BL21 (DE3) were purchased from Bioline, USA. *E. coli* BW25113 Δ*emrE*, Δ*mdfA* and Δ*acrB::kan* cells were used for acriflavine transport assays against an efflux sensitive background (33).

Preparation of chemically competent E. coli cells

Chemically competent cells of the *E. coli* triple efflux mutant were prepared according to the calcium wash method. Briefly, *E. coli* cells were grown to mid-exponential phase (OD_{600nm} = 0.4) and immediately incubated on ice for 30 minutes. Cells were harvested at 3000 × g for 15 minutes at 4°C and resuspended with ice-cold 100 mM $MgCl_2$ solution. Cell suspensions were pelleted at 2000 × g for 15 minutes at 4°C. Cell pellets were resuspended in ice-cold 100 mM $CaCl_2$ solution and chilled on ice for 20 minutes. Cell suspensions were pelleted at 2000 × g for 15 minutes at 4°C and resuspended in ice cold 85 mM $CaCl_2$ with 15% glycerol. Cell suspensions were pelleted at 1000 × g for 15 minutes and resuspended to a final OD_{600nm} = 200 in 2 mL of ice cold 85 mM $CaCl_2$ with 15% glycerol. Samples were snap-frozen in liquid nitrogen and stored at – 80°C for transformation.

Transformation of chemically competent *E. coli* cells.

Transformation of *E. coli* BL21 (DE3) or BW25113 (Δ*emrE*, Δ*mdfA* and Δ*acrB::kan)* with pTTQ18-$RSGH_6$ or pTTQ18-ABUW_1191_{RSGH6} was achieved using the heat shock method (34) with the following modifications. Briefly, 50 µL of chemically competent *E. coli* were thawed on

ice and incubated with 5 ng of plasmid DNA for 30 minutes, followed by heat-shock at 42°C for 40 seconds. *E. coli* samples were immediately transferred to ice to incubate for 2 minutes prior to recovery in S.O.C media (Thermo Fischer) for 1 hour at 37°C, 200 rpm. Recovered cell culture was plated on LB-agar supplemented with 100 μg/mL ampicillin for selection and incubated overnight at 37°C. Following transformation, all *E. coli* cultures harbouring pTTQ18-$RSGH_6$ (empty vector) or pTTQ18-$ABUW\_1191_{RSGH6}$ were prepared in LB-media supplemented with 100 μg/mL ampicillin and grown at 37°C, 200 rpm unless otherwise specified.

Small scale culture and expression analyses of ABUW_1191 in *E. coli*

Overnight cultures of *E. coli* BL21 (DE3) harbouring pTTQ18-$RSGH_6$ or pTTQ18-$ABUW\_1191_{RSGH6}$ were grown in 50 mL of Luria-Bertani (LB) broth (10 g/L NaCl, 10 g/L tryptone, 5 g/L yeast extract) supplemented with 100 μg/mL carbenicillin and 20 mM glycerol at 37°C, shaking at 200 rpm. Overnight cultures were diluted 1:100 in fresh LB media supplemented with 100 μg/mL carbenicillin and 20 mM glycerol and grown at 37°C, shaking at 200 rpm to a final OD_{600nm} = 0.8. Expression of ABUW_1191 was induced with IPTG (0.2 mM final concentration) for 3 hours. Cell cultures were harvested by centrifugation (12,000 × g) for 15 minutes at 4°C. *E. coli* mixed membranes were extracted according to the water-lysis spheroplast method as published (32). Briefly, cell pellets were resuspended in 10 mL 0.2 M Tris-HCl, pH 8.0 and gently mixed on rollers for 20 minutes at room temperature. At time zero, 4.85 mL of sucrose buffer (0.2 M Tris-HCl, pH 8.0, 1 M sucrose, 1 mM EDTA) was added. At 1.5 minutes, 65 μL of freshly prepared 10 mg/mL lysozyme solution was added. At 2 minutes, 9.6 mL MilliQ water was added, and the sample was gently mixed on rollers for 20 minutes. The spheroplasts were sedimented at 25,000 × g for 20 minutes, then resuspended in 15 mL MilliQ water and incubated at room temperature for 30 minutes. Mixed membranes were sedimented at 25,000 × g for 20 minutes, washed thrice with NaPi buffer (0.1 M disodium hydrogen phosphate, 0.1 M sodium dihydrogen phosphate, pH 7.2). Membrane pellets were resuspended in 500 μL of NaPi buffer, pH 7.2 containing 1 mM β-mercaptoethanol and were snap-frozen with liquid nitrogen and stored at –80°C prior to further SDS-PAGE and western blot

analyses. Total protein content was quantified using a Pierce™ BCA Protein Assay Kit (Thermo Scientific) (35). SDS-PAGE of mixed membrane samples followed the method published by Henderson and MacPherson (36). Heterologous expression of ABUW_1191 in mixed membranes of *E. coli* was detected by the western blotting using an anti-$RGSH_6$–horseradish peroxidase conjugate (Bio-Rad).

Antimicrobial sensitivity screening

Biolog phenotype microarrays (PMs) were used to explore the antimicrobial profile of ABUW_1191 against 240 unique antimicrobials using the bacterial chemical sensitivity panel (PM11-20) (37). A full list of antimicrobials tested is available (Appendix B). Biolog phenotype microarrays were performed as described (38). *E. coli* BL21 (DE3) harbouring pTTQ18-$RSGH_6$ or pTTQ18-ABUW_1191_{RSGH6} were streaked onto LB agar plates supplemented with 100 μg/mL ampicillin and grown overnight at 37°C. Individual colonies were streaked onto a fresh LB-ampicillin agar plate and grown overnight at 37°C. Colonies were collected and suspended in Biolog GN IF-0a solution to 85% transmittance, measured by a Biolog turbidimeter. Cell suspensions were diluted 1:200 in Biolog IF-10b solution and supplemented with 1:100 dilution of Biolog redox dye mix A. PM plates were inoculated with IPTG (0.05 mM final concentration) and inoculated with 100 μL of bacterial cell culture in each well across PM11-PM20. PM plates were sealed with Breathe-Easy® film (Diversified Biotech) to allow for gas exchange. Plates were incubated and imaged using a Biolog OmniLog instrument to measure colorimetric change at 37°C, with shaking for 72 hours.

Minimum inhibitory concentration assays

Minimum inhibitory concentration (MICs) assays according to the microbroth serial dilution method was performed as described with the following modifications (39). LB media was used for MICs, except for silver nitrate where LB media excluding sodium chloride was used throughout this assay to avoid precipitation of the silver salt. Briefly, fresh transformants of *E. coli* BL21 (DE3) harbouring pTTQ18-$RSGH_6$ or pTTQ18-ABUW_1191_{RSGH6} were grown in fresh media overnight supplemented with 100 μg/mL ampicillin. Overnight bacterial cultures were

diluted 1:100 in fresh media supplemented with ampicillin (100 μg/mL) for positive selection and grown to mid-exponential phase (OD_{600nm} = 0.6). Cells were further diluted in 1:100 in fresh media and inoculated into 96-well plate containing media supplemented with 0.05 mM and two-fold serial dilution of acriflavine or silver nitrate. Plates were sealed with Breathe-Easy® film (Diversified Biotech) and incubated at 37°C at 200 rpm for 24 hours before total growth was measured as absorbance at OD_{600nm} by PheraSTAR FSX instrument (BMG LabTech).

Fluorometric transport assays

Overnight cell cultures of *E. coli* BW25113 (Δ*emrE*, Δ*mdfA* and Δ*acrB::kan)* cells harbouring pTTQ18-$RSGH_6$ or pTTQ18-$ABUW\_1191_{RSGH6}$ were grown in LB media containing 100 μg/mL ampicillin at 37°C, 200 rpm shaking. Protein expression was induced at OD_{600nm} = 0.8 with 0.05 mM IPTG for 1 hour. Cells were washed thrice with HEPES buffer (20 mM HEPES-KOH pH 7.0, 145 mM NaCl, 5 mM KCl) and resuspended to a final OD_{600nm} = 3 in 1 mL of HEPES buffer. Cells were treated with 10 μM CCCP and 5 μM acriflavine and incubated at 37°C in the dark for 1 hour. Cells were washed thrice with HEPES buffer to remove excess dye and protonophore. Cell pellets were resuspended immediately prior to transport assay initiation. All transport assays were performed using a Biotek HT synergy multiplate reader with excitation and emission wavelengths of 450 nm and 510 nm respectively. Assays began with an initial read to adjust for autofluorescence, followed by the injection of 0.5% w/v glucose in HEPES buffer (final concentration) to initiate transport-mediated efflux of acriflavine out of the bacterial cells.

Results and discussion

ABUW_1191 is part of the soft-core genome of *A. baumannii*

Pan-genome analysis of *A. baumannii* indicated that ABUW_1191 is almost always present across *A. baumannii* genomes (*n* = 170/172), and thus is part of the soft-core genome of this species. Genomes that did not appear to host an ortholog includes *A. baumannii* strain KBN10P02143 (GCF_001514375.1), *A. baumannii* strain 15A5 (GCF_002082705.1) and *A. baumannii* SMC_Paed_Ab_BL01 (GCF_002843665.1). Local genetic neighbourhood analysis reveals

ABUW_1191 is almost always adjacent to uroporphyrinogen decarboxylase gene (*hemE*, ABUW_1190) and a gene encoding a domain of unknown function protein (DUF3015, ABUW_1192) (Figure 1). In the case of *A. baumannii* (GCF_002504145), this organisation is disrupted by an IS5 family transposon IS*Aba*27 insertion between *hemE* and DUF187 ortholog. Uroporphyrinogen decarboxylase is an enzyme important for the biosynthesis of tetrapyrroles (40). The enzyme specifically catalyses the decarboxylation of four acetate groups of uroporphyrinogen III to yield coproporphyrinogen III for heme biosynthesis (40). Analysis of conserved genes further downstream of ABUW_1191 (Figure 1), reveal the gene is almost always conserved nearby the acinetobactin biosynthesis gene cluster *basIJH* and a class C β-lactamase gene *ampC* (ABUW_1194). Acinetobactin is a major siderophore of *A. baumannii* important for iron scavenging and a major virulence factor (41). In other *Acinetobacter* species and *Alkanindiges hydrocarboniclasticus*, the ortholog of ABUW_1191 is similarly located adjacent to the uroporphyrinogen decarboxylase gene (Figure 2).

Phylogenetic analysis of the DUF817 family

The phylogenetic tree comprised of ABUW_1191 and homologs is presented in Figure 3. The phylogenetic tree is predominately comprised of members from the Proteobacteria, Firmicutes and Actinobacteria phyla. Overall, the phylogenetic tree divides into two main clusters, cluster 1 (families I-VII) and cluster 2 (families VIII-XIII). ABUW_1191 and its *Acinetobacter* orthologs forms their own deeply rooted group, classified as family IV within cluster 1. This family is almost exclusively comprised of *Acinetobacter* spp. proteins, except for members from *Serratia* sp. S1B and *Alkanindiges hydrocarboniclasticus* from the Gammaproteobacteria and *Pararhodobacter marinus* from the Alphaproteobacteria.

Overall, cluster 1 is mostly comprised of members from the Proteobacteria and Actinobacteria, largely from the *Micrococcales* order of the Actinobacteria and the *Hyphomicrobiales* and the *Rhodobacterales* orders within the Alphaproteobacteria. Cluster 2 is mostly comprised of proteins from the *Bacillales* order within the Firmicutes, the *Streptomycetales* order within the Actinobacteria and the *Burkholderiales* and the *Rhizobiales* from the Proteobacteria. The DUF817

family thus appears to be mostly found in soil and plant-associated bacteria, which is an intriguing observation that may provide clues to its physiological role(s).

In silico prediction structure of ABUW_1191 reveals a novel protein fold

Currently, there is no solved structure for a DUF817 family protein. AlphaFold2 predicts that ABUW_1191 forms a novel integral membrane protein fold topology. This structure consists of eight tightly packed transmembrane helices followed by a C-terminal β-sheet 'cap' comprising of five β-strands arranged in a single antiparallel β-sheet across the cytoplasmic based of the transmembrane helical bundle (Figure 4 and 5). AlphaFold2 provided lDDT analyses of confidence maps the transmembrane region and β-sheet region with very high confidence (>90%) (Figure 6). Ramachandran plot analysis confirms that 96.2% of residues are found in favoured regions, 2.9% were found in additional allowed regions and 0.8% were found in disallowed regions (Figure 6).

ABPS (Adaptive Poisson-Boltzmann Solver) electrostatic potential mapped to the putative ABUW_1191 structure revealed a largely hydrophobic transmembrane surface with highly polar cytoplasmic and periplasmic regions (Figure 5). ConSurf analyses revealed the internal transmembrane region is highly conserved, whereas the peripheral residues and cytoplasmic β-sheet cap are variable (Figure 5). Based both on visual inspection and estimations by MOLEonline, three distinct tunnel regions can be observed: two lateral tunnels in the hydrophobic transmembrane domain, and one tunnel towards the periplasmic face of ABUW_1191 (Figure 5). The vertical tunnel spans ~50 Å in length with a maximum radius of ~3 Å and is lined with five ionisable residues (Figure 5, Figure S1, Table S2). The two lateral tunnels are hydrophobic, with no ionizable residues and are estimated to be ~45 Å in length with a maximum radius of ~4 Å (Figure 5, Figure S2, Table S3) and ~57 Å in length with a maximum radius of ~4 Å (Figure 5, Figure S3, Table S4). DALI analyses did not match the predicted fold of ABUW_1191 to any known PDB structure. The orientation of the three tunnels in the predicted structure of ABUW_1191 makes it tempting to speculate that ABUW_1191 function is to transport a substrate from the lipid bilayer to the periplasm.

ABUW_1191 confers increased tolerance to a diverse range of antimicrobials in *E. coli*

To determine whether ABUW_1191 from *A. baumannii* confers a resistance phenotype, it was heterologously expressed as a His-tagged fusion in *E. coli.* The coding region of ABUW_1191 was chemically synthesised and cloned into the pTTQ18-RGH_6 expression vector and both pTTQ18-$RGSH_6$ and pTTQ18-ABUW_1191_{RGSH6} was transformed into *E. coli* BL21 (DE3) cells. Expression of the ABUW_1191 construct was confirmed by presence of a ~20 kDa band on SDS-PAGE and a western blot (Appendix C).

Biolog phenotype microarray analysis indicated that ABUW_1191 conferred increased respiration in the presence of a diverse range of antimicrobials, including aztreonam, cefmetazole, cefotaxime, streptomycin, dihydrostreptomycin, paromomycin, polymyxin B, tinidazole and DTAB. In addition to these therapeutics, ABUW_1191 also conferred increased respiration on potassium tellurite, sodium salicylate, dichlofluanid, tolyfluanid, caffeine, compound 48/80, FCCP, oxycarboxin and umbelliferone, suggesting ABUW_1191 confers increased tolerance to multiple drugs (Figure 7). Tolerance conferred to β-lactams conferred by ABUW_1191 implies a potential connection with the previous observation that ABUW_1191 is typically encoded nearby the *ampC* β-lactamase gene (Figure 1).

MIC analyses indicated that ABUW_1191 conferred log 2-fold increased MIC to silver nitrate, consistent with our previous TraDIS data (Table 1) see Chapter 2. MIC analysis also indicated that ABUW_1191 conferred log 2-fold increased MIC to acriflavine, an antimicrobial fluorophore and common substrate of drug efflux pumps (Table 1).

Fluorometric transport assay demonstrates efflux mediated by ABUW_1191

Fluorometric acriflavine transport assays were performed using *E. coli* BW25113 (Δ*emrE*, Δ*mdfA* and Δ*acrB::kan*) cells to monitor total acriflavine efflux in an efflux sensitive background. Expression of ABUW_1191 in efflux sensitive cells revealed an increase in total acriflavine efflux over time compared to cells harbouring an empty vector as a control (pTTQ18-$RSGH_6$) (Figure 8).

These results suggest that the antimicrobial resistance profile conferred by ABUW_1191 may be via an active efflux mechanism.

Conclusions

This study reports on the first attempt to characterise a gene of unknown function, ABUW_1191, from the DUF817 family of proteins of unknown function. Its conservation in the core genome of *A. baumannii* nearby siderophore biosynthesis cluster and heme synthesis gene, suggests ABUW_1191 is playing an important physiological role(s) in this opportunistic pathogen. The findings described herein, in conjunction with previous literature results, suggest that this protein plays an important role in virulence which could be explored as a putative, novel virulence factor for this pathogen. Biolog phenotype microarrays, MIC analysis and fluorescent transport assays provide support that ABUW_1191 may confer a multidrug resistance phenotype, possibly via an efflux mechanism. This is consistent with identification of this gene as a silver nitrate fitness factor for *A. baumannii* (see Chapter 2). The predicted structure of ABUW_1191 provides support for a novel transport structure including three putative channels that provide a possible route in transport within the predicted structure that might suggest possible selection of substrate from the inner membrane bilayer. Future studies will focus on the purification of the ABUW_1191 protein, including screening potential ligands by nano-DSF or nano-ITC and reconstitution of the protein in proteoliposomes, followed by structural analysis. Such physio-chemical characterization of ABUW_1191 should clarify the biochemical and physiological function of this protein.

References

1. J. Mistry, *et al.*, Pfam: The protein families database in 2021. *Nucleic Acids Res.* **49**, D412–D419 (2021).

2. S. Y. Liau, D. C. Read, W. J. Pugh, J. R. Furr, A. D. Russell, Interaction of silver nitrate with readily identifiable groups: relationship to the antibacterial action of silver ions. *Lett. Appl. Microbiol.* **25**, 279–283 (1997).

3. J. R. Morones-Ramirez, J. A. Winkler, C. S. Spina, J. J. Collins, Silver enhances antibiotic activity against Gram-negative bacteria. *Sci. Transl. Med.* **5**, 190ra81 (2013).

4. P. Dibrov, J. Dzioba, K. K. Gosink, C. C. Häse, Chemiosmotic mechanism of antimicrobial activity of Ag(+) in *Vibrio cholerae*. *Antimicrob. Agents Chemother.* **46**, 2668–2670 (2002).

5. A. Gupta, K. Matsui, J.-F. Lo, S. Silver, Molecular basis for resistance to silver cations in *Salmonella*. *Nat. Med.* **5**, 183–188 (1999).

6. X.-Z. Li, H. Nikaido, K. E. Williams, Silver-resistant mutants of *Escherichia coli* display active efflux of Ag+ and are deficient in porins. *J. Bacteriol.* **179**, 6127–6132 (1997).

7. A. Y. Peleg, H. Seifert, D. L. Paterson, *Acinetobacter baumannii*: Emergence of a successful pathogen. *Clin. Microbiol. Rev.* **21**, 538–582 (2008).

8. A. F. Sanchez-Larrayoz, *et al.*, Complexity of complement resistance factors expressed by *Acinetobacter baumannii* needed for survival in human serum. *J. Immunol.* **199**, 2803–2814 (2017).

9. S. Crépin, *et al.*, The lytic transglycosylase MltB connects membrane homeostasis and *in vivo* fitness of *Acinetobacter baumannii*. *Mol. Microbiol.* **109**, 745–762 (2018).

10. S. R. Eddy, Profile hidden Markov models. *Bioinformatics* **14**, 755–763 (1998).

11. S. C. Potter, *et al.*, HMMER web server: 2018 update. *Nucleic Acids Res.* **46**, W200–W204 (2018).

12. R. C. Edgar, MUSCLE: Multiple sequence alignment with high accuracy and high throughput. *Nucleic Acids Res.* **32**, 1792–1797 (2004).

13. N. Saitou, M. Nei, The neighbor-joining method: A new method for reconstructing phylogenetic trees. *Mol. Biol. Evol.* **4**, 406–425 (1987).

14. J. Felsenstein, Confidence limits on phylogenies: An approach using the bootstrap. *Evolution* **39**, 783–791 (1985).

15. E. Zuckerkandle, L. Pauling, Evolutionary divergence and convergence in proteins. *Evol. Genes Proteins*, 97–166 (1965).

16. S. Kumar, G. Stecher, M. Li, C. Knyaz, K. Tamura, MEGA X: Molecular evolutionary genetics analysis across computing platforms. *Mol. Biol. Evol.* **35**, 1547–1549 (2018).

17. I. Letunic, P. Bork, Interactive tree of life (iTOL) v5: An online tool for phylogenetic tree display and annotation. *Nucleic Acids Res.* **49**, W293-296 (2021).

18. F. L. Short, *et al.*, The *Acinetobacter baumannii* disinfectant resistance protein, AmvA, is a spermidine and spermine efflux pump. *Commun. Biol.* **4**, 1-12 (2021).

19. C. L. M. Gilchrist, Y.-H. Chooi, Clinker & clustermap.js: Automatic generation of gene cluster comparison figures. *Bioinformatics* **37**, 2473–2475 (2021).

20. C. K. Saha, R. S. Pires, H. Brolin, M. Delannoy, G. C. Atkinson, FlaGs and webFlaGs: Discovering novel biology through the analysis of gene neighbourhood conservation. *Bioinformatics* **37**, 1312–1314 (2021).

21. J. Jumper, *et al.*, Highly accurate protein structure prediction with AlphaFold. *Nature* **596,** 583-589 (2021).

22. M. Mirdita, *et al.*, ColabFold: making protein folding accessible to all. *Nat. Methods* **19**, 679–682 (2022).

23. M. Steinegger, J. Söding, MMseqs2 enables sensitive protein sequence searching for the analysis of massive data sets. *Nat. Biotechnol.* **35**, 1026–1028 (2017).

24. R. A. Laskowski, M. W. MacArthur, D. S. Moss, J. M. Thornton, PROCHECK: a program to check the stereochemical quality of protein structures. *J. Appl. Crystallogr.* **26**, 283–291 (1993).

25. M. Landau, *et al.*, ConSurf 2005: The projection of evolutionary conservation scores of residues on protein structures. *Nucleic Acids Res.* **33**, W299-302 (2005).

26. H. Ashkenazy, *et al.*, ConSurf 2016: An improved methodology to estimate and visualize evolutionary conservation in macromolecules. *Nucleic Acids Res.* **44**, W344–W350 (2016).

27. L. Pravda, *et al.*, MOLEonline: A web-based tool for analyzing channels, tunnels and pores (2018 update). *Nucleic Acids Res.* **46**, W368–W373 (2018).

28. L. Holm, DALI and the persistence of protein shape. *Protein Sci.* **29**, 128–140 (2020).

29. W. Delano, The PyMOL molecular graphics system. *CCP4 Newsl. Protein Crystallogr.* **40**, 82–92 (2002).

30. M. J. R. Stark, Multicopy expression vectors carrying the *lac* repressor gene for regulated high-level expression genes in *Escherichia coli*. *Gene* **51**, 255–267 (1987).

31. M. V. Dilworth, *et al.*, Microbial expression systems for membrane proteins. *Methods* **147**, 3–39 (2018).

32. A. Ward, *et al.*, "The amplified expression, identification, purification, assay and properties of hexahistidine-tagged bacterial membrane transport proteins" in *Membrane Transport - A Practical Approach*, S. A. Baldwin, Ed. (2000), pp. 141–166.

33. N. Tal, S. Schuldiner, A coordinated network of transporters with overlapping specificities provides a robust survival strategy. *Proc. Natl. Acad. Sci. U. S. A.* **106**, 9051–9056 (2009).

34. A. Froger, J. E. Hall, Transformation of plasmid DNA into *E. coli* using the heat shock method. *J. Vis. Exp.*, 253 (2007).

35. P. K. Smith, *et al.*, Measurement of protein using bicinchoninic acid. *Anal. Biochem.* **150**, 76–85 (1985).

36. P. J. F. Henderson, A. J. S. Macpherson, "Assay, genetics, proteins, and reconstitution of proton-linked galactose, arabinose, and xylose transport systems of *Escherichia coli*" in *Methods in Enzymology*, (1986), pp. 387–429.

37. B. R. Bochner, Global phenotypic characterization of bacteria. *FEMS Microbiol. Rev.* **33**, 191–205 (2009).

38. A. M. Mackie, K. A. Hassan, I. T. Paulsen, S. G. Tetu, "Biolog phenotype microarrays for phenotypic characterisation of microbial cells" in *Methods in Molecular Biology*, (2014), pp. 123–130.

39. I. Wiegand, K. Hilpert, R. E. W. W. Hancock, Agar and broth dilution methods to determine the minimal inhibitory concentration (MIC) of antimicrobial substances. *Nat. Protoc.* **3**, 163–175 (2008).

40. J. Fan, Q. Liu, Q. Hao, M. Teng, L. Niu, Crystal structure of uroporphyrinogen decarboxylase from *Bacillus subtilis*. *J. Bacteriol.* **189**, 3573–3580 (2007).

41. J. R. Sheldon, E. P. Skaar, *Acinetobacter baumannii* can use multiple siderophores for iron acquisition, but only acinetobactin is required for virulence. *PLoS Pathog.* **16**, e1008995 (2020).

42. X. Robert, P. Gouet, Deciphering key features in protein structures with the new ENDscript server. *Nucleic Acids Res.* **42**, W320–W324 (2014).

43. V. Mariani, M. Biasini, A. Barbato, T. Schwede, lDDT: A local superposition-free score for comparing protein structures and models using distance difference tests. *Bioinformatics* **29**, 2722–2728 (2013).

Figures and tables

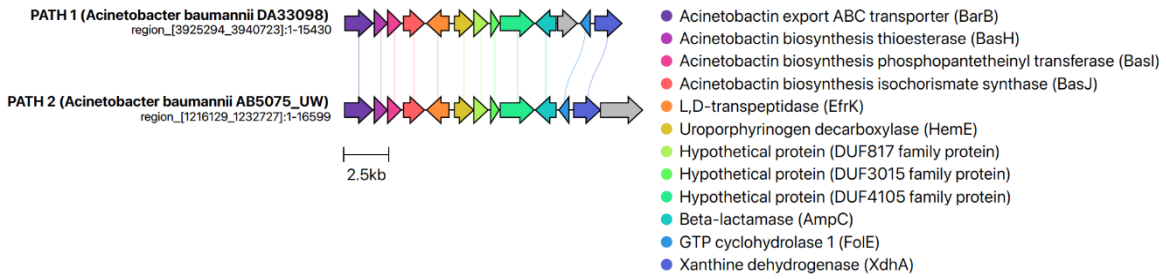

Figure 1: Visualization of the genomic context of DUF817 protein across *A. baumannii* genomes (*n* = 172). DUF817 is conserved as part of the soft-core genome (*n* = 170/172) with high-level of synteny. The top two alternate pathways are numbered 1 and 2 respectively. Path 1 (number of genomes = 50/170) is represented by *A. baumannii* DA33098. Path 2 (number of genomes = 25/170) is represented by *A. baumannii* AB5075_UW. *Coloured* genes are conserved genes with 100% identity across genomes. *Grey* genes represent unique genes across pathways. Gene conservation was visualised with Clinker (19) and annotated in Illustrator.

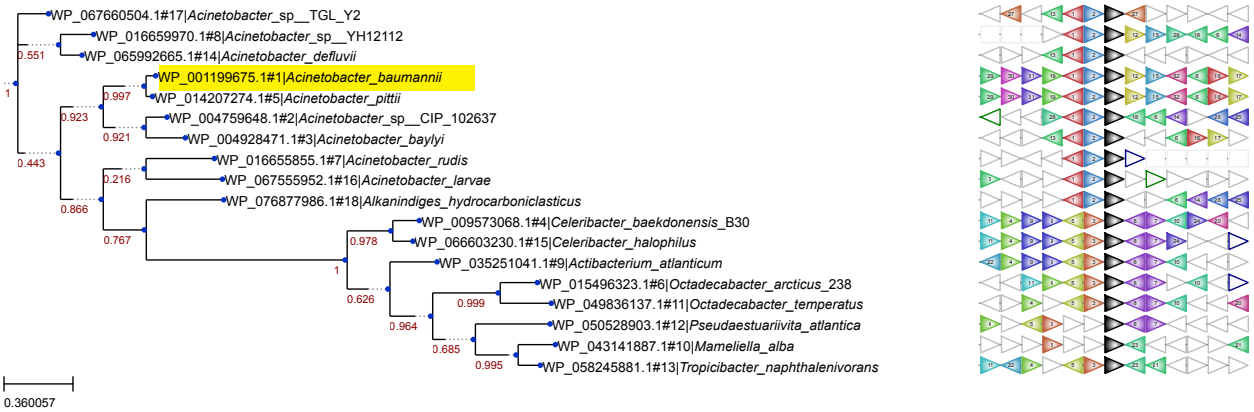

Figure 2: Visualisation of the genomic context of DUF817 (*black*) across distant RefSeq homologs from family IV and V from the phylogenetic tree. Genes that are present in two or more regions are colored and numbered (Table S1). Non conserved genes are blank. *Purple* and *green* outlined genes are pseudogenes and RNA genes respectively. Branch values are provided in bootstrap support values. Figure generated by WebFLaGs (20).

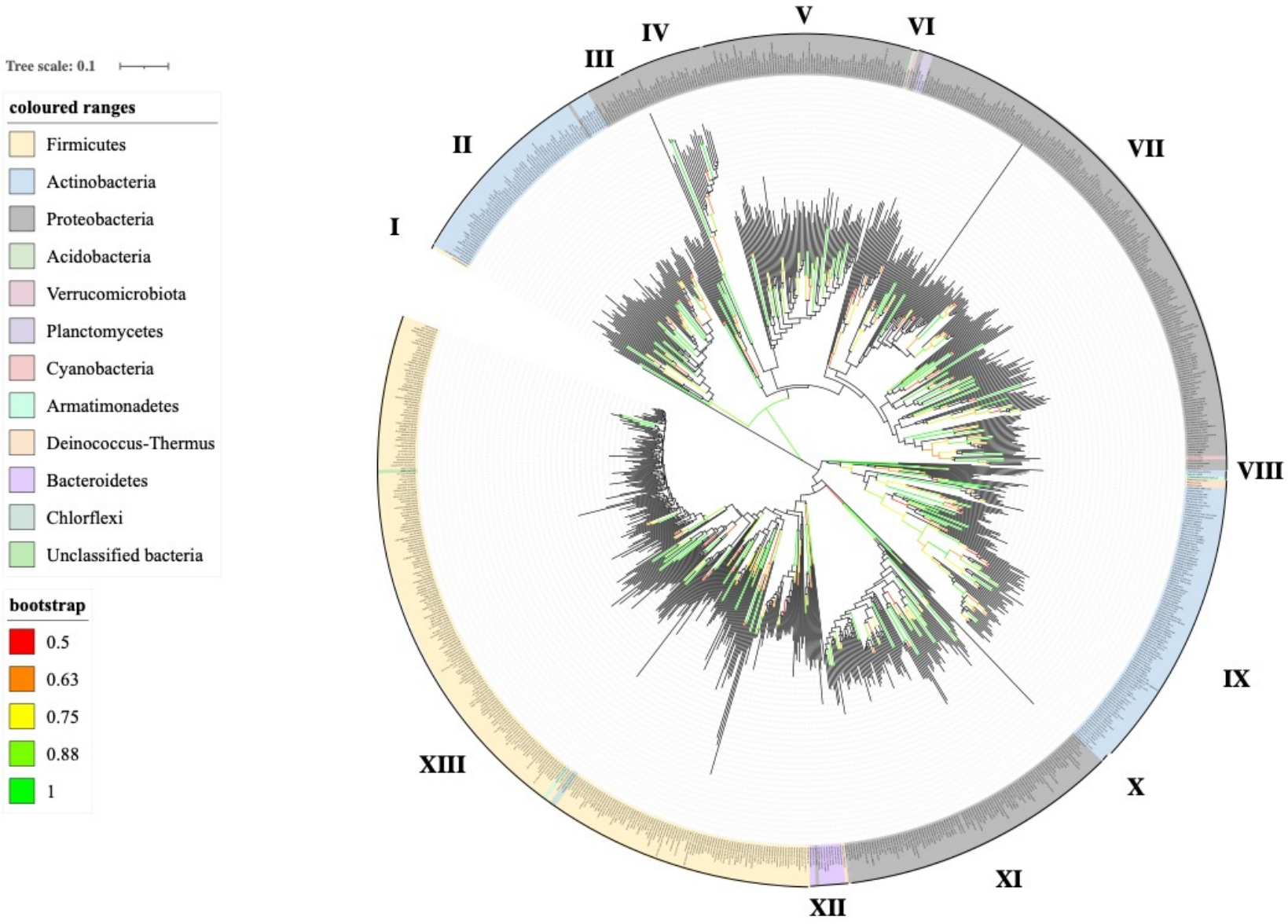
Tree scale: 0.1
coloured ranges
Firmicutes
Actinobacteria
Proteobacteria
Acidobacteria
Verrucomicrobiota
Planctomycetes
Cyanobacteria
Armatimonadetes
Deinococcus-Thermus
Bacteroidetes
Chlorflexi
Unclassified bacteria
bootstrap
0.5
0.63
0.75
0.88
1
I
II
III
IV
V
VI
VII
VIII
IX
X
XI
XII
XIII

Figure 3: Phylogenetic tree of DUF817 family. The phylogenetic tree was constructed by the neighbour-joining method across (n = 880) ABUW_1191 homologous sequences with E-values ≤ 10^{-20}. The phylogenetic tree was constructed in MEGAX and visualised in iTOL (13–17). Branches were drawn to scale where branch lengths represent the number of substitutions per site. The tree is colourised according to taxonomic phylum. Bootstrap values of at least n = 1000 iterations ≤0.5 are represented as coloured branches from *red* to *green* (0.5-1.0), respectively.

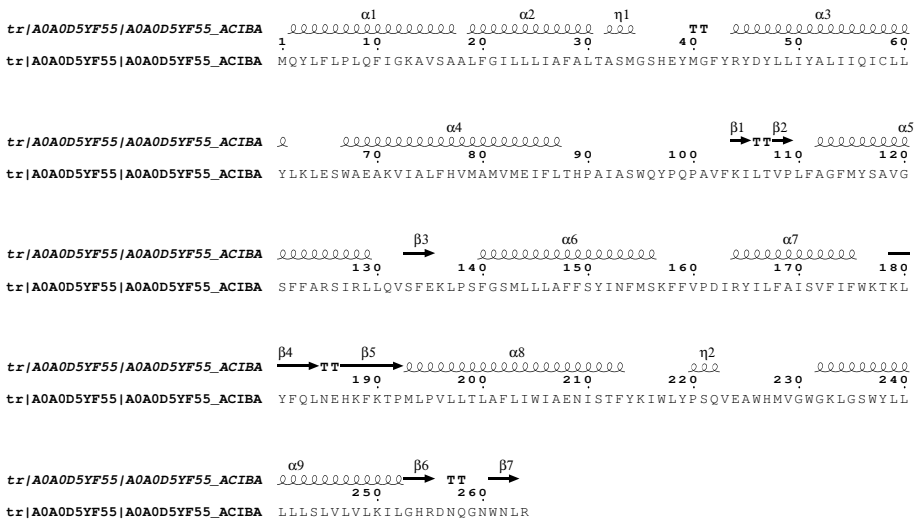

Figure 4: Sequence alignment with predicted secondary structure features from AlphaFold2 structures of ABUW_1191 revealing the presence of nine α-helices (α), five β-strands (β), and two 310-helices (η) present in ABUW_1191. Figure prepared with ESPript webserver (42).

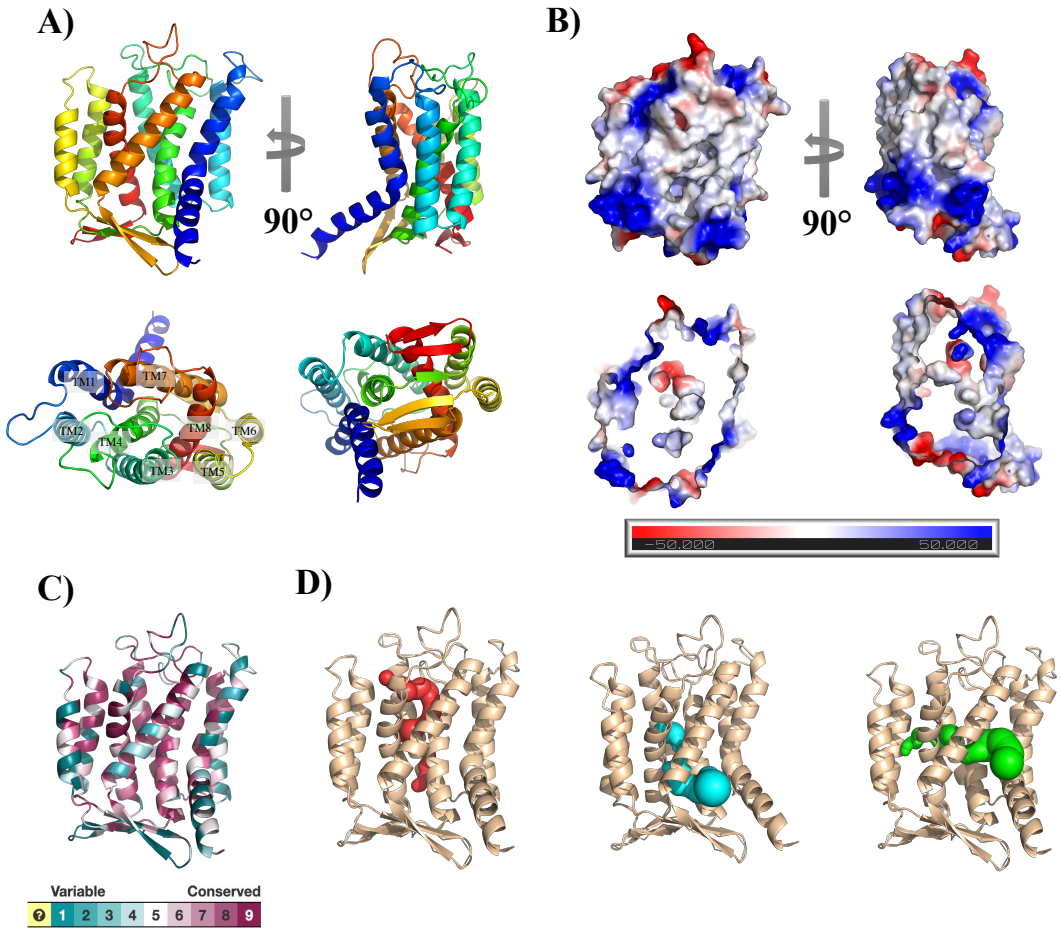

Figure 5: AlphaFold2 prediction of the ABUW_1191 A) Rainbow representation of ABUW_1191 from front-facing profile and side-facing profile reveals a single ABUW_1191 protomer comprised small eight transmembrane helices including N-terminal kinked helix. Top-down view revealing transmembrane pore region central to eight transmembrane helices. Bottom-up view revealing the presence of a five-member antiparallel β-sheet that caps the transmembrane protein at the cytoplasmic face. B) APBS electrostatics view of the distribution of charge on the surface and within the ABUW_1191 structure. C) ConSurf analysis of ABUW_1191 coloured by conservation from variable (*cyan*) to conserved (*magenta*) (25, 26). D) MOLEonline estimation of ~50 Å long transmembrane channel (*red*) and hydrophobic lateral tunnels ~56 Å (*blue*) and ~45 Å (*green*) in length respectively (27). All figures were visualised in Pymol (29).

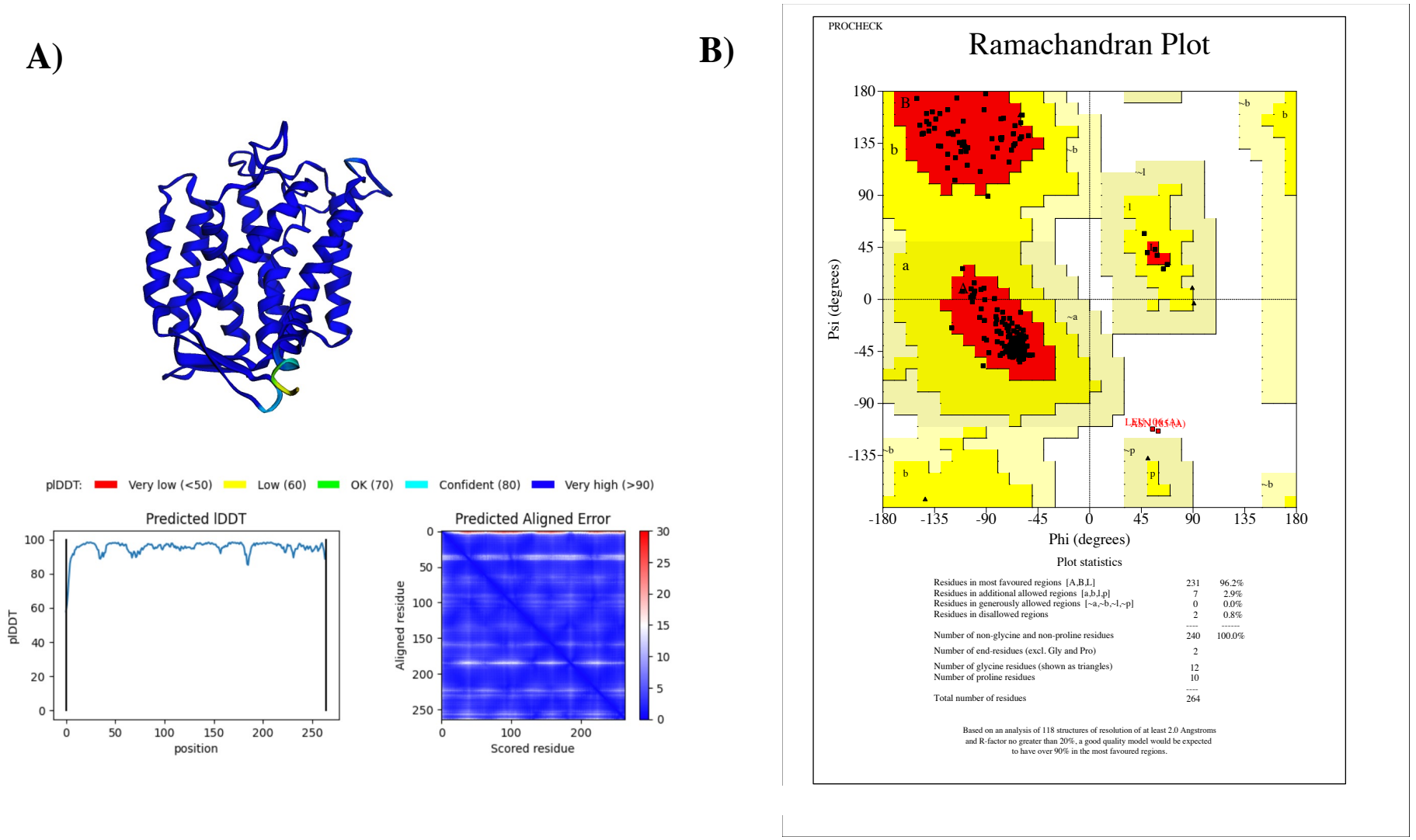

Figure 6: Assessment of ABUW_1191 model quality. **A)** lDDT confidence analysis of ABUW_1191 generated by AlphaFold2 (21, 43).

B) ABUW_1191 Ramachandran plot generated PROCHECK for the assessment of model quality (24)

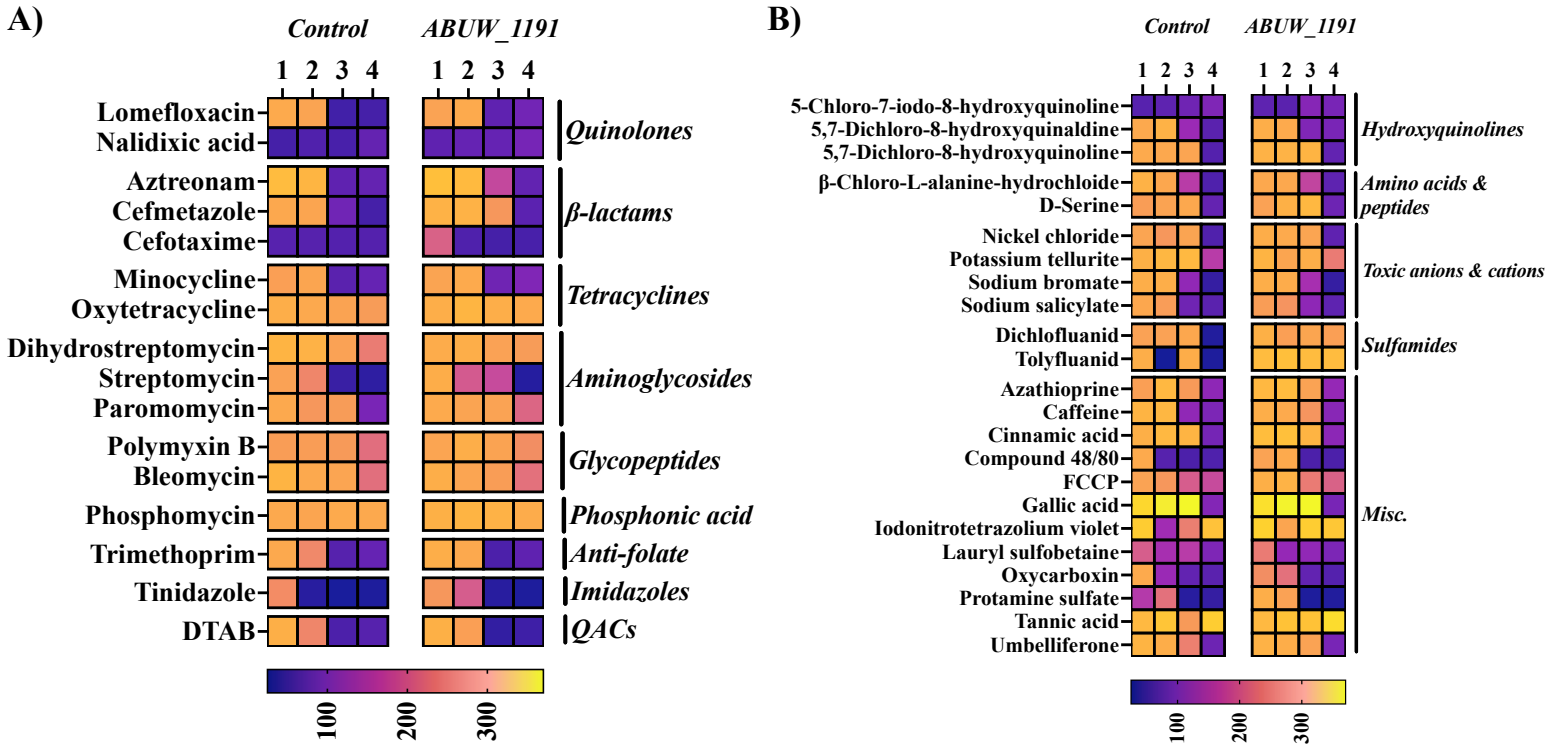

Figure 7: Resistance profile of ABUW_1191. Antimicrobial resistance phenotypes determined from the expression of ABUW_1191 in *E. coli* BL21 cells. Results are displayed as a heatmap using a colored scale from no growth (*dark blue*) to maximum growth (*yellow*). Biolog phenotypes are represented in two heatmap panels. A) antimicrobials and B) toxic bioactive compounds. Phenotypes are organized according to antimicrobial class. Columns represent log 2-fold increase in antimicrobial concentration across four wells of the Biolog PM.

Table 1: MICs of *E. coli* BL21 (DE3) pTTQ18 (control) or pTTQ18 (ABUW_1191)

Drug	MIC (μg/mL) for cells transformed with		Drug category
	pTTQ18	pTTQ18 (ABUW_1191)	
Silver nitrate	3	6	Biocide
Acriflavine	9.38	18.75	Dye

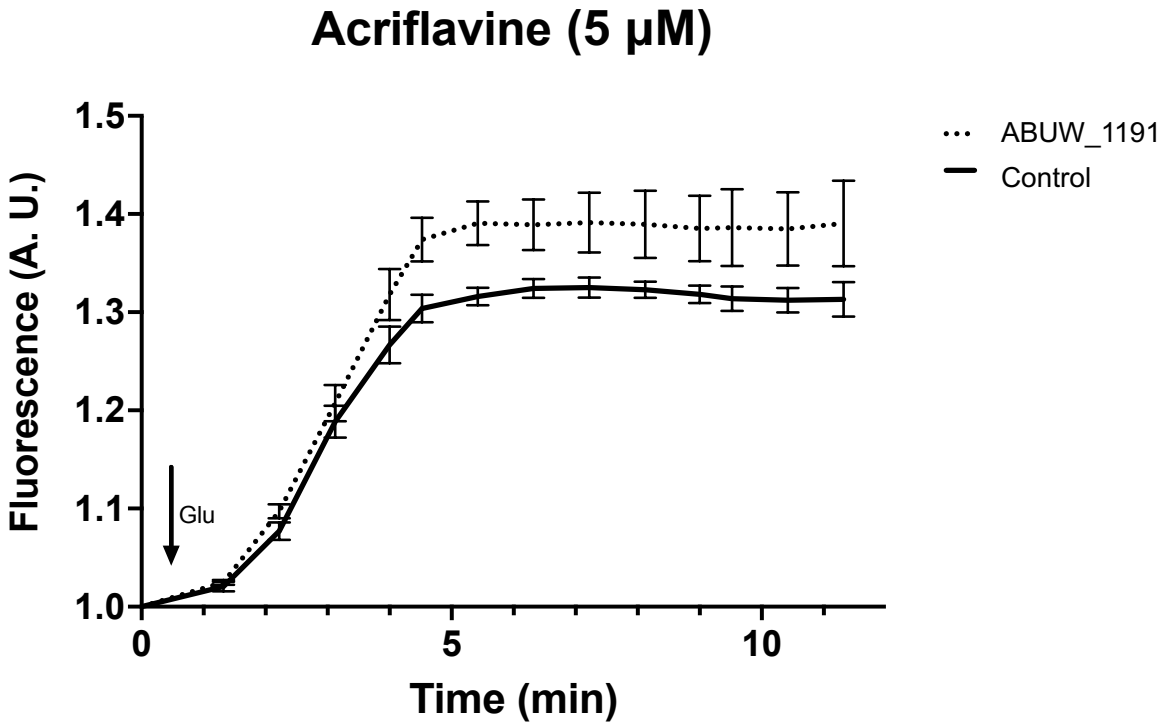

Figure 8: Acriflavine transport assay. Direct efflux of acriflavine associated with ABUW_1191 expression in *E. coli* BW25113 (Δ*emrE*, Δ*mdfA* and Δ*acrB::kan*) cells. Acriflavine loaded cells after one hour of incubation in the presence of CCCP were measured to determine difference in efflux rate of acriflavine between IPTG induced *E. coli* BW25113 (Δ*emrE*, Δ*mdfA* and Δ*acrB::kan*) expressing pTTQ18-ABUW_1191$_{RSGH6}$ (*dotted line*) verses an pTTQ18-RSGH$_6$ empty vector control (*solid line*). Black arrow depicts point of injection of 0.5% v/v glucose (final concentration) to initiate active efflux of acriflavine. Values are a means of three independent experiments and error bars are represented by the standard error of the mean. Statistical

significance was determined using an unpaired t-test. Acriflavine efflux was found to be statistically significant between ABUW_1191 and control groups (p-value <0.05).

Supporting information

Table S1: FlaGs output of conserved genes of RefSeq homologs ABUW_1191

Number	RefSeq Accession	Gene
1	WP_004928477.1	L,D-transpeptidase
2	WP_067660507.1	uroporphyrinogen decarboxylase
3	WP_066603232.1	serine hydroxymethyltransferase
4	WP_035250835.1	propionate-CoA ligase PrpE
5	WP_082176073.1	NAD kinase
6	WP_206541105.1	GTP cyclohydrolase I FolE
7	WP_044037149.1	alpha/beta fold hydrolase
8	WP_139222460.1	hypothetical protein
9	WP_009573072.1	response regulator
10	WP_035250829.1	hypothetical protein
11	WP_058245887.1	NADP-dependent malic enzyme
12	WP_000914200.1	DUF3015 family protein
13	WP_067660513.1	pirin-like bicupin family protein
14	WP_076877982.1	Smr/MutS family protein
15	WP_233733243.1	DUF4105 domain-containing protein
16	WP_233733247.1	xanthine dehydrogenase small subunit
17	WP_001076804.1	xanthine dehydrogenase molybdopterin binding subunit
18	WP_005176472.1	cupin domain-containing protein
19	WP_000983829.1	acinetobactin biosynthesis isochorismate synthase BasJ
20	WP_009573063.1	translation elongation factor 4
21	WP_043141875.1	aldo/keto reductase
22	WP_058245886.1	hypothetical protein
23	WP_058246404.1	DMT family transporter
24	WP_066603216.1	entericidin A/B family lipoprotein
25	WP_076877981.1	anthranilate phosphoribosyltransferase
26	WP_004759654.1	indole-3-glycerol phosphate synthase TrpC
27	WP_081405971.1	IS5 family transposase
28	WP_180047200.1	diguanylate cyclase
29	WP_233733223.1	ATP-binding cassette domain-containing protein
30	WP_233733224.1	alpha/beta fold hydrolase
31	WP_233733231.1	4'-phosphopantetheinyl transferase superfamily protein
32	WP_001211238.1	class C extended-spectrum β-lactamase ADC-26

Channel 1

Physico-chemical Properties

Length:	49.9	Bottleneck:	1.1
Hydropathy:	0	Charge:	1
Polarity:	7.5	Mutability:	71
LogP:	1.38	LogD:	1.06
LogS:	-0.7	Ionizable:	5

3D view

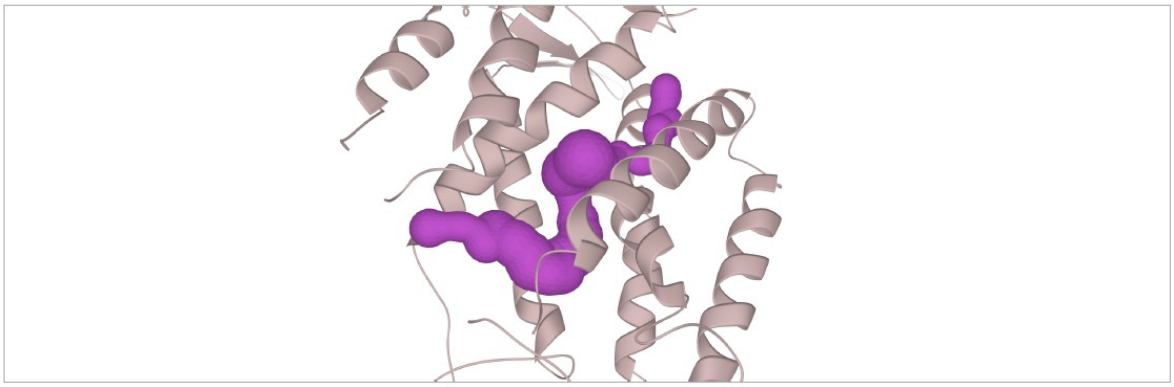

2D view

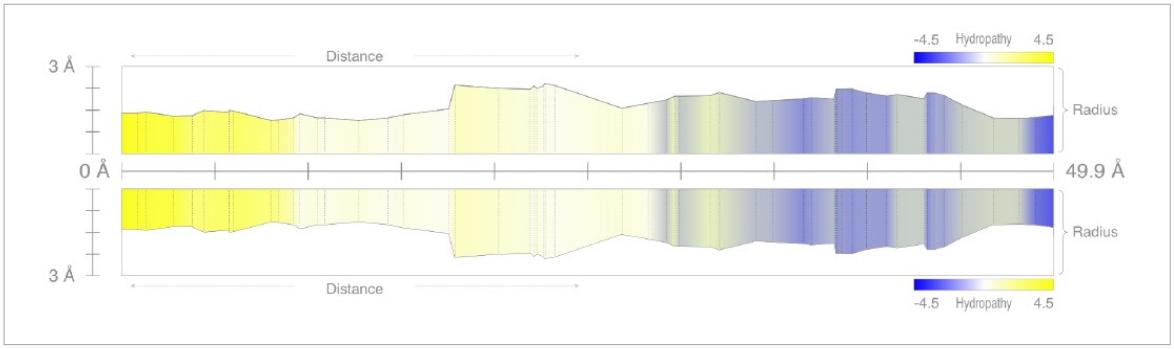

Figure S1: ABUW_1191 putative transmembrane channel 1, properties calculated by MOLE online (27). 3D visualisation of ABUW_1191 model in LiteMol showing transmembrane cavity spanning cytoplasmic domain towards periplasmic domain in ABUW_1191. 2D view reveals diameter and length of pore region in Angstroms. Mapped colours represent hydropathic (*yellow*) and hydrophilic (*blue*) residues respectively. Figure generated from MOLEonline report.

Table S2: Residues lining ABUW_1191 putative channel 1

Pore-lining residues		
VAL72	PHE154	SER244
ILE73	LYS157	VAL248
PHE76	ARG164	LEU252
GLU84	GLU208	
TRP95	TRP217	
MET115	TYR219	
TYR116	LYS233	
SER117	SER236	
VAL119	TRP237	
GLY120	LEU240	
ALA124	LEU243	

Channel 2

Physico-chemical Properties

Length:	44.7	Bottleneck:	0.9
Hydropathy:	2.02	Charge:	0
Polarity:	1.09	Mutability:	74
LogP:	1.21	LogD:	1.21
LogS:	-0.77	Ionizable:	0

3D view

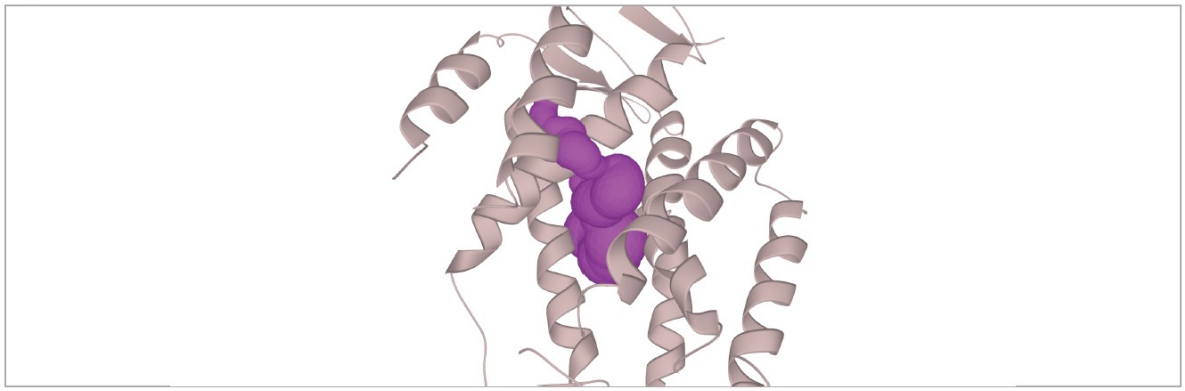

2D view

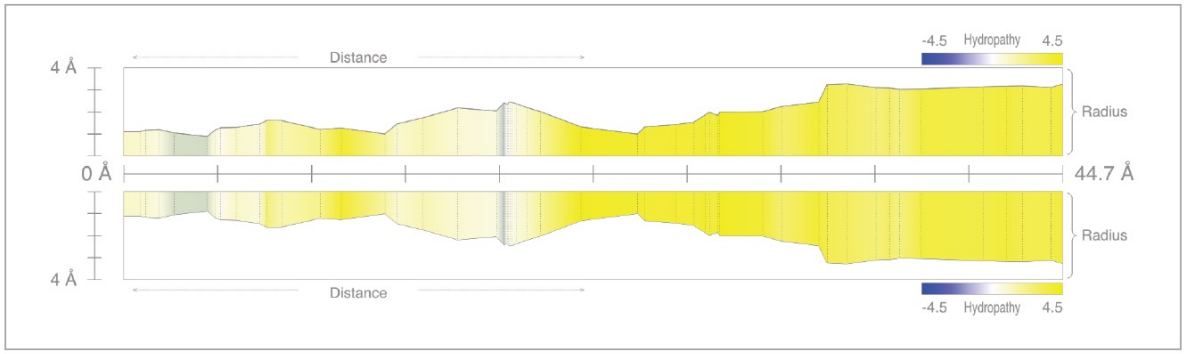

Figure S2: ABUW_1191 putative transmembrane channel 2, properties calculated by MOLEonline (27). 3D visualisation of ABUW_1191 model in LiteMol showing transmembrane cavity spanning the lateral width in ABUW_1191. 2D view reveals diameter and hydrophobic nature of this channel, with length of pore region measured in Angstroms. Mapped colours represent hydropathic (*yellow*) and hydrophilic (*blue*) residues respectively. Figure generated from MOLEonline report.

Table S3: Residues lining ABUW_1191 putative channel 2

Pore-lining residues of channel 2		
ILE11	LEU146	LEU242
ALA14	ALA147	LEU243
VAL15	SER150	LEU243
ALA18	TYR151	SER244
ILE22	LEU200	
LEU25	LEU203	
PHE76	ILE204	
TYR116	ALA207	
VAL119	TRP237	
PHE122	LEU239	
PHE123	LEU240	

Channel 3

Physico-chemical Properties

Length:	56.8	Bottleneck:	1
Hydropathy:	2.26	Charge:	0
Polarity:	0.96	Mutability:	73
LogP:	1.38	LogD:	1.38
LogS:	-0.97	Ionizable:	0

3D view

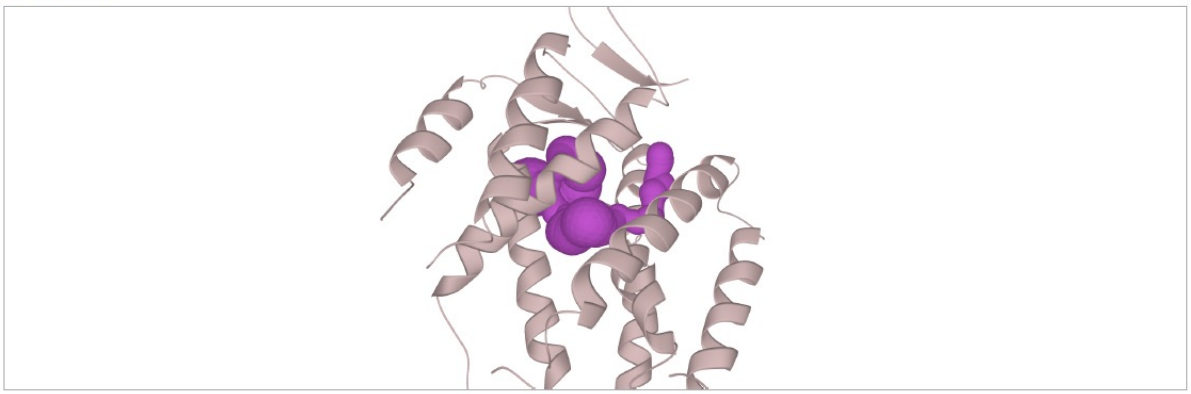

2D view

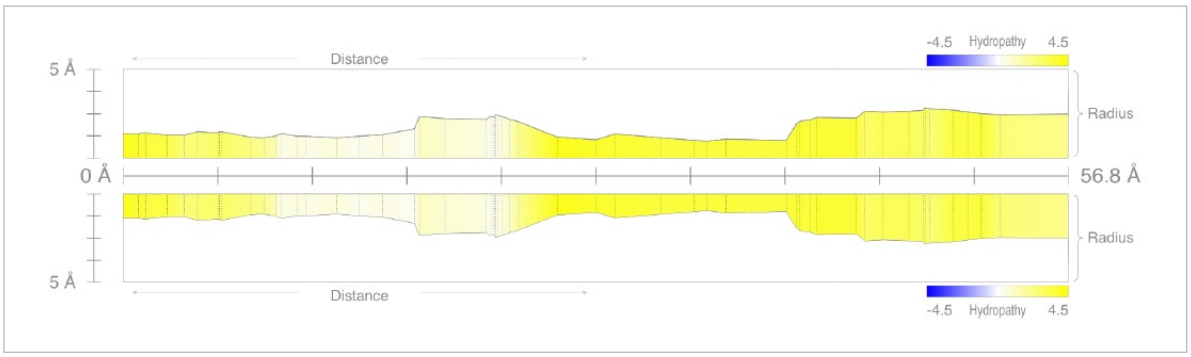

Figure S3: ABUW_1191 putative transmembrane channel 3, properties calculated by MOLEonline (27). 3D visualisation of ABUW_1191 model in LiteMol showing the additional hydrophobic lateral channel spanning the width in ABUW_1191. 2D view reveals diameter and hydrophobic nature of this channel, with length of pore region measured in Angstroms. Mapped colours represent hydropathic (*yellow*) and hydrophilic (*blue*) residues, respectively. Figure generated from MOLEonline report.

Table S4: Residues lining ABUW_1191 putative channel 3.

Pore-lining residues of channel 3		
PHE10	SER126	TRP237
VAL72	LEU130	LEU240
ILE73	VAL132	LEU241
PHE76	PHE134	LEU243
TYR116	LEU180	SER244
SER117	THR191	LEU245
VAL119	VAL196	VAL248
GLY120	LEU197	LEU252
PHE122	THR199	
PHE123	LEU200	
ALA124	ILE204	

Chapter 6: A tool for the direct visualisation of rapid drug efflux out of individual bacterial cells

Authors

Stephanie S. Nagy[1,2], Joris M.H. Goudsmits[3,4], Sophia C. Goodchild[1], Karl A. Hassan[5], Antoine M. van Oijen[4,6], Andrew Robinson[4,6] and Ian T. Paulsen.[1,2*]

Author affiliations

[1]School of Natural Sciences, Faculty of Science and Engineering, Macquarie University, Sydney, NSW, Australia

[2]ARC Centre of Excellence in Synthetic Biology, Macquarie University, Sydney, NSW, Australia

[3]School of Mathematical and Physical Sciences, University of Technology Sydney, Sydney, NSW, Australia

[4]Molecular Horizons Institute and School of Chemistry and Molecular Bioscience, University of Wollongong, Wollongong, NSW, Australia.

[5]School of Environmental and Life Sciences, University of Newcastle, Newcastle, NSW, Australia.

[6]Illawarra Health and Medical Research Institute, Wollongong, NSW, Australia.

***Corresponding author:** Distinguished Professor Ian T. Paulsen, ian.paulsen@mq.edu.au

Abstract

Multidrug efflux systems are integral membrane proteins that can rapidly export noxious compounds out of the cell and are a key mechanism of intrinsic and adaptive resistance to survive antimicrobial challenge. Isogenic bacterial populations will have different numbers of efflux pump expression due to stochastic variations in gene expression, which can promote differential levels of resistance within a population. Bacterial drug efflux pumps are typically studied in at the population level, where the population average may obscure differences between subpopulations within these bacterial communities. In this work, a combination of microfluidics and single-cell epifluorescence microscopy allowed for the design and construction of a microfluidic chip to observe direct efflux out of bacterial cells in real-time. Herein, we demonstrate that this technique is suitable to observe differential rates of drug efflux within a wild type population of *Escherichia coli*, where distinct sub-populations are observed with differential fast, medium, and slow efflux rates. At submicromolar concentrations of rhodamine 6G (R6G), single-molecule resolution of R6G export was visualised and found undergo different transition states across a population of cells. This work provides proof-of-concept for a microfluidic chip approach that enables the study of efflux pumps at the single-cell level, enabling subtleties in efflux pump expression, function, and efflux rate across an isogenic population to be unmasked.

Introduction

Antimicrobial resistance (AMR) is a significant threat to modern medicine, where deaths due to antimicrobial resistant infections is expected to rise to 10 million deaths globally by 2050 (1). AMR bacterial pathogens have acquired and express a diverse range of different mechanisms to confer resistance to antibiotics. These resistance mechanisms can be classed into four main categories, including: i) drug inactivation, ii) target modification, iii) reduced permeability, and iv) increased efflux v) metabolic bypass, and vi) target protection (2). Multidrug efflux pumps are polyspecific in nature and can recognise and transport a range of unrelated antimicrobial classes to confer antimicrobial resistance. Multidrug efflux pumps can also provide intrinsic or adaptive resistance to allow the cell to survive and develop high-level resistance under antimicrobial challenge (3–5). Natural variations in gene expression arising from mRNA transcription and protein translation can lead to remarkably different efflux phenotypes within an isogenic bacterial population and, hence, promote survival under rapidly changing and harsh conditions due to a bet hedging mechanism (6–8). Therefore, differential expression of a drug efflux pump(s) across an isogenic bacterial population can lead to different antimicrobial efflux rates and subsequently different drug resistance phenotypes between cells in an isogenic population (9).

Conventionally, drug efflux function has been studied at the population-level, thus masking the presence of any hetergeneous efflux sub-populations (10, 11). Therefore, population methods may not accurately report the efflux dynamics of the multidrug efflux pump of interest. Advances in single-cell technologies have allowed researchers to start probing individual cell-to-cell phenotypes related to antimicrobial resistance, including drug efflux pumps. A swathe of techniques have been developed for this purpose, including the use of flow cytometry and single-cell microfluidics which are typically used to measure relative drug accumulation as a proxy for differences in drug efflux between individual cells (12–15). To the best of our knowledge, a single-cell technique to directly visualise and quantify heterogeneous drug efflux rates as a measure of real-time, direct antimicrobial export out of individual cells has not been developed.

In this study, we designed a microfluidic chip to measure drug efflux rates for individual cells in real-time, and ask the question; can we quantify heterogeneous efflux rates across an isogenic population of cells? We validated our microfluidic chip by studying the efflux rate distribution of a wild type population of *Escherichia coli* BW25113 cells, the isogenic parent of the KEIO collection (16). This study provides a proof-of-concept that will pave the way for development of direct, quantitative evaluations of efflux rates within isogenic populations utilising microfluidics.

Materials and methods

Microfluidic chip design

The microfluidic chip design utilises a PDMS-based chip that is cheap, porous, non-fluorescent and biocompatible (17). The schematic and dimensions of the microfluidic chip are provided in Figure 1. Briefly, the microfluidic chip is approximately 50 μm thick, and is comprised of a main channel, 18 mm in length that is connected to 9 side channels, 1 mm (l) × 4 mm (w), comprised of one independent side channel (s0) and eight side channels (s1-8) that connect to a reverse flow chamber via a serpentine channel (Figure 1). The serpentine channel and reverse flow chamber allow for hydrostatic pressure-driven reverse flow, to separate buffer in the main channel from the side channels which harbour the dye-loaded cells. This allows for control over the start of each independent transport assay across the eight side channels. The main channel connects to a syringe pump and all nine side channels (s0-8) connect to a secondary syringe pump via a bidirectional 11-port microfluidic valve (M-SWITCH™, Fluigent) for independent flow control across each channel. The reverse flow chamber connects to an external buffer reservoir. The perimeter of the microfluidic chip connects to a vacuum line to prevent any air bubbles generating during the transport assay. The microfluidic chip was fabricated with polydimethylsiloxane (PDMS, Sylgard® 184, Sigma-Aldrich) by replicate mould on a SU-8 photoresist master wafer.

SU-8 master wafer fabrication

The SU8 master wafer was prepared as follows. First, a silicon wafer was cleaned by washing in isopropanol and baked at 150°C for 15 minutes to remove excess moisture. A base layer ~2 μm thick was prepared with SU-8 2002 (MicroChem) by spreading the photoresist with a spin-coater set to 500 rpm at 100 rpm/second for 10 seconds, followed by spinning at 2000 rpm set to 200 rpm/second for a total of 40 seconds. The wafer was placed on a hot plate set to 65°C for 5 minutes, then ramped to 95°C to soft bake for 5 minutes, before being hard baked for 20 minutes at 150°C. A 100 μm thick SU-8 layer was prepared with SU-8 2075 (MicroChem) by spreading the photoresist with a spin-coater set to 500 rpm at 100 rpm/second for 10 seconds, followed by spinning at 1510 rpm set to 200 rpm/second for 40 seconds. The photoresist coated wafer was soft baked at 65°C for 5 minutes before the temperature was ramped to 95°C to bake for a further 15 minutes. The SU-8 photoresist was etched using a laser scanning lithographer (μPG 101, Heidelberg Instruments) to generate the microfluidic pattern designed as described (see Figure 1). Post-exposure bake was performed at 65°C for 5 minutes and ramped up to 95°C for 30 minutes. The SU-8 master wafer was developed in SU-8 developer (MicroChem) at room temperature with gentle agitation for 15 minutes. The developed SU-8 wafer was hard-baked at 150°C for 30 minutes. The master wafer was silanized to reduce PDMS adhesion to the wafer by addition of a few drops of silane (trichloro(1,1,2,2-perfluorooctyl) silane) directly onto the SU-8 wafer and vacuum desiccation for 15 minutes, followed by a post-silanization bake at 150°C for 10 minutes.

PDMS microfluidic chip fabrication

Disposable PDMS microfluidic chips were prepared as follows. PDMS (Sylgard® 184, Sigma-Aldrich), was mixed in a ratio of 10:1 polymer:curing agent and thoroughly mixed to ensure equal distribution of curing agent throughout the polymer. The mixture was centrifuged at 1000 × *g* for 15 minutes to remove most air bubbles generated during mixing. The PDMS mixture was poured onto the SU-8 master wafer and placed into a vacuum chamber to degas until all visible air bubbles were removed. The PDMS was cured by baking in an oven set to 150°C for 20 minutes. Once cool, the PDMS elastomer was removed from the SU-8 master and cut to glass slide dimensions

using a razor blade. Inlets and outlets of the master channel, reverse flow chamber, side channels and vacuum line were punched with a 0.75 mm biopsy punch (WellTech). Glass coverslips (0.17 mm) were cleaned under atmospheric plasma for one minute using a plasma cleaner (Zepto LF, Diener electronic). Immediately following this process, the PDMS and the cleaned glass coverslip were exposed to atmospheric plasma for 40 seconds. Once activated by plasma, the PDMS was immediately bonded, channel sides down to the glass coverslip. The bonded PDMS chip was baked at 100°C for 20 minutes to enhance covalent bonding between the PDMS chip and glass coverslip. All outlets were fitted with polyethylene tubing (PE-60, 0.76 mm inner diameter, 1.22 mm outer diameter, Instech Laboratories, Inc.) and sealed with epoxy to create airtight connections to the microfluidic chip. Microfluidic flow of the PDMS chip was controlled using two syringe pumps with 50 mL plastic syringes. The first syringe pump was interfaced with the main channel outlet of the microfluidic chip. The second syringe pump was interfaced with an 11-port microfluidic switch (M-SWITCH™, Fluigent) which connected to the nine side channels, allowing the microfluidic flow of each side channel to be controlled independently and initiate efflux assays across each channel in a controlled manner. The syringe pumps, microfluidic switch and PE-60 tubing were rinsed thoroughly with MilliQ water prior to transport assay experiments and were thoroughly rinsed with 70% ethanol at the end of each experiment. The microfluidic chips and tubing were then primed with MilliQ water to remove air at a slow flow rate. Once excess air was removed from the chip, the microfluidic chip was then primed with the HEPES assay buffer (20 mM HEPES-KOH, pH 7.0, 145 mM NaCl, 5 mM KCl) for single-cell efflux experiments.

Microscopy setup for single-cell efflux experiments

All single cell efflux measurements were acquired using a Nikon Eclipse Ti2 inverted fluorescence microscope, equipped with a 1.49 NA 100 × objective and 512 × 512-pixel EM-CCD camera (C9100-13, Hamamatsu). Excitation light was provided using continuous-wave optically pumped semidiode lasers at 514 nm wavelength (150 mW max. output) and 568 nm wavelength (200 mW max. output) (Sapphire LP, Coherent). To image R6G fluorescence, we collected light

emitted between 525-555 nm (ET540/30m filter, Chroma). Time-lapse movies were recorded to visualise real-time R6G export out of *E. coli* cells. Two sets of image acquisitions were acquired in each assay. A bright-field image was collected at 37 ms exposure. R6G fluorescence was acquired using 50 ms exposure times and EM gain of 175. A heating stage was set to 37°C to maintain optimal temperature for *E. coli* cells throughout the experiments. All images were processed and analysed in Fiji (18).

Characterisation of hydrostatic reverse flow and ideal flow rate for rapid mixing.

To characterise microfluidic flow rates viable for single-cell efflux experiments, initial flow rate experiments involved priming the microfluidic chips with MilliQ water and introducing a rhodamine B solution into the main channel to visualise the direction of flow of the fluorescent dye within the chip. This was used to determine the presence and absence of mixing of two solutions prior to directed flow-rate within a single cell channel, and the rate of complete mixing of two solutions once directed into the flow channel. For this purpose, flow rates of 10 μL/min, 20 μL/min and 50 μL/min were tested.

Bacterial strains and cell cultures for single cell transport experiments.

E. coli BW25113 cultures were grown in EZ-rich media (Teknova) supplemented with 0.2% v/v glucose to minimise background fluorescence during single cell imaging. Overnight cultures were grown in 500 μL of EZ-glucose media at 37°C, 800 rpm. The next day, cultures were diluted 1:100 into fresh EZ-glucose media and grown at 37°C, 200 rpm until OD_{600nm} = 0.6) was reached. Cells were then harvested at 5,000 × g for 5 minutes, washed thrice in HEPES assay buffer and resuspended to a final volume of 1 mL to concentrate the cells. Cell suspensions were then treated with 10 μM CCCP and 1 μM R6G before incubating at 37°C, for 1 hour in the dark, allowing for accumulation of R6G in the *E. coli* BW25113 cells via passive diffusion. Cells were washed thrice at 15,000 × g for 1 minute in HEPES assay buffer. The sample was kept as a cell pellet and only resuspended to a final volume of 1 mL immediately prior to single-cell transport assays.

Single-cell R6G efflux assays

E. coli cells loaded with R6G were introduced into the main channel at a flow rate of 20 µL/min and allowed to flow into each side channel for a couple of minutes to promote cell adhesion to the glass slide surface. To determine that dye loss is not due to photobleaching or the flow of the HEPES assay buffer, a bright-field image was collected and time-lapse imaging of *E. coli* BW25113 cells was initialised prior to flushing with a continuous flow of HEPES assay buffer at a flow rate of 20 µL/min for 100 seconds. After the control experiment data was acquired, the main channel inlet was switched to the HEPES assay buffer reservoir that had been supplemented with 65 µM of sodium formate (HEPES-SF). The main channel was flushed with HEPES-SF solution for 20 minutes to ensure no buffer front was present before transport assays were recorded. Each efflux assay involved the collection of a bright-field image and initiation of the time-lapse series before directing continuous flow of HEPES-SF over dye-loaded *E. coli* cells for a total of 100 seconds per assay.

Image analysis and data visualisation

Image analysis was performed using Fiji (18). Time-lapse series, comprising of 2000 frames were loaded into the Fiji software and the frame in which buffer exchange first occured was noted as the zero time-point for fluorescence decay analysis. Individual cells were manually selected using a selection brush (12 pixels wide) to create regions of interest (ROI). Manually created cell outlines were added to the ROI manager, in which only non-overlapping, in-focus cells that remained adhered to the surface throughout the time-lapse acquisition were chosen. The ROI were collated into an ROI manager in Fiji, and the fluorescence decay over time was measured across the time-lapse series to track the rate of R6G efflux out of individual cells. To quantify the single-cell efflux rates across the isogenic populations, raw fluorescence intensity data was imported to GraphPad Prism. Single-phase decay analysis was used to obtain the half-life of fluorescence decay over time, correlating to the R6G efflux rate in each cell, as measured from the point of buffer exchange to the end of the time-lapse series. To determine the distribution of efflux rates within the isogenic

bacterial population, the half-life of fluorescence decay for individual cells were mapped to a frequency distribution plot.

Results

Microfluidic chip design

To measure *in vivo* fluorimetric drug efflux transport assays at the population level, bacterial cells at mid-exponential growth phase were treated with a protonophore to dissipate the proton-motive force gradient, inhibiting active transport processes and allowing for passive diffusion of membrane-permeable dye to accumulate within the cell (11). Measurement of drug export was initiated through the introduction of a carbon source in the buffer to re-establish the proton-motive force gradient, enabling observation of changes in fluorescence intensity over time. To describe how the microfluidic chip has been designed to accommodate this experiment, the buffer separation and exchange features will be described using the terms Buffer A and Buffer B to denote the assay buffer without and with carbon source, respectively.

To develop a microfluidic chip amenable to study drug efflux experiments at the single cell level, we required the chip to have four main features.

i) a main channel — as a point of entry of Buffer A and Buffer B and to introduce dye-loaded cells into the microfluidic chip;

ii) a side channel— as an isolated area for the collection of dye-loaded cells where Buffer B is introduced for the re-establishment of active efflux and can be directed in a controlled manner for time-lapse imaging of R6G export at the single cell level;

iii) controlled separation of Buffer A and Buffer B with similar viscosity and physicochemical properties, to prevent passive diffusion of Buffer B from entering side-channels containing dye-loaded cells in assay buffer until required; and

iv) controlled buffer exchange within the side-channels, at a fast rate but without the presence of a buffer front or completely detaching *E. coli* cells adhered to the glass slide surface.

The design features to achieve these four main elements are depicted as a 2D-schematic in Figure 1.

The most challenging component of this research was to design a chip that could allow for separation and rapid mixing of two buffers with similar physicochemical properties without a buffer front affecting the timed initiation of the transport assay across a population of individual cells within the imaging area. Initially, we implemented a design where the user would intentionally introduce a small air bubble when exchanging Buffer A for Buffer B within the main channel to create a physical air barrier separating the two solutions. The bubble would be large enough to block the side-channel inlets from the main channel until buffer exchange was needed (by slowly flowing the air bubble over to block the next channel). However, the air bubble was unreliable and often collapsed mid-experiment leading to unintentional exposure to Buffer B before efflux experiments could be measured. Furthermore, the lack of a vacuum line to facilitate this air bubble, and the porous nature of PDMS led to many other unintentional air bubbles appearing throughout the chip, often blocking the channels or dislodging too many cells from the glass surface as they flowed through these channels. In response to these challenges, we re-designed the chip to facilitate buffer exchange through reverse flow and implemented the use of a vacuum line to remove introduction of air throughout the time frame of the efflux assay experiment.

In a single-cell efflux experiment with this design, Buffer A is equilibrated through the microfluidic chip by directing flow through the main channel, side-channels, and reverse flow chamber. The hydrostatic reverse flow is established to allowed for passive reverse flow of Buffer A out of the side-channels into the main channel. Dye-loaded *E. coli* cells were loaded into each side-channel for single-cell export experiments. Buffer B is flushed through the main channel

and allowed to equilibrate within the main channel. Real-time single-cell efflux experiments were initiated for each separate side-channel through direction of Buffer B from the main channel into the side-channel of choice for time-lapse imaging of decay of fluorescence intensity over time as a function of active transport of R6G dye out of individual *E. coli* cells.

Our initial experiments involved a set of controls to confirm the microfluidic chip design was suitable for single-cell export experiments. The first investigation involved testing the flow direction and flow rates achieved by equilibrating the microfluidic chip with MilliQ water to represent Buffer A, and introducing a fluorescent rhodamine B solution to represent Buffer B and allow the flow direction to be visualised in the absence of *E. coli* cells. Our experiment revealed controlled separation of Buffer A filled side-channels that flowed out of the side-channels into the main-channel to prevent passive diffusion of the Buffer B solution from the main channel into side-channels (Figure 2).

Following this successful proof of concept, we needed to determine the flow rate that would allow for rapid buffer exchange to occur between Buffer A and Buffer B to occur without a significant buffer front and which would lead to delays in efflux initiation across a population of *E. coli* cells depending on their location within the different side-channels. The conical nature of the side-channel allowed for tight, rapid mixing to occur near the surface and flow evenly across our bacterial cells further down the channel. Furthermore, our experiments to test different flow rates determined a flow rate of 20 μL/min was optimal for rapid buffer exchange between the MilliQ water and the rhodamine B solution without the presence of a significant buffer front or dislodging too many *E. coli* cells from the glass surface (Figure 3). These results confirmed our microfluidic chip design was amenable to reliable buffer separation, to prevent initiation of efflux assays before measurement and allowed for rapid buffer exchange at a suitable flow rate for reliable, simultaneous initiation of efflux to measure individual efflux rates across a single-cell population of *E. coli.*

***In vivo* single-cell observation of heterogenous R6G efflux in *E. coli* cells**

As described in the methods section, we ran a control experiment on wild type *E. coli* cells in the presence of the HEPES assay buffer only and found that the level of R6G fluorescence profile remained relatively stable throughout the course of a transport experiment and was not decreased by photobleaching or the presence of 20 μL/min flow of HEPES assay buffer over the individual *E. coli* cells (Figure 4).

Mid-exponential phase *E. coli* cells loaded with 1 μM of R6G and treated with CCCP were washed and collected into eight independent side channels. Initiation of active efflux was induced with the introduction of HEPES-SF and rapid decay of fluorescence intensity of R6G was measured across each individual cell as a time-lapse series for 100 seconds. This experiment was repeated across the remaining seven side-channels, and fluorescence decay over time as a function of R6G efflux was acquired for a total of $n = 65$ cells. A representative bright-field image and corresponding time-lapse series are presented in Figure 5. A frequency distribution of individual efflux rates, represented as half-time of fluorescence decay in seconds, is presented in Figure 5. Representative fast and slow efflux rates of individual cells detected across this experiment are presented in Figure 6. Data of half-time, k-constant, and R-squared values for each cell measured is available in Table S1.

Bright-field and epifluorescence imaging revealed *E. coli* cells appeared healthy and exhibited a normal cell morphology prior to transport assay initiation. Introduction of HEPES-SF reveals a rapid loss of cells within the flow channel and suggests the need for modification of a glass slide, such as APTES to improve cell adhesion to the glass surface. However, as up to eight channels were accommodated on a single microfluidic chip, we were able to count up to 65 individual cells across the experiment that remained attached to the glass surface throughout the entire efflux assay. Non-linear regression analyses of fluorescence decay rates (single-phase decay plots) revealed a diverse distribution of fluorescence decay half-lives ($t_{1/2}$) across the bacterial cells measured. Frequency distribution analyses revealed three populations to emerge from a population of *E. coli* cells exporting R6G (Figure 5); a fast efflux population centred on $t_{1/2} = 6$ seconds, a

medium efflux population centred on $t_{1/2}$ = 18 seconds and a slower efflux population centred on $t_{1/2}$ = 22 seconds. The average fluorescence decay half-life was $t_{1/2}$ = 13.43 seconds upon initiation of R6G efflux by HEPES-SF. This data further supports the notion that within an isogenic population, stochastic heterogeneity can affect antimicrobial efflux rates out of individual bacterial cells. The average half-life was not representative of the main population efflux rate, where a majority of individual cells were identified to have a $t_{1/2}$ of approximately 8 seconds. Representative fluorescence decay curves of individual cells measured show different transition states during R6G transport, where some facilitate rapid, one-phase efflux of R6G out of the cell, while others show the presence of at least two phases of R6G efflux to occur (Figure 6).

Observation of single-molecule transport of R6G out of individual *E. coli* cells.

In a follow up experiment, we loaded a wild type population of *E. coli* BW25113 cells with a sub-micromolar concentration of R6G solution (<1 μM). At this concentration, we were able to observe individual foci associated close to the cell membrane, corresponding to R6G localisation within single cells (Figure 7, Appendix D). The total number of foci observed in this experiment was different across a population of *E. coli* BW25113 cells. Most cells contained multiple R6G foci associated at the cell membrane near the cell poles of the bacterial cell. Some cells only contained one R6G foci, while other cells did not have any visible foci (Figure 7, Appendix D). Not all foci were located at the cell poles; those with multiple foci appeared to have foci also associated with the cell membrane towards the centre of the cell (Figure 7, Appendix D).

We repeated the fluorescence decay experiments with sub-micromolar R6G, and as described in the methods, except we focused specifically to the foci. R6G fluorescence traces were produced for each foci. Three distinct transition states were observed within a population and representative R6G transport cycles are presented in Figure 7. Most foci appeared to export R6G as expected for normal fluorescence single-phase decay. However, we were also able to detect sharp, single-step R6G transport cycle and a two-step R6G transport cycle to occur at the single-molecule level (Figure 7). This data reveals that differences in mechanism of R6G transport for individual cells (possibly discrete efflux pumps) can be observed in our assay.

Discussion

Multidrug efflux pumps are a main mechanism of antibiotic resistance in Gram-negative bacteria, where intrinsic and adaptive expression of a single multidrug efflux pump can confer a significant multidrug resistance phenotype (3, 19). The stochastic nature of protein expression is expected to contribute to different levels of native efflux pump expression and efflux phenotypes across an isogenic bacterial population (8, 9, 20). Therefore, it is important to continue to develop new tools to quantify differences in drug efflux rates across a bacterial population, which may impact overall heterogeneity in efflux mediated antimicrobial resistance.

Current methods to study *in vivo* efflux activity have been developed to study efflux rates at the population-level (11). However, these population-based methods will average the efflux rate across an otherwise heterogeneous efflux population. Several approaches to examine drug accumulation in single cell bacterial populations have been developed to examine drug efflux in an indirect fashion (12–15). The limitation to using drug accumulation as a proxy for drug efflux is that it is not possible to directly determine efflux rates or to identify mechanistic differences in efflux at the single-molecule level. In this study we combined the use of microfluidics and epifluorescence microscopy to develop the first rapid, real-time single-cell efflux assay to quantify heterogeneity in efflux across an isogenic population as a function of direct antimicrobial export out of the cell. We demonstrate that individual cells can be tracked as regions of interest, and measurement of different fluorescence decay rates can be measured in under 100 seconds, providing a rapid and convenient test to study whole cell efflux of an antimicrobial fluorophore in bacteria.

Our microfluidic chip is convenient and can be easily fabricated in-house at low cost without the need for specialist equipment. In addition, our microfluidic chip is capable of simultaneous separation of two buffer solutions, allowing for strict control of the flow rate and direction of transport assay buffer required to initiate active transport of dye out of individual cells collected in each side-channel. Hence, we can readily quantify drug export as a function of intracellular fluorescence decay across all cell populations that remain adhered to the glass surface across the

time-lapse series and repeat this process in up to eight replicate channels per experiment. Time-lapse imaging allows us to easily identify the exact time-point in which buffer exchange occurs as the point in time where bacterial cells are exposed to carbon source to re-establish electrochemical gradients and begin active export. At this time point, the start point for phase decay analysis is established, and real-time measurement of fluorescence decay in each individual cell can be studied.

Using this approach, we determined that within an isogenic wild type population of *E. coli*, efflux of R6G was heterogeneous and efflux rates were observed across a spectrum of fast, average and slow fluorescence decay half-times. Most cells demonstrated R6G fluorescence decay half-times between approximately 6 and 8 seconds, which is significantly different to the ensemble population average fluorescence decay half-time of approximately 13 seconds. This data not only shows very clear distinct subpopulations of efflux dynamics across a wild-type population, but also emphasised the importance of single cell efflux analyses in these populations, as true averages mask differences within the population.

When sub-micromolar concentrations of R6G were loaded into wild type *E. coli* cells, we also observed the capability for our microfluidic chip to be used to resolve R6G export to the single-molecule level. Most cells in this population harboured multiple R6G foci or a singular R6G foci localised at the membrane interface at the cell poles. This is consistent with previous observations that the *E. coli* AcrAB-TolC multidrug efflux pump is largely localised to the poles of the cell (9). Hence, it is likely that each of these foci represent a single R6G efflux pump. Furthermore, we also observed three distinct R6G efflux transition states for these foci within a single *E. coli* cell population across a population (Figure 7). First, we observed a single-step change in fluorescence intensity that may represent the rapid efflux of a single-molecule of R6G. Secondly, we observed a two-step change in fluorescence intensity that may represent the sequential transport of two R6G molecules. Thirdly, we observed a gentle one-phase decay of fluorescence intensity. Hence, it is also tempting to speculate that these different decay profiles represent distinct mechanisms of efflux corresponding to different classes of transporter. However,

attributing these different R6G efflux dynamics to specific transporters from ABC, RND, MFS and other efflux pump families will require further experimentation with gene knockouts and/or fluorescently-tagged transporters.

We were able to detect and observe membrane-bound R6G fluorescence foci across the population. Most cells in this population harboured multiple R6G foci or a singular R6G foci localised at the membrane interface at the cell poles. This is consistent with previous observations that the *E. coli* AcrAB-TolC multidrug efflux pump is largely localised to the poles of the cell (9).

Our experiment is a proof-of-concept study. We have demonstrated the ability to study heterogeneous R6G efflux rates within isogenic bacterial population at the single-cell and single-molecule resolution. Our immediate next steps will focus on improving replicates and resolution of single-cell and single-molecule R6G experiments to verify the reproducibility of the phenotypes reported in this chapter. We also intend to further optimise our microfluidic chip. Surface modification tactics, such as the application of APTES ((3-aminopropyl) triethoxysilane) functionalised glass coverslips that form strong covalent bonds with the LPS of Gram-negative cells (21) will be explored to improve cell adhesion to the glass surface and increase the sample numbers in each side-channel.

Conclusions

In this study, we have developed a new approach to studying drug efflux of bacterial cells, using a combination of microfluidics and epifluorescence single-cell microscopy. We report on the first visualisation of R6G efflux at the single-cell and single-molecule level in *E. coli*. Our proof-of-concept study provides a step forward in how drug efflux systems are studied in single-cell populations, with potential benefits to unmask subtleties in drug efflux function not otherwise observed in population-level experiments. With minimal adaption, this new experimental platform should be amenable to other fluorescent probes, particularly with advances in photostability and brightness (11, 22, 23), to study efflux function at the single-cell and

single-molecule level across a range of bacterial strains and heterologous drug efflux pump expression systems.

References

1. C. J. L. Murray, *et al.*, Global burden of bacterial antimicrobial resistance in 2019: a systematic analysis. *Lancet* **399**, 629–655 (2022).
2. E. M. Darby, *et al.*, Molecular mechanisms of antibiotic resistance revisited. *Nat. Rev. Microbiol.* **21**, 280–295 (2023).
3. L. J. V. Piddock, Clinically relevant chromosomally encoded multidrug resistance efflux pumps in bacteria. *Clin. Microbiol. Rev.* **19**, 382–402 (2006).
4. H. Nikaido, J.-M. Pagès, Broad-specificity efflux pumps and their role in multidrug resistance of Gram-negative bacteria. *FEMS Microbiol. Rev.* **36**, 340–363 (2012).
5. A. E. Ebbensgaard, A. Løbner-Olesen, J. Frimodt-Møller, The role of efflux pumps in the transition from low-level to clinical antibiotic resistance. *Antibiotics* **9**, 1–7 (2020).
6. A. Raj, A. van Oudenaarden, Nature, nurture, or chance: Stochastic gene expression and its consequences. *Cell* **135**, 216–226 (2008).
7. H. J. E. Beaumont, J. Gallie, C. Kost, G. C. Ferguson, P. B. Rainey, Experimental evolution of bet hedging. *Nature* **462**, 90–93 (2009).
8. M. Ackermann, A functional perspective on phenotypic heterogeneity in microorganisms. *Nat. Rev. Microbiol.* **13**, 497–508 (2015).
9. T. Bergmiller, *et al.*, Biased partitioning of the multidrug efflux pump AcrAB-TolC underlies long-lived phenotypic heterogeneity. *Science.* **356**, 311–315 (2017).
10. B. A. Mitchell, I. T. Paulsen, M. H. Brown, R. A. Skurray, Bioenergetics of the staphylococcal multidrug export protein QacA. *J. Biol. Chem.* **274**, 3541–3548 (1999).
11. J. M. A. Blair, L. J. V. Piddock, How to measure export via bacterial multidrug resistance efflux pumps. *MBio* **7**, 1–6 (2016).
12. M. A. Sánchez-Romero, J. Casadesús, Contribution of phenotypic heterogeneity to adaptive antibiotic resistance. *Proc. Natl. Acad. Sci.* **111**, 355–360 (2014).
13. Y. Pu, *et al.*, Enhanced efflux activity facilitates drug tolerance in dormant bacterial cells. *Mol. Cell* **62**, 284–294 (2016).
14. J. Cama, *et al.*, Single-cell microfluidics facilitates the rapid quantification of antibiotic accumulation in Gram-negative bacteria. *Lab Chip* **20**, 2765–2775 (2020).
15. A. Reuter, *et al.*, Direct visualisation of drug-efflux in live *Escherichia coli* cells. *FEMS Microbiol. Rev.* **44**, 782–792 (2020).
16. F. Grenier, D. Matteau, V. Baby, S. Rodrigue, Complete genome sequence of *Escherichia coli* BW25113. *Genome Announc.* **6**, 90005 (2018).

17. M. P. Wolf, G. B. Salieb-Beugelaar, P. Hunziker, PDMS with designer functionalities—Properties, modifications strategies, and applications. *Prog. Polym. Sci.* **83**, 97–134 (2018).

18. J. Schindelin, *et al.*, Fiji: An open-source platform for biological-image analysis. *Nat. Methods* **9**, 676–682 (2012).

19. J. Sun, Z. Deng, A. Yan, Bacterial multidrug efflux pumps: Mechanisms, physiology and pharmacological exploitations. *Biochem. Biophys. Res. Commun.* **453**, 254–267 (2014).

20. I. El Meouche, M. J. Dunlop, Heterogeneity in efflux pump expression predisposes antibiotic-resistant cells to mutation. *Science.* **362**, 686–690 (2018).

21. Q. Lu, J. Wang, A. Faghihnejad, H. Zeng, Y. Liu, Understanding the molecular interactions of lipopolysaccharides during *E. coli* initial adhesion with a surface forces apparatus. *Soft Matter* **7**, 9366–9379 (2011).

22. M. R. L. Stone, M. S. Butler, W. Phetsang, M. A. Cooper, M. A. T. Blaskovich, Fluorescent antibiotics: New research tools to fight antibiotic resistance. *Trends Biotechnol.* **36**, 523–536 (2018).

23. J. B. Grimm, *et al.*, A general method to fine-tune fluorophores for live-cell and *in vivo* imaging. *Nat. Methods* **14**, 987–994 (2017).

Figures and Tables

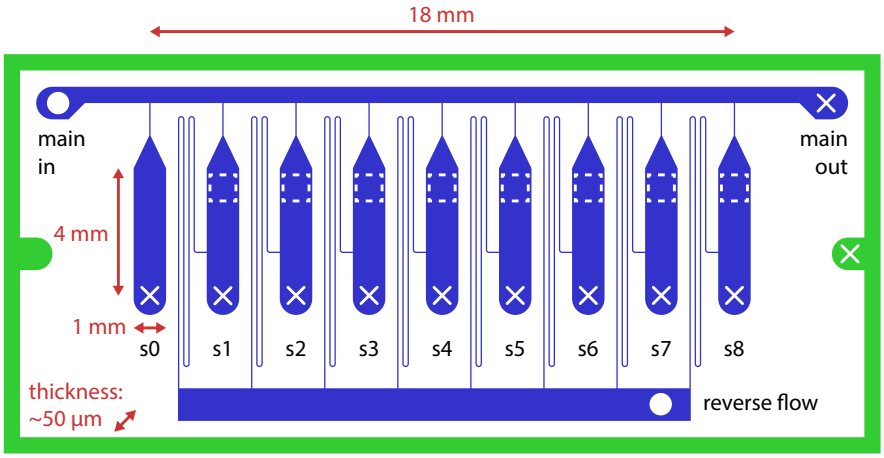

Figure 1: Schematic of the microfluidic chip designed used for the R6G efflux experiment. The main channel is 1800 µm in length, with channel height of 50 µm for continuous flow of HEPES assay buffer, cell delivery and HEPES-SF buffer. Cells are confined into side-channels, 100 µm in width and 4000 µm in length to allow multiple individual *E. coli* cells to be collected into a monolayer within a single channel (s1-s8).

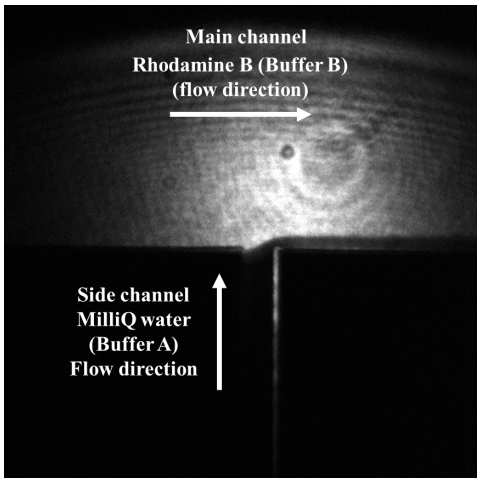

Figure 2: Epifluorescent image (λ_{Ex} = 514 nm) displaying the strict separation of Buffer A and buffer B solutions by implementing hydrostatic reverse flow, preventing passive diffusion and mixing of Buffer B from reaching cells prior to transport assay initiation.

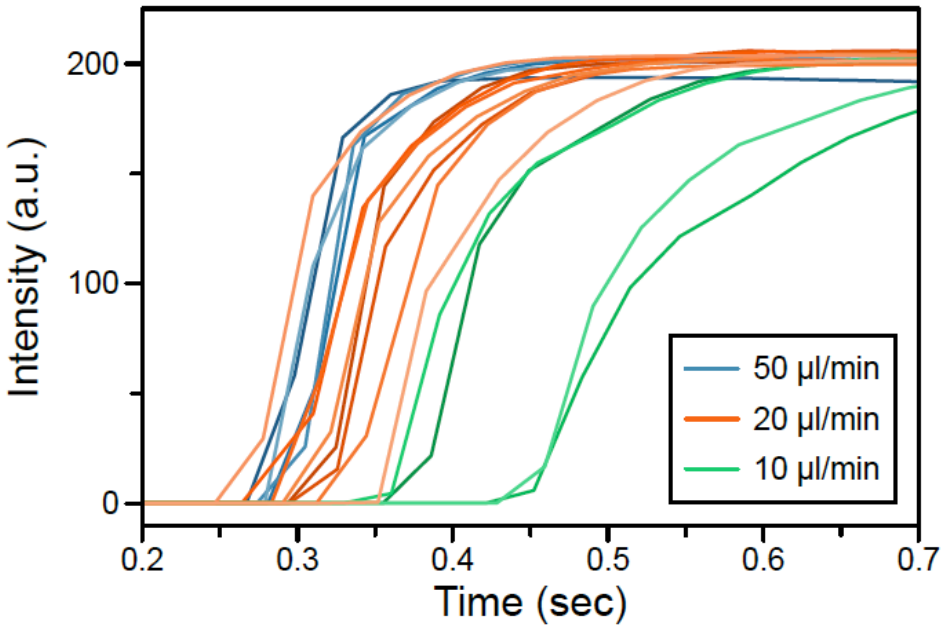

Figure 3: Buffer exchange between MilliQ water and rhodamine B solution at specific point within side-channels. Three flow rates were tested at 50 µL/min (*blue*) 20 µL/min (*orange*) and 10 µl/min (*green*) to determine the flow rate sufficient for rapid buffer exchange with minimal buffer front for single cell R6G efflux assays. The 20 µL/min flow rate was seen to be rapid enough for buffer exchange without complete dissociation of *E. coli* cells attached to the glass surface.

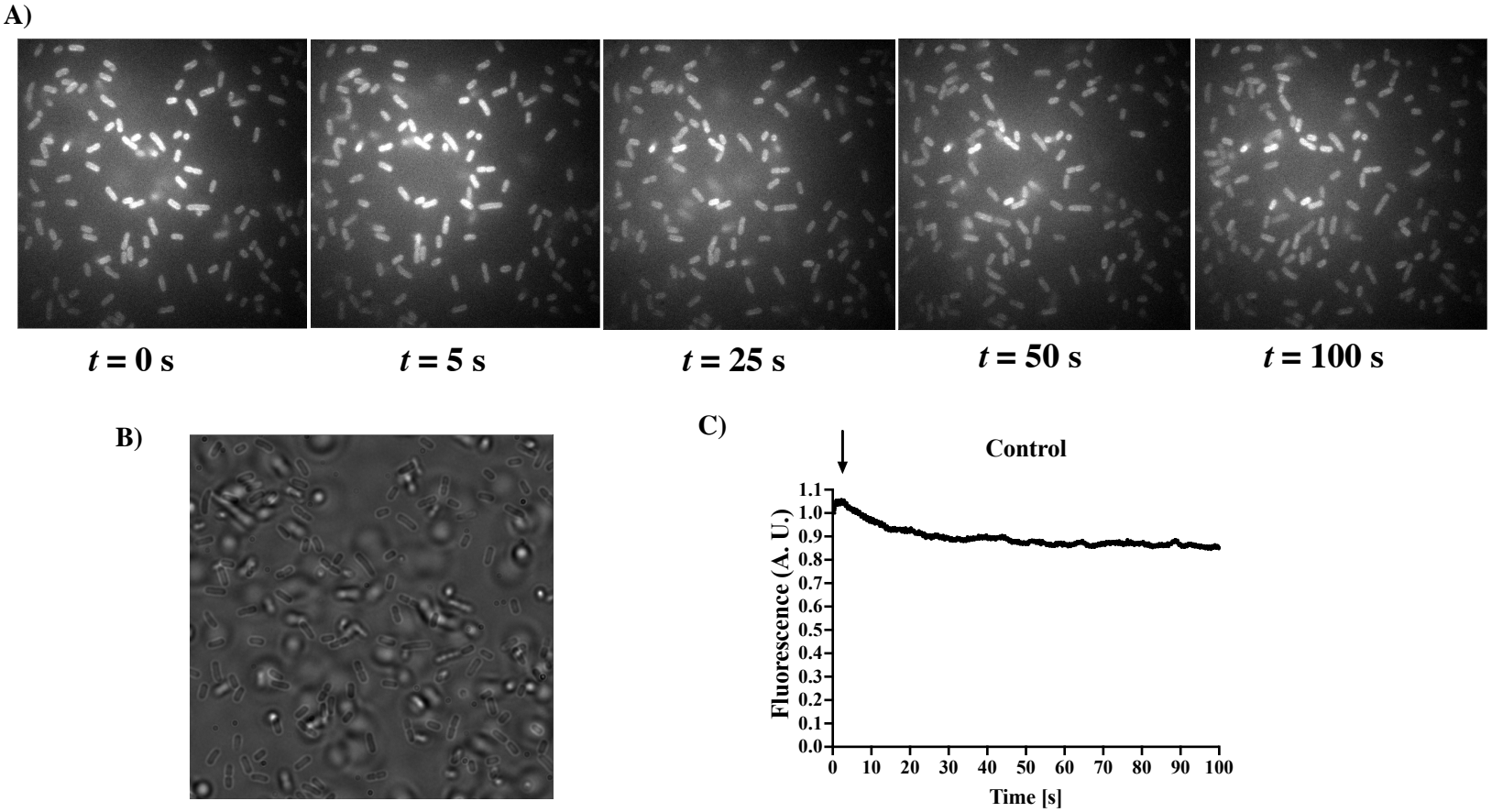

Figure 4: Single cell R6G transport control experiment. HEPES assay buffer was flowed over the cells for the 100 seconds to determine if fluorescence is lost due to buffer flow and/or photobleaching from the laser excitation. B) *E. coli* cells in focus are adhered to the glass slide, *E. coli* cells out of focus are not adhered to the glass slide and are removed upon buffer exchange. C) Normalised fluorescence decay average over 100 second timeframe, reveals only a small loss of intracellular fluorescence without initiation of a transport experiment.

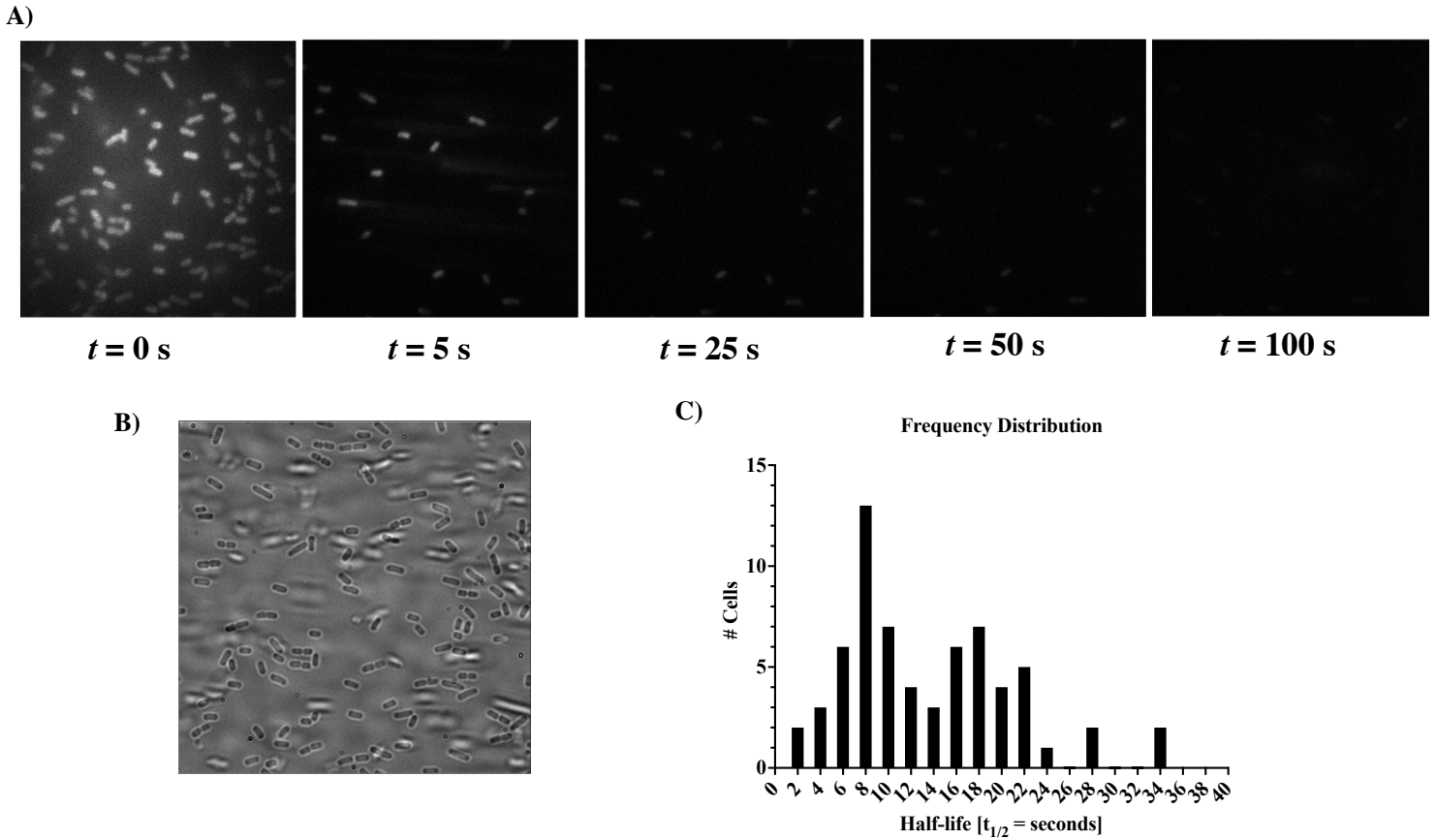

Figure 5: Single-cell R6G export experiment across wild type *E. coli* BW25113 cells. A) Representative time-lapse series of R6G single-cell efflux assay across a 100 second time frame. B) Bright-field image of bacterial cells prior to transport assay initialization; *E. coli* cells in focus are adhered to the glass slide, *E. coli* cells out of focus are not adhered to the glass slide and are removed upon buffer exchange. C) Frequency distribution plot of fluorescence decay half-time across *E. coli* BW25113 cells (n = 65).

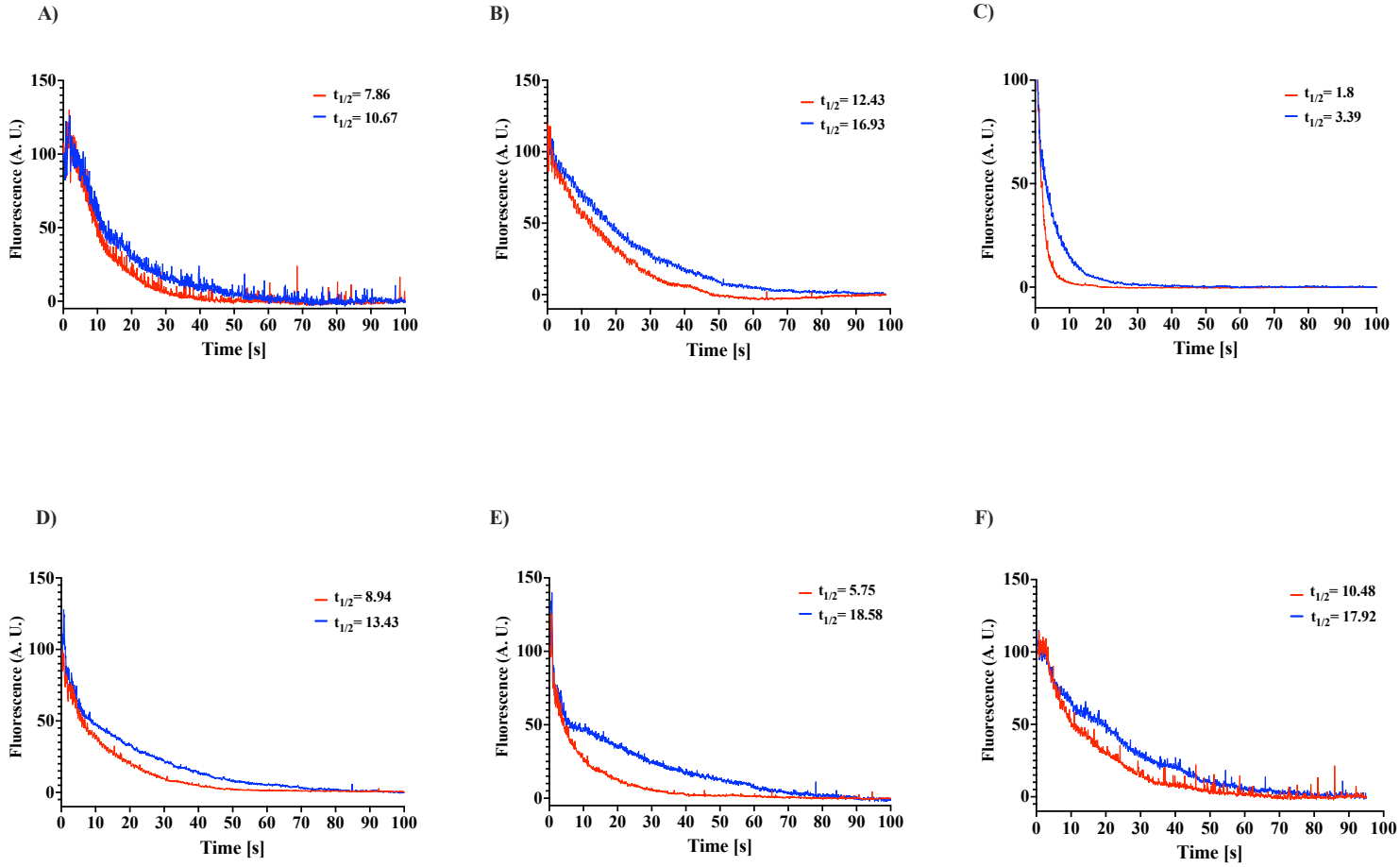

Figure 6: A representative selection of normalized R6G fluorescence decay curves for two individual cells in the same channel (*blue* and *red*) showing different fluorescence decay rates and/or profiles. Differential fluorescence decay rates were observed across multiple cells in each channel. The half-time (seconds) of fluorescence decay of each curve is presented in the legend. Relatively faster (*red)* and slower (*blue*) rates were observed across each channel, and differences in transition states can be observed, including one-phase decay (Panels C, D, E) and two-phase decay states (Panels A, B, D, E, F).

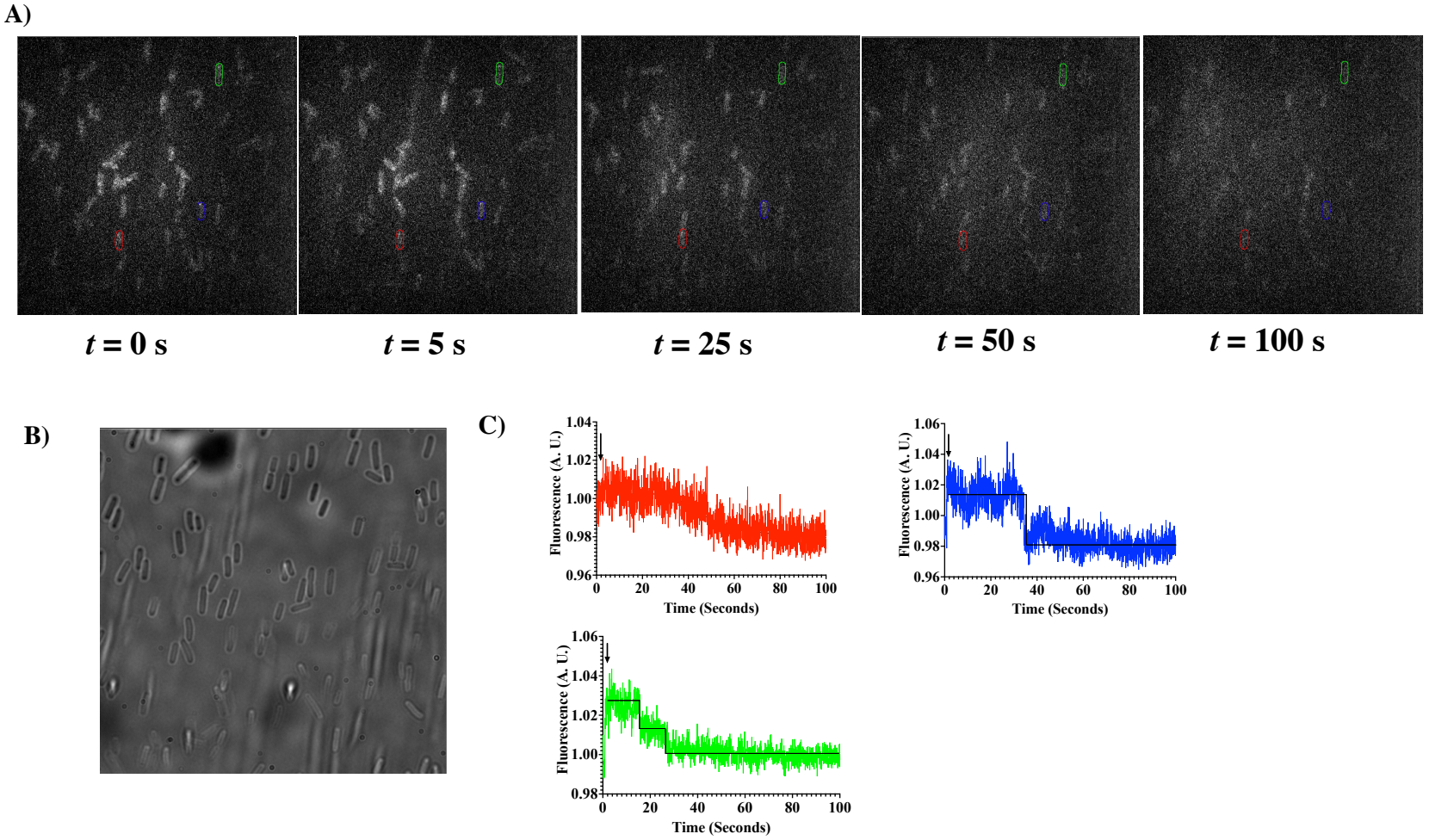

Figure 7: Single-molecule R6G efflux experiment. A) Time-lapse series of single-molecule R6G export over 100 second timeframe. B) Brightfield image of cell sample prior to initiation of R6G transport assay. C) Representative fluorescent decay of three population states observed across foci within cell samples studied; solid *grey* lines were added manually to highlight the patterns of efflux transition states observed for individual foci within the same cell sample.

Supporting information

Table 1: Phase decay analysis of single-cell R6G efflux experiment.

Cell #	Rate constant [s^{-1}]	Half-Life [s]	R-squared
Cell 1	0.0649	10.67	0.9792
Cell 2	0.0882	7.862	0.9766
Cell 3	0.1121	6.181	0.9552
Cell 4	0.0797	8.692	0.977
Cell 5	0.0923	7.514	0.9659
Cell 6	0.0878	7.893	0.9081
Cell 7	0.0848	8.172	0.9558
Cell 8	0.0822	8.428	0.9638
Cell 9	0.0791	8.765	0.978
Cell 10	0.0443	15.65	0.939
Cell 11	0.0591	11.73	0.9602
Cell 12	0.0409	16.93	0.9569
Cell 13	0.039	17.77	0.9638
Cell 14	0.0558	12.43	0.9568
Cell 15	0.0283	24.47	0.9552
Cell 16	0.0304	22.78	0.9611
Cell 17	0.2043	3.393	0.9906
Cell 18	0.3567	1.943	0.8827
Cell 19	0.385	1.8	0.872
Cell 20	0.0775	8.942	0.99
Cell 21	0.0822	8.428	0.9928
Cell 22	0.0516	13.43	0.9731
Cell 23	0.0458	15.14	0.9637
Cell 24	6.821	9.841	0.9714
Cell 25	3.324	4.796	0.9425
Cell 26	6.726	9.704	0.9616
Cell 27	13.22	19.07	0.9629
Cell 28	11.05	15.95	0.964
Cell 29	6.953	10.03	0.9322
Cell 30	7.837	11.31	0.9347
Cell 31	7.682	11.08	0.945
Cell 32	0.0661	10.48	0.9886

Cell #	Rate constant [s^{-1}]	Half-Life [s]	R-squared value
Cell 33	0.0703	9.86	0.9866
Cell 34	0.0766	9.051	0.9864
Cell 35	0.0653	10.62	0.9759
Cell 36	0.0719	9.647	0.9698
Cell 37	0.0387	17.92	0.9899
Cell 38	0.0318	21.78	0.9874
Cell 39	0.0302	22.95	0.961
Cell 40	0.039	17.8	0.98
Cell 41	0.0347	19.99	0.9849
Cell 42	0.0249	27.86	0.9726
Cell 43	0.0377	18.38	0.9539
Cell 44	0.0552	12.57	0.976
Cell 45	0.0467	14.83	0.9916
Cell 46	0.0439	15.8	0.9873
Cell 47	0.0332	20.85	0.9835
Cell 48	0.0344	20.13	0.9793
Cell 49	0.0207	33.47	0.9706
Cell 50	0.0363	19.11	0.9693
Cell 51	0.0252	27.5	0.9703
Cell 52	0.0984	7.042	0.9275
Cell 53	0.0324	21.42	0.9572
Cell 54	0.2131	3.253	0.7884
Cell 55	0.1197	5.79	0.9731
Cell 56	0.0897	7.728	0.9803
Cell 57	0.102	6.798	0.9661
Cell 58	0.0373	18.58	0.9376
Cell 59	0.0391	17.74	0.9367
Cell 60	0.0717	9.669	0.9757
Cell 61	0.0428	16.21	0.9648
Cell 62	0.0462	15.02	0.916
Cell 63	0.0311	22.31	0.9617
Cell 64	0.0208	33.31	0.9249
Cell 65	0.0385	17.99	0.9473

Chapter 7: Identification of a novel ciprofloxacin tolerance gene, *aciT*, which contributes to filamentation in *Acinetobacter baumannii*

Published as: Naidu, V., Shah, B., Kamath, K. S., Chien, A., Nagy, S., Pokhrel, A., Molloy, M., Hassan, K. A., & Paulsen, I. T. (2021). Identification of a novel ciprofloxacin tolerance gene, *aciT*, which contributes to filamentation in *Acinetobacter baumannii*. *Antimicrobial Agents and Chemotherapy*, 65(6), 1-9. [e01400]. https://doi.org/10.1128/AAC.01400-20.

AMERICAN SOCIETY FOR MICROBIOLOGY | Antimicrobial Agents and Chemotherapy®

MECHANISMS OF RESISTANCE

Identification of a Novel Ciprofloxacin Tolerance Gene, *aciT*, Which Contributes to Filamentation in *Acinetobacter baumannii*

Varsha Naidu,[a] Bhumika Shah,[a] Karthik S. Kamath,[a,b] Arthur Chien,[c] Stephanie Nagy,[a] Alaska Pokhrel,[a] Mark Molloy,[a,d] Karl A. Hassan,[a,e] Ian T. Paulsen[a]

[a]Department of Molecular Sciences, Faculty of Science and Engineering, Macquarie University, Sydney, NSW, Australia
[b]Australian Proteome Analysis Facility (APAF), Macquarie University, Sydney, NSW, Australia
[c]The Microscopy Unit, Faculty of Science and Engineering, Macquarie University, Sydney, NSW, Australia
[d]Faculty of Medicine and Health, University of Sydney, Sydney, NSW, Australia
[e]School of Environmental and Life Sciences, University of Newcastle, Newcastle, NSW, Australia

ABSTRACT Fluoroquinolones are one of the most prescribed broad-spectrum antibiotics. However, their effectiveness is being compromised by high rates of resistance in clinically important organisms, including *Acinetobacter baumannii*. We sought to investigate the transcriptomic and proteomic responses of the clinical *A. baumannii* strain AB5075-UW upon exposure to subinhibitory concentrations of ciprofloxacin. Our transcriptomics and proteomics analyses found that the most highly expressed genes and proteins were components of the intact prophage *phiOXA*. The next most highly expressed gene (and its protein product) under ciprofloxacin stress was a hypothetical gene, ABUW_0098, named here the *A*cinetobacter *c*iprofloxacin *t*olerance (*aciT*) gene. Disruption of this gene resulted in higher susceptibility to ciprofloxacin, and complementation of the mutant with a cloned *aciT* gene restored ciprofloxacin tolerance to parental strain levels. Microscopy studies revealed that *aciT* is essential for filamentation during ciprofloxacin stress in *A. baumannii*. Sequence analysis of *aciT* indicates the encoded protein is likely to be localized to the cell membrane. Orthologs of *aciT* are found widely in the genomes of species from the *Moraxellaceae* family and are well conserved in *Acinetobacter* species, suggesting an important role. With these findings taken together, this study has identified a new gene conferring tolerance to ciprofloxacin, likely by enabling filamentation in response to the antibiotic.

KEYWORDS *Acinetobacter*, fluoroquinolone, antibiotic resistance, ciprofloxacin, filamentation, pathogen

Acinetobacter baumannii is a Gram-negative bacterium that is considered a serious threat to global health care due to increasing rates of multidrug resistance (MDR) in clinical isolates. MDR clinical isolates of *A. baumannii* can be a challenge to treat for clinicians as few therapeutic options are available. The World Health Organization (WHO) has classified *A. baumannii* as one of the top three priority pathogens for which new antibiotic development is needed urgently. Broad-spectrum antibiotics, including fluoroquinolones such as ciprofloxacin, have been extensively used to treat infections caused by *A. baumannii*. Ciprofloxacin is listed as an essential medicine by the WHO and has been reported by the CDC to be one of the most prescribed oral antibiotics. Surveillance studies have shown significant increases in resistance rates for ciprofloxacin in *A. baumannii*, thereby compromising its use in health care. Discovery and characterization of novel ciprofloxacin-resistant genes are therefore critical for future inhibitory drug designs.

Fluoroquinolones exert their antibacterial activity by interfering with the function of type IIA topoisomerases—DNA gyrase and topoisomerase IV (1). Type IIA topoisomerases modulate the topological state of DNA through negative supercoiling of DNA and by

Citation Naidu V, Shah B, Kamath KS, Chien A, Nagy S, Pokhrel A, Molloy M, Hassan KA, Paulsen IT. 2021. Identification of a novel ciprofloxacin tolerance gene, *aciT*, which contributes to filamentation in *Acinetobacter baumannii*. Antimicrob Agents Chemother 65:e01400-20. https://doi.org/10.1128/AAC.01400-20.

Address correspondence to Ian T. Paulsen, Ian.Paulsen@mq.edu.au.

Received 6 July 2020
Returned for modification 12 August 2020
Accepted 20 March 2021
Accepted manuscript posted online 5 April 2021
Published 18 May 2021

decatenating newly replicated DNA during transcription and replication. Quinolones form a stable ternary complex with topoisomerase and DNA, preventing DNA strands from religating, resulting in double-stranded DNA breaks (2).

In the well-studied *Escherichia coli* model, stalling of replication forks leads to RecA-mediated autoproteolytic cleavage of the repressor LexA (3), which eventually self-cleaves, leading to the derepression of more than 30 genes associated with DNA repair and error-prone DNA polymerases (4). Collectively this process is referred to as the SOS DNA damage response (5). The cell division inhibitor SulA which is part of the SOS response, temporarily arrests cell division, allowing time for DNA repair to occur (6). During this process, bacterial cells change shape to form long filamentous structures. Filamentation has been described to occur in response to stressful environments, including DNA damage, antibiotics (7), and desiccation (8), and to subvert host innate defenses (9). In *E. coli*, filamentation in response to sub-MICs of ciprofloxacin has been shown to generate multiple mutant chromosomes that asymmetrically divide at the filament tips, giving rise to resistant offspring cells (10): hence, filamentation is a significant precursor in the evolution of resistance. Homologs of LexA and SulA, as well as several other DNA damage and cell division genes, have not been identified in *Acinetobacter* species (11, 12). It is unclear how *Acinetobacter* responds to genotoxic antibiotic ciprofloxacin at the core genome level.

In *A. baumannii*, mutations that lead to ciprofloxacin resistance tend to primarily emerge at the Ser81 codon of the DNA gyrase subunit GyrA, followed by secondary mutations in the Ser84 codon of the topoisomerase IV subunit ParC (13–16). Collectively, codon substitutions at these locations in the *gyrA* and *parC* genes have been shown to increase resistance to the fluoroquinolone ciprofloxacin by ~128-fold (17). In our current study, the global response to ciprofloxacin was investigated using transcriptomics and proteomics in the ciprofloxacin-resistant *A. baumannii* isolate AB5075-UW, which carries a mutation at the Ser81 codon of GyrA. This enabled the identification of genes in the core *A. baumannii* genome that are involved in tolerance to ciprofloxacin.

RESULTS AND DISCUSSION

Global transcriptomic and proteomic response to ciprofloxacin. An international clonal complex I *A. baumannii* strain AB5075-UW (18), with a ciprofloxacin MIC of 125 μg/ml (see Fig. S1A in the supplemental material) was exposed to a subinhibitory concentration (31.25 μg/ml) of ciprofloxacin for 1 h. Subsequently, the transcriptomic and proteomic responses were analyzed via transcriptome sequencing (RNA-Seq) and SWATH-MS (sequential window acquisition of all theoretical fragment ion spectra mass spectrometry) (19), respectively. This combined approach provided quantitative expression data for 3,983 out of 3,987 genes in total (20) in transcriptomics and 2,063 proteins in proteomics (21), representing 51.7% of the putative AB5075-UW proteome. The transcriptomics and proteomics data showed that 1,135 genes and 917 proteins were significantly (adjusted *P* value of 0.05) differentially expressed when exposed to 31.25 μg/ml ciprofloxacin (see Data Set S1 in the supplemental material). The Pearson correlation coefficient between mRNA abundance and protein abundance was 0.84 when gene expression and protein abundance data were filtered based on an adjusted *P* value of 0.05 (Fig. 1A).

A total of 153 genes had higher transcript levels, and 159 genes had lower transcript levels, by a $\log_2$ fold change of $>$1.5 (adjusted *P* value of 0.05) (Fig. 1B). In contrast, proteomics data showed higher expression of 21 proteins and lower expression of 14 proteins, by a $\log_2$ fold change of $>$1.5 (adjusted *P* value of 0.05) (Fig. 1B). These data were filtered to investigate the intersecting genes and proteins. The 16 intersecting abundant genes (and respective proteins) include components of the intact prophage *phiOXA*, components of the CRISPR-Cas system, and the hypothetical proteins ABUW_0369 and ABUW_0098 (Fig. 1C). Induction of prophage gene expression in response to ciprofloxacin stress has been previously described in other pathogenic

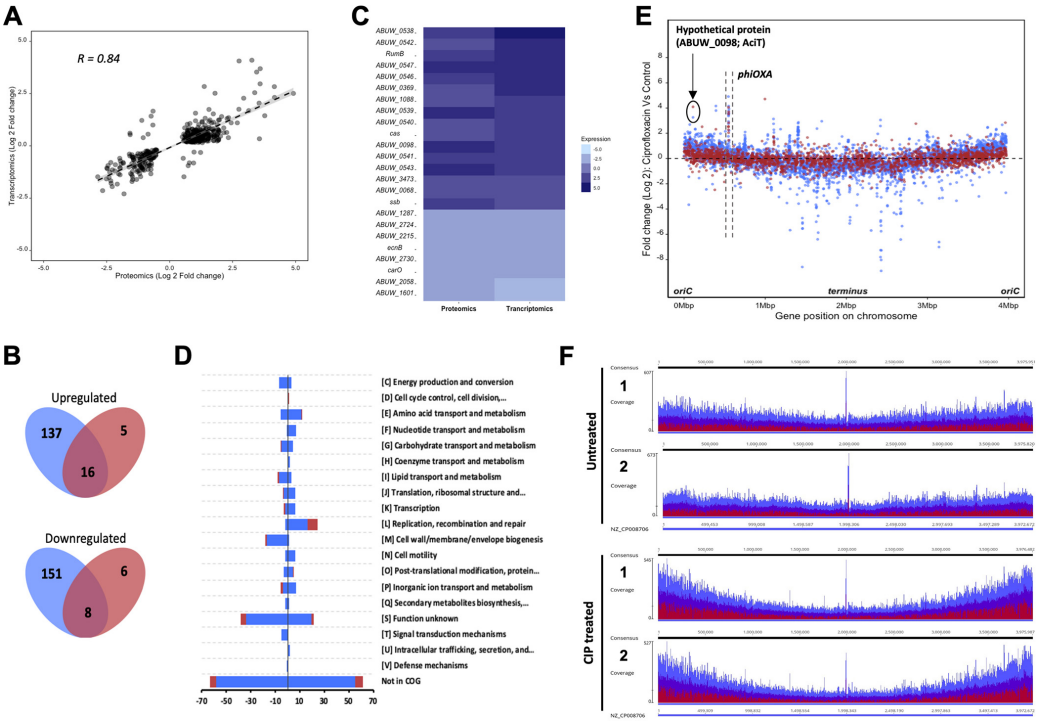

FIG 1 (A) Correlation between transcriptomics and proteomics data after they were filtered based on an adjusted *P* value of 0.05. The Pearson correlation coefficient between both data sets is 0.84. (B) Venn diagram depicting the relationship between genes and proteins that had a $\log_2$ fold change of greater or less than 1.5 (adjusted *P* value of <0.05). The proteomics data set is represented by the blue oval, and the transcriptomics data set is represented by red. The expression of 16 intersecting genes and proteins was greater than 1.5 ($\log_2$ fold change), and the expression of 8 was less than 1.5 ($\log_2$ fold change). (C) Intersecting genes and proteins from the Venn diagram were identified and plotted in a heat map. (D) Functional class analysis of genes/proteins based on COG categories. Bars represent the number of genes (blue) or proteins (red) in each COG category that had either increased or decreased expression by a $\log_2$ fold change of greater than 1.5 or less than 1.5 (adjusted *P* value of <0.05), respectively. (E) The transcriptional (blue) and proteomic (red) response of *A. baumannii* AB5075-UW to ciprofloxacin shock treatment. Each point in the graph represents a single ORF within the genome, arranged according to their location in the genome on the *x* axis and their fold change ($\log_2$) in expression on the *y* axis, following treatment with 31.25 μg/ml ciprofloxacin for 1 h. (F) Distribution of DNA reads along AB5075-UW chromosome of ciprofloxacin-treated (31.25 μg/ml, 1 h) and control (no treatment). The height of the graph shows the coverage of reads represented as minimum (red), average (purple), and maximum (blue).

organisms, such as *Salmonella enterica* serovar Typhimurium and *Staphylococcus aureus*, wherein ciprofloxacin is shown to facilitate phage-mediated gene transfer and expression of phage-encoded virulence factors, respectively (22, 23). In contrast, 8 intersecting genes (and representative proteins) showing lower expression include those coding for functions such as hypothetical proteins, the outer membrane protein CarO, and entericidin B (EcnB) (Fig. 1C).

Functional class analysis of differentially expressed genes and proteins identified enrichment of COG (Clusters of Orthologous Genes database) categories associated with DNA replication, recombination and repair, and cell envelope (Fig. 1D). In transcriptomics, several genes associated with DNA damage and repair were highly expressed, including the translesion polymerase genes *umuC* and *umuDAb* (expressed by $\log_2$ fold changes of 3.0 and 2.6, respectively).

The RND (resistance-nodulation-division) efflux pump AdeIJK has previously been shown to confer intrinsic resistance to ciprofloxacin in the *A. baumannii* strain ATCC 17978 (17). The genes encoding AdeIJK were not highly expressed in our transcriptomics or proteomics data. However, we conducted MIC tests with AB5075-UW Δ*adeI*, Δ*adeJ*, Δ*adeK*, and Δ*adeN* mutants that have been inactivated by transposon mutation

(20) to test their susceptibility to ciprofloxacin (Fig. S1B). AdeN belongs to the TetR family of regulators and represses the activity of AdeIJK efflux pumps (24). The *adeN* mutant had a 2-fold decrease in susceptibility to ciprofloxacin, while *adeIJK* mutants were more susceptible than the parental strain (Fig. S1B). This suggests that while *adeIJK* expression was not induced in AB5075-UW, it plays an important role in intrinsic resistance to ciprofloxacin (25).

Ciprofloxacin stress increases expression and gene dosage shift near the origin of replication (*oriC*). As shown in Fig. 1E, when transcriptomics and proteomics data are mapped as a function of gene position in the genome, transcription of genes proximal to the origin of replication (*oriC*) increases. We postulated that this may be due to a higher number of gene copies closer to the *oriC* during ciprofloxacin stress. To show that this was gene dosage dependent, we treated AB5075-UW with ciprofloxacin, using the same conditions as in transcriptomics and proteomics analyses (31.25 μg/ml for 1 h), and performed whole-genome sequencing. As shown in Fig. 1F, the gene dosage closer to *oriC* was much higher in ciprofloxacin-treated cells than in the no-treatment cells. Replication forks in the bacteria start from the *oriC* and extend bidirectionally toward the terminus region of the chromosome. In healthy exponentially growing cells, bidirectional replication of the bacterial chromosome leads to a higher replication-associated gene dosage closer to the *oriC* (26). Genes that are essential for transcription and translation tend to be located close to the *oriC*; as a result, these genes benefit from a higher dosage, and their transcription activity increases, presumably contributing toward bacterial fitness (26). Ciprofloxacin-mediated stalling of replication forks reduces the rate of DNA elongation; however, since new rounds of replication are continuously initiated, the replication-associated *oriC-ter* gene dosage increases, leading to more copies of genes closer to the *oriC*, and thus a higher likelihood of transcription/translation.

ABUW_0098 is a novel gene that confers tolerance to ciprofloxacin. The hypothetical gene of unknown function ABUW_0098 and its encoded protein were overexpressed in transcriptomics and proteomics analyses by $\log_2$ fold changes of 3.26 and 4.10, respectively. To investigate whether ABUW_0098 provides tolerance to ciprofloxacin, we cloned the ABUW_0098 gene with its predicted endogenous promoter (405-bp upstream region of ABUW_0098) into the shuttle vector pVRL1Z (27), and the resulting plasmid, pVRL1Z$_{ABUW_0098}$, was used to complement the AB00272 (ABUW_0098-inactivated) mutant strain (see Fig. S2B in the supplemental material) (20). Growth measurements were performed on five *A. baumannii* constructs. These included the AB00272 mutant and the AB00272 mutant complemented with pVRL1Z$_{ABUW_0098}$, as well as controls, including the AB5075-UW parental strain, AB5075-UW with empty pVRL1Z plasmid, and the AB00272 mutant with empty pVRL1Z plasmid.

We found that AB00272 mutant strain and AB00272 with empty pVRL1Z plasmid showed higher susceptibility to ciprofloxacin than AB5075-UW and AB5075-UW expressing empty pVRL1Z plasmid (Fig. 2A to D). Complementation of the AB00272 mutant with pVRL1Z$_{ABUW_0098}$ restored complete tolerance to ciprofloxacin at 31.25 μg/ml (Fig. 2B) and partial tolerance at 46.87 μg/ml (Fig. 2C) and 62.5 μg/ml (Fig. 2D). Interestingly, in all scenarios changes in the growth rate of all strains were only observed at approximately 45 min (double cell density) after addition of ciprofloxacin.

We sought to investigate the morphologies of all five constructs used in the growth curve experiment (see Fig. S4 in the supplemental material). Cells were imaged at four different time points, which included no treatment (before adding antibiotic) and at 1, 2, and 4 h after addition of 31.25 μg/ml of ciprofloxacin (Fig. 2E; see Fig. S3 in the supplemental material). AB5075-UW and AB5075-UW carrying empty pVRL1Z were elongated by 5 to 10$\times$ their original size at the 2-h time point (Fig. S4), consistent with phenotypes observed in *E. coli* (10, 28). Strikingly, the AB00272 mutant carrying empty pVRL1Z showed no signs of filamentation at any time point (Fig. 2E). Restoring the ABUW_0098 gene in AB00272 did not result in filamentation, similar to AB5075-UW expressing pVRL1Z (Fig. 2E); this could be attributed to the gene copy number. To test this, we introduced pVRL1Z$_{ABUW_0098}$ into AB5075-UW and compared its morphology with that of

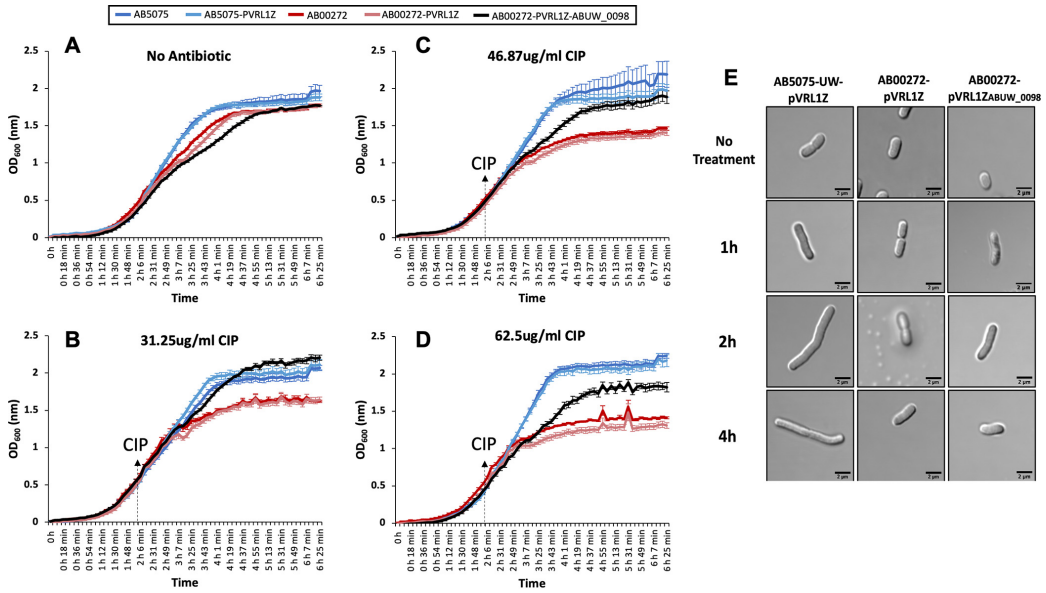

FIG 2 (A) Graph shows 6.25-h growth rate in Mueller-Hinton broth of AB5075-UW (parental strain, blue line), AB5075-UW expressing empty pVRL1Z plasmid (light blue), the AB00272 mutant strain (ABUW_0098 gene insertionally inactivated) (red), AB00272 mutant strain expressing empty pVRL1Z plasmid (light red), and AB00272 mutant strain complemented with pVRL1Z$_{ABUW_0098}$ (black). (B) All AB5075-UW constructs shocked with 31.25 μg/ml of ciprofloxacin after 2 h 6 min of growth. (C) All AB5075-UW constructs shocked with 46.87 μg/ml of ciprofloxacin after 2 h 6 min of growth. (D) All AB5075-UW constructs shocked with 62.5 μg/ml of ciprofloxacin after 2 h 6 min of growth (OD$_{600}$ of ~0.5). Growth of the ΔABUW_0098 mutant strain, AB00272, was significantly inhibited in the presence of ciprofloxacin. Error bars show the standard errors from three independent experiments. (E) Cell morphology of AB5075-UW expressing empty pVRL1Z plasmid, the AB00272 mutant strain expressing empty pVRL1Z plasmid, and the AB00272 mutant strain complemented with pVRL1Z$_{ABUW_0098}$ grown without antibiotics to mid-log phase (no treatment) followed by exposure to a sub-MIC of ciprofloxacin (31.25 μg/ml) at 1, 2, and 4 h. Scale bar, 2 μm.

AB5075-UW expressing empty pVRL1Z at 1, 2, and 4 h after addition of 31.25 μg/ml of ciprofloxacin. We found that while AB5075-UW expressing pVRL1Z$_{ABUW_0098}$ was able to form filamentous structures (see Fig. S6 in the supplemental material), the frequency of filamentation may be less than that of AB5075-UW expressing empty pVRL1Z.

We also investigated whether the downstream gene (ABUW_0099) had any role in filamentation during ciprofloxacin exposure. Growth measurements were performed on two different transposon insertion mutants (AB00274 and AB00275) with this gene inactivated. We found that there was no significant difference in growth rates between the parental AB5075-UW strain and ABUW_0099 mutants when exposed to ciprofloxacin (see Fig. S5 in the supplemental material). Furthermore, unlike the ABUW_0098 mutant, the ability of AB00274 and AB00275 to form filaments was not perturbed in the presence of ciprofloxacin (Fig. S6). A study recently published showed a novel gene, *advA* (ABUW_0096), located approximately 1,700 bp upstream of ABUW_0098, to be localized to cell division sites and to cause cells to adapt filamentous morphologies when deleted (29). Mutations in *advA* caused cells to become hypersensitive to fluoroquinolones and β-lactams.

In the well-studied *E. coli* model, SulA, which is membrane associated (30), is known to inhibit cell division by sequestering FtsZ, preventing the formation of Z rings (31, 32). The inhibition of cell division causes *E. coli* to become filamentous, while *sulA* mutants are not able to form filaments (31). The ability to form filamentous structures in response to fluroquinolones has been shown to give rise to resistant cells in *E. coli* (10). Several canonical proteins associated with cell division, including FtsE, FtsX, and SulA, are not found in the core genome of *Acinetobacter* and *Psychrobacter* species (12). Orthologs of ABUW_0098 are well conserved in *Acinetobacter* species and are found widely in other

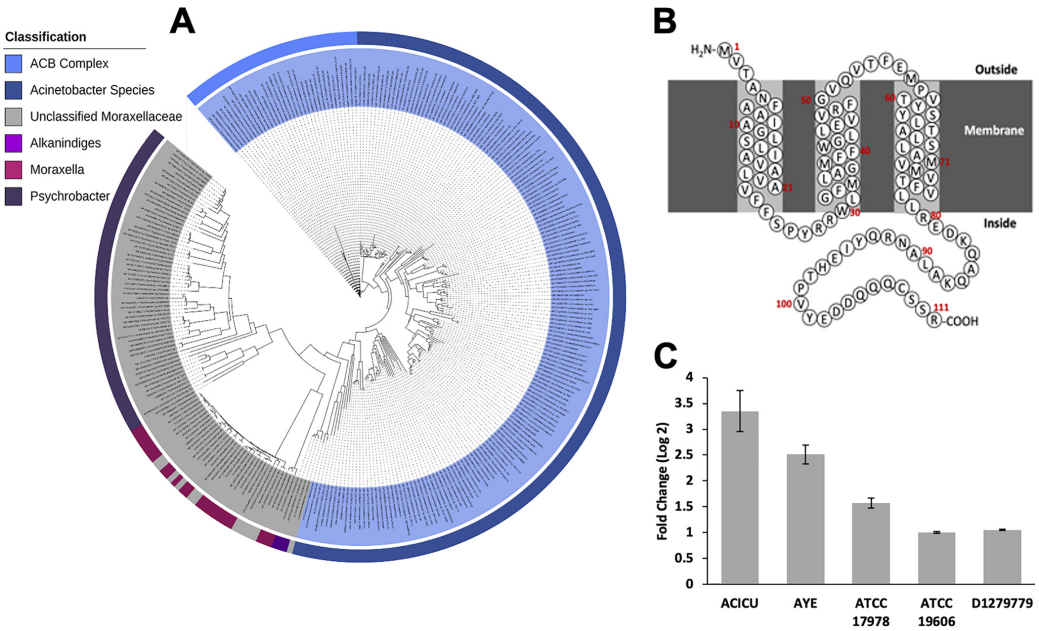

FIG 3 (A) Tree showing the phylogenetic relationship of ABUW_0098 protein. The tree was generated using iTOL from a Clustal Omega alignment of protein sequence obtained from the National Center for Biotechnology Information database. (B) Predicted transmembrane topology of the ABUW_0098 protein (AciT) based on predictions made using TMHMM (36). This protein is predicted to have three transmembrane α-helices. (C) Induction of ABUW_0098 (*aciT*) homologs by ciprofloxacin in *A. baumannii* strains ACICU, AYE, ATCC 17978, ATCC 19606, and D1279779. A subinhibitory concentration of ciprofloxacin was added to the medium when cells were in the exponential growth phase. The bars represent a change in *aciT* gene expression compared with an untreated control after 1 h of growth in the presence of ciprofloxacin. Error bars show the standard errors from at least 2 biological and 4 technical replicates.

bacteria in the family *Moraxellaceae* (Fig. 3A), suggesting the possibility that ABUW_0098 may interfere with FtsZ formation of Z rings. Sequence analysis (33) indicates that the protein encoded by ABUW_0098 has three predicted transmembrane α-helices and is most likely localized to the cell membrane (Fig. 3B). We used quantitative real-time PCR (qRT-PCR) analyses to determine whether ciprofloxacin induces the gene expression of *aciT* orthologs in other *A. baumannii* strains, including ACICU, AYE, ATCC 17978, ATCC 19606, and D1279779. Each strain was treated with subinhibitory concentrations of ciprofloxacin for 1 h. We found that ciprofloxacin caused a strong induction of *aciT* in ciprofloxacin-resistant *A. baumannii* strains ACICU and AYE ($\log_2$ fold change of >2). In contrast, expression of *aciT* in ciprofloxacin-susceptible *A. baumannii* strain ATCC 17978 was moderately induced ($\log_2$ fold change of 1.5) and weakly induced in ATCC 19606 ($\log_2$ fold change of 1) and D1279779 ($\log_2$ fold change of 1.05) (Fig. 3C). In a recent study with ATCC 17978, the supplementary transcriptomic data presented showed that expression of *aciT* (A1S_3385) was greater than 2-fold at $\log_2$ when exposed to ciprofloxacin, and introduction of a single *gyrA* resistance allele in ATCC 17978 resulted in ciprofloxacin-induced expression of *aciT* to be greater than 3-fold at $\log_2$ (17). The variations in ciprofloxacin-induced expression of *aciT* could be attributed to many factors, which include the concentration of antibiotic used, variations at the strain level, or differences in *aciT* induction between ciprofloxacin-susceptible and -resistant strains.

The data presented in this study demonstrate that a previously uncharacterized gene, ABUW_0098, is important for tolerance to ciprofloxacin in *A. baumannii*. We have named ABUW_0098 the *Acinetobacter* ciprofloxacin tolerance (*aciT*) gene. In *Acinetobacter* species, which lack the cell division inhibitor SulA, we propose that AciT may fulfil an equivalent

functional role. The discovery of *aciT* demonstrates the significant value of genome-wide expression studies to identify novel drug targets and tolerance factors in multidrug-resistant bacteria.

MATERIALS AND METHODS

Bacterial strains, plasmids, reagents, and growth media. The bacterial strains used in this study include *A. baumannii* strains AB5075-UW, ATCC 17978, ACICU, and AYE and *E. coli* strain HST08. AB5075-UW and its transposon mutants were obtained from the Manoil laboratory three-allele collection (20). All bacterial cultures were maintained at 37°C in MH broth with shaking (200 rpm) unless specified otherwise. *E. coli* strain HST08 was used as a host for plasmid propagation. The parent plasmid used in this study was pVRL1Z (27). Strains carrying pVRL1Z plasmid variants were cultured in low-salt LB medium containing 25 μg/ml Zeocin for *E. coli* and 300 μg/ml for *A. baumannii*.

Gene cloning, PCR, and complementation. The coding region of ABUW_0098 with its predicted endogenous promoter (450-bp upstream region of ABUW_0098) was purchased from Integrated DNA Technologies (see Table S2 in the supplemental material). This gene fragment was cloned in the pVRL1Z plasmid, using EcoRI and NotI restriction enzymes. Insertion of the gene fragment in the plasmid was confirmed via PCR followed by Sanger sequencing using universal M13 forward and reverse primers (see Table S1 in the supplemental material). Disruption of the ABUW_0098 gene in the mutant strain AB00272 was confirmed by gene-specific primers spanning the ABUW_0098 gene (Table S1).

Antibiotic susceptibility assays. Susceptibility assays were conducted in Mueller-Hinton (MH) broth using the both microdilution method as described previously (34).

Ciprofloxacin growth rate assay. Overnight cultures of individual AB5075-UW constructs were diluted (1/100) in MH broth and grown in 96-well plates at 37°C with shaking at 200 rpm in the PHERAstar FSX (BMG Labtech, Germany), with optical density (OD) measurements recorded every 6 min. Once the cultures reached an exponential phase of ~0.5 at the optical density at 600 nm (OD_{600}), the appropriate concentration of ciprofloxacin was added, and cultures were allowed to grow continuously for an additional 4 h 20 min with regular OD measurements every 6 min.

Microscopic imaging. Overnight cultures of individual strains were diluted (1/100) in MH broth and grown at 37°C with shaking at 200 rpm until cells reached the exponential phase at an OD_{600} of ~0.5. Approximately 50 μl of cells was harvested at this point and fixed (3% glutaraldehyde–0.1 M phosphate buffer solution). Cultures were then treated with 31.25 μg/ml ciprofloxacin and allowed to grow for a further 4 h. During this time, cells were harvested at 1, 2, and 4 h and fixed immediately. Fixed cells were immobilized on poly-L-lysine-coated cover slides. Imaging was performed with an Olympus FV3000 confocal microscope (Olympus, Tokyo, Japan) using FluoView software (Olympus, Tokyo, Japan). The differential interference contrast (DIC) image was obtained by a 405-nm laser and transmitted detector with a 100× oil immersion objective (Olympus UApo N, 1.49 NA, infinity-corrected 0.13- to 0.19-mm working distance/FN22). Each image was saved in the OIF file format. Image processing was done using ImageJ software.

Cell treatments. *A. baumannii* AB5075-UW cells were grown overnight in 5 ml MH broth. MH broth was reseeded with cultures at 1:100, and the cultures were grown for ~2 h at 37°C to an OD_{600} of 0.6 with shaking (200 rpm) in 100-ml cultures. Three samples were treated with 31.25 μg/ml ciprofloxacin, whereas the other three samples were not treated and used as the control. Cultures were grown for a further 1 h, at which point they were split into a 30-ml culture for RNA isolation and a 70-ml culture for protein isolation.

Protein extraction and analysis. Bacterial cells were prepared for proteomic analysis as detailed in reference 35. For protein extraction, cells were first washed with phosphate-buffered saline (PBS; pH 7.4), resuspended in lysis buffer (50 mM Tris-HCl [pH 8.8], 1% SDS [wt/vol], 8 M urea, EDTA-free protease inhibitor cocktail), and lysed by bead beating. Protein disulfide bonds were reduced using dithiothreitol (DTT) and alkylated using iodoacetamide (IAA). Subsequently, samples were desalted using methanol-chloroform precipitation and redissolved in 50 mM Tris-HCl (pH 8.8)–8 M urea. After the pellet was dissolved, samples were diluted with 50 mM Tris-HCl (pH 8.8) to reduce the concentration of urea to 1.6 M. The bicinchoninic acid (BCA) assay was performed as per manufacturer's instructions to determine the protein concentrations.

An equal amount of protein sample was digested with LysC protease at 37°C overnight, followed by proteolysis with trypsin at 37°C. The digests were desalted using a C_{18} reverse-phase spin column, and samples were divided into two fractions: one for the generation of the reference ion library, using information-dependent acquisition mass spectrometry (IDA-MS), and another for label-free relative quantification, using SWATH-MS (19).

To create a reference peptide ion library, first, a pool of tryptic peptides was generated by combining a fraction of sample from all the biological conditions. Peptides were prefractionated using strong cation-exchange chromatography and high-pH reverse-phase chromatography. Fractionated peptides were separated by reverse-phase (RP) liquid chromatography using a nano-liquid chromatography (nano-LC) system and detected in a TripleTOF 5600 (SCIEX) mass spectrometer operated in IDA-MS mode. The peptide ion library was generated by searching IDA-MS data against the *A. baumannii* (strain AB5075-UW) reference protein sequence (3,839 sequences [source, Uniprot]), using the ProteinPilot 5.0 search engine with the Paragon algorithm at a 1% false-discovery rate.

For label-free relative quantification of proteins using SWATH-MS, equal amounts of peptides of the individual samples were separated over a reverse-phase linear gradient of 5.5 to 33% of solvent B (90% [vol/vol] acetonitrile–0.1% [vol/vol] formic acid) over 60 min at a flow rate of 600 nl/min using a nano-LC system in conjunction with a TripleTOF 5600 (SCIEX). The mass spectrometer was operated in positive nanoflow electrospray analysis mode, and SWATH-MS acquisition was performed in a 60-variable *m/z*

window method over an *m/z* range of 400 to 1,250, selected based on the distribution of intensities of the precursor *m/z* values in the IDA data sets. Collision energies were calculated for 2+ precursors with *m/z* values of the lowest *m/z* + 20% for each window width, and a collision energy spread of 5 eV was used.

The reference ion library was imported into PeakView software 2.1 using the SWATH MicroApp 2.0 (SCIEX) and matched against SWATH-MS data from individual replicates. Cumulative protein areas from extracted ion chromatograms, representing the quantitative value of individual proteins, were exported to Excel for further analysis.

RNA extraction and analysis. Cells for RNA extraction was centrifuged immediately and suspended in QIAzol (Qiagen). RNA extraction was carried out using the miRNeasy RNA extraction kit from Qiagen, as per the manufacturer's instructions. DNA was eliminated using the Turbo DNase kit (Ambion) as per the manufacturer's instructions. RNA integrity was determined using the Agilent Bioanalyzer, followed by rRNA depletion using the Ribo-Zero rRNA removal kit for Gram-negative bacteria (Illumina, Inc., USA). The cDNA library was generated using the TruSeq stranded total RNA sample preparation kit (Illumina, Inc., USA) and samples sequenced on an Illumina HiSeq4000 platform. This yielded 20 million 100-bp paired-end (PE) reads per sample approximately. The EDGE-pro (Estimated Degree of Gene Expression in Prokaryotic Genomes) pipeline was used to align reads to the *A. baumannii* AB5075-UW reference genome (GenBank accession no. CP008706.1), using Bowtie2, and to generate the raw read counts.

DNA extraction and analysis. MH broth was reseeded with *A. baumannii* AB5075-UW cells at 1:100 from overnight cultures, and the cultures were grown for ~2 h at 37°C with shaking (200 rpm). Cultures at an OD_{600} of 0.6 with and without the 31.25-μg/ml ciprofloxacin treatment were grown for 1 h at 37°C with shaking. Two biological replicates were prepared. The total DNA of each sample was extracted using the DNeasy UltraClean Microbial kit, following the manufacturer's instructions. Geneious 2020.2.4 was used to map the raw sequencing reads to the AB5075-UW genome available from the NCBI database (NZ_CP008706.1).

Quantitative real-time PCR analyses of *aciT* expression. *A. baumannii* strains ACICU, AYE, and ATCC 17978 were grown as described above for AB5075-UW RNA and protein extraction. Cultures at an OD_{600} of 0.6 with and without the subinhibitory concentration of ciprofloxacin (15.625 μg/ml for ACICU, 31.25 μg/ml for AYE, and 0.125 μg/ml for ATCC 17978) (Fig. S1C and D) were grown for 1 h at 37°C with shaking. Total RNA was isolated using the miRNeasy RNA extraction kit from Qiagen, as per the manufacturer's instructions. DNA was eliminated using the Turbo DNase kit (Ambion) as per the manufacturer's instructions. Reverse transcription and qRT-PCR were performed using the Roche KAPA SYBR Fast one-step qRT-PCR kit, as per manufacturer's instructions The *rpoB* gene encoding the beta subunit of RNA polymerase was used as an internal reference control.

Data analysis. All statistical analysis and data visualization were performed with the R program (v.4.0.0), unless specified otherwise. The DESeq2 package (v.1.28.1), based on the negative binomial generalized linear model with default settings, was used to estimate the differential expression for transcriptomics and proteomics. Differential expression was generated by comparing treated samples against untreated samples. The Benjamini-Hochberg adjustment was used to select differentially expressed genes.

Data availability. The DNA and RNA sequence data that support the findings of this study have been deposited in the NCBI Sequence Read Archive (SRA) under accession no. PRJNA673281.

SUPPLEMENTAL MATERIAL

Supplemental material is available online only.

SUPPLEMENTAL FILE 1, PDF file, 0.6 MB.

SUPPLEMENTAL FILE 2, XLSX file, 0.9 MB.

ACKNOWLEDGMENTS

We thank Bart Eijkelkamp for providing the pVRL1Z plasmids used in this study and Liam Elbourne for advice on data analysis.

This work was supported by an Australian Government Research Training Program scholarship (RTP) to V.N. and NHMRC (National Health and Medical Research Council) project grants APP1120298 to I.T.P. and K.A.H. I.T.P. is supported by ARC (Australian Research Council) Laureate Fellowship FL140100021. K.A.H. is supported by ARC Future Fellowship FT180100123.

The authors have no conflicts of interest to declare.

REFERENCES

1. Bax BD, Chan PF, Eggleston DS, Fosberry A, Gentry DR, Gorrec F, Giordano I, Hann MM, Hennessy A, Hibbs M, Huang J, Jones E, Jones J, Brown KK, Lewis CJ, May EW, Saunders MR, Singh O, Spitzfaden CE, Shen C, Shillings A, Theobald AJ, Wohlkonig A, Pearson ND, Gwynn MN. 2010. Type IIA topoisomerase inhibition by a new class of antibacterial agents. Nature 466:935–940. https://doi.org/10.1038/nature09197.
2. Willmott CJ, Critchlow SE, Eperon IC, Maxwell A. 1994. The complex of DNA gyrase and quinolone drugs with DNA forms a barrier to transcription by RNA polymerase. J Mol Biol 242:351–363. https://doi.org/10.1006/jmbi.1994.1586.
3. Little JW, Edmiston SH, Pacelli LZ, Mount DW. 1980. Cleavage of the Escherichia coli lexA protein by the recA protease. Proc Natl Acad Sci U S A 77:3225–3229. https://doi.org/10.1073/pnas.77.6.3225.
4. Butala M, Zgur-Bertok D, Busby SJ. 2009. The bacterial LexA transcriptional repressor. Cell Mol Life Sci 66:82–93. https://doi.org/10.1007/s00018-008-8378-6.

5. Little JW, Mount DW. 1982. The SOS regulatory system of Escherichia coli. Cell 29:11–22. https://doi.org/10.1016/0092-8674(82)90085-x.
6. Bi E, Lutkenhaus J. 1993. Cell division inhibitors SulA and MinCD prevent formation of the FtsZ ring. J Bacteriol 175:1118–1125. https://doi.org/10.1128/jb.175.4.1118-1125.1993.
7. Ryan DM, Monsey D. 1981. Bacterial filamentation and in vivo efficacy: a comparison of several cephalosporins. J Antimicrob Chemother 7:57–63. https://doi.org/10.1093/jac/7.1.57.
8. Stackhouse RR, Faith NG, Kaspar CW, Czuprynski CJ, Wong AC. 2012. Survival and virulence of Salmonella enterica serovar enteritidis filaments induced by reduced water activity. Appl Environ Microbiol 78:2213–2220. https://doi.org/10.1128/AEM.06774-11.
9. Justice SS, Hunstad DA, Seed PC, Hultgren SJ. 2006. Filamentation by Escherichia coli subverts innate defenses during urinary tract infection. Proc Natl Acad Sci U S A 103:19884–19889. https://doi.org/10.1073/pnas.0606329104.
10. Bos J, Zhang Q, Vyawahare S, Rogers E, Rosenberg SM, Austin RH. 2015. Emergence of antibiotic resistance from multinucleated bacterial filaments. Proc Natl Acad Sci U S A 112:178–183. https://doi.org/10.1073/pnas.1420702111.
11. Hare JM, Perkins SN, Gregg-Jolly LA. 2006. A constitutively expressed, truncated umuDC operon regulates the recA-dependent DNA damage induction of a gene in Acinetobacter baylyi strain ADP1. Appl Environ Microbiol 72:4036–4043. https://doi.org/10.1128/AEM.02774-05.
12. Robinson A, Brzoska AJ, Turner KM, Withers R, Harry EJ, Lewis PJ, Dixon NE. 2010. Essential biological processes of an emerging pathogen: DNA replication, transcription, and cell division in Acinetobacter spp. Microbiol Mol Biol Rev 74:273–297. https://doi.org/10.1128/MMBR.00048-09.
13. Hooper DC. 1999. Mechanisms of fluoroquinolone resistance. Drug Resist Updat 2:38–55. https://doi.org/10.1054/drup.1998.0068.
14. Jacoby GA. 2005. Mechanisms of resistance to quinolones. Clin Infect Dis 41(Suppl 2):S120–S126. https://doi.org/10.1086/428052.
15. Vila J, Ruiz J, Goni P, Jimenez de Anta T. 1997. Quinolone-resistance mutations in the topoisomerase IV parC gene of Acinetobacter baumannii. J Antimicrob Chemother 39:757–762. https://doi.org/10.1093/jac/39.6.757.
16. Vila J, Ruiz J, Goni P, Marcos A, Jimenez de Anta T. 1995. Mutation in the gyrA gene of quinolone-resistant clinical isolates of Acinetobacter baumannii. Antimicrob Agents Chemother 39:1201–1203. https://doi.org/10.1128/aac.39.5.1201.
17. Geisinger E, Vargas-Cuebas G, Mortman NJ, Syal S, Dai Y, Wainwright EL, Lazinski D, Wood S, Zhu Z, Anthony J, van Opijnen T, Isberg RR. 2019. The landscape of phenotypic and transcriptional responses to ciprofloxacin in Acinetobacter baumannii: acquired resistance alleles modulate drug-induced SOS response and prophage replication. mBio 10:e01127-19. https://doi.org/10.1128/mBio.01127-19.
18. Jacobs AC, Thompson MG, Black CC, Kessler JL, Clark LP, McQueary CN, Gancz HY, Corey BW, Moon JK, Si Y, Owen MT, Hallock JD, Kwak YI, Summers A, Li CZ, Rasko DA, Penwell WF, Honnold CL, Wise MC, Waterman PE, Lesho EP, Stewart RL, Actis LA, Palys TJ, Craft DW, Zurawski DV. 2014. AB5075, a highly virulent isolate of Acinetobacter baumannii, as a model strain for the evaluation of pathogenesis and antimicrobial treatments. mBio 5:e01076-14. https://doi.org/10.1128/mBio.01076-14.
19. Gillet LC, Navarro P, Tate S, Rost H, Selevsek N, Reiter L, Bonner R, Aebersold R. 2012. Targeted data extraction of the MS/MS spectra generated by data-independent acquisition: a new concept for consistent and accurate proteome analysis. Mol Cell Proteomics 11:O111.016717. https://doi.org/10.1074/mcp.O111.016717.
20. Gallagher LA, Ramage E, Weiss EJ, Radey M, Hayden HS, Held KG, Huse HK, Zurawski DV, Brittnacher MJ, Manoil C. 2015. Resources for genetic and genomic analysis of emerging pathogen Acinetobacter baumannii. J Bacteriol 197:2027–2035. https://doi.org/10.1128/JB.00131-15.
21. Love MI, Huber W, Anders S. 2014. Moderated estimation of fold change and dispersion for RNA-seq data with DESeq2. Genome Biol 15:550–558. https://doi.org/10.1186/s13059-014-0550-8.
22. Bearson BL, Brunelle BW. 2015. Fluoroquinolone induction of phage-mediated gene transfer in multidrug-resistant Salmonella. Int J Antimicrob Agents 46:201–204. https://doi.org/10.1016/j.ijantimicag.2015.04.008.
23. Goerke C, Koller J, Wolz C. 2006. Ciprofloxacin and trimethoprim cause phage induction and virulence modulation in Staphylococcus aureus. Antimicrob Agents Chemother 50:171–177. https://doi.org/10.1128/AAC.50.1.171-177.2006.
24. Rosenfeld N, Bouchier C, Courvalin P, Perichon B. 2012. Expression of the resistance-nodulation-cell division pump AdeIJK in Acinetobacter baumannii is regulated by AdeN, a TetR-type regulator. Antimicrob Agents Chemother 56:2504–2510. https://doi.org/10.1128/AAC.06422-11.
25. Damier-Piolle L, Magnet S, Bremont S, Lambert T, Courvalin P. 2008. AdeIJK, a resistance-nodulation-cell division pump effluxing multiple antibiotics in Acinetobacter baumannii. Antimicrob Agents Chemother 52:557–562. https://doi.org/10.1128/AAC.00732-07.
26. Couturier E, Rocha EP. 2006. Replication-associated gene dosage effects shape the genomes of fast-growing bacteria but only for transcription and translation genes. Mol Microbiol 59:1506–1518. https://doi.org/10.1111/j.1365-2958.2006.05046.x.
27. Lucidi M, Runci F, Rampioni G, Frangipani E, Leoni L, Visca P. 2018. New shuttle vectors for gene cloning and expression in multidrug-resistant Acinetobacter species. Antimicrob Agents Chemother 62:e02480-17. https://doi.org/10.1128/AAC.02480-17.
28. Wickens HJ, Pinney RJ, Mason DJ, Gant VA. 2000. Flow cytometric investigation of filamentation, membrane patency, and membrane potential in Escherichia coli following ciprofloxacin exposure. Antimicrob Agents Chemother 44:682–687. https://doi.org/10.1128/aac.44.3.682-687.2000.
29. Geisinger E, Mortman NJ, Dai Y, Cokol M, Syal S, Farinha A, Fisher DG, Tang AY, Lazinski DW, Wood S, Anthony J, van Opijnen T, Isberg RR. 2020. Antibiotic susceptibility signatures identify potential antimicrobial targets in the Acinetobacter baumannii cell envelope. Nat Commun 11:4522. https://doi.org/10.1038/s41467-020-18301-2.
30. Schoemaker JM, Gayda RC, Markovitz A. 1984. Regulation of cell division in Escherichia coli: SOS induction and cellular location of the sulA protein, a key to lon-associated filamentation and death. J Bacteriol 158:551–561. https://doi.org/10.1128/JB.158.2.551-561.1984.
31. Huisman O, D'Ari R, George J. 1980. Further characterization of sfiA and sfiB mutations in Escherichia coli. J Bacteriol 144:185–191. https://doi.org/10.1128/JB.144.1.185-191.1980.
32. Chen Y, Milam SL, Erickson HP. 2012. SulA inhibits assembly of FtsZ by a simple sequestration mechanism. Biochemistry 51:3100–3109. https://doi.org/10.1021/bi201669d.
33. Sonnhammer EL, von Heijne G, Krogh A. 1998. A hidden Markov model for predicting transmembrane helices in protein sequences. Proc Int Conf Intell Syst Mol Biol 6:175–182.
34. Wiegand I, Hilpert K, Hancock RE. 2008. Agar and broth dilution methods to determine the minimal inhibitory concentration (MIC) of antimicrobial substances. Nat Protoc 3:163–175. https://doi.org/10.1038/nprot.2007.521.
35. Kamath KS, Krisp C, Chick J, Pascovici D, Gygi SP, Molloy MP. 2017. Pseudomonas aeruginosa proteome under hypoxic stress conditions mimicking the cystic fibrosis lung. J Proteome Res 16:3917–3928. https://doi.org/10.1021/acs.jproteome.7b00561.
36. Krogh A, Larsson B, von Heijne G, Sonnhammer EL. 2001. Predicting transmembrane protein topology with a hidden Markov model: application to complete genomes. J Mol Biol 305:567–580. https://doi.org/10.1006/jmbi.2000.4315.

Chapter 8: Rapid microevolution of biofilm cells in response to antibiotics

Published as: Penesyan, A., Nagy, S. S., Kjelleberg, S., Gillings, M. R., & Paulsen, I. T. (2019). Rapid microevolution of biofilm cells in response to antibiotics. *npj Biofilms and Microbiomes*, 5, 1-14. [34]. https://doi.org/10.1038/s41522-019-0108-3.

npj | Biofilms and Microbiomes

www.nature.com/npjbiofilms

ARTICLE OPEN

Rapid microevolution of biofilm cells in response to antibiotics

Anahit Penesyan[1,2], Stephanie S. Nagy[1], Staffan Kjelleberg[3,4,5], Michael R. Gillings[6] and Ian T. Paulsen[1]*

Infections caused by *Acinetobacter baumannii* are increasingly antibiotic resistant, generating a significant public health problem. Like many bacteria, *A. baumannii* adopts a biofilm lifestyle that enhances its antibiotic resistance and environmental resilience. Biofilms represent the predominant mode of microbial life, but research into antibiotic resistance has mainly focused on planktonic cells. We investigated the dynamics of *A. baumannii* biofilms in the presence of antibiotics. A 3-day exposure of *A. baumannii* biofilms to sub-inhibitory concentrations of antibiotics had a profound effect, increasing biofilm formation and antibiotic resistance in the majority of biofilm dispersal isolates. Cells dispersing from biofilms were genome sequenced to identify mutations accumulating in their genomes, and network analysis linked these mutations to their phenotypes. Transcriptomics of biofilms confirmed the network analysis results, revealing novel gene functions of relevance to both resistance and biofilm formation. This approach is a rapid and objective tool for investigating resistance dynamics of biofilms.

npj Biofilms and Microbiomes (2019)5:34 ; https://doi.org/10.1038/s41522-019-0108-3

INTRODUCTION

Acinetobacter baumannii is a Gram-negative pathogen found in hospitals worldwide.[1] It is responsible for opportunistic infections of the bloodstream, urinary tract, and other soft tissues, and can account for up to 20% of infections in Intensive Care Units, causing serious morbidity and mortality.[1,2] *Acinetobacter baumannii* belongs to a group of six pathogens responsible for many multidrug-resistant (MDR) nosocomial infections (the ESKAPE pathogens: *Enterococcus faecium*, *Staphylococcus aureus*, *Klebsiella pneumoniae*, *Acinetobacter baumannii*, *Pseudomonas aeruginosa*, and *Enterobacter* spp.).[3] In 2017, *A. baumannii* was listed at the top of the highest priority "Critical" group of antibiotic-resistant pathogens identified by the World Health Organization as in need of further research.[4]

The success of this pathogen is due to a combination of cellular resistance mechanisms and the additional protection provided by its biofilm lifestyle.[5] *Acinetobacter baumannii* has an arsenal of tools to defend against antimicrobials, including classical mechanisms of antibiotic resistance, such as enzymatic inactivation of antibiotics, target and membrane modifications, and active export of drugs via membrane-localized drug efflux transporters.[6–8] These mechanisms have been extensively studied in planktonically grown *A. baumannii*. Transcriptomic and mutational studies under antibiotic challenge using *A. baumannii* planktonic cultures identified mutations and differentially expressed genes directly linked with these known mechanisms of resistance to particular antibiotics.[9,10]

Resistance and pathogenicity of *A. baumannii* is enhanced by its ability to form biofilms.[5] *Acinetobacter baumannii* biofilms can form on various surfaces, including medical devices, where they are persistent sources of contamination and infection.[11] The National Institutes of Health (NIH) estimates that biofilms account for over 80% of microbial infections in the body.[12] Biofilms are a major obstacle to treatment because their cells can display up to a 1000-fold increase in antibiotic resistance compared to planktonic cells.[13,14] Biofilms provide additional resistance[5] (also referred to as "biofilm tolerance"[15–17]) via biofilm-specific mechanisms such as the shielding effect of the biofilm matrix that leads to restricted penetration of antimicrobials,[18] the slower growth rate in deep layers of biofilms,[19] and the presence of persister cells.[20]

Biofilms are recognized as the predominant form of bacterial life, with the majority of bacteria living as biofilm communities in diverse environments, including within host organisms.[15,21] Nevertheless, compared to the wealth of data collected using planktonic cultures during the history of microbiological research, the biofilm mode of life remains largely underexplored, leading to a growing interest in the ecology of microbial biofilms, and the factors involved in biofilm development and survival. In particular, understanding the processes that occur in biofilms when exposed to antibiotics is important, because this could give us insight into how advantageous phenotypes arise, and help identify the genomic basis of these phenotypes.

The ability of bacteria to adapt to new environmental conditions arises from their short generation times and genomic variability, allowing rapid emergence of favorable mutations. Methods for investigating the effect of mutations on bacterial phenotype, such as knock-out strains and transposon mutagenesis, are often time-consuming, involve extensive sample manipulation, and often focus on single gene targets. In contrast, whole genome sequencing can rapidly identify suites of naturally occurring mutations, and also reveal potential synergy between different mutations.

This study investigated how genetic and phenotypic diversity was generated within biofilms of a highly virulent strain of *A. baumannii*. We assessed the transcription profiles of biofilms grown in the presence and absence of sub-inhibitory concentration of antibiotics ciprofloxacin and tetracycline, and examined the genetic consequences of biofilm growth in the presence of antibiotics, identifying de novo mutations by using whole genome sequencing. Thus, we were able to link phenotypes with genotypes and with population level gene expression patterns in one experimental analysis, providing a holistic assessment of

[1]Department of Molecular Sciences, Faculty of Science and Engineering, Macquarie University, Sydney, NSW 2109, Australia. [2]School of Chemical Engineering, University of New South Wales, Sydney, NSW 2052, Australia. [3]Singapore Centre for Environmental Life Sciences Engineering, 60 Nanyang Drive, SBS-01N-27, Singapore 637551, Singapore. [4]School of Biological Sciences, Nanyang Technological University, 60 Nanyang Drive, Singapore 637551, Singapore. [5]School of Biological, Earth and Environmental Sciences, University of New South Wales, Sydney, NSW 2052, Australia. [6]Department of Biological Sciences, Faculty of Science and Engineering, Macquarie University, Sydney, NSW 2109, Australia. *email: ian.paulsen@mq.edu.au

Published in partnership with Nanyang Technological University

npj nature partner journals

processes that occur in biofilms, and, subsequently, drive genomic changes under the exposure to sub-inhibitory concentration of antibiotics.

To assess changes in antibiotic susceptibility, the MIC (minimum inhibitory concentration) levels of biofilm dispersal cells were assessed against the antibiotics in a broth microdilution assay, and compared to the MIC levels of initial planktonic cultures. The MIC broth microdilution assay tests the level of antibiotic resistance in the planktonic state, that is, the level of resistance determined by classical "cellular" antibiotic resistance mechanisms[5] and does not capture the additional resistance provided by biofilm mode of life. Additional resistance provided by the biofilm lifestyle ("biofilm tolerance") is directly related to the ability to form biofilms,[5] which was tested separately. Thus, by using the broth microdilution MIC assay (to test "cellular" level resistance), and biofilm formation assays (to assess the ability to form biofilms), we were able to separate these two phenotypes, both of which can significantly contribute to the overall resilience of biofilms.

Acinetobacter baumannii is intrinsically resistant to many antibiotics, and consequently ciprofloxacin and tetracycline were used in this study, due to the relatively low level of resistance of *A. baumannii* AB5075-UW to these two antibiotics. These antibiotics are chemically diverse and belong to different classes, with different modes of actions. Ciprofloxacin (fluoroquinolone) functions via inhibiting DNA gyrase and topoisomerases involved in transcription, thereby inhibiting cell division.[22] Tetracycline (tetracycline class) inhibits protein synthesis by binding to the 30S subunit of microbial ribosomes.[23] Earlier studies also demonstrated that both ciprofloxacin and tetracycline are able to permeate biofilms,[18,24] which is important to maximize the exposure of biofilm cells to antibiotics.

RESULTS AND DISCUSSION

Understanding the dynamics of biofilms exposed to antibiotics is important for developing control strategies and for tracking the evolution of resistance. With this in mind, we exposed biofilms of a highly virulent clinical strain of *A. baumannii*, AB5075-UW, to sub-inhibitory concentrations of two antibiotics: ciprofloxacin and tetracycline. Phenotypic and genomic analyses were undertaken on cells dispersing from biofilms, while the biofilms were investigated using transcriptomics. This multipronged approach examined processes occurring in biofilm communities, reflected in differential gene expression, while simultaneously examining genomic changes in cells dispersing from biofilms.

Ability to form biofilms

Biofilm formation can increase the resistance/tolerance of biofilms by orders of magnitude. Therefore, the ability to form biofilms has serious implications for antibiotic therapy. Biofilm formation was assessed using spectrophotometric quantification of biofilms stained with crystal violet (CV). Compared to the initial planktonic isolates, biofilm effluent isolates (with or without antibiotic exposure) showed increased biofilm formation capability (Fig. 1). Many tetracycline-exposed biofilm effluent isolates showed an additional increase in biofilm formation. Increased biofilm formation in the presence of tetracycline has been reported in other bacteria[25,26] and can complicate treatment of biofilm-related infections, because the treatment itself promotes biofilm formation and enhances biofilm-specific resistance mechanisms (also known as "biofilm tolerance").[5] Here we demonstrate that these phenotypes can be fixed within populations of biofilm dispersal cells, which then display enhanced biofilm formation even after treatment has ceased.

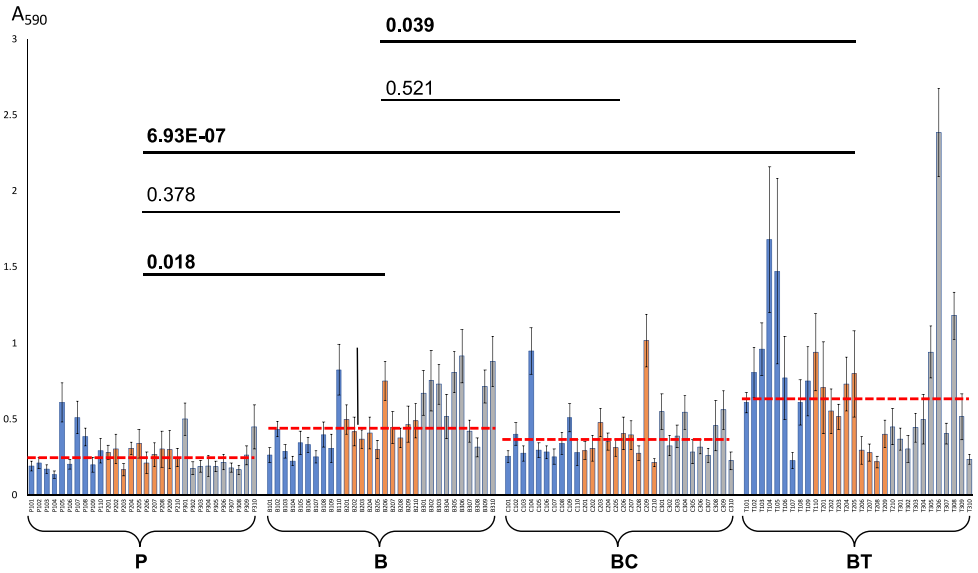

Fig. 1 Results of biofilm formation assay. *X*-axis: 30 planktonic isolates P101–P310 (P samples), 30 antibiotic-free biofilm effluent isolates B101–B310 (B samples), 30 ciprofloxacin-exposed biofilm effluent isolates C101–C310 (BC samples), and 30 tetracycline-exposed biofilm effluent isolates T101–T310 (BT samples). Each sample type includes 10 isolates from each biological replicate 1 (blue bars), biological replicate 2 (orange bars), and biological replicate 3 (gray bars). The *Y*-axis represents corresponding absorbance values of 5-fold diluted crystal violet extracts at 590 nm (A_{590}). Error bars represent standard deviations between 24 technical replicates. The average value for each sample type is indicated by red dashed lines. *P* values denote differences between sample pairs based on nested mixed-factor ANOVA test followed by Turkey's HSD post hoc test. *P* values showing statistically significant ($p < 0.05$) differences are presented in bold

Cells from ciprofloxacin-exposed biofilms showed no net change in biofilm formation in comparison to those from antibiotic-free biofilms and from planktonic cultures (Fig. 1). Some individual isolates from the ciprofloxacin and tetracycline treatments were outliers, exhibiting 5 to 10 times higher biofilm formation than planktonic cells (Fig. 1). This strongly suggested the accumulation of mutation(s) that enhanced biofilm formation.

Evolution of antibiotic resistance

Cells recovered from antibiotic-exposed biofilms showed consistent increases in antibiotic resistance in the MIC assay, above their initial MICs (Fig. 2). Out of 30 random isolates recovered from ciprofloxacin-exposed biofilms, the overwhelming majority (93%) showed increased resistance towards ciprofloxacin (2-fold or more increase in the MIC), with most (76%) showing at least a 4-fold increase in ciprofloxacin resistance. Many ciprofloxacin-exposed isolates (80%) also showed increased resistance to tetracycline, with one-third of the isolates showing high levels of resistance (4-fold and above increase in the MIC) (Fig. 2).

Similar effects were also observed in cells from tetracycline-exposed biofilms. More than half (53%) of the isolates displayed at least a 2-fold increase in resistance to tetracycline, with eight exhibiting high-level resistance, at 4-fold increases in the MIC or more. Nine of the tetracycline-exposed isolates also gained increased resistance to ciprofloxacin, in some cases exhibiting a 4-fold increase in the MIC. However, the net difference in average ciprofloxacin MIC levels between the set of 30 tetracycline-exposed isolates and the initial planktonic isolates was not statistically significant (Fig. 2), suggesting that despite an increased ciprofloxacin resistance observed in several isolates, tetracycline does not lead to a significant net increase in cross-resistance towards ciprofloxacin. In contrast, exposure of biofilms to ciprofloxacin led to a statistically significant net increase in the MIC levels for both antibiotics in cells dispersed from these biofilms (Fig. 2).

To further investigate whether biofilm-derived isolates gained cross-resistance against other antibiotics, the isolates were tested for their susceptibility to colistin and erythromycin, both of which differ structurally and functionally from antibiotics to which the biofilms were exposed. Our choice of antibiotics was limited due to the innate resistance of AB5075-UW to a broad range of antibiotics. Many of the isolates that showed increased resistance towards ciprofloxacin and/or tetracycline were also resistant towards erythromycin (Supplementary Fig. 1). This suggests the fixation of mutations for MDR in the resistant isolates. Significant increase in the levels of erythromycin MIC was observed in the population of ciprofloxacin-exposed isolates compared to initial planktonic isolates and compared to antibiotic-free biofilms (Supplementary Fig. 1). Similar pleiotropic effects have been observed in studies with planktonic *Escherichia coli*,[27,28] whereas our study demonstrates that these effects also extend to biofilm communities. However, for tetracycline-exposed isolates, no statistically significant net difference was observed overall between the erythromycin MIC levels of tetracycline-exposed isolates, antibiotic-free biofilms, and initial planktonic isolates (Supplementary Fig. 1), reinforcing the fact that tetracycline exposure had a limited effect on the development of cross-resistance in the population of antibiotic-exposed cells. No significant changes were observed in the levels of colistin resistance between the treatments, although sporadic emergence of resistance was observed.

Unexpectedly, more than two-thirds of cells recovered from antibiotic-free biofilms also developed a moderate increase in tetracycline resistance, and, overall, exhibited a statistically significant increase in net tetracycline resistance compared to planktonic isolates (p value = 0.013) (Fig. 2). Interestingly, as was observed in the biofilm formation assay (Fig. 1), tetracycline exposure also led to enhanced biofilm formation seen in many tetracycline-exposed isolates, and in a slight increase in the net biofilm formation among the 30 tetracycline-exposed isolates, compared to isolates from antibiotic-free biofilms (p value =

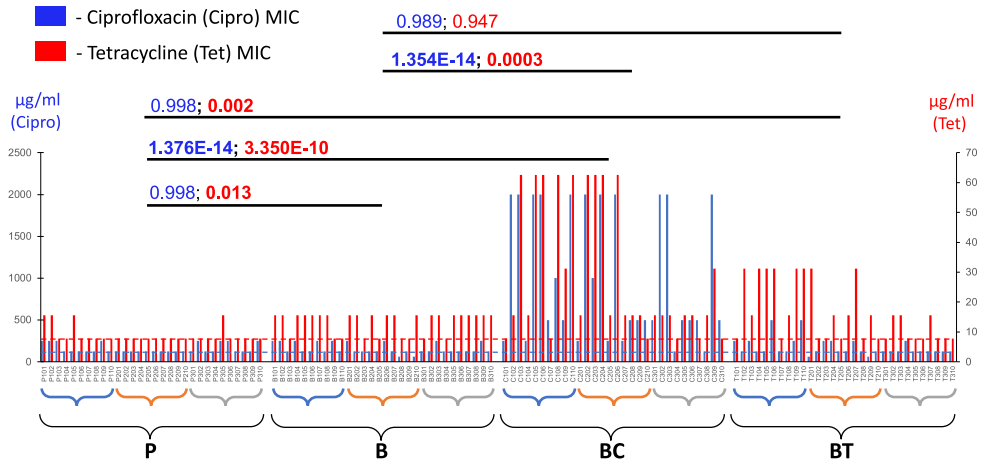

Fig. 2 Results of the minimum inhibitory concentration (MIC) antibiotic susceptibility assay. *X*-axis: 30 planktonic isolates P101–P310 (P samples), 30 antibiotic-free biofilm effluent isolates B101–B310 (B samples), 30 ciprofloxacin-exposed biofilm effluent isolates C101–C310 (BC samples), and 30 tetracycline-exposed biofilm effluent isolates T101–T310 (BT samples). Each sample type includes 10 isolates from each biological replicate 1 (blue parentheses), biological replicate 2 (orange parentheses), and biological replicate 3 (gray parentheses). Blue bars represent the MIC levels of ciprofloxacin (in µg/ml, measured on the primary *Y*-axis on the left), and red bars—the MIC levels of tetracycline (in µg/ml, measured on the right-hand *Y*-axis). Consensus MIC levels in the initial planktonic cultures are shown by the horizontal blue (for ciprofloxacin MIC) and red (for tetracycline MIC) dashed lines. *P* values denote differences between sample pairs based on nested mixed factor ANOVA test followed by Turkey's HSD post hoc test. *P* values showing statistically significant ($p < 0.05$) differences are presented in bold

0.039). Such effects suggest a mild synergistic effect between mechanisms of biofilm formation and tetracycline resistance. It is widely accepted that enhanced biofilm formation leads to an increased resistance to various antibiotics and other environmental stressors via biofilm-specific resistance mechanisms.[5] This indicates that tetracycline may act to promote MDR by enhancing the protection mechanisms provided by the biofilm. Such biofilm-specific effects are overlooked in broth microdilution MIC assays that test resistance levels in a planktonic state, and as a consequence, do not detect a significant net increase in antibiotic resistance in the MIC assay for tetracycline-exposed isolates (Fig. 2, Supplementary Fig. 1).

In contrast, ciprofloxacin exposure leads to the development of MDR via classical "cellular level" mechanisms[5] that operate in individual cells. These effects result in significantly increased antibiotic resistance that can be detected by the broth microdilution MIC assays performed on planktonic cells (Fig. 2, Supplementary Fig. 1). Thus, our data suggest two distinct pathways for the development of MDR under ciprofloxacin *vs*. tetracycline exposure: (1) via increasing "cellular" drug resistance mechanisms (as tested in the MIC assay), especially seen for ciprofloxacin, often with a cross-resistance towards tetracycline and erythromycin, and (2) via increasing biofilm formation (as seen in the biofilm formation assay), as suggested for tetracycline.

Genomic DNA sequencing and mutation analysis: Network analysis

Cells dispersing from biofilms have been reported to have high rates of phenotypic variation.[29] To investigate the potential genetic basis of diversity in biofilm effluent cells, we sequenced the genomes of 30 random isolates from each treatment type, as well as the initial inoculum. Genome sequencing detected multiple mutations in each isolate (Supplementary Data 1). The majority of mutations were insertions and deletions and mutations mediated by the IS*Aba13* mobile element, followed by synonymous/intergenic and non-synonymous single-nucleotide polymorphisms (SNPs). A number of mutations mediated by mobile genetic elements IS*Aba1* and IS*Aba125* were also detected, as well as loss of plasmids 1 and 2 from various isolates (Table 1).

From planktonic growth experiments, the doubling time of AB5075 in a rich medium at 37 °C is estimated to be ~ 1 h,[30] and the spontaneous mutation rate of multidrug resistant *A. baumannii* strains can vary from 0 to 2.1×10^{-6} mutations per cell division.[31] However, the effects of doubling time and mutation rate on the number of mutations observed are not straightforward. The timing of mutation occurrence has a great impact on the overall number of mutations detected, since the earlier a mutation occurs, the greater the likelihood; it will be passed on and multiplied within subsequent generations, compared to a mutation appearing at a later timepoint. Furthermore, the biofilm mode of growth represents an additional challenge for such calculations, due to the heterogeneity and differences in the cellular activity across the biofilm layers.[32,33] Therefore, we chose not to make such calculations and estimates, instead using de facto results on the number and nature of mutations as detected based on bioinformatic analyses.

Although it is hard to estimate exact mutation rates in biofilms, the number of mutations observed in this study was surprisingly high. A study by Hammerstrom et al.[34] showed the emergence of a hypermutator phenotype characterized by inactivation of the *mutS* gene (encoding an essential protein for the DNA mismatch repair) in *A. baumannii*, when grown to evolve tigecycline resistance over 26 days, with gradually increasing concentrations of tigecycline, up to 32 times the initial MIC. No *mutS* gene mutations were observed in our data (Supplementary Data 1). The emergence of several mutations, mainly SNPs, and the development of resistance towards streptomycin was reported in a recent study of planktonically grown *Salmonella enterica* serovar Typhimurium LT2, in the presence of sub-inhibitory concentrations of streptomycin.[35] Our study showed an abundance of not only SNPs but also a high number of mutations related to structural rearrangements such as insertions and deletions. The latter may not be unexpected as biofilms are known to promote genomic rearrangements and increased rates of horizontal gene transfer.[36]

Cells from antibiotic treatments displayed a higher number of IS-mediated mutations compared to antibiotic-free samples (Table 1), in agreement with reports that these mobile elements increase their rates of mobilization in the presence of antibiotics.[37] Conversely, fewer instances of plasmid loss were detected in antibiotic-exposed cells, despite the fact that neither of the *A. baumannii* plasmids carry known ciprofloxacin or tetracycline resistance genes.

Description of main correlation patterns in network analysis. To examine the emergence of specific mutations in each sample type, as well as their possible effect on phenotype, network analyses were performed. These analyses were based on co-

Table 1. Summary of mutations detected in P, B, BC, and BT samples, and the distribution of mutations across the three biological replicates (represented by R1, R2, and R3, respectively)

	P				B				BC				BT				
	R1	R2	R3	Total (P)	R1	R2	R3	Total (B)	R1	R2	R3	Total (BC)	R1	R2	R3	Total (BT)	Total (per mutation type)
SNP non-synonymous	1	1	1	3	4	2	9	15	9	6	3	18	4	1	9	14	50
SNP synonymous	4	2	1	7	9	4	4	17	12	6	7	25	7	9	10	26	75
SNP intergenic	10	0	2	12	8	0	6	14	10	0	1	11	17	0	1	18	55
Insertions/deletions	1	12	5	18	6	7	9	22	6	13	8	27	10	21	10	41	108
Loss of plasmid 1	1	3	6	10	5	7	6	18	3	4	1	8	1	1	1	3	39
Loss of plasmid 2	0	0	2	2	0	1	1	2	0	0	0	0	0	0	0	0	4
IS*Aba1* mediated	1	1	0	2	1	5	0	6	0	0	9	9	2	1	2	5	22
IS*Aba13* mediated	10	1	9	20	12	4	10	26	21	16	8	45	25	10	7	42	133
IS*Aba125* mediated	0	0	0	0	1	0	1	2	0	3	0	3	2	6	1	9	14
Total (per replicate)	28	20	26		46	30	46		61	48	37		68	49	41		
Total (per sample type)	74				122				146				158				

P planktonic samples, *B* antibiotic-free biofilm samples, *BC* ciprofloxacin-exposed biofilm samples, *BT* tetracycline-exposed biofilm samples

occurrence patterns (i) between the presence of specific mutations and the sample type/growth regime, (ii) between the presence of specific mutations and phenotypic traits (antibiotic resistance measured by the MIC analyses, and biofilm formation tested in the microtiter plate assay), and (iii) between specific mutations and biological replicates.

A strong positive correlation between a mutation and a sample type suggests that the particular treatment regime acted as a selective pressure that favored the fixation of that mutation, because the mutation conferred a phenotypic advantage under those growth conditions. Conversely, negative correlations indicate the reduced likelihood of certain mutations being fixed under particular growth conditions.

A positive correlation between a gene mutation and a phenotype implies a positive effect of that mutation on the emergence of the given phenotype, while negative correlations imply a negative effect on a given phenotype.

Positive/negative correlations between a mutation and a biological replicate indicate the prevalence/absence of that mutation in that biological replicate.

Correlations directly linking specific mutations with sample origin and/or a phenotype. Several mutations in locus ABUW_0885 (mainly synonymous SNPs; nodes labeled 5.1–5.6 in Fig. 3) were linked with resistance to both antibiotics, as well as to enhanced biofilm formation. Despite a relatively large number of synonymous/intergenic SNPs included in the analyses (Table 1), only those five synonymous SNPs directly correlated with either a specific sample type or a phenotype, and, interestingly, all five synonymous mutations were in the same locus ABUW_0885 (nodes 5.2–5.6 in Fig. 3, Table 2). The limited effect of synonymous mutations may not be surprising as they do not change protein sequence, and, hence, often do not impact cellular fitness. However, in some cases synonymous SNPs can contribute to changes in phenotype and undergo selection.[38] ABUW_0885 encodes a large, possibly secreted, protein often annotated as "biofilm-associated protein" (Bap). Bap proteins of *A. baumannii* are important for adherence to surfaces, including human epithelial cells, and for the development of the three-dimensional architecture of mature biofilms.[39] Sequence analysis of the protein encoded by ABUW_0885 using the InterPro tool[40] revealed multiple repeats, immunoglobulin (Ig)-like folds, and a type I secretion C-terminal target domain. The relatively high number of point mutations identified in ABUW_0885 suggests that it might be a hot spot for genetic and phenotypic variability. Similar repeat-containing genes with a high occurrence of mutations have been previously termed "contingency loci"—regions of hypermutable DNA that mediate high-frequency, stochastic, heritable changes that drive rapid evolution and adaptation of bacteria under changing environmental conditions.[41]

In ciprofloxacin-exposed samples, mutations were often directly linked to increased ciprofloxacin resistance, or resistance to both ciprofloxacin and tetracycline (as tested in MIC assays) (Fig. 3, Table 2). These include mutations in *smpB* and ABUW_3609 (nodes 20 and 23.1, respectively). SmpB in association with SsrA (tmRNA) plays an important role in rescuing stalled ribosomes and detoxifying toxic protein products under stress conditions. In earlier studies, deletion of these genes led to increased susceptibility to a range of antibiotics and environmental stresses,[42] but increased resistance to fluoroquinolones, possibly due to a preventive effect on chromosome fragmentation.[43] Likewise, in our study a mutation in *smpB* could have decreased or abolished the activity of the protein, leading to similar effects specific to the fluoroquinolone ciprofloxacin.

Three types of non-synonymous point mutations were detected in the *adeS* gene in effluent cells from ciprofloxacin-exposed biofilms (nodes 13.1–13.3 in Fig. 3, Table 2). Two of these affected codon 318 and resulted in the substitution of glycine with valine or aspartic acid, respectively (nodes 13.1 and 13.2 in Fig. 3, Table 2). These mutations showed strong association with resistance to both tetracycline and ciprofloxacin in the network analysis. The third non-synonymous point mutation (node 13.3), affecting codon 167, showed a weak association with tetracycline resistance (Fig. 3). AdeS is a sensor which, in conjugation with the AdeR response regulator, regulates the expression of the AdeABC RND family multidrug efflux system—one of the major mechanisms of MDR in *A. baumannii*. Mutations in *adeS* can lead to the constitutive expression or overexpression of this efflux system.[44,45] Corroborating our mutation analysis, the AdeABC efflux pump was highly up-regulated in the transcriptomic data from ciprofloxacin-exposed biofilm samples, and, to a lesser degree, in tetracycline-exposed biofilm samples and antibiotic-free biofilms (Fig. 4, Supplementary Fig. 2, Supplementary Data 3). Based on InterPro analysis,[40] codon 318 is located within the ATPase domain of the *adeS* histidine kinase, whereas codon 167 is within the dimerization/phospho-acceptor domain. Thus, in addition to identifying gene mutations linked to particular phenotypes, our data can identify mutations in different parts of a gene that may have different phenotypic impacts. In the case of *adeS* histidine kinase, mutations in the ATPase domain, particularly those affecting codon 318, may have greater impact on the expression of the *adeS*-regulated AdeABC efflux pump, and, subsequently, on antibiotic resistance, compared to mutations in phospho-acceptor domain.

Mutations in two neighboring genes, ABUW_3824 (nodes 25.1 and 25.2 in Fig. 3, Table 2) and ABUW_3825 (nodes 26.1–26.4), encoding a family 1 glycosyl transferase and a hypothetical protein, respectively, were common in both ciprofloxacin- and tetracycline-exposed biofilm samples. These mutations were often linked with antibiotic resistance phenotypes, suggesting that they might confer antibiotic resistance and were selected in the presence of antibiotics (Fig. 3). Genomic analysis showed that these genes are within the K-locus, which determines the production of capsular polysaccharide known to protect against killing by host serum, and to increase virulence.[46,47] The K-locus in strain AB5075-UW includes genes with locus tags ABUW_3815–ABUW_3833, flanked by *lldP* and *fkpA*. A similar organization of the K-cluster occurs in other *A. baumannii* strains.[46] Geisinger and Isberg[47] have reported an increase in the K-locus exopolysaccharide when grown in the presence of sub-inhibitory concentrations of chloramphenicol and erythromycin, due to increased transcription of K-locus genes.[47] Whether mutations in K-locus genes identified in our study lead to changes in the production in the capsular polysaccharides is not known. However, our study demonstrates mutational changes in the K-locus at a genomic level in the biofilm effluent cells with the potential to translate into fixed alterations in the production of the polysaccharide. In our transcriptomic data, various sets of K-locus genes were significantly up- or down-regulated depending on the growth regime (Supplementary Fig. 2, Supplementary Data 3), suggesting that the treatments might result in variation of the K-capsule structure.

IS*Aba13* mobile element-mediated mutations affecting ABUW_3609 were detected in antibiotic-exposed biofilm samples (nodes 23.1–23.3 in Fig. 3, Table 2). This locus encodes the DNA-binding H-NS protein. These mutations were linked to resistance phenotypes, as well as to enhanced biofilm formation (Fig. 3). IS-mediated mutations in an H-NS protein have been linked to high-level colistin resistance in *A. baumannii*[48] and led to enhanced adherence to human pneumocytes and an increase in virulence.[49] The latter was accompanied by up-regulation of type VI secretion system and pili. Up-regulation of these genes was also observed in our transcriptomic data (Supplementary Fig. 2, Supplementary Data 3). Taken together, these suggest that antibiotic exposure may facilitate the emergence of H-NS mutants, and, subsequently, lead

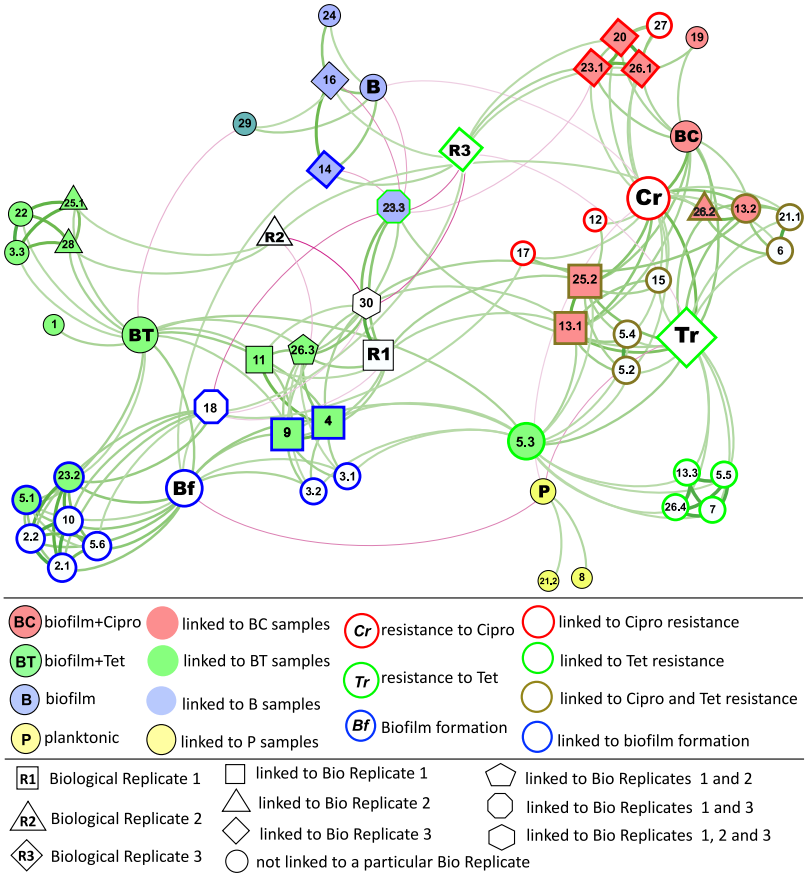

Fig. 3 The network linking mutations with the growth regime, phenotypes, and biological replicates. The force-directed representation of the network is constructed based on co-occurrence patterns and correlations (p value <0.01) between mutations and the growth regime, between mutations and phenotypic measures, and between mutations and biological replicates. Growth regime/sample types are presented as color-filled nodes: P—planktonic culture (yellow-filled), B—antibiotic-free biofilm effluent (blue-filled), BC—ciprofloxacin-exposed biofilm effluent (red-filled), BT—tetracycline-exposed biofilm effluent (green-filled). Phenotypes are presented as color-outlined nodes: Bf (blue-outlined)—biofilm formation, measured in microtiter plate assay; Cr (red-outlined)—resistance to ciprofloxacin measured in MIC assay; and Tr (green-outlined)—resistance to tetracycline measured in MIC assay. P, B, BT, and BC nodes represent the sample type; Bf, Cr, and Tr nodes represent a phenotype; R1, R2, and R3 represent biological replicates 1, 2, and 3, respectively; all other nodes denote mutations directly linked with a specific sample type and/or phenotype. The fill color of nodes corresponds to the sample type that the mutation directly correlates with (linked to P—yellow-filled, to B—blue-filled, to BC—red-filled, to BT—green-filled). The node outline color corresponds to the phenotype with which the mutation is directly linked to (linked to Bf—blue-outlined, to Cr—red-outlined, to Tr –green-outlined). Mutations directly linked to both ciprofloxacin and tetracycline resistance are outlined in khaki. Mutations linked to a particular biological replicate are indicated as squares (linked to replicate 1), triangles (linked to replicate 2), diamonds (linked to replicate 3), pentagons (linked to replicates 1 and 2), octagons (linked to replicates 1 and 3), and a hexagon (linked to replicates 1, 2, and 3). The size of the node is relative to the node authority. Edges (the lines connecting the nodes) represent correlations between two nodes, positive correlations are presented in green, and negatives in magenta. Edge thickness/intensity represents the strength of correlation. The full description of each mutation is presented in Table 2

to increased antibiotic resistance and virulence. H-NS has several roles in the cell, most notably in gene regulation and the silencing of horizontally acquired foreign DNA that often encodes virulence factors and antibiotic resistance determinants.[50] The mutations affecting ABUW_3609 may lead to inactivation of this gene, and, therefore, activation or "de-silencing" of horizontally acquired genes. These may include genes involved in antibiotic resistance, resulting in the emergence of antibiotic-resistant phenotypes.

Mutations in ABUW_2055, encoding a fimbrial adhesin, appeared in antibiotic-free biofilm samples and had a positive correlation with increased biofilm formation (node 14 in Fig. 3). The link between ABUW_2055 and biofilm formation is not surprising as fimbrial adhesins, also called attachment pili, are polymeric fibers that play an important role in surface attachment and biofilm formation.[51]

A mutation in *csuB* (ABUW_1489), part of the *csu* operon that codes

Table 2. Description of mutations that directly correlate (p value <0.01) with a growth regime, a phenotype, or a biological replicate

		Label	Mutation	Annotation	Gene/s	Gene product/s
SNPs	Non-synonymous	2.1	A → G	K5E (AAA → GAA)	*rplX*	50S ribosomal protein L24
		2.2	A → T	K6N (AAA → AAT)	*rplX*	50S ribosomal protein L24
		4	G → A	Intergenic (−98/−30)	ABUW_0747/ABUW_0748	Putative transcriptional regulator Cro/CI family/HP
		5.1	A → C	E2690A (GAG → GCG)	ABUW_0885	Biofilm-associated protein
		6	C → T	P233L (CCG → CTG)	ABUW_0944	Oxidoreductase α (molybdoprotein)-subunit
		10	C → T	A20V (GCA → GTA)	ABUW_1489	CsuB, putative secreted protein related to type I pili
		13.1	C → A	G318V (GGC → GTC)	*adeS*	AdeS kinase
		13.2	C → T	G318D (GGC → GAC)	*adeS*	AdeS kinase
		13.3	C → A	D167Y (GAT → TAT)	*adeS*	AdeS kinase
		14	G → A	R41H (CGT → CAT)	ABUW_2055	Fimbrial protein
		17	T → A	L102I (TTA → ATA)	ABUW_2540	Transposase
		27	C → T	Intergenic (+446/−139)	ABUW_4067/ABUW_4068	HP/HP
		30	G → A	Intergenic (+110/−135)	ABUW_1900/ABUW_1901	Oxidoreductase FAD, FMN binding/HP
	Synonymous	5.2	A → G	A2635A (GCA → GCG)	ABUW_0885	Biofilm-associated protein
		5.3	T → C	G1510G (GGT → GGC)	ABUW_0885	Biofilm-associated protein
		5.4	A → G	L2636L (TTA → TTG)	ABUW_0885	Biofilm-associated protein
		5.5	A → T	V2367V (GTA → GTT)	ABUW_0885	Biofilm-associated protein
		5.6	T → A	T1913T (ACT → ACA)	ABUW_0885	Biofilm-associated protein
InDels	Insertions	1	(CTTTGGATT)10 → 11	Intergenic (+257/−590)	*tyrS*/ABUW_0015	Tyrosyl-tRNA synthetase/16S rRNA gene
		8	+C	Intergenic (−206/−47)	ABUW_1059/ABUW_1060	HP/HP
		25.1	(T)5 → 6	Coding (737/1212 nt)	ABUW_3824	Family 1 glycosyl transferase
	Deletions	3.1	(A)5 → 4	Coding (236/1239 nt)	ABUW_0633	Putative methyltransferase
		15	(A)7 → 6	Coding (198/888 nt)	ABUW_2169	Putative membrane protein
		18	Δ1 bp	Coding (85/708 nt)	*vfr*	Virulence factor regulator, cAMP receptor-like protein
		19	Δ1 bp	Intergenic (−132/+517)	ABUW_3017/ggt	Integrase/gamma-glutamyltransferase
		21.1	(CGGTGCAGT)19 → 7	Coding (313–420/1368 nt)	*filE*	Pilus assembly protein
		21.2	Δ135 bp	Coding (421–555/1368 nt)	*filE*	Pilus assembly protein
		22	Δ141 bp	Partial loss of the gene	[ABUW_3448]	Glycosyl transferase, group 1
IS*Aba1*	Insertions	3.2	IS*Aba1* (−) + 9 bp	Coding (356–364/1239 nt)	ABUW_0633	Putative methyltransferase
		11	IS*Aba13* (−) + 9 bp	Coding (327–335/654 nt)	ABUW_1731	Transcriptional regulator, TetR family
		20	IS*Aba1* (+) + 9 bp	Coding (169–177/477 nt)	*smpB*	SsrA-binding protein
		26.1	IS*Aba1* (+) + 9 bp	Coding (229–237/1254 nt)	ABUW_3825	HP
IS*Aba13*	Insertions	16	IS*Aba13* (−) + 9 bp	Coding (170–178/1470 nt)	ABUW_2208	Adenylate guanylate cyclase
		23.1	IS*Aba13* (+) + 9 bp	Coding (70–78/327 nt)	ABUW_3609	DNA-binding protein HNS
		23.2	IS*Aba13* (−) + 9 bp	Coding (70–78/327 nt)	ABUW_3609	DNA-binding protein HNS
		23.3	IS*Aba13* (+) + 9 bp	Intergenic (−27/+160)	ABUW_3609/ABUW_3610	DNA-binding protein HNS/thioesterase superfamily protein
		25.2	IS*Aba13* (−) + 9 bp	Coding (779–787/1212 nt)	ABUW_3824	Family 1 glycosyl transferase
		26.2	IS*Aba13* (+) + 9 bp	Coding (1008–1016/1254 nt)	ABUW_3825	HP
		26.3	IS*Aba13* (+) + 9 bp	Coding (1224–1232/1254 nt)	ABUW_3825	HP
	Deletions	7	Δ9965 bp	IS*Aba13*-mediated	[ABUW_1758]–ABUW_1764	Putative acetyl esterase/lipase; extracellular serine protease; sulfate permease; HP; gdhB2 quinoprotein glucose dehydrogenase-B; UspA domain protein; GGDEF family protein
		9	Δ8706 bp	IS*Aba13*-mediated	ABUW_1759–ABUW_1764	Extracellular serine protease; sulfate permease; HP; gdhB2 quinoprotein glucose dehydrogenase-B; UspA domain protein; GGDEF family protein
		12	Δ871 bp	IS*Aba13*-mediated	[ABUW_1764]	GGDEF family protein
		24	Δ34,453 bp	IS*Aba13*-mediated	ABUW_3804–[ABUW_3830]	HP; HP; FE/S-dependent 2-methylisocitrate dehydratase; 2-methylcitrate synthase; methylisocitrate lyase; GntR family transcriptional regulator; aromatic amino acid aminotransferase; D-lactate dehydrogenase; K-capsule biosynthesis genes
IS*Aba125*		3.3	IS*Aba125* (+) + 3 bp	Coding (696–698/1239 nt)	ABUW_0633	Putative methyltransferase
		26.4	IS*Aba125* (+) + 3 bp	Coding (695–697/1254 nt)	ABUW_3825	HP
		28	Δ1985 bp	Between IS*Aba125*	ABUW_4087–ABUW_4089	HP; transposase
Loss of plasmid		29	Δ83,610 bp	Loss of plasmid 1	[repAci6]–ABUW_4123	Loss of plasmid 1

Labels correspond to node labels presented in Fig. 3. In the "Mutation" and "Annotation" columns, for SNPs the arrow shows changes in the codon. In the "Mutation" column, short repeat insertion/deletions are presented as the repeat sequence, in parentheses, followed by the number indicating changes in the number of corresponding repeat; for IS-mediated insertions—the IS element involved is given, followed by the strand ("+" or "−"), followed by the number of base pairs involved in the target site amplification. In "Annotation" column, for intergenic mutations, numbers within parentheses represent the position of the mutation, in nucleotide numbers, relative to the two neighboring genes: upstream (with "−" sign) or downstream (with "+" sign) of each gene. For InDels, the numbers within parentheses represent the positions of nucleotides affected in a coding sequence, out of the full number of the nucleotides in the gene. In the "Gene Product/s" column "HP" denotes a hypothetical protein. The slash separates the two genes on each side of an intergenic mutation

for proteins involved in a chaperon-usher pili assembly system important for pilus assembly and biofilm formation,[52,53] was linked to increased biofilm formation in our analyses (node 10 in Fig. 3). Peleg et al.[54] showed that the *csu* operon was only present in pathogenic strains of *A. baumannii*, suggesting this is an important virulence factor.

A mutation in *vfr* (node 18 in Fig. 3) encoding the virulence factor regulator was also positively correlated with biofilm formation. Up-regulation of *vfr* was observed in the transcriptomic data of biofilm

samples (Supplementary Data 3). This locus has been implicated in quorum sensing and flagellar biogenesis,[55,56] both of which are important determinants of biofilm formation.

Correlations between tetracycline exposure and biofilm formation. Several genes were commonly mutated in tetracycline-exposed samples. However, these mutations often positively correlated with increased biofilm formation rather than increased resistance to tetracycline, as can also be seen by the close proximity of nodes representing tetracycline exposure and biofilm formation (nodes BT and Bf, respectively, Fig. 3). This reinforces a possible synergy between biofilm formation and tetracycline resistance mechanisms. Among these mutations was a large 8706 bp deletion involving genes ABUW_1759–ABUW_1764 found in tetracycline-exposed cells and linked to enhanced biofilm formation (node 9, Fig. 3). This region encodes several proteins, including a diguanylate cyclase/phosphodiesterase containing GGDEF and EAL domains. This protein is involved in the regulation of c-di-GMP levels and is known to affect physiological processes including biofilm formation.[57]

Mutations in a putative SAM-dependent methyltransferase (ABUW_0633) also arose predominantly in tetracycline-exposed biofilm dispersal cells (Fig. 3). Mutations in SAM-dependent methyltransferases have been linked to the increased resistance to doxycycline and tigecycline.[58,59] Considering the structural similarities of these two antibiotics with tetracycline (all belonging to the tetracycline class of antibiotics), we can speculate that mutations in ABUW_0633 also have a role in increasing tetracycline resistance. Tetracycline-class antibiotics inhibit protein synthesis by preventing the aminoacyl tRNA subunit from binding to the acceptor site of the 30S ribosomal subunit. Webb et al.[58] suggested that a SAM-dependent methyltransferase that has been shown to confer resistance to doxycycline in in *Burkholderia pseudomallei* probably methylates the tetracycline binding site of the 30S ribosomal subunit. Subsequently, alteration of this gene function through mutation or deletion might change ribosomal methylation patterns, which in turn decreases binding efficiency.[58] However, based on our analysis, none of the mutations in ABUW_0633 (nodes 3.1–3.3 in Fig. 3) was directly linked with tetracycline resistance, but mainly correlated with increased biofilm formation. This suggests that increased biofilm formation in these cells may be at least partially responsible for the increased tetracycline resistance.

The intergenic mutation between ABUW_0747 and ABUW_0748 that can affect the promoter region of the two genes (node 4 in Fig. 3) predominantly occurred in tetracycline-exposed isolates. The presence of this mutation also correlated with biofilm formation and not tetracycline resistance. ABUW_0747 and ABUW_0748 are part of a prophage (predicted to include genes ABUW_0733–ABUW_0815[60]) and encode Cro/CI family transcriptional regulators involved in controlling the life cycle of the phage and its transformation into the lytic phase. Clusters of genes in this phage were significantly up and down-regulated during biofilm growth in our transcriptomics data, and were mainly down-regulated under tetracycline exposure (Fig. 4, Supplementary Fig. 2, Supplementary Data 3). Bacteriophage life cycles have been linked with biofilm development.[61] Whether the putative phage ABUW_0733–ABUW_0815 has a role in biofilm formation in *A. baumannii* and/or in antibiotic resistance is not known.

Thus, our study revealed an interesting phenomenon. Mutations that appeared in the tetracycline-exposed cells were primarily linked with increased biofilm formation, and not directly with increased tetracycline resistance, based on the *p* value threshold for each correlation. Corroborating these data, the biofilm formation assays showed that many tetracycline-exposed isolates had a notable increase in their capacity to form biofilms, compared to antibiotic-free biofilm effluent isolates (Fig. 1), suggesting that tetracycline exposure may drive the emergence of mutations that result in increased biofilm formation. Ultimately, such events could lead to serious consequences, as increased biofilm formation can result in increased resistance to a wide range of antibiotics and environmental stressors via biofilm-specific resistance mechanisms.[5]

Loss of plasmid 1. Complete loss of the largest plasmid, plasmid 1 (shown as node 29 on Fig. 3) positively correlated with antibiotic-free biofilm samples, indicating this event was common in antibiotic-free biofilms. However, loss of plasmid 1 was negatively correlated with tetracycline exposure, suggesting there may be selective pressure to retain plasmid 1 in the presence of tetracycline. Interestingly, despite having several annotated genes involved in resistance towards antibiotics such as streptomycin, no tetracycline resistance genes are known to be harbored on plasmid 1. Similarly, no loss of plasmid 2 was observed for antibiotic-exposed cells (Table 1).

Differences in mutational spectra between biological replicates. As demonstrated in Fig. 3, there were only a limited number of mutations that were prevalent or absent in specific biological replicates, as evident by few positive and negative edges linking a particular replicate (represented by nodes R1, R2, and R3) with specific mutations. Moreover, the nodes representing biological replicates are relatively centrally located within the network, in close proximity to each other. This implies that there were strong similarities between biological replicates in their overall mutational spectrum, and none of the replicates showed a strong inclination towards a specific growth regime or a phenotype. In accordance with the latter, the nodes representing biological replicates had no direct correlation with a growth regime or a phenotype, except biological replicate 3 (node R3) that showed a negative correlation with tetracycline resistance (node Tr). Corroborating this observation from the network analysis, in our MIC assay the isolates originating from biological replicate 3 showed notably decreased tetracycline resistance compared to isolates from other replicates (Fig. 2).

All three biological replicates correlated with an intergenic SNP indicated by node 30, replicate 1 showing a strong positive correlation, while replicates 2 and 3 displayed negative correlations with this node in the network figure (Fig. 3). Apart from these correlations, the mutation represented by node 30 was not directly linked with a particular phenotype or a sample type, and, thus, had no phenotypic implications and was not enriched in a particular sample type. Upon inspection (Supplementary Data 1), it became apparent that this mutation was consistently and exclusively detected in isolates carrying numbers 101–110, from all sample types P, B, BC, and BT. This implies that this mutation was present in the original clone used to inoculate the overnight culture (from which the planktonic isolates P101–P110 were obtained) for biological replicate 1 and was also detected in nearly all random biofilm isolates originating from biological replicate 1. The mutation was absent in isolates originating from replicates 2 and 3. This shows that there was a degree of variability among the initial clones used for inoculation of triplicate overnight cultures and, once again, highlights the power of our mutation analysis.

Correlations between mutations. Multiple correlations were observed between mutations, highlighting the potential for interplay between genes in generating advantageous phenotypes (Fig. 3, Table 2, Supplementary Data 2).

A strong positive correlation between two mutations indicates that these mutations often co-occur within the same genome, for which there are two likely explanations: there are (i) cumulative effects where the two mutations may be co-dependent and act in tandem, possibly having a synergistic effect on the phenotype; or (ii) compensatory effects where emergence of one mutation under given growth conditions requires a second mutation to rescue any

fitness defect imposed by the first mutation.

There were strong positive correlations observed between the IS*Aba1*-mediated mutation in the *smpB* gene (node 20 in Fig. 3, Table 2) and the insertion of IS*Aba13* into ABUW_3609, encoding a DNA-binding H-NS protein (node 23.1). These mutations emerged together in ciprofloxacin-exposed samples, were directly linked with ciprofloxacin resistance, and, according to the literature, might play a role in chromosome architecture and stability.[43,62]

Strong correlations were observed between all three mutations in the *adeS* gene (nodes 13.1–13.3 in Fig. 3), the sensor kinase involved in AdeABC efflux pump regulation, and mutations in either ABUW_3824 or ABUW_3825 (nodes 25.2, 26.2, and 26.4), involved in the biosynthesis of the K-capsule. This suggests a possible functional link between the two mechanisms. Both of these may affect membrane permeability of the antibiotics, and/or changes in the K-capsule might ameliorate toxic effects of AdeS-mediated overexpression of AdeABC. Such interconnectivity between gene functions remains largely unexplored.

Two mutations in *rplX* gene, encoding ribosomal protein L24, were linked with enhanced biofilm formation. These two mutations, leading to amino acid substitutions in positions 5 and 6 (nodes 2.1 and 2.2 in Fig. 3), were strongly correlated with each other and were only found as co-occurring mutations.

Also strongly linked were mutations in ABUW_3824 and ABUW_3448 (nodes 25.1 and 22 in Fig. 3), both of which encode similar glycosyl transferases. These two mutations in turn were also correlated with a mutation in ABUW_0633 (node 3.3) and the deletion of uncharacterized plasmid genes ABUW_4087–ABUW_4089 (node 28).

Negative correlations between mutations indicate that the two mutations are not likely to be present in the same genome, possibly due to the lethal, or highly disadvantageous phenotypic effects that one mutation may have in the presence of the other. Such relationships also suggest functional links between affected genes. An example is the intergenic mutation between the genes ABUW_3609–ABUW_3610 (node 23.3), which is negatively correlated with mutations in *vfr* (node 18), ABUW_2055 (node 14), and ABUW_2208 (node 16), many of which are enriched in the antibiotic-free biofilms or linked with increased biofilm formation (Fig. 3). It is likely that the intergenic mutation affects expression of ABUW_3609, as an IS*Aba13* insertion in ABUW_3609 (node 23.2) is linked with increased biofilm formation.

Interactions between various mutations observed in this study were unexpected, as these links had not been identified previously. Because our study involved whole genome-wide analysis of all mutations, it was possible to reveal multiple mutations per genome and, subsequently, investigate correlations between the presence and absence of mutations in different parts of the genome. Such analyses can identify novel interactions between genes, which have been previously overlooked, and provide targets for future studies.

RNA-sequencing transcriptomics

As soon as effluent isolates were collected from each biofilm sample, whole biofilms were harvested and used for RNA extraction and transcriptomics to identify genes whose transcription was up- or down-regulated in each of the treatments. Nearly half the genes (1516 out of 3895 genes, including plasmid genes) of *A. baumannii* AB5075-UW were significantly (p adj. <0.05) up- or down-regulated in biofilms compared to stationary phase planktonic cultures (Supplementary Fig. 2, Supplementary Data 3). This reflects profound physiological differences between planktonic and biofilm lifestyles.

Among the most up-regulated genes in biofilms were genes involved in the synthesis of ribosomal proteins (Supplementary Fig. 2). This has been observed previously, for example, in comparisons between gene expression levels in biofilms and stationary phase cultures of *E. coli*.[63] In *Gardnerella vaginalis*, ribosomal proteins were down-regulated in comparison to planktonic cells in exponential phase.[64] Consequently, differences in the expression of ribosomal proteins are probably related to differences in cellular activity between the stationary phase cultures and exponentially growing planktonic cultures, whereby the ribosomal turnover in biofilms is higher compared to stationary phase planktonic cultures, but lower in comparison to exponentially growing planktonic cultures. A number of other genes involved in basic metabolic processes such as protein synthesis, carbohydrate metabolism, and cell division were also up-regulated in biofilms (Supplementary Fig. 2, Supplementary Data 3), further suggesting that differences in cellular activity lie behind the differential expression of genes involved in these processes.

In comparison to stationary phase planktonic cultures, genes encoding universal stress proteins and catalases were down-regulated in biofilms, supporting ideas that the stationary phase is characterized by nutrient limitation, changes in pH, and the accumulation of toxic by-products.[65,66]

Among the highly up-regulated and down-regulated genes in all biofilm samples were genes/gene clusters involved in the biosynthesis of proteins for type VI secretion systems, efflux, cell surface modification, and pili, as well as membrane proteins and lipoproteins of unknown function (Supplementary Fig. 2, Supplementary Data 3). These gene products often have important roles in cell interaction and communication, which is of paramount importance in biofilm formation and functioning. All biofilm samples, with or without antibiotic exposure, exhibited up-regulation of drug efflux transport systems. While these systems are best known for their role in MDR, they were up-regulated in biofilms even in the absence of antibiotics. This suggests that such systems have a biofilm-specific role that has been largely overlooked. There are a few reports that suggest a link between efflux transporters and biofilm formation. For example, an efflux transporter component TolC was found to promote cell aggregation in *E. coli*.[67] In *P. aeruginosa*, an ABC-family efflux pump was preferentially expressed in biofilms compared to planktonic cells, conferring biofilm-specific antibiotic resistance.[68] Despite these reports suggesting the importance of efflux in biofilms, the role of efflux transporters in biofilms remains largely unknown[69]

The operon that includes genes *nuoA-nuoN* (ABUW_3165–ABUW_3177) and encodes NADH dehydrogenase I was significantly up-regulated in biofilm samples (Supplementary Fig. 2). In the rhizosphere-dwelling bacterium *Pseudomonas fluorescens*, the *nuo*-encoded NADH dehydrogenase I was essential for plant root colonization.[70] Since biofilm formation is an essential trait for colonization, we speculate that the *nuo* operon has a role in biofilm formation in *A. baumannii*.

To identify specific transcriptional responses to each antibiotic, transcriptomic data from antibiotic-exposed biofilm samples were compared to data from antibiotic-free biofilms (Fig. 3). The addition of antibiotics further increased the up-regulation of genes related to antibiotic resistance, most notably, the RND family efflux transport system AdeABC, involved in resistance to a variety of antibiotics.[71] Several other putative multidrug efflux systems were also up-regulated. Ciprofloxacin exposure led to an increase in the expression of genes in phage and phage-like islands previously identified in the genome of AB5075-UW,[60] whereas tetracycline generally had the opposite effect by down-regulating these genes (Fig. 4, Supplementary Fig. 2).

Ciprofloxacin exposure resulted in increased expression of *tniABC* genes involved in transposition, *tra* genes involved in translocation/plasmid conjugation, and the genes *recA* and *umuD* (Fig. 4, Supplementary Fig. 2). The DNA recombination and repair protein RecA, in conjunction with UmuD polymerase, plays a central role in the induction of SOS pathway of DNA repair and mutagenesis. The SOS response also promotes homologous

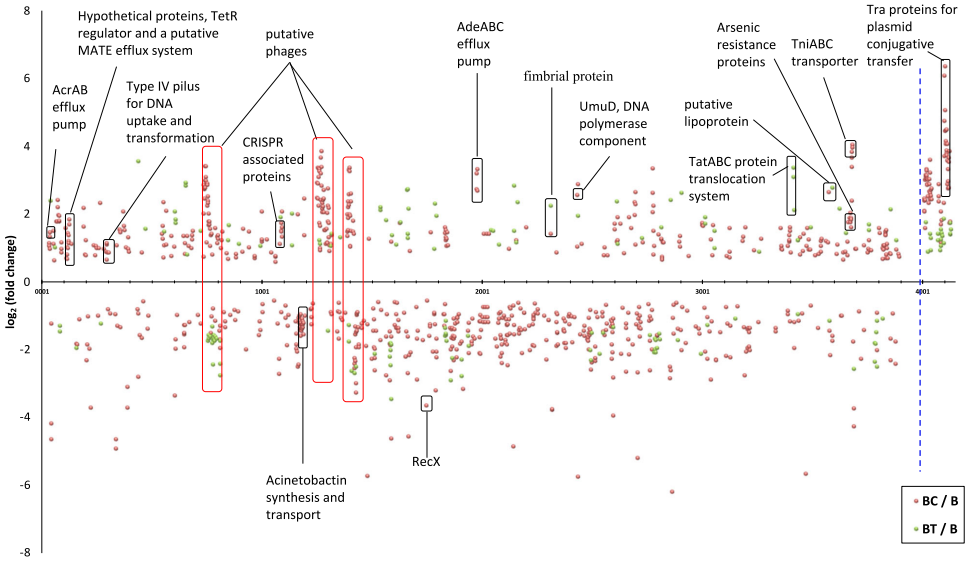

Fig. 4 Transcriptomic changes observed in antibiotic-exposed biofilms compared to antibiotic-free biofilm samples. Transcriptomic changes (log_2 fold change; *p* adj <0.05) detected in ciprofloxacin- and tetracycline-exposed biofilm samples are presented by orange and green circles, respectively. The *X*-axis represents locus tag numbers of the AB5075-UW main chromosome and the largest plasmid 1 (separated by the blue dashed line). Putative phage genes are outlined by red rectangles. Three independent biological replicates were used for evaluating significance

recombination and horizontal gene transfer,[72] processes important for phage transduction, conjugation, and DNA repair. The *recX* gene, which encodes the inhibitor of RecA and has a preventive effect on the induction of the SOS response,[73] was significantly down-regulated under ciprofloxacin exposure.

Induction of *recA*-facilitated homologous recombination by ciprofloxacin has been previously reported in other bacteria.[74–76] Up-regulation of phage transduction, type IV pili-related transformation systems, and plasmid conjugation genes observed in this study is probably the result of *recA*-mediated induction of the SOS pathway under ciprofloxacin exposure. Other genes up-regulated by ciprofloxacin included the CAS genes, part of the CRISPR-related defense system against bacteriophage and conjugative plasmid transfer. This is probably a consequence of the up-regulation of chromosomally encoded phage and plasmid-encoded conjugation genes.

Tetracycline exposure led to differential expression of uncharacterized hypothetical proteins, putative transporters, and the twin-arginine translocation *tatABC* genes involved in proofreading and translocation of large folded proteins across the cytoplasmic membrane[77] (Fig. 4, Supplementary Fig. 2). High-level up-regulation of *tatABC* genes (up to 40-fold) suggests a possible novel mechanism of action for TatABC in tetracycline resistance in biofilms.

Intriguingly, among the most up- or down-regulated genes in biofilm samples were a large number of genes/gene clusters encoding hypothetical proteins with no known function (Supplementary Fig. 2, Supplementary Data 3). Differential expression in these genes reached more than 1000-fold highlighting significant gaps in our knowledge of how biofilms form and persist. These currently unknown gene products could be key factors in biofilm function and could be explored as targets for controlling biofilm formation in medical and environmental contexts.

Implications and concluding remarks

Biofilms are recognized as the predominant lifestyle for the majority of microorganisms. They represent cell communities with significant physiological differences from their planktonic counterparts.[15,78,79] Consequently, many processes that have been studied using planktonic cultures may not apply to biofilms. This is a particular problem for antibiotic resistance research, with the realization that microbial resistance in biofilms far exceeds the resistance levels observed in planktonic cultures.[13,21] The unique properties of biofilms provide protection against antibiotics.[5] Biofilm-specific processes such as cell differentiation and increased rates of horizontal gene transfer can further facilitate the dissemination of antibiotic resistance.[36]

Dispersal of cells from biofilms is an essential process in the biofilm life cycle and is associated with formation of genetic variants that help to ensure successful re-colonization,[80] and genetic diversification during biofilm growth has been demonstrated in *P. aeruginosa*.[81] Here, we demonstrate that the emergence of genomic variants within biofilm dispersal cells is largely synchronized with changes in the environment. Thus, after 6 days of biofilm growth, only 3 days of which were in the presence of sub-inhibitory concentration of antibiotics, *A. baumannii* biofilm dispersal cells had accumulated a wide diversity of mutations that conferred phenotypic changes that were advantageous in the presence of antibiotics. Moreover, we could also trace mutations to changes in specific gene expression profiles in these biofilms.

Our data demonstrate the remarkable ability of microorganisms to adapt to particular environments via rapid evolution, driven by generation of mutations that are subsequently fixed in cell populations. These genomic changes conferred fitness advantages that could overcome environmental pressures such as antibiotic exposure. In particular, our work demonstrates the alarming

emergence of resistant phenotypes within a very short time period after exposure to sub-inhibitory concentrations of antibiotics. It provides us with an unprecedented window into the consequences of antibiotic exposure on bacteria in various natural and medical settings. These rapid and dramatic effects of antibiotic exposure on biofilm cells might not have been fully appreciated.

Sequencing technologies have developed to the point where whole genome sequencing has become a trivial task. Using DNA-sequencing to understand mutation, transcription, and phenotypic changes to organisms is now practical. We can move beyond understanding the effect of specific single mutations on phenotype. Direct investigation of the natural emergence of mutations under selective pressures via high-throughput genome sequencing, with minimal sample manipulation, allows an unbiased and potentially global understanding of bacterial evolutionary processes. The consequence of interplay between specific mutations can thus be studied.

In summary, our data highlight the genomic flexibility of bacteria to quickly adapt to changing environments. These responses can involve multiple mutations within a single genome that, combined, may generate novel phenotypes, thus challenging the "one mutation–one phenotype" paradigm. By using the power of large-scale genome sequencing and transcriptomics, it is possible to decipher processes and natural adaptations occurring in bacteria. This will help to identify mutations with potential roles in biofilm formation and antibiotic resistance. Since biofilms are the prevalent form of microbial life in many environments, the results of our study and our approach are applicable to a wide range of microorganisms, both in clinical and environmental settings. In turn, these findings will become a roadmap for future studies to focus on the role of newly discovered genes and gene combinations in the development of resistant phenotypes. These are potential targets in the war on bacterial resistance.

METHODS

Strains and growth conditions

A previously sequenced and characterized, highly virulent strain of *A. baumannii*, AB5075-UW,[60,82] was used. The strain was maintained on a cation-adjusted Mueller–Hinton (MH) medium (Becton, Dickinson and Company).

Biofilm growth and antibiotic exposure

Biofilms were grown in Tygon R-3603 tubes (VWR International) attached to a peristaltic pump delivering fresh medium at a rate of 4 ml/h. Three single colonies of AB5075-UW were inoculated into liquid MH medium in three separate tubes (a separate colony per tube). One hundred microliters of diluted overnight culture of AB5075-UW (at 1.6×10^4 cells per ml) were inoculated into sterile tubes, using three independent biological replicates for each treatment, each replicate in a separate tube/channel (three channels per treatment). After 3 days of growth at 37 °C to allow biofilm establishment, one set of triplicate samples was left antibiotic-free, while the MH medium for the second set was supplemented with 62.5 µg/ml ciprofloxacin (0.5 MIC), and the growth medium for the third set of samples was supplemented with 2 µg/ml tetracycline (0.25 MIC). In order to choose an appropriate concentration of antibiotics for these biofilm experiments, an MIC test was performed using the broth microdilution method as described below. The concentration of antibiotics chosen represented the minimum concentrations that excluded any growth inhibitory effects in the MIC test. After the addition of antibiotics, biofilms were grown for a further 3 days, at which time the biofilm effluent cells were collected for DNA-sequencing. Biofilms formed inside the tubes were harvested for use in RNA extraction and sequencing.

DNA extraction, sequencing, and mutation analysis

After 72 h of growth, 1 ml of biofilm effluent containing cells detaching from biofilms were collected from each channel. Effluents were diluted 1000-fold and spread on fresh solid MH medium to grow colonies overnight. Ten random, distantly located single colonies were picked from each biological replicate, totaling 90 isolates. These included 30 biofilm effluent isolates grown under ciprofloxacin exposure (BC samples), 30 effluent isolates grown under the tetracycline exposure (BT samples), and 30 effluent isolates derived from antibiotic-free biofilms (B samples). Isolates were also collected from the initial overnight planktonic cultures that were used to inoculate biofilms by spreading the aliquot of the diluted culture, in corresponding biological triplicates, on MH solid medium and collecting 10 distantly located random single colonies per biological replicate, totaling 30 isolates derived from the initial planktonic culture (P samples).

Genomic DNA was extracted from all 120 isolates individually using the DNeasy kit (Qiagen) and the manufacturer's protocol. Genomic DNA samples were submitted to the Ramaciotti Center for Gene Function Analysis (UNSW, Sydney, Australia), where samples were sequenced using HiSeq2500, yielding 120 million paired end reads of 250 bp in length.

Sequence data were trimmed from low-quality data using Trimmomatic software[83] and the quality of sequence data was assessed using FastQC (Babraham Bioinformatics). Paired end reads were combined using Flash.[84] The Breseq algorithm[85] was used for mutation analysis of each individual sample, using combined sequencing reads derived from each isolate. The complete genomic sequence of AB5075-UW available from GenBank (Accession: PRJNA243297) was used as a reference. Mutations with <50% frequency (as estimated by Breseq) were excluded.

Network analysis using mutation data

Pearson's correlations based on mutation co-occurrences and quantitative phenotypic data were calculated in R using the Hmisc 4.1-0 package.[86] The correlation data obtained (as presented in Supplementary Data 2) was imported into the network visualization software Gephi[87] to generate networks based on the ForceAtlas2 layout algorithm.[88] Only correlations with p value <0.01 were included in network analyses. Only mutations directly linked with major nodes (those representing growth regimes, phenotypes, and biological replicates) are shown. Full unfiltered correlation results are presented in Supplementary Data 2.

RNA extraction, sequencing, and analysis

After 72 h of growth following the addition of antibiotics and immediately upon collection of biofilm effluent cells, tubes containing biofilms (three independent biological replicates for each treatment, each replicate in a separate tube/channel, as stated previously) were washed with MH medium to remove planktonic or loosely attached cells. Qiazol reagent was added directly to the biofilms in tubes to lyse and collect the cell material. RNA extraction was performed using the miRNeasy kit (Qiagen) according to the manufacturer's protocol. RNA samples were submitted to the Ramaciotti Center for Gene Function Analysis (UNSW, Sydney, Australia) for ribosomal RNA depletion and sequencing. RNA samples were sequenced on the NextSeq500 platform generating 400 million paired end reads, 75 bp in length.

Sequence data were trimmed from low-quality data using Trimmomatic software.[83] The quality of sequence data was assessed using FastQC (Babraham Bioinformatics). Genome mapping was performed using the EDGE-pro algorithm.[89] Differential expression was calculated in R using the Deseq2 package.[90] To validate the differential expression data, the RNA-sequencing analysis was also performed using the Rockhopper software[91] and the Tophat/Cufflinks/Cuffdiff pipeline,[92] both of which yielded results similar to the EDGE-pro/Deseq2 output.

Quantification of biofilm formation

The capacity of each isolate to form biofilms was tested by the ability of the cells to adhere to the wells of 96-well microtiter dishes (Cellstar, flat bottom, Greiner Bio-One) followed by CV staining of the biofilms formed, as described by O'Toole and Kolter[93] with slight modifications. Briefly, overnight cultures of each isolate, in triplicate, were inoculated (resulting in 1:100 dilution of the overnight culture) into wells of 96-well microtiter plates containing 100 µl cation-adjusted MH liquid medium. Inoculated plates were incubated at 37 °C with shaking (100 r.p.m.) for 20 h. After incubation, the growth was confirmed as the OD_{600} using a PHERAstar microplate reader (BMG Labtech), after which the liquid medium was removed from each well and the wells rinsed twice with phosphate-buffered saline (PBS, pH 7.4, Sigma) to remove loosely attached cells. A 0.2% (w/v) aqueous solution of CV stain (Sigma) was applied for 15 min followed by PBS washing, twice, to remove the excess stain. Ethanol

(150 µl, 100%) was added to each well to extract the CV stain. The extract was diluted 5-fold and absorbance of the CV stain read at 590 nm using the microplate reader.

To evaluate net differences in biofilm formation between isolates originating from planktonic (P), antibiotic-free biofilm (B), ciprofloxacin-exposed biofilm (BC), and tetracycline-exposed biofilm (BT) samples, a three-level mixed-factor nested analysis of variance (ANOVA) was used (technical replicates nested within each isolate, isolates nested within samples in separate biological replicates, and biological replicates nested within sample types) revealing significant heterogeneity between samples ($F_{3,8} = 12.97$; $p = 0.002$). The post hoc Tukey's HSD (honestly significant difference) test was employed to reveal differences between sample pairs.

Antibiotic susceptibility testing

Antibiotic susceptibility of each isolate was tested using an MIC broth microdilution method,[94] using 2-fold dilutions of antibiotics starting from 1000 µg/ml for ciprofloxacin, 125 µg/ml for tetracycline, 30 µg/ml for colistin, and 1000 µg/ml for erythromycin.

To evaluate net differences in MICs between isolates originating from P, antibiotic-free B, ciprofloxacin-exposed BC, and tetracycline-exposed BT samples, a mixed-factor nested ANOVA was used (MICs for individual isolates nested within samples in separate biological replicates, and biological replicates nested within sample types), followed by the post hoc Tukey's HSD to reveal differences between sample pairs. The ANOVA test revealed statistically significant heterogeneity between samples in all MIC tests, including for ciprofloxacin ($F_{3,8} = 40.83$; $p = 3.38E-05$), tetracycline ($F_{3,8} = 5.22$; $p = 0.027$), and erythromycin ($F_{3,8} = 4.96$; $p = 0.031$). Due to the nature of MIC microdilution assay, MIC values often do not follow a normal distribution, as was also apparent in our study when tested using data distribution histograms. To achieve normal distribution, the data was log-transformed prior to ANOVA calculations, as described in ref. .[95]

Reporting summary

Further information on experimental design is available in the Nature Research Reporting Summary linked to this article.

DATA AVAILABILITY

The DNA and RNA sequence data that support the findings of this study have been deposited in the NCBI Sequence Read Archive (SRA) with the accession number SRP155796.

Received: 30 May 2019; Accepted: 3 October 2019;
Published online: 06 November 2019

REFERENCES

1. Peleg, A. Y., Seifert, H. & Paterson, D. L. *Acinetobacter baumannii*: emergence of a successful pathogen. *Clin. Microbiol. Rev.* **21**, 538–582 (2008).
2. Vincent, J. et al. International study of the prevalence and outcomes of infection in intensive care units. *JAMA* **302**, 2323–2329 (2009).
3. Rice, L. B. Federal funding for the study of antimicrobial resistance in nosocomial pathogens: No ESKAPE. *J. Infect. Dis.* **197**, 1079–1081 (2008).
4. World Health Organization. *Global Priority List of Antibiotic-resistant Bacteria to Guide Research, Discovery, and Development of New Antibiotics* (World Health Organization, Geneva, 2017).
5. Penesyan, A., Gillings, M. & Paulsen, I. T. Antibiotic discovery: Combatting bacterial resistance in cells and in biofilm communities. *Molecules* **20**, 5286–5298 (2015).
6. Gordon, N. C. & Wareham, D. W. Multidrug-resistant *Acinetobacter baumannii*: mechanisms of virulence and resistance. *Int. J. Antimicrob. Agents* **35**, 219–226 (2010).
7. Paulsen, I. T. Multidrug efflux pumps and resistance: regulation and evolution. *Curr. Opin. Microbiol.* **6**, 446–451 (2003).
8. Nikaido, H. Multiple antibiotic resistance and efflux. *Curr. Opin. Microbiol.* **1**, 516–523 (1998).
9. Esterly, J. S., Richardson, C. L., Eltoukhy, N. S., Qi, C. & Scheetz, M. H. Genetic mechanisms of antimicrobial resistance of *Acinetobacter baumannii*. *Ann. Pharmacother.* **45**, 218–228 (2011).
10. Qin, H. et al. Comparative transcriptomics of multidrug-resistant *Acinetobacter baumannii* in response to antibiotic treatments. *Sci. Rep.* **8**, 3515 (2018).
11. Eijkelkamp, B. A. et al. Adherence and motility characteristics of clinical *Acinetobacter baumannii* isolates. *FEMS Microbiol. Lett.* **323**, 44–51 (2011).
12. National Institutes of Health. *Research on Microbial Biofilms*. Report No. PA-03-047 (National Institutes of Health, Bethesda, 2002).
13. Hoyle, B. D. & Costerton, J. W. Bacterial resistance to antibiotics: the role of biofilms. *Prog. Drug Res.* **37**, 91–105 (1991).
14. Ceri, H. et al. The Calgary Biofilm Device: new technology for rapid determination of antibiotic susceptibilities of bacterial biofilms. *J. Clin. Microbiol.* **37**, 1771 (1999).
15. Flemming, H.-C. et al. Biofilms: an emergent form of bacterial life. *Nat. Rev. Microbiol.* **14**, 563 (2016).
16. Ciofu, O. & Tolker-Nielsen, T. Tolerance and resistance of *Pseudomonas aeruginosa* biofilms to anntimicrobial agents—how *P. aeruginosa* can escape antibiotics. *Front. Microbiol.* **10**, 913 (2019).
17. Olsen, I. Biofilm-specific antibiotic tolerance and resistance. *Eur. J. Clin. Microbiol. Infect. Dis.* **34**, 877–886 (2015).
18. Shigeta, M. et al. Permeation of antimicrobial agents through *Pseudomonas aeruginosa* biofilms: a simple method. *Chemotherapy* **43**, 340–345 (1997).
19. Costerton, J. W., Stewart, P. S. & Greenberg, E. P. Bacterial biofilms: a common cause of persistent infections. *Science* **284**, 1318–1322 (1999).
20. Lewis, K. Persister cells and the riddle of biofilm survival. *Biochemistry (Mosc.)* **70**, 267–274 (2005).
21. Costerton, J. W., Lewandowski, Z., Caldwell, D. E., Korber, D. R. & Lappin-Scott, H. M. Microbial biofilms. *Annu. Rev. Microbiol.* **49**, 711–745 (1995).
22. Drlica, K. & Zhao, X. DNA gyrase, topoisomerase IV, and the 4-quinolones. *Microbiol. Mol. Biol. Rev.* **61**, 377–392 (1997).
23. Chopra, I. & Roberts, M. Tetracycline antibiotics: mode of action, applications, molecular biology, and epidemiology of bacterial resistance. *Microbiol. Mol. Biol. Rev.* **65**, 232–260 (2001).
24. Stone, G., Wood, P., Dixon, L., Keyhan, M. & Matin, A. Tetracycline rapidly reaches all the constituent cells of uropathogenic *Escherichia coli* biofilms. *Antimicrob. Agents Chemother.* **46**, 2458–2461 (2002).
25. Linares, J. F., Gustafsson, I., Baquero, F. & Martinez, J. L. Antibiotics as intermicrobial signaling agents instead of weapons. *Proc. Natl Acad. Sci. USA* **103**, 19484–19489 (2006).
26. Boehm, A. et al. Second messenger signalling governs *Escherichia coli* biofilm induction upon ribosomal stress. *Mol. Microbiol.* **72**, 1500–1516 (2009).
27. Imamovic, L. & Sommer, M. O. Use of collateral sensitivity networks to design drug cycling protocols that avoid resistance development. *Sci. Transl. Med.* **5**, 204ra132 (2013).
28. Oz, T. et al. Strength of selection pressure is an important parameter contributing to the complexity of antibiotic resistance evolution. *Mol. Biol. Evol.* **31**, 2387–2401 (2014).
29. Koh, K. S. et al. Phenotypic diversification and adaptation of *Serratia marcescens* MG1 biofilm-derived morphotypes. *J. Bacteriol.* **189**, 119–130 (2007).
30. Ajiboye, T. O., Skiebe, E. & Wilharm, G. Phenolic acids potentiate colistin-mediated killing of *Acinetobacter baumannii* by inducing redox imbalance. *Biomed. Pharmacother.* **101**, 737–744 (2018).
31. Karami-Zarandi, M. et al. Variable spontaneous mutation rate in clinical strains of multidrug-resistant *Acinetobacter baumannii* and differentially expressed proteins in a hypermutator strain. *Mutat. Res.* **800-802**, 37–45 (2017).
32. Wentland, E. J., Stewart, P. S., Huang, C.-T. & McFeters, G. A. Spatial variations in growth rate within *Klebsiella pneumoniae* colonies and biofilm. *Biotechnol. Prog.* **12**, 316–321 (1996).
33. Stewart, P. S. & Franklin, M. J. Physiological heterogeneity in biofilms. *Nat. Rev. Microbiol.* **6**, 199–210 (2008).
34. Hammerstrom, T. G., Beabout, K., Clements, T. P., Saxer, G. & Shamoo, Y. *Acinetobacter baumannii* repeatedly evolves a hypermutator phenotype in response to tigecycline that effectively surveys evolutionary trajectories to resistance. *PLoS ONE* **10**, e0140489 (2015).
35. Wistrand-Yuen, E. et al. Evolution of high-level resistance during low-level antibiotic exposure. *Nat. Commun.* **9**, 1599 (2018).
36. Madsen, J. S., Burmolle, M., Hansen, L. H. & Sorensen, S. J. The interconnection between biofilm formation and horizontal gene transfer. *FEMS Immunol. Med. Microbiol.* **65**, 183–195 (2012).
37. Zhu, Y.-G. et al. Continental-scale pollution of estuaries with antibiotic resistance genes. *Nat. Microbiol.* **2**, 16270 (2017).
38. Agashe, D. et al. Large-effect beneficial synonymous mutations mediate rapid and parallel adaptation in a bacterium. *Mol. Biol. Evol.* **33**, 1542–1553 (2016).
39. Brossard, K. A. & Campagnari, A. A. The *Acinetobacter baumannii* biofilm-associated protein plays a role in adherence to human epithelial cells. *Infect. Immun.* **80**, 228–233 (2012).
40. Finn, R. D. et al. InterPro in 2017—beyond protein family and domain annotations. *Nucleic Acids Res.* **45**, D190–D199 (2017).

41. Moxon, R., Bayliss, C. & Hood, D. Bacterial contingency loci: the role of simple sequence DNA repeats in bacterial adaptation. *Annu. Rev. Genet.* **40**, 307–333 (2006).
42. Li, J., Ji, L., Shi, W., Xie, J. & Zhang, Y. *Trans*-translation mediates tolerance to multiple antibiotics and stresses in *Escherichia coli*. *J. Antimicrob. Chemother.* **68**, 2477–2481 (2013).
43. Brito, L. et al. Absence of tmRNA has a protective effect against fluoroquinolones in *Streptococcus pneumoniae*. *Front. Microbiol.* **7**, 2164 (2016).
44. Marchand, I., Damier-Piolle, L., Courvalin, P. & Lambert, T. Expression of the RND-type efflux pump AdeABC in *Acinetobacter baumannii* is regulated by the AdeRS two-component system. *Antimicrob. Agents Chemother.* **48**, 3298–3304 (2004).
45. Peleg, A. Y., Adams, J. & Paterson, D. L. Tigecycline efflux as a mechanism for nonsusceptibility in *Acinetobacter baumannii*. *Antimicrob. Agents Chemother.* **51**, 2065–2069 (2007).
46. Kenyon, J. J. & Hall, R. M. Variation in the complex carbohydrate biosynthesis loci of *Acinetobacter baumannii* genomes. *PLoS ONE* **8**, e62160 (2013).
47. Geisinger, E. & Isberg, R. R. Antibiotic modulation of capsular exopolysaccharide and virulence in *Acinetobacter baumannii*. *PLoS Pathog.* **11**, e1004691 (2015).
48. Deveson Lucas, D. et al. Emergence of high-level colistin resistance in an *Acinetobacter baumannii* clinical isolate mediated by inactivation of the global regulator H-NS. *Antimicrob. Agents Chemother.* **62**, e02442–17 (2018).
49. Eijkelkamp, B. A. et al. H-NS plays a role in expression of *Acinetobacter baumannii* virulence features. *Infect. Immun.* **81**, 2574–2583 (2013).
50. Lucchini, S. et al. H-NS mediates the silencing of laterally acquired genes in bacteria. *PLoS Pathog.* **2**, e81 (2006).
51. Berne, C., Ducret, A., Hardy, G. G. & Brun Y. V. Adhesins involved in attachment to abiotic surfaces by Gram-negative bacteria. *Microbiol. Spectr.* **3**, https://doi.org/10.1128/microbiolspec.MB-0018-2015 (2015).
52. Tomaras, A. P., Dorsey, C. W., Edelmann, R. E. & Actis, L. A. Attachment to and biofilm formation on abiotic surfaces by *Acinetobacter baumannii:* Involvement of a novel chaperone-usher pili assembly system. *Microbiology* **149**, 3473–3484 (2003).
53. Pakharukova, N. et al. Structural basis for *Acinetobacter baumannii* biofilm formation. *Proc. Natl Acad. Sci. USA* **115**, 5558–5563 (2018).
54. Peleg, A. Y. et al. The success of *Acinetobacter* species; genetic, metabolic and virulence attributes. *PLoS ONE* **7**, e46984 (2012).
55. Dasgupta, N., Ferrell, E. P., Kanack, K. J., West, S. E. & Ramphal, R. *fleQ*, the gene encoding the major flagellar regulator of *Pseudomonas aeruginosa*, is sigma70 dependent and is downregulated by Vfr, a homolog of *Escherichia coli* cyclic AMP receptor protein. *J. Bacteriol.* **184**, 5240–5250 (2002).
56. Fuchs, E. L. et al. In vitro and in vivo characterization of the *Pseudomonas aeruginosa* cyclic AMP (cAMP) phosphodiesterase CpdA, required for cAMP homeostasis and virulence factor regulation. *J. Bacteriol.* **192**, 2779–2790 (2010).
57. Tamayo, R., Pratt, J. T. & Camilli, A. Roles of cyclic diguanylate in the regulation of bacterial pathogenesis. *Annu. Rev. Microbiol.* **61**, 131–148 (2007).
58. Webb, J. R., Price, E. P., Currie, B. J. & Sarovich D. S. Loss of methyltransferase function and increased efflux activity leads to doxycycline resistance in *Burkholderia pseudomallei*. *Antimicrob. Agents Chemother.* **61**, e00268–17 (2017).
59. Chen, Q. et al. Decreased susceptibility to tigecycline in *Acinetobacter baumannii* mediated by a mutation in *trm* encoding SAM-dependent methyltransferase. *J. Antimicrob. Chemother.* **69**, 72–76 (2014).
60. Gallagher, L. A. et al. Resources for genetic and genomic analysis of emerging pathogen *Acinetobacter baumannii*. *J. Bacteriol.* **197**, 2027–2035 (2015).
61. Rice, S. A. et al. The biofilm life cycle and virulence of *Pseudomonas aeruginosa* are dependent on a filamentous prophage. *ISME J.* **3**, 271–282 (2008).
62. Lim, C. J., Kenney, L. J. & Yan, J. Single-molecule studies on the mechanical interplay between DNA supercoiling and H-NS DNA architectural properties. *Nucleic Acids Res.* **42**, 8369–8378 (2014).
63. Schembri, M. A., Kjærgaard, K. & Klemm, P. Global gene expression in *Escherichia coli* biofilms. *Mol. Microbiol.* **48**, 253–267 (2003).
64. Castro, J. et al. Comparative transcriptomic analysis of *Gardnerella vaginalis* biofilms vs. planktonic cultures using RNA-seq. *NPJ Biofilms Microbiomes* **3**, 3 (2017).
65. Jaishankar, J. & Srivastava, P. Molecular basis of stationary phase survival and applications. *Front Microbiol.* **8**, 2000 (2017).
66. Navarro Llorens, J. M., Tormo, A. & Martínez-García, E. Stationary phase in Gram-negative bacteria. *FEMS Microbiol. Rev.* **34**, 476–495 (2010).
67. Imuta, N. et al. The *Escherichia coli* efflux pump TolC promotes aggregation of enteroaggregative *E. coli* 042. *Infect. Immun.* **76**, 1247–1256 (2008).
68. Zhang, L. & Mah, T. F. Involvement of a novel efflux system in biofilm-specific resistance to antibiotics. *J. Bacteriol.* **190**, 4447–4452 (2008).
69. Soto, S. M. Role of efflux pumps in the antibiotic resistance of bacteria embedded in a biofilm. *Virulence* **4**, 223–229 (2013).
70. Camacho Carvajal, M. M., Wijfjes, A. H., Mulders, I. H., Lugtenberg, B. J. & Bloemberg, G. V. Characterization of NADH dehydrogenases of *Pseudomonas fluorescens* WCS365 and their role in competitive root colonization. *Mol. Plant Microbe Interact.* **15**, 662–671 (2002).
71. Wieczorek, P. et al. Multidrug resistant *Acinetobacter baumannii*—the role of AdeABC (RND family) efflux pump in resistance to antibiotics. *Folia Histochem. Cytobiol.* **46**, 257–267 (2008).
72. Beaber, J. W., Hochhut, B. & Waldor, M. K. SOS response promotes horizontal dissemination of antibiotic resistance genes. *Nature* **427**, 72–74 (2004).
73. Venkatesh, R. et al. RecX protein abrogates ATP hydrolysis and strand exchange promoted by RecA: insights into negative regulation of homologous recombination. *Proc. Natl Acad. Sci. USA* **99**, 12091–12096 (2002).
74. López, E. & Blázquez, J. Effect of subinhibitory concentrations of antibiotics on intrachromosomal homologous recombination in *Escherichia coli*. *Antimicrob. Agents Chemother.* **53**, 3411–3415 (2009).
75. Thi, T. D. et al. Effect of *recA* inactivation on mutagenesis of *Escherichia coli* exposed to sublethal concentrations of antimicrobials. *J. Antimicrob. Chemother.* **66**, 531–538 (2011).
76. Valencia, E. Y., Esposito, F., Spira, B., Blázquez, J. & Galhardo, R. S. Ciprofloxacin-mediated mutagenesis is suppressed by subinhibitory concentrations of amikacin in *Pseudomonas aeruginosa*. *Antimicrob. Agents Chemother.* **61**, e02107–e02116 (2017).
77. Robinson, C. et al. Transport and proofreading of proteins by the twin-arginine translocation (Tat) system in bacteria. *Biochim. Biophys. Acta Biomembr.* **1808**, 876–884 (2011).
78. Booth, S. C. et al. Differences in metabolism between the biofilm and planktonic response to metal stress. *J. Proteome Res.* **10**, 3190–3199 (2011).
79. Stipetic, L. H. et al. A novel metabolomic approach used for the comparison of *Staphylococcus aureus* planktonic cells and biofilm samples. *Metabolomics* **12**, 75 (2016).
80. McDougald, D., Rice, S. A., Barraud, N., Steinberg, P. D. & Kjelleberg, S. Should we stay or should we go: mechanisms and ecological consequences for biofilm dispersal. *Nat. Rev. Microbiol.* **10**, 39–50 (2012).
81. McElroy, K. E. et al. Strain-specific parallel evolution drives short-term diversification during *Pseudomonas aeruginosa* biofilm formation. *Proc. Natl Acad. Sci. USA* **111**, E1419–E1427 (2014).
82. Jacobs, A. C. et al. AB5075, a highly virulent isolate of *Acinetobacter baumannii*, as a model strain for the evaluation of pathogenesis and antimicrobial treatments. *mBio* **5**, e01076–14 (2014).
83. Bolger, A. M., Lohse, M. & Usadel, B. Trimmomatic: a flexible trimmer for Illumina sequence data. *Bioinformatics* **30**, 2114–2120 (2014).
84. Magoc, T. & Salzberg, S. L. FLASH: fast length adjustment of short reads to improve genome assemblies. *Bioinformatics* **27**, 2957–2963 (2011).
85. Deatherage, D. E. & Barrick, J. E. Identification of mutations in laboratory-evolved microbes from next-generation sequencing data using breseq. *Methods Mol. Biol.* **1151**, 165–188 (2014).
86. Harrell, F. E. *Package 'Hmisc'*. https://cran.r-project.org/web/packages/Hmisc/Hmisc.pdf (2017). Accessed 9 Jan 2018.
87. Bastian, M., Heymann, S. & Jacomy M. Gephi: an open source software for exploring and manipulating networks. *Proceedings of the Third International AAAI Conference on Weblogs and Social Media.* 361–362 (2009).
88. Jacomy, M., Venturini, T., Heymann, S. & Bastian, M. ForceAtlas2, a continuous graph layout algorithm for handy network visualization designed for the gephi software. *PLoS ONE* **9**, e98679 (2014).
89. Magoc, T., Wood, D. & Salzberg, S. L. EDGE-pro: Estimated Degree of Gene Expression in prokaryotic genomes. *Evol. Bioinform.* **9**, 127–136 (2013).
90. Love, M. I., Huber, W. & Anders, S. Moderated estimation of fold change and dispersion for RNA-seq data with DESeq2. *Genome Biol.* **15**, 550 (2014).
91. McClure, R. et al. Computational analysis of bacterial RNA-seq data. *Nucleic Acids Res.* **41**, e140 (2013).
92. Trapnell, C. et al. Differential gene and transcript expression analysis of RNA-seq experiments with TopHat and Cufflinks. *Nat. Protoc.* **7**, 562 (2012).
93. O'Toole, G. A. & Kolter, R. Initiation of biofilm formation in *Pseudomonas fluorescens* WCS365 proceeds via multiple, convergent signalling pathways: a genetic analysis. *Mol. Microbiol.* **28**, 449–461 (1998).
94. EUCAST. Determination of minimum inhibitory concentrations (MICs) of antibacterial agents by broth dilution. *Clin. Microbiol. Infect.* **9**, ix–xv (2003).
95. McDonald, J. H. *Handbook of Biological Statistics* 3rd edn (Sparky House Publishing, 2014).

ACKNOWLEDGEMENTS

This work was supported by the Australian National Health and Medical Research Council Project Grant 1120298. ITP is supported by the Australian Research Council Laureate Fellowship FL140100021. The funders had no role in study design, data collection and interpretation, or the decision to submit the work for publication.

AUTHOR CONTRIBUTIONS

A.P. and I.T.P. conceived the project and designed the experiments. A.P. performed all the experiments and collected the data, with the exception of antibiotic susceptibility testing done by S.S.N. A.P. analyzed the data. A.P., S.K., M.R.G., and I.T.P. interpreted the data and wrote the manuscript.

COMPETING INTERESTS

The authors declare no competing interests.

ADDITIONAL INFORMATION

Supplementary information is available for this paper at https://doi.org/10.1038/s41522-019-0108-3.

Correspondence and requests for materials should be addressed to I.T.P.

Chapter 9: Discussion and future directions

Acinetobacter baumannii is an opportunistic, nosocomial pathogen that has acquired a diverse range of antimicrobial resistance mechanisms (1, 2). An important resistance mechanism are multidrug efflux systems that can directly expel noxious compounds out of the cell before bactericidal concentrations are reached (3). Direct efflux of noxious compounds allow bacterial pathogens to survive antimicrobial therapy and subsequently develop more specific resistance mechanisms (4).

Advances in modern genome sequencing and increasing accessibility of high-throughput genomic sequencing technologies, such as TraDIS and transcriptomics has provided an exciting opportunity to sequence drug resistant isolates and study global fitness and gene responses to antimicrobial challenge (5, 6). Such high-throughput approaches have led to the discovery of new efflux pumps and even novel efflux pump families (7-9). The work presented throughout this thesis features the use of high-throughput methods, such as TraDIS (Chapter 2) and transcriptomics (Chapter 7-8) at sub-inhibitory concentrations of biocides and antimicrobials to identify novel genes conferring antimicrobial resistant phenotypes in *A. baumannii* (Chapter 3-5). In addition to this work, we developed a new method for real-time visualisation of heterogeneity in drug efflux rates within an isogenic bacterial population (Chapter 6).

In Chapter 2, TraDIS was utilised to understand fitness factors contributing to biocide tolerance to ten distinct biocides that were important for resistance to both biocides and antibiotics in *A. baumannii*. In Chapter 6, transcriptomics and proteomics were applied to investigate the global gene response of *A. baumannii* AB5075_UW to subinhibitory ciprofloxacin challenge. In Chapter 7, transcriptomics was applied to study the global gene response to ciprofloxacin and tetracycline antibiotics in biofilms. Drug efflux pumps played a central role in the global gene responses across all three studies (Chapter 2, 7, 8). In Chapter 2, TraDIS analysis identified a number of well-characterised drug efflux pumps of *A. baumannii* (AdeABC, AdeIJK, ArpAB, AmvA) and known efflux pump regulators (AdeRS, AdeN, AmvR and TetR) that were important fitness

determinants for a diverse range of biocides. This suggests biocide exposure in clinical settings may play a role in the emergence of antibiotic resistant pathogens. In Chapter 7, transcriptomic and proteomic studies of subinhibitory exposure of *A. baumannii* to ciprofloxacin, revealed the AdeIJK RND efflux system contributed to intrinsic resistance of this pathogen to ciprofloxacin. In Chapter 8, genome sequencing and subsequent transcriptomic analysis of biofilm isolates exposed to ciprofloxacin or tetracycline at subinhibitory concentrations for three days showed frequent, co-occurring mutations in the transcriptional regulator *adeS* gene, potentially leading to constitutive overexpression of the AdeABC multidrug efflux system. Subsequent transcriptomic analyses showed significant upregulation of AdeABC efflux system genes in biofilms compared to planktonic cultures.

The high-throughput nature of these experiments led to the identification of a swathe of hypothetical proteins of unknown function conferring significant increased fitness or higher gene expression in response to biocides, ciprofloxacin, or tetracycline. Following the biofilm study, transcriptomics revealed significant increased expression of a range of hypothetical genes of unknown function, including an uncharacterised member of the MATE family of drug efflux pumps (Chapter 8). Such genes might simultaneously play important roles in both biofilm formation and drug resistance. Ciprofloxacin transcriptomic analyses in Chapter 7 indicated that the ABUW_0098 gene (*aciT*) is upregulated by ciprofloxacin shock. Initially, we thought this might be a potential new ciprofloxacin efflux system, but further work showed that AciT confers tolerance to ciprofloxacin via formation of a filamentous cellular morphology. Interestingly, the biofilm work in Chapter 8 indicated that expression of *aciT* is also upregulated in response to ciprofloxacin in biofilms.

In addition to these published works, Chapter 2 identified three hypothetical membrane proteins of unknown function that confer fitness to silver nitrate that may represent new efflux pumps. Chapters 3-5 explored the potential roles of these hypothetical proteins in drug efflux. These genes included *yadGH* (ABUW_1247/1248) encoding an ABC-2 transporter of unknown function, ABUW_0700 encoding an ArAE transporter of unknown function and ABUW_1191 encoding a

DUF817 protein of unknown function. These chapters describe a combination of bioinformatics and drug resistance and transport assays to investigate their function.

Silver is a soft transition metal and commonly used anti-infective agent that can act as a bactericidal or bacteriostatic biocide with a pleiotropic mechanism of action to inhibit bacterial cell growth (10, 11). These mechanisms include generation of reactive oxygen species (ROS) through the displacement of iron by binding to iron-sulfur centres, disruption of DNA replication through pyrimidine dimerization, and disrupting the surface of the cell envelope leading to downstream effects such as electron transport chain inhibition and proton leakage (10–15). Silver resistance is largely mediated by the differential expression of porins and metal efflux systems (11). Due to the pleiotropic mechanism of action of silver ions on bacteria, we sought to further understand the function of the three novel genes through bioinformatic analysis and phenotypic assays (Chapter 3-5).

In Chapter 3, we investigated the YadGH ABC transporter in *A. baumannii* AB5075_UW, which may represent a new multidrug efflux pump and/or may also represent a lipid or polysaccharide transport system contributing to cell envelope homeostasis. Bioinformatics analyses reveal the conservation of *yadGH* near a genome region of high synteny related to cell envelope integrity and redox. Further *in silico* analyses with AlphaFold2 predicted a structure that suggests a possible role in lipid export. Biolog phenotype microarrays provided further evidence for a putative role in cell envelope stress response as heterologous expression of YadGH in *E. coli* conferred greater respiration on QAC detergents dequalinium chloride and domiphen bromide, two antiseptics that primarily damage bacterial cell envelope (16–18). Furthermore, *yadGH* expression appeared to specifically confer higher respiration activity on heterocyclic nitrogenous compounds including nitrofurans and nitroimidazoles, that form reactive nitrogen intermediates to exert bactericidal activity by damaging rRNA, DNA and proteins involved in normal cellular function (19, 20). Therefore, the overlap in selectivity for antimicrobials involved in membrane disruption and oxidative stress response, and conserved adjacency to an oxygen-insensitive nitroreductase is consistent with the role of *yadGH* in silver tolerance to *A. baumannii*.

Further MIC and efflux assays revealed *yadGH* was able to confer increased resistance and efflux of acriflavine, suggesting it may function as a multidrug efflux pump. Acriflavine has pleiotropic effects on the cell including DNA intercalation and cell membrane disruption (21, 22). It is unclear whether the acriflavine efflux observed in whole-cell assays is directly attributable to YadGH, or whether indirect effects on the integrity or composition of the cell envelope are leading to changes in expression of other multidrug efflux pumps. Investigation of the effects of a *yadH* knockout mutant in *A. baumannii* revealed pleiotropic effects on the cell envelope including changes in fatty acid composition, capsule loss and increased permeability and aggregation.

Further work needs to be undertaken to clearly delineate the physiological role of YadGH and identify the ligand of this ABC transporter. Future directions could include recombinant purification of the YadGH transport complex and biophysical assays such as nanoDSF, nanoITC and SPR could be used to identify the ligand(s) of this ABC transporter. Following identification of YadGH substrates, we could pursue proteoliposome transport assays to validate direct transport of radiolabelled substrate. Identification of the real ligand(s) of this transporter would likely suggest further physiological follow-up experiments.

In Chapter 4, we investigated ABUW_0700 encoding an aromatic acid exporter family protein of unknown function. Members related to this family include AaeB, a *p*-hydroxybenzoic acid transporter that acts as a metabolic relief valve under acid stress in *E. coli*, and the distantly related ALMT family of organic acid transporters that play an important role in metal detoxification and nutrient acquisition in plants (23, 24).

Bioinformatic analysis indicated that ABUW_0700 is part of the core *A. baumannii* genome and conserved adjacent to genes involved in xenobiotic detoxification, redox and peptidoglycan maintenance. *In silico* analyses revealed the ABUW_0700 predicted structure was comprised of twelve transmembrane helices and two large cytoplasmic domains, with a large transmembrane cavity that is positively charged, suggesting that it binds to an anionic ligand.

Heterologous expression of ABUW_0700 in *E. coli* conferred increased respiration to aromatic antimicrobial compounds and toxic anions, but also cations. MICs revealed that ABUW_0700 conferred increased resistance to sulfadiazine, silver nitrate and acriflavine, and whole-cell transport assays suggested acriflavine resistance was mediated by increased efflux. Considering the resistance profile characterised for ABUW_0700 were not all anionic in nature, it is suggested that ABUW_0700 may also confer antimicrobial tolerance through other mechanisms separate to anion transport.

Future directions to clarify whether ABUW_0700 functions as a drug and/or anion efflux pump, could include recombinant purification of the ABUW_0700 transporter protein and biophysical assays to determine its ligand(s). Reconstitution of ABUW_0700 protein into proteoliposomes will provide an opportunity to determine transport of radiolabelled substrate across a lipid bilayer to deduce whether ABUW_0700 may represent an aromatic acid metabolic relief valve and/or novel multidrug efflux protein. In addition to these experiments, gene knockout and complementation of ABUW_0700 should be conducted to test resistance phenotypes compared to parental *A. baumannii* AB5075_UW strain. This strain can also be used to investigate whether ABUW_0700 confers similar impacts to cell envelope homeostasis as YadGH, since ABUW_0700 was identified in the same silver nitrate TraDIS experiment.

In Chapter 5, we investigated ABUW_1191 encoding a DUF817 protein from *A. baumannii*. In Chapter 2, ABUW_1191 was shown to be important for fitness on silver nitrate but, detrimental to fitness on four other biocide compounds that act on cell membranes, including chlorhexidine, CTAB, hypochlorous acid and glutaraldehyde. This suggests that ABUW_1191 impacts the cell envelope in a manner that can lead to differential outcomes depending on the biocide employed.

Bioinformatic analyses revealed ABUW_1191 was encoded as part of the soft-core genome in *A. baumannii* adjacent to genes involved in virulence and resistance, including the acinetobactin siderophore cluster, heme biosynthesis gene, *hemE* and class C β-lactamase gene, *ampC.* As silver can bind to iron-sulfur clusters and lead to the displacement of iron, conservation of ABUW_1191

involved in silver tolerance in a conserved genome region involved in iron-homeostasis is suggestive of a putative role in metal detoxification and homeostasis.

In silico analyses predicted that ABUW_1191 had a unique structure fold, comprised of eight transmembrane helices with an antiparallel β-sheet cap over the cytoplasmic pore. In addition to the central transmembrane pore were two lateral pores that appear as pathways for substrate translocation from the lipid bilayer leaflet to the periplasmic space.

Heterologous expression of ABUW_1191 in *E. coli* revealed a multidrug resistant phenotype including the β-lactam antimicrobials aztreonam, cefotaxime and cefmetazole. Our bioinformatics highlighted that ABUW_1191 is almost always conserved nearby an *ampC* β-lactamase gene (ABUW_1194), where members of this class are known to contribute to aztreonam and cefotaxime resistance in *A. baumannii* (25). Furthermore, ABUW_1191 also conferred resistance to potassium tellurite, a potent superoxide generator that can lead to inactivation of iron-sulfur clusters and generation of ROS in cytoplasmic space of Gram-negative bacteria (26, 27). MICs indicated that ABUW_1191 conferred increased resistance to silver nitrate and acriflavine. Whole-cell transport assays showed increased acriflavine efflux conferred by ABUW_1191.

Our study provides a foundational characterisation of ABUW_1191, and similar to the other two proteins, future directions could include purification of ABUW_1191, followed by biophysical assays and reconstitution into proteoliposomes. This would hopefully clarify the ligand(s) of ABUW_1191 and its physiological role in the cell. Experiments relating to cell membrane composition, cell permeability, flow cytometry and capsule production and oxidative stress tolerance should be pursued to identify whether presence or absence of ABUW_1191 has significant impacts on *A. baumannii* cell envelope integrity which can influence silver tolerance and multidrug resistance phenotypes in this pathogen.

Chapter 6 describes the development of a novel technique for single cell visualization and quantitation of efflux rates within individual cells in an isogenic bacterial population. Natural

variations in drug efflux pump expression can lead to different efflux-mediated resistance phenotypes in individual cells within an isogenic bacterial population (28, 29).

We studied heterogeneity in R6G efflux mediated by wild-type *E. coli* BW25113, following the same experimental principles as one would follow a traditional whole cell fluorometric transport assay, with the exception that washed and resuspended cells are flowed into a microfluidic chip connected to syringe pumps rather than loaded into a cuvette for fluorometric analyses. The design of the microfluidic chip enabled strict control over the timing and flow of buffer to initiate the transport assay process to allow for rapid efflux rates across a population of individual *E. coli* cells. We were able to clearly define different efflux rates occurring within an isogenic bacterial population. By using low concentrations of R6G we were able to visualize single-molecule foci largely localized at the cell poles across a bacterial population, that may represent individual efflux pumps transporting R6G. We observed three distinct R6G fluorescence transition states at this resolution which could reflect the activity of different types of multidrug efflux pump families.

The design and successful demonstration of our microfluidic chip opens a wealth of experimental possibilities looking at multidrug efflux pumps at a single-cell and single-molecule level. For example, it could be applied to study drug efflux across a range of different fluorophores and fluorescent antimicrobial compounds. It could be potentially linked with gene knockout strains or fluorescently-tagged efflux pumps to link the different observed single-molecule efflux dynamics to individual transporters. The microfluidic chip functionality could be further optimized, for example by modification of the glass slide surface to enhance bacterial cell adhesion. This microfluidic chip system could also be used to study other types of transporters such as nutrient uptake systems with labelled fluorescent substrates. Moreover, our device provides a versatile platform that may be adapted to examine the efficacy of novel efflux inhibitors at the single-cell level. The device can allow for the potential characterization of novel efflux inhibitors for the complete or partial efflux inhibition across a heterologous efflux population. If only a sub-population of cells are inhibited, or partially inhibited, this can lead to further development of mutagenesis and antimicrobial resistance (21, 30).

In summary, the continual exposure of antimicrobial agents to bacteria is driving drug resistance and to expand our understanding of antimicrobial resistance, it is imperative to identify and develop new techniques to study novel efflux systems and subtleties in their function. This thesis provides a toolkit to preliminarily characterise hypothetical membrane proteins of unknown function as putative drug efflux pumps and provides a new method to study heterogeneity in efflux rates *in vivo*. Here we have characterised the genomic context, putative structure, and preliminary multidrug resistant and efflux phenotype of three unique genes selected under sub-inhibitory biocide exposure of *A. baumannii.* We have also developed a rapid method to study heterogeneity in drug efflux rates within an isogenic population of cells, which will allow for further understanding of heterogeneity in efflux function to be studied at the individual cell level.

In conclusion, multidrug efflux systems play significant roles in antimicrobial resistance and have potentially significant roles contributing to biofilm formation and virulence in bacterial pathogens. The development of efflux pump inhibitors to combat efflux mediated resistance seems like a straightforward therapeutic strategy, however, so far, no efflux pump inhibitor has successfully been brought to market largely due to toxicity or pharmacokinetic issues (31, 32). This is likely due to the fact that canonical bacterial efflux pump families generally have mammalian homologs, leading to undesirable toxicity side-effects of these inhibitors. The discovery of novel efflux pump families may provide a new avenue to understand drug resistance mechanisms yet to be discovered and provide new therapeutic targets to ameliorate their effects. Furthermore, a thorough understanding of the physiological roles played by current and novel efflux systems can provide information to construct strategies to select against them or inhibit their mode of action. Together, we can hopefully utilise our knowledge of the ecology and evolution of these drug efflux systems to help overcome and further understand the role of efflux in the AMR crisis and develop effective therapeutic strategies to combat resistance in multidrug resistant pathogens, including *A. baumannii*.

References

1. A. Y. Peleg, H. Seifert, D. L. Paterson, *Acinetobacter baumannii*: Emergence of a successful pathogen. *Clin. Microbiol. Rev.* **21**, 538–582 (2008).

2. C. M. Harding, S. W. Hennon, M. F. Feldman, Uncovering the mechanisms of *Acinetobacter baumannii* virulence. *Nat. Rev. Microbiol.* **16**, 91–102 (2018).

3. P. J. F. Henderson, *et al.*, Physiological functions of bacterial "multidrug" efflux pumps. *Chem. Rev.* **121**, 5417–5478 (2021).

4. A. E. Ebbensgaard, A. Løbner-Olesen, J. Frimodt-Møller, The role of efflux pumps in the transition from low-level to clinical antibiotic resistance. *Antibiot. (Basel, Switzerland)* **9,** 855 (2020).

5. A. K. Cain, *et al.*, A decade of advances in transposon-insertion sequencing. *Nat. Rev. Genet.* **21**, 526–540 (2020).

6. L. Li, S. G. Tetu, I. T. Paulsen, K. A. Hassan, A transcriptomic approach to identify novel drug efflux pumps in bacteria. *Methods Mol. Biol.* **1700**, 221–235 (2018).

7. K. A. Hassan, *et al*., Transcriptomic and biochemical analyses identify a family of chlorhexidine efflux proteins. *Proc. Natl. Acad. Sci. U. S. A.* **110**, 20254–20259 (2013).

8. K. A. Hassan, Q. Liu, P. J. F. Henderson, I. T. Paulsen, Homologs of the *Acinetobacter baumannii* AceI transporter represent a new family of bacterial multidrug efflux systems. *MBio* **6**, e01982-14 (2015).

9. K. A. Hassan, *et al*., Fluorescence-based flow sorting in parallel with transposon insertion site sequencing identifies multidrug efflux systems in *Acinetobacter baumannii*. *MBio* **7**, e01200-16 (2016).

10. K. Mijnendonckx, N. Leys, J. Mahillon, S. Silver, R. Van Houdt, Antimicrobial silver: Uses, toxicity and potential for resistance. *BioMetals* **26**, 609–621 (2013).

11. O. McNeilly, R. Mann, M. Hamidian, C. Gunawan, Emerging concern for silver nanoparticle resistance in *Acinetobacter baumannii* and other bacteria. *Front. Microbiol.* **12,** 652863 (2021).

12. F. F. Xu, J. A. Imlay, Silver(I), mercury(II), cadmium(II), and zinc(II) target exposed enzymic iron-sulfur clusters when they toxify *Escherichia coli*. *Appl. Environ. Microbiol.* **78**, 3614–3621 (2012).

13. H. J. Park, *et al.*, Silver-ion-mediated reactive oxygen species generation affecting bactericidal activity. *Water Res.* **43**, 1027–1032 (2009).

14. S. M. Swasey, L. E. Leal, O. Lopez-Acevedo, J. Pavlovich, E. G. Gwinn, Silver (I) as DNA glue: Ag+-mediated guanine pairing revealed by removing Watson-Crick constraints. *Sci. Rep.* **5**, 1–9 (2015).

15. P. Dibrov, J. Dzioba, K. K. Gosink, C. C. Häse, Chemiosmotic mechanism of antimicrobial activity of Ag(+) in *Vibrio cholerae*. *Antimicrob. Agents Chemother.* **46**, 2668–2670 (2002).

16. M. C. Jennings, K. P. C. Minbiole, W. M. Wuest, Quaternary ammonium compounds: an antimicrobial mainstay and platform for innovation to address bacterial resistance. *ACS Infect. Dis.* **1**, 288–303 (2016).

17. C. Bailly, Medicinal applications and molecular targets of dequalinium chloride. *Biochem. Pharmacol.* **186,** 114467 (2021).

18. P. Gao, *et al.*, Identification and validation of a novel lead compound targeting 4-diphosphocytidyl-2-C-methylerythritol synthetase (IspD) of mycobacteria. *Eur. J. Pharmacol.* **694**, 45–52 (2012).

19. C. G. Giske, Contemporary resistance trends and mechanisms for the old antibiotics colistin, temocillin, fosfomycin, mecillinam and nitrofurantoin. *Clin. Microbiol. Infect.* **21**, 899–905 (2015).

20. C. W. Ang, A. M. Jarrad, M. A. Cooper, M. A. T. Blaskovich, Nitroimidazoles: Molecular fireworks that combat a broad spectrum of infectious diseases. *J. Med. Chem.* **60**, 7636–7657 (2017).

21. H. Nakamura, A. Suganuma, Membrane mutation associated with sensitivity to acriflavine in Escherichia coli. *J. Bacteriol.* **110**, 329–335 (1972).

22. M. Kawai, J. I. Yamagishi, Mechanisms of action of acriflavine: Electron microscopic study of cell wall changes induced in *Staphylococcus aureus* by acriflavine. *Microbiol. Immunol.* **53**, 481–486 (2009).

23. T. K. Van Dyk, L. J. Templeton, K. A. Cantera, P. L. Sharpe, F. S. Sariaslani, characterization of the *Escherichia coli* AaeAB efflux pump: a metabolic relief valve? *J. Bacteriol.* **186**, 7196–7204 (2004).

24. T. Sharma, I. Dreyer, L. Kochian, M. A. Piñeros, The ALMT family of organic acid transporters in plants and their involvement in detoxification and nutrient security. *Front. Plant Sci.* **7**, 1488 (2016).

25. J.-M. Rodríguez-Martínez, L. Poirel, P. Nordmann, Genetic and functional variability of AmpC-type β-lactamases from *Acinetobacter baumannii*. *Antimicrob. Agents Chemother.* **54**, 4930–4933 (2010).

26. T. G. Chasteen, D. E. Fuentes, J. C. Tantaleán, C. C. Vásquez, Tellurite: History, oxidative stress, and molecular mechanisms of resistance: Review article. *FEMS Microbiol. Rev.* **33**, 820–832 (2009).

27. I. L. Calderón, *et al.*, Tellurite-mediated disabling of [4Fe-4S] clusters of *Escherichia coli* dehydratases. *Microbiology* **155**, 1840–1846 (2009).

28. I. El Meouche, M. J. Dunlop, Heterogeneity in efflux pump expression predisposes antibiotic-resistant cells to mutation. *Science.* **362**, 686–690 (2018).

29. T. Bergmiller, *et al.*, Biased partitioning of the multidrug efflux pump AcrAB-TolC underlies long-lived phenotypic heterogeneity. *Science.* **356**, 311–315 (2017).

30. E. E. Whittle, *et al.*, Flow Cytometric Analysis of Efflux by Dye Accumulation. *Frontiers in Microbiology* **10** (2019).

31. T. Opperman, S. Nguyen, Recent advances toward a molecular mechanism of efflux pump inhibition. *Front. Microbiol.* **6**, 421 (2015).

32. G. Spengler, A. Kincses, M. Gajdács, L. Amaral, New roads leading to old destinations: Efflux pumps as targets to reverse multidrug resistance in bacteria. *Mol.* **22**, 468 (2017).

Appendix A: Biocide TraDIS supplementary data

Supplementary data for Chapter 2 “Genomic fitness profiling of *Acinetobacter baumannii* reveals modes of action for common biocides and mechanisms of biocide-antibiotic antagonism” can be accessed online: https://www.researchsquare.com/article/rs-157820/latest and is provided in “Supplementaryinformation.xlsx”. The Biocide TraDIS values against all ten distinct biocides for *yadGH* (Chapter 3) and ABUW_0700 (Chapter 4) are available in excel sheet titled “Transporters” and for ABUW_1191 (Chapter 5) in the excel sheet titled “Hypothetical”.

Appendix B: Antimicrobials screened with Biolog PM11-20

PM11	Compound	PM12	Compound
A1-4	Amikacin	A1-4	Penicillin G
A5-8	Chlortetracycline	A5-8	Tetracycline
A9-12	Lincomycin	A9-12	Carbenicillin
B1-4	Amoxicillin	B1-4	Oxacillin
B5-8	Cloxacillin	B5-8	Penimepicycline
B9-12	Lomefloxacin	B9-12	Polymyxin B
C1-4	Bleomycin	C1-4	Paromomycin
C5-8	Colistin	C5-8	Vancomycin
C9-12	Minocycline	C9-12	D, L-Serine hydroxamate
D1-4	Capreomycin	D1-4	Sisomicin
D5-8	Demeclocycline	D5-8	Sulfamethazine
D9-12	Nafcillin	D9-12	Novobiocin
E1-4	Cefazolin	E1-4	2,4-Diamino-6,7-diisopropylpteridine
E5-8	Enoxacin	E5-8	Sulfadiazine
E9-12	Nalidixic acid	E9-12	Benzethonium chloride
F1-4	Chloramphenicol	F1-4	Tobramycin
F5-8	Erythromycin	F5-8	Sulfathiazole
F9-12	Neomycin	F9-12	5-Fluoroorotic acid
G1-4	Ceftriaxone	G1-4	Spectinomycin
G5-8	Gentamicin	G5-8	Sulfamethoxazole
G9-12	Potassium tellurite	G9-12	L-Aspartic-β-hydroxamate
H1-4	Cephalothin	H1-4	Spiramycin
H5-8	Kanamycin	H5-8	Rifampicin
H9-12	Ofloxacin	H9-12	Dodecyltrimethylammonium bromide

PM13	Compound	PM14	Compound
A1-4	Ampicilliin	A1-4	Acriflavine
A5-8	Dequalinium chloride	A5-8	Furaltadone
A9-12	Nickel chloride	A9-12	Sanguinarine
B1-4	Azlocillin	B1-4	9-Aminoacridine
B5-8	2,2'-Dipyridyl	B5-8	Fusaric acid
B9-12	Oxolinic acid	B9-12	Sodium arsenate
C1-4	6-Mercaptopurine	C1-4	Boric acid
C5-8	Doxycycline	C5-8	1-Hydroxypyridine-2-thione
C9-12	Potassium chromate	C9-12	Sodium cyanate
D1-4	Cefuroxime	D1-4	Cadmium chloride
D5-8	5-Fluorouracil	D5-8	Iodoacetate
D9-12	Rolitetracycline	D9-12	Sodium dichromate
E1-4	Cytosine-1-β-D-arabinofuranoside	E1-4	Cefoxitin
E5-8	Geneticin (G418)	E5-8	Nitrofurantoin
E9-12	Ruthenium red	E9-12	Sodium metaborate
F1-4	Cesium chloride	F1-4	Chloramphenicol
F5-8	Glycine	F5-8	Piperacillin
F9-12	Thallium (I) acetate	F9-12	Sodium metavanadate
G1-4	Cobalt chloride	G1-4	Chelerythrine
G5-8	Manganese chloride	G5-8	Carbenicillin
G9-12	Trifluoperazine	G9-12	Sodium nitrite
H1-4	Cupric chloride	H1-4	EGTA
H5-8	Moxalactam	H5-8	Promethazine
H9-12	Tylosin	H9-12	Sodium orthovanadate

PM15	Compound	PM16	Compound
A1-4	Procaine	A1-4	Cefotaxime
A5-8	Guanidine hydrochloride	A5-8	Phosphomycin
A9-12	Cefmetazole	A9-12	5-Chloro-7-iodo-8-hydroxyquinoline
B1-4	D-Cycloserine	B1-4	Norfloxacin
B5-8	EDTA	B5-8	Sulfanilamide
B9-12	5,7-Dichloro-8-hydroxyquinaldine	B9-12	Trimethoprim
C1-4	5,7-Dichloro-8-hydroxyquinoline	C1-4	Dichlofluanid
C5-8	Fusidic acid	C5-8	Protamine sulfate
C9-12	1,10-Phenanthroline	C9-12	Cetylpyridinium chloride
D1-4	Phleomycin	D1-4	1-Chloro-2,4-dinitrobenzene
D5-8	Domiphen bromide	D5-8	Diamide
D9-12	Nordihydroguaiaretic acid	D9-12	Cinoxacin
E1-4	Alexidine	E1-4	Streptomycin
E5-8	5-Nitro-2-furaldehyde semicarbazone	E5-8	5-Azacytidine
E9-12	Methyl viologen	E9-12	Rifamycin SV
F1-4	3,4-Dimethoxybenzyl alcohol	F1-4	Potassium tellurite
F5-8	Oleandomycin	F5-8	Sodium selenite
F9-12	Puromycin	F9-12	Aluminum sulfate
G1-4	CCCP	G1-4	Chromium chloride
G5-8	Sodium azide	G5-8	Ferric chloride
G9-12	Menadione	G9-12	L-Glutamic-γ-hydroxamate
H1-4	2-Nitroimidazole	H1-4	Glycine hydroxamate
H5-8	Hydroxyurea	H5-8	Chloroxylenol
H9-12	Zinc chloride	H9-12	Sorbic acid

PM17	Compound	PM18	Compound
A1-4	D-Serine	A1-4	Ketoprofen
A5-8	β-Chloro-L-alanine hydrochloride	A5-8	Sodium pyrophosphate decahydrate
A9-12	Thiosalicylic acid	A9-12	Thiamphenicol
B1-4	Sodium salicylate	B1-4	Trifluorothymidine
B5-8	Hygromycin B	B5-8	Pipemidic acid
B9-12	Ethionamide	B9-12	Azathioprine
C1-4	4-Aminopyridine	C1-4	Poly-L-lysine
C5-8	Sulfachloropyridazine	C5-8	Sulfisoxazole
C9-12	Sulfamonomethoxine	C9-12	Pentachlorophenol
D1-4	Oxycarboxin	D1-4	Sodium *m*-arsenite
D5-8	3-Amino-1,2,4-triazole	D5-8	Sodium bromate
D9-12	Chlorpromazine	D9-12	Lidocaine
E1-4	Niaproof	E1-4	Sodium metasilicate
E5-8	Compound 48/80	E5-8	Sodium *m*-periodate
E9-12	Sodium tungstate	E9-12	Antimony (III) chloride
F1-4	Lithium chloride	F1-4	Semicarbazide
F5-8	DL-Methionine hydroxamate	F5-8	Tinidazole
F9-12	Tannic acid	F9-12	Aztreonam
G1-4	Chlorambucil	G1-4	Triclosan
G5-8	Cefamandole nafate	G5-8	3,5-Diamino-1,2.4-triazole
G9-12	Cefoperazone	G9-12	Myricetin
H1-4	Cefsulodin	H1-4	5-Fluoro-5’-deoxyuridine
H5-8	Caffeine	H5-8	2-Phenylphenol
H9-12	Phenylarsine oxide	H9-12	Plumbagin

PM19	Compound	PM20	Compound
A1-4	Josamycin	A1-4	Amitriptyline
A5-8	Gallic acid	A5-8	Apramycin
A9-12	Coumarin	A9-12	Benserazide
B1-4	Methyltrioctylammonium chloride	B1-4	Orphenadrine
B5-8	Harmane	B5-8	D, L-Propanolol
B9-12	2,4-Dinitrophenol	B9-12	Tetrazolium violet
C1-4	Chlorhexidine	C1-4	Thioridazine
C5-8	Umbelliferone	C5-8	Atropine
C9-12	Cinnamic acid	C9-12	Ornidazole
D1-4	Disulphiram	D1-4	Proflavine
D5-8	Iodonitrotetrazolium violet	D5-8	Ciprofloxacin
D9-12	Phenylmethylsulfonyl fluoride	D9-12	18-Crown-6 ether
E1-4	FCCP	E1-4	Crystal violet
E5-8	D, L-Thioctic acid	E5-8	Dodine
E9-12	Lawsone	E9-12	Hexachlorophene
F1-4	Phenethicillin	F1-4	4-Hydroxycoumarin
F5-8	Blasticidin S	F5-8	Oxytetracycline
F9-12	Sodium caprylate	F9-12	Pridinol
G1-4	Lauryl sulfobetaine	G1-4	Captan
G5-8	Dihydrostreptomycin	G5-8	3,5-Dinitrobenzene
G9-12	Hydroxylamine	G9-12	8-Hydroxyquinoline
H1-4	Hexammine cobalt (III) chloride	H1-4	Patulin
H5-8	Thioglycerol	H5-8	Tolyfluanid
H9-12	Polymyxin B	H9-12	Troleandomycin

Appendix C: SDS-PAGE and western blot analysis of YadGH (Chapter 3), ABUW_0700 (Chapter 4) and ABUW_1191 (Chapter 5)

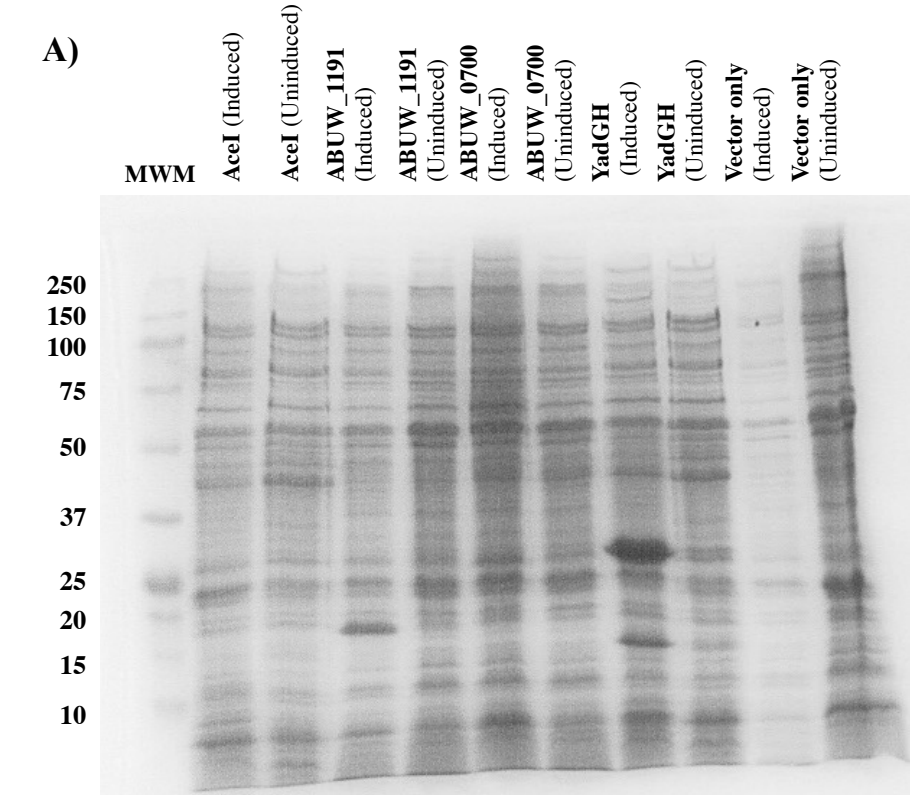

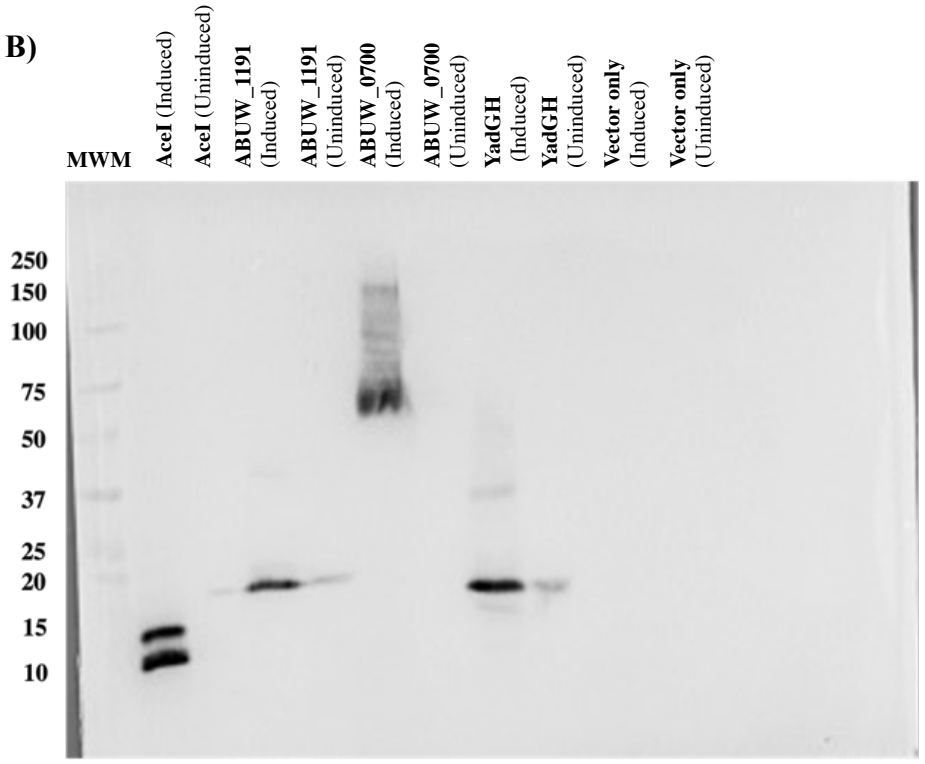

A) SDS-PAGE and B) anti-His_6 western blot of all three hypothetical membrane proteins of unknown function against pTTQ18 empty vector (negative control) and pTTQ18-AceI (positive control) visualised with Coomassie brilliant blue and anti-His_6 probe (Bio-Rad), respectively. MMW (Molecular weight marker, 250 kDa precision plus, Bio-Rad).

AceI positive control appears as two bands at ~10kDa and ~15 kDa as expected. ABUW_1191 appears as a clear band at ~20 kDa, ABUW_0700 is not clearly visible in the SDS-PAGE gel but appears as a smeared wave-like band at ~70kDa in the western blot. The SDS-PAGE gel for YadGH shows a band at ~20 kDa that may represent YadH and a band at ~30 kDa that may represent YadG. In the western blot, YadH can be visualised as a clear band at 20 kDa, the second band at ~37 kDa may represent a YadH dimer, or a His-rich protein contaminant.

Appendix D: Single-cell R6G efflux assay supplementary data

A supplementary file titled “single-molecule movie.mov” is provided with this thesis to assist visualisation of individual foci observed in the single-molecule efflux assay described in Chapter 6.

Appendix E: Biosafety approval letter

MACQUARIE UNIVERSITY

Office of the Deputy Vice-Chancellor (Research)

Research Office
C5C Research HUB East, Level 3, Room 324
MACQUARIE UNIVERSITY NSW 2109 AUSTRALIA

Phone **+61 (0)2 9850 4194**
Fax +61 (0)2 9850 4465
Email biosafety@mq.edu.au

6 February 2015

Professor Ian Paulsen
Department of Chemistry and Biomolecular Sciences
Faculty of Science and Engineering
Macquarie University

Dear Professor Paulsen,

Re: "Characterizing bacterial transporter, regulator and metabolic genes" (Ref: 5201401141)

NOTIFICATION OF A NOTIFIABLE LOW RISK DEALING (NLRD)

The above application has been reviewed by the Institutional Biosafety Committee (IBC) and has been approved as an NLRD, effective 6 February 2015.

This approval is subject to the following standard conditions:

- The NLRD is conducted by persons with appropriate training and experience, within a facility certified to either Physical Containment level 1 (PC1) or PC2.
- Working requiring Quarantine Containment level 2 (QC2) does not commence until the facility has been certified
- Only persons who have been *assessed by the IBC* as having appropriate training and experience may conduct the dealing. This includes persons involved in all parts of the dealing e.g. researchers, couriers and waste contractors. A copy of the IBC's record of assessment must be retained by the project supervisor.
- NLRDs classified under Part 1 of Schedule 3 of the Regulations must be conducted in a facility (or class of facilities) that is certified to at least a PC1 level **and** that is mentioned in the IBC record of assessment as being appropriate for the dealing;
- NLRDs classified under Part 2.1 of Schedule 3 of the Regulations must be conducted in a facility (or class of facilities) that is certified to at least a PC2 level **and** that is mentioned in the IBC record of assessment as being appropriate for the dealing;
- Any transport of the GMO must be conducted in accordance with the Regulator's *Guidelines for the Transport of GMOs* available at: http://www.ogtr.gov.au/internet/ogtr/publishing.nsf/Content/transport-guide-1
- A copy of the IBC's record of assessment has been attached to this approval.
- The record of assessment must be kept by the person or organisation for 8 years after the date of assessment by the IBC (regulation 13 C of the *Gene Technology Regulations 2001*).
- All NLRDs undertaken by Macquarie University will be reported to the OGTR at the end of every financial year.
- If the dealing involves organisms that may produce disease in humans, the NLRDs must be conducted in accordance with the vaccination requirements set out in the Australian Standard AS/NZS 2243.3:2010

- The Chief Investigator must inform the Biosafety Committee if the work with GMOs is completed or abandoned.

Please note the following standard requirements of approval:

1. Approval will be for a period of 5 years subject to the provision of annual reports. If, at the end of this period the project has been completed, abandoned, discontinued or not commenced for any reason, you are required to submit a Final Report. If you complete the work earlier than you had planned you must submit a Final Report as soon as the work is completed. Please contact the Committee Secretary at biosafety@mq.edu.au for a copy of the annual report.

A Progress/Final Report for this study will be due on: 1 February 2016

2. If you will be applying for or have applied for internal or external funding for the above project it is your responsibility to provide the Macquarie University's Research Grants Management Assistant with a copy of this email as soon as possible. Internal and External funding agencies will not be informed that you have final approval for your project and funds will not be released until the Research Grants Management Assistant has received a copy of this email.

If you need to provide a hard copy letter of approval to an external organisation as evidence that you have approval, please do not hesitate to contact the Committee Secretary at the address below.

Please retain a copy of this email as this is your formal notification of final Biosafety approval.

Yours Sincerely

Associate Professor Subramanyam Vemulpad

Chair, Macquarie University Institutional Biosafety Committee

Encl. Copy of record submitted by Macquarie University to the OGTR.

Biosafety Secretariat
Research Office
Level 3, Research Hub, Building C5C East
Macquarie University
NSW 2109 Australia

T: +61 2 9850 6848
F: +61 2 9850 4465

http://www.mq.edu.au/research